NASA CR 65761

~~CONFIDENTIAL~~

LUNAR TV CAMERA

Final Report

(U)

Volume 4

Contract No. NAs 9-3548

1 June 1967

CLASSIFICATION CHANGE

To UNCLASSIFIED
By authority of GDS-GP-4
Changed by L. Shirley Date 8/75
Classified Document Master Control Station, NASA
Scientific and Technical Information Facility

Prepared for

NATIONAL AERONAUTICS AND SPACE ADMINISTRATION
Manned Space Flight Center, IESD
Houston, Texas

AVAILABLE TO U.S. GOVERNMENT

Delimited by NASA 5/17/2013

AGENCIES & U.S. GOVERNMENT

CONTRACTORS ONLY

By

WESTINGHOUSE DEFENSE AND SPACE CENTER
Aerospace Division
Baltimore, Maryland

Delimited by NASA 5/17/2013

Contractors Only

GROUP 4 DOCUMENT
DOWNGRADED AT 3-YEAR INTERVALS
DECLASSIFIED AFTER 12 YEARS
DOD DIR 5200.10

LIBRARY COPY

JUL 10 1967

MANNED SPACECRAFT CENTER
HOUSTON, TEXAS

NOTICE: This material contains information affecting the national defense of the United States within the meaning of the Espionage Laws, Title 18, U. S. C., Sections 793 - 794, the transmission or the revelation of which in any manner to an unauthorized person is prohibited by law.

X67-23886 (ACCESSION NUMBER)
(THRU)
335 (PAGES)
20 (CODE)
CR-65761 (NASA CR OR TMX OR AD NUMBER)
14 (CATEGORY)
FACILITY FORM 602

~~CONFIDENTIAL~~

6693D

PRECEDING PAGE BLANK NOT FILMED.

CONFIDENTIAL

C67-7866

LUNAR TV CAMERA

Final Report

(U)

Volume 4

Contract No. NAs 9-3548

1 June 1967

PRECEDING PAGE BLANK NOT FILMED.

Prepared for

NATIONAL AERONAUTICS AND SPACE ADMINISTRATION
Manned Space Flight Center, IESD
Houston, Texas

By

WESTINGHOUSE DEFENSE AND SPACE CENTER
Aerospace Division
Baltimore, Maryland

PRECEDING PAGE BLANK NOT FILMED.

GROUP 4 DOCUMENT
DOWNGRADED AT 3-YEAR INTERVALS
DECLASSIFIED AFTER 12 YEARS
DOD DIR 5200.10

NOTICE: This material contains information affecting the national defense of the United States within the meaning of the Espionage Laws, Title 18, U. S. C., Sections 793 - 794, the transmission or the revelation of which in any manner to an unauthorized person is prohibited by law.

Agencies and Contractors

Delimited by NASA 5/17/2013

CONFIDENTIAL

This page intentionally left blank.

FOREWORD

This volume was prepared by the Westinghouse Electronic Tube Division under subcontract to the Westinghouse Defense and Space Center, Aerospace Division, Baltimore, Maryland on NASA Contract No. NAS 9-3548. The work was sponsored by the Instrumentation Equipment Systems Division of the Houston Manned Space Center. Max Engert was the project engineer for NASA(MSC).

The program results presented began in October 1964 and were completed in December 1966. Program Manager, R. A. White, was responsible for the program management of the tube development and manufacture and H. S. Wilcox was Engineering Director.

The chief contributors and their fields of interest were Dr. G. Goetze on the overall tube conception and design, A. van der Jagt on the heater cathode, Dr. G. Goetze, A. H. Boerio, R. R. Beyer, H. R. De Vries, and K. F. Boll on the target, J. Vine on the electron optics, A. J. Haley on reliability and D. E. Morehart on tube test.

This report is the final "Technical Report" and includes all work done on contract NAS 9-3548. Due to the voluminous material and classification of some aspects of the work, the report is composed of four volumes.

VOLUME I	This volume describes the overall objectives and requirements and includes unclassified design, development and performance details.
VOLUME II	This volume includes classified* design and performance details.
VOLUME III	This volume describes the development and qualification tests and contains classified* performance details.

VOLUME IV This volume is classified* and describes development, manufacturing, and performance details of the SEC Camera Tube.

Declassified by NASA 8/1975

* Class ential.

Page

VIBRATION I..... 34

VIBRATION II..... 38

VIBRATION III..... 41

MECHANICAL SHOCK..... 47

ACOUSTIC NOISE..... 51

ACCELERATION..... 53

THERMAL VACUUM..... 56

HUMIDITY..... 62

LEAD BEND..... 64

TEST EQUIPMENT USED..... 66

6.2 Target Breakdown Voltage..... 68

6.3 Shelf Life Considerations.... 69

6.4 Life Tests..... 72

TABLE OF CONTENTS

		Page
1.	INTRODUCTION	1
2	DESIGN CONSIDERATIONS	3
3.	MANUFACTURING	5
	3.1 Cracked Button Stems	6
	3.2 Stripped Seals and Cracks in Image Section	6
	3.3 Low Photoresponse	6
	3.4 Poor Cathode Emission	7
4.	ELECTRICAL TESTING	9
5.	RELATED INVESTIGATIONS	15
	5.1 Electrical Breakdown Through the Faceplate	15
	5.2 Ribbon Cathode Development	16
	5.3 Target Burn-In Problems	16
	5.4 Resolution Study	17
6.	RELIABILITY	19
	6.1 Environmental Testing	19
	QUALIFICATION PROCEDURE	22
	RESULTS FROM LCT NO. 432	23
	RESULTS FROM LCT NO. 411	29

LIST OF APPENDIXES

APPENDIX A	INVESTIGATION OF ELECTRICAL LEAKAGE THROUGH FIBER OPTIC FACEPLATES.
APPENDIX B	THERMIONIC CATHODE EMISSION
APPENDIX C	RIBBON CATHODE DEVELOPMENT
APPENDIX D	TARGET BURN-IN INVESTIGATION
APPENDIX E	THE EFFECT OF INTENSE EXPOSURES ON SEC TARGETS
APPENDIX F	MOISTURE DAMAGE TO THE SEC TARGET
APPENDIX G	A RESOLUTION STUDY PROGRAM FOR THE LUNAR CAMERA TUBE
APPENDIX H	THE INFLUENCE OF THE READING BEAM DIAMETER ON RESOLUTION
APPENDIX I	HUMIDITY TEST
APPENDIX J	AN SEC TARGET WITH HIGH STORAGE CAPACITY

Reverse page intentionally left blank

1. INTRODUCTION

Westinghouse Aerospace Division's Purchase Order No. 86KP-87-96641-OS provided for the fabrication and delivery of twenty Secondary Electron Conduction Lunar Camera Tubes. In addition to this, the Westinghouse Electronic Tube Division was required to conduct extensive environmental, electrical and life tests. As supplemental tasks,Westinghouse Electronic Tube Division carried out several investigations. They were:

(1) A Resolution Study for the Lunar Camera Tube

(2) Moisture Damage to the SEC Target

(3) The Ribbon Cathode Development for the Lunar Camera Tube

(4) A SEC Target with High Storage Capacity

(5) Investigation of Target "Burn-In"

(6) The Influence of the Reading Beam Diameter on Resolution

Establishment of Reliability and Quality Control plans was required in addition to a high degree of documentation to provide traceability of parts and processes.

In spite of detailed electrical testing, there remains a subjective component in final evaluation of the tube for suitability to its ultimate use. As a result, considerably more than twenty operable tubes were delivered from which tubes for the missions were selected.

This report deals with the production of tubes and investigations to facilitate this by increasing yield and improving performance.

2. DESIGN CONSIDERATIONS

Changes in design of the tube as described in the contract proposal have not been radical. They have evolved out of the necessity for reliability in manufacture and for optimizing performance without causing a tube/camera interface problem.

The first design (WX-30298) utilized a 1 watt cathode in the scanning section to get started, since the 1 watt design was available for immediate use. This was subsequently replaced with a .2 watt pelletized cathode assembly bought from Sylvania Electric Products when the WX-31034 was designed. Considerable effort was expended to ruggedize this cathode by assuring a rigid anchor of the heater and cathode leads in its support ceramic. The amount of support is necessarily limited since additional mass or increased heat conductivity of supporting members tends to lower its efficiency drastically. The ultimate performance of the assembly still depends upon the integrity of the assembly as received from the supplier. (See Ribbon Cathode Development Report, Appendix C).

The target mesh assembly was modified to minimize the signal generated by a change in capacitance caused by a variation in spacing between target and mesh during vibration. The modification consisted of changing the unsupported area of target and mesh from a circle whose diameter was the

diagonal of the raster, to a rectangle only slightly larger in each dimension than the raster area. The intent was to reduce the excursion of the membranes and raise the resonant frequency.

A major concern was the survival during vibration of the SEC material deposited on the target substrate. Extensive tests beyond specified limits indicate that the destruction level is well above our limits.

A requirement caused by the tube/camera interface necessitated change in suppliers of our fiber optic faceplate and resulted in a chemical incompatibility between the new fiber optic plate and photocathode processing. An entire new approach to photocathode processing was required to produce a satisfactory photocathode without damaging the target. (See Section 5 for further details).

The exhaust tubulation was removed from the button stem resulting in a net reduction of overall length, an improved method of affixing flying leads, and improved reliability through reduction of cracks and leaks in that area. Exhaust is now carried out through a side-arm appendage which is removed from the tube after processing.

3. MANUFACTURING

Production was initiated in the Image Tube Technology Laboratory where assembly was carried out by technicians under the direction of the lunar camera tube engineering section.

In September 1965, the lunar camera tube manufacturing program was physically moved to the image manufacturing department which up to this point had been concerned with the construction of image orthicons and vidicons. The imposition of detailed control, complete documentation and rigorous inspection was perhaps the most difficult facet of this move, However, the assumption by the manufacturing organization of the scheduling and assembly details permitted the rapid introduction of modifications such as "side-arm exhaust", ruggedization modifications, and photocathode processing by the engineering department.

Manufacturing capability was limited by the availability of exhaust positions and one of the first changes was a reduction of the exhaust cycle from 3 days to 1 day through the use of higher temperatures compatible with the target. Considerable attention was given to the possibility of gas or ion spots in the tube due to residual gas as a result of the shortened exhaust cycle. But this did not prove to be a problem, possibly due to rigorous cleaning and a pre-exhaust vacuum bake and storage of the major tube sub-assemblies under vacuum until the day of final assembly and exhaust.

As is common with image tube manufacturing, certain problems appear in epidemic proportions from time to time. The lunar camera tube was no exception, but probably because of the precise documentation required of us, causes were quickly discovered and remedial work initiated at once although many tubes had to be "run through the mill" before an effective fix could be found. The next four paragraphs briefly describe four of these problems.

3.1 Cracked Button Stems

This problem was caused by the difficulty of annealing the button stem after sealing of the tubing to the exhaust system and subsequent tipoff. The situation was avoided by eliminating the tubulation from the button stem and using a Parker compression fitting to connect to the exhaust system through an appendage on the image section. Removal from the system was affected by pinching off a connecting copper tubulation.

3.2 Stripped Seals and Cracks in Image Section

This problem resulted in high scrap in assembly, and occasionally showed up in completed tubes. Improved cleaning of parts prior to glassing not only reduced scrap in assembly, but permitted higher exhaust processing temperatures without risk of cracks in finished tubes.

3.3 Low Photoresponse

This is an ever present problem that required constant vigilence on the part of manufacturing engineering. As can be seen from the control

chart (Figure 3), the variation in sensitivity from tube to tube can be greater than the average value of sensitivity for the tubes. The control chart also demonstrates clearly that the average photoresponse increased significantly (beyond the 3 sigma limits of the control chart) as we gained experience making this photocathode. Three innovations are believed responsible for this improvement:

(a) Improved cleaning of the fiber optic prior to assembly in the tube,

(b) Vacuum prebake of the image section of the tube after the fiber optic assembly is heliarc welded on, and

(c) Higher exhaust temperatures prior to photocathode processing.

3.4 Poor Cathode Emission

An epidemic of tubes having no or low thermionic cathode emission was traced to improperly cured high temperature cement which was used in the process of ruggedizing the cathode. A change in the design of this cathode was made which eliminated the cement entirely and features supports brazed to supporting ceramics. Modifications were also made in cathode processing on exhaust to minimize poisoning of the cathode by products of photocathode processing and incidentally to minimize poisoning of the photocathode by products of thermionic cathode breakdown.(See Appendix B).

During the period of manufacturing in the factory, the entire "clean room" area was re-built and equipment was upgraded to meet the rigorous

demands for "Lunar Quality".

Training and retention of trained assemblers was a serious problem particularly during the summer vacation period. During some periods production was nearly shut down when rejection of assemblies reduced yield almost to zero. Rejections were sometimes for appearance defects which probably would not affect performance or reliability. However, it was necessary to maintain an inflexible posture with respect to quality in order to assure no relaxation in the more critical operations.

4. ELECTRICAL TESTING

A test set was constructed to operate and evaluate the performance of the tubes at 10, 2.5 and .625 frames/second both in a static condition and under vibration on a sine wave vibrator in an area adjacent to the test set. From the start our major difficulty was the isolation of our tube and test set from the electrical noise in the factory. Use of a screen room attenuated the noise but did not eliminate it, particularly when the tube was operated in the .625 frames/second mode.

Electrical testing was performed in four steps for a shipped tube:

(a) Initial test to determine advisability of further processing and test.

(b) 48 hours operation in overscan and reduced light level. This "dynamic aging" was designed to stabilize the tube operation prior to characteristic tests.

(c) Characteristic tests to determine if tube is potentially suitable for shipment. If so, it is subjected to sine wave vibration, thermal shock and hold under a positive pressure of argon.

(d) Final "pre-ship" to determine if any change has taken place during prior tests and operations.

TYPICAL PERFORMANCE AND DISTRIBUTION OF

OPERATING PARAMETERS WX-31034

Figures 1 to 3

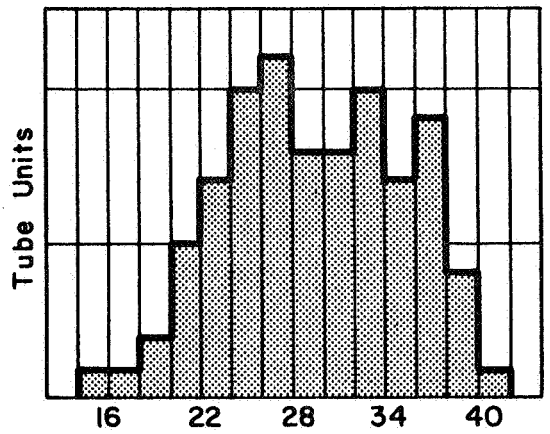

Frequency Histogram
Aperture Response at 250 Lines

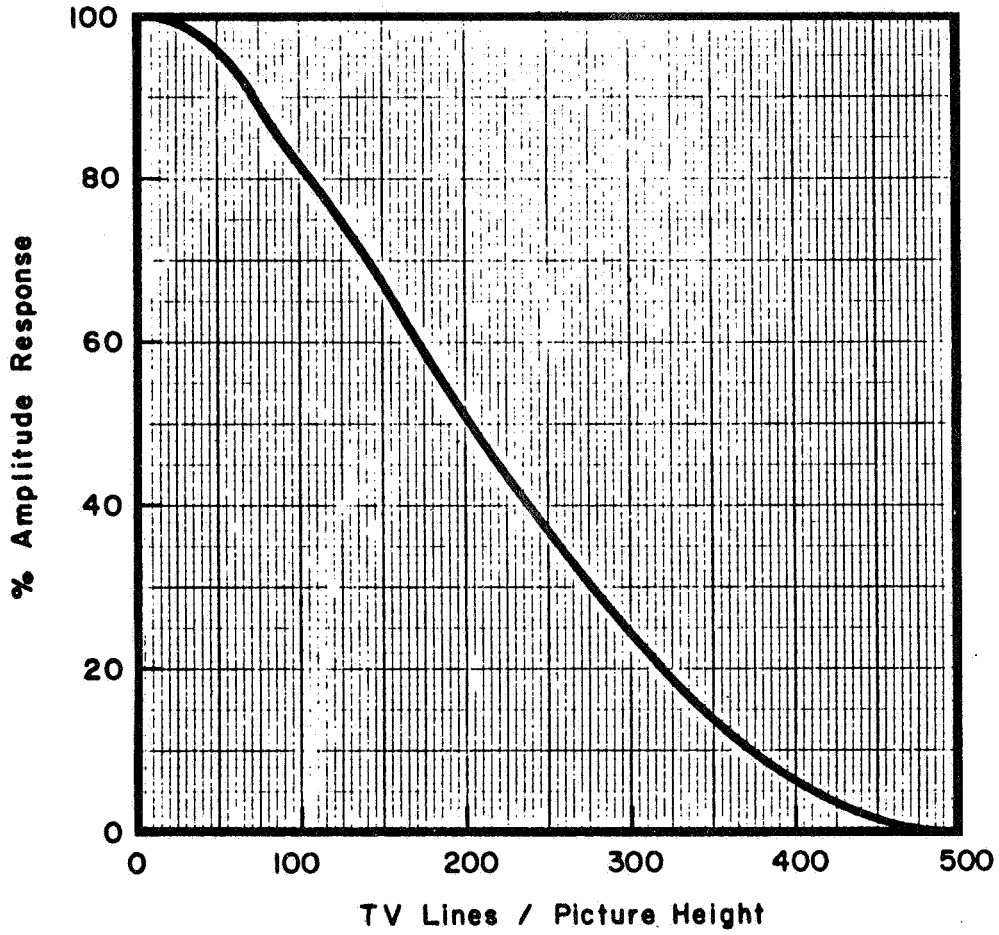

Fig. 1
Aperture Response vs TV Line Number
(Typical)

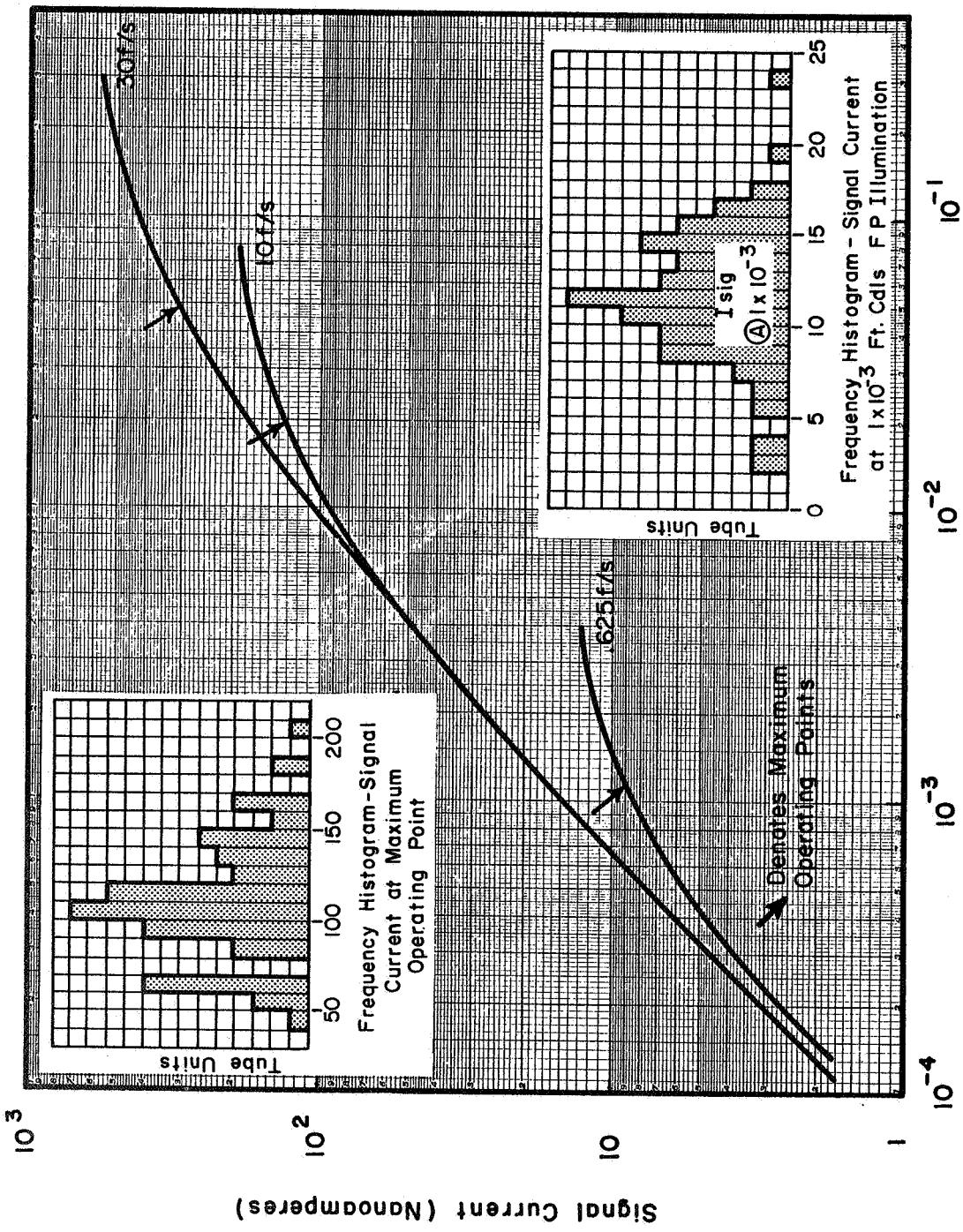

Fig. 2
Typical Operating Characteristic Curve 6693D-PF-14

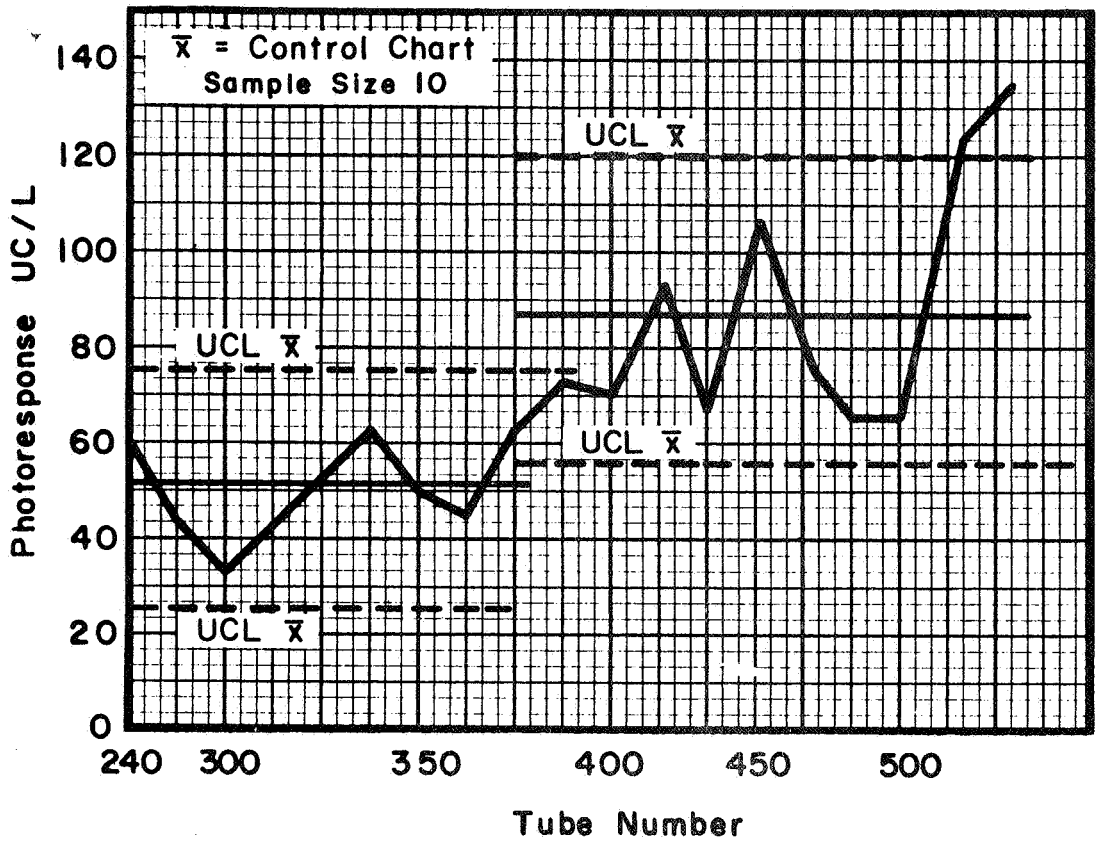

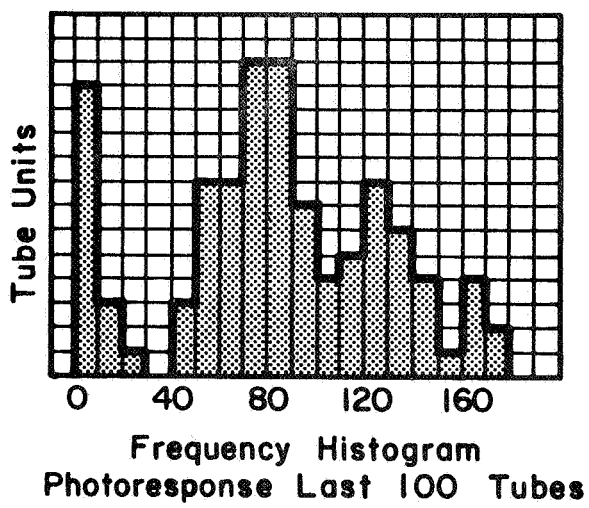

Fig. 3
Photoresponse Curve

Reverse page intentionally left blank

5. RELATED INVESTIGATIONS

During the course of this contract, several investigations were performed with the goal of improving the performance and/or reliability of the device. A brief summary follows and the detailed reports are appended.

5.1 Electrical Breakdown Through The Faceplate

As operated in the camera the fiber optic faceplate must withstand an electrical stress of 8 kV between the planar outside surface and the spherical inner surface that provides the substrate for the photocathode.

Early tubes demonstrated an intermittent spurious signal that appeared as a flash in the resulting picture presentation. The source was traced to an electrical discharge occurring in the body of the faceplate. The Mosaic fiber optic conducted about one nanoampere at 8 kV in its raw state and up to 10,000 nanoamperes on a finished tube. Similar tests of Corning faceplates showed about .5 nanoamperes and 50 nanoamperes respectively without the discharge typical of the Mosaic plate.

Production was immediately changed to utilize 100% Corning plates and this immediately precipitated a photocathode problem, since it was found that the Corning fiber optic was not compatible with the photocathode processing technique then in use. It was necessary to devise a schedule that

incorporated a higher temperature and still not damage the target. It was finally possible to adjust the schedule to the point that photoresponse on the average equaled our previous results with Mosaic plates and individual tubes exceeded our best previous results.

A copy of the report on this investigation is included as Appendix A.

5.2 Ribbon Cathode Development

As previously mentioned, the present design of thermionic cathode is purchased as an assembly and modified to ruggedize it. But there have been inherent difficulties with this, not the least of which is variation of quality beyond our immediate control.

A back-up design was initiated by A. van der Jagt in September 1965, the result of which is a directly heated ribbon cathode supported between two cantilevered springs. Its vibration characteristics seem excellent and reliability would be vastly improved over present design. It has sufficient emission to operate the tube at the .2 watt input, but the necessity of a directly heated cathode posed sufficient camera re-design problems to prevent incorporation into any tubes. This work is reported in Appendix C.

5.3 Target Burn-In Problems

As the project progressed, it was learned that intense lights would appear in the field of view and be such a size that it would not activate the automatic light control function. As a result, a high contrast,

high intensity light would be imaged through the lens of the camera to the tube. Investigation showed that the photocathode was not affected by incident light of this magnitude (several hundred foot candles). Our attention was then given to determining the tolerance of the target to the results of this exposure. Several tubes were subjected to conditions simulating those described above and various combinations of photocathode voltage, illumination and time were run to determine, if possible, parameters for the onset of damage.

Within the limits of our investigation it was determined that irreversible damage does not take place when the tube is operated to produce an output current no higher than that of the maximum operating point. The maximum operating point being the signal current at $E_{photok} = -8$ kV and illumination raised to the point that resolution starts to smear. A constant current curve produced by decreasing photocathode voltage to compensate for increased illumination describes the A.L.C. and defines the upper limit before onset of damage. Above this point, the permanent reduction in gain is a function of primary current, photocathode voltage and time. This work is reported in Appendix D.

5.4 Resolution Study

A separate study to determine the resolution capabilities of the WX-31034 was carried on concurrently with the production program. This study was valuable in pointing out just which parts of the tube were limiting the resolution and in establishing design centers.

The findings of the report established that the aperture response and limiting resolution for the tube as produced was close to the theoretical limits for this design. The final report for the resolution study is in Appendix G.

6. RELIABILITY

The end use of the tube necessitated considerable experimentation, test and evaluation to assure a high degree of reliability. The goal of the reliability program was control of manufacturing material and processes to assure that tubes delivered for the mission were, statistically speaking, from the same population as those tubes from which information was derived by destructive tests.

6.1 Environmental Testing

Environmental testing was used as a design tool to determine the optimum tube configuration as well as a method of assurance that the tube as manufactured will operate and survive under conditions of the mission.

6.1.1 Development of Ruggedized Design

Mechanical design of the ruggedized tube was carried out by breaking the tube into three functionally different sub-assemblies. They are the image section, the target-mesh section and the scanning section.

Mechanical samples of each section were subjected to vibration, analyzed and modified where necessary. This method permitted us to make many assemblies in a short time and eliminate the possibility of spurious results due to non-environmental defects. A number of complete

operable tubes were then tested to destruction to verify the design. Tests were devised to identify resonances in specific structures so that every tube could be vibrated at non-destructive levels and any incipient problems could be detected and corrected.

Specific changes made as a result of this program are described in Section 2.

6.1.2 Qualification Tests

The following section of the report covers the program to determine the suitability of design and construction of the WX-31034 with respect to the environmental requirements of the qualification tests specified in paragraph 4.3.2 of Purchasing Department Specification 21341, Revision C. The environmental tests are part of the larger qualification test program which includes life test of 7 of the 9 test samples. The remaining two tubes are subjected to environmental tests but both tubes are not subjected to the same tests.

Certain environmental requirements are imposed as part of the acceptance tests for the 20 or so tubes shipped for eventual operation in camera systems as well as the 9 qualification test samples. No failures occurred in qualification samples or in tubes given acceptance tests and shipped.

Operating environmental tests were performed with considerable difficulty. In no case was a picture comparable to that achieved

in the test set. This was primarily due to long lead length and difficulty in shielding. In all cases the operating environmental pictures indicated only that no perceptible change took place during or after the test with that set up. Pictures of good definition were taken in the standard test set-up before and after each environmental test

Humidity tests were run in the operating mode for only part of the prescribed time on one tube (432), and the second tube (411) was subjected to humidity tests without operation because of the effect of humidity on optical focus and associated equipment such as the deflection yoke. Details are given in Engineering Memo No. 88 included as Appendix I of this report.

The procedure followed in qualification testing was to perform the tests in the order specified and to check the tube in the test set upon completion of each test and perform a final test after the last environmental test, comparing it with initial results. To keep this presentation within reasonable size, only the initial and final test results are shown, but the conditions of test and applicable supporting data are included in order of the tests outlined in the qualification procedure listed on the following page.

QUALIFICATION PROCEDURE

Acceptance Requirements	Tube	-	to	-	Tube	-	to	-
	411				432			
Test Preliminaries	X	5/24		5/26	X	6/8		6/15
Electrical Tests	X	5/26		5/26	X	6/15		6/15
Argon Hold	X	6/8		6/15	X	6/16		6/23
Checked	X	6/18		6/18	X	6/23		6/23
Vibration I	X	6/18		6/18	X	6/23		6/23
Glass Strain	X	6/18		6/18	X	6/23		6/23
Checked	X	6/19		6/19	X	6/24		6/24
Environmental Tests								
Vibration II	X	6/29		6/29				
Vibration III	X	6/30		6/30				
Checked	X	8/1		8/1				
Mechanical Shock	X	8/3		8/3				
Checked	X	8/8		8/8				
Acoustic Noise					X	6/29		6/29
Acceleration					X	6/30		6/30
Checked					X	7/1		7/1
Thermal Vacuum (low temp.)					X	7/5		7/6
Thermal Vacuum (high temp.)					X	7/27		7/28
Checked					X	8/1		8/1
Temperature Cycling					X	8/8		8/8
Checked					X	8/9		8/9
Temperature Storage (low)	X	8/8		8/23				
Temperature Storage (high)	X	8/23		9/7				
Checked	X	9/7		9/7				
Humidity	X	9/13		9/23	X	9/6		9/16
Checked	X	9/23		9/23	X	9/16		9/16
	454				293			
Lead Bend	X	9/27			X	9/27		

RESULTS FROM LCT NO. 432

(Elmira LCT Test Set Model E 154A)

1. Electrical Set Up Parameters For Photographs.
2. Electrical Tests Before Qualification Program (Photographs)
    a. Monitor
    b. Spurious Signal
    c. Center Resolution
3. List of Tests Performed on LCT Tube No. 432.
4. Post Humidity
5. Post Thermal Cycling Photographs
    a. Monitor
    b. Spurious Signal
    c. Center Resolution

1. TUBE #432

SET UP PARAMETERS FOR PHOTOGRAPHS

Eg_1 = -52 volts
Eg_{1co} = -87 volts
Eg_2 = 300 volts
$Eg_{3,6}$ = 600 volts
Eg_4 = 97 volts
Eg_5 = 300 volts
Eg_7 = 25 volts
Esj = 35 volts
Epc = -8 KV
E_H = 1.5 volts
I_H = 149 ma
I_{HAL} = -8 ma
I_{VAL} = +7 ma
Isj = 7.5×10^{-9} amp. at 1×10^{-3} ft-c. (10 f/s)

CONFIDENTIAL

2. ELECTRICAL TESTS BEFORE QUALIFICATION PROGRAM

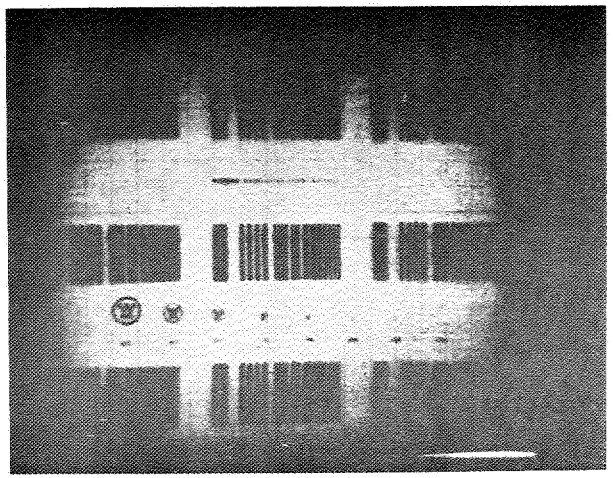

a. Monitor

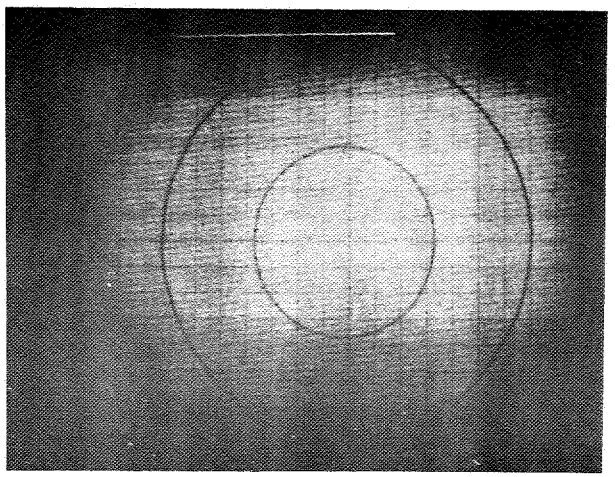

b. Spurious Signal

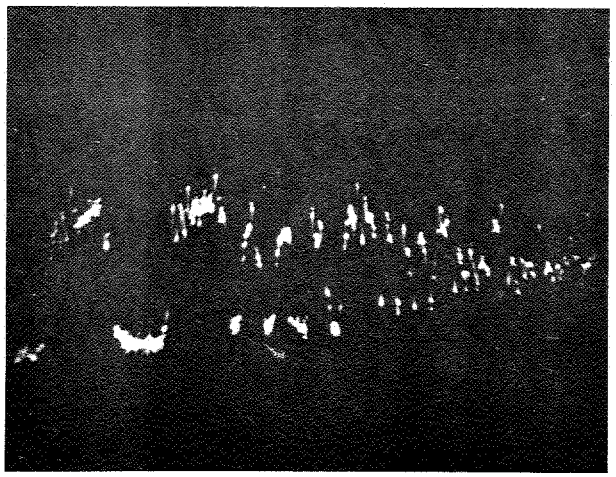

c. Center Resolution

93% at 30 lines
70% at 100 lines
46% at 200 lines
23% at 300 lines
8% at 400 lines

6693D-PF-1

CONFIDENTIAL

CONFIDENTIAL

3. LIST OF TESTS PERFORMED ON LCT TUBE NO. 432

Test	Paragraph	Description	Performed by
Argon Hold	3.4.4	168 hr. in 4 PSI Argon	D. Morehart
Glass Strain	3.4.5.11	Down shock from 100°C to 0°C	D. Morehart
Vibration I	3.4.5.1	2.5g Non-operating Sine Wave	D. Morehart
Acoustic Noise	3.4.5.5	.0002 dyne/cm^2 acoustic noise	D. Morehart A. Armstrong
Acceleration	3.4.5.6	7g Acceleration	D. Morehart A. Armstrong
Thermal Vacuum	3.4.5.7	-54°C +70°C 10^{-6}	D. Morehart A. Armstrong
Temperature Cycling	3.4.5.9	-54°C to 25°C to 70°C to 25°C	D. Morehart
Humidity	3.4.5.13	95%+ Humidity (See Eng. Memo #88 (Fig.2)	

CONFIDENTIAL

4. POST HUMIDITY

Unable to remove yoke.

See Appendix I

5. POST THERMAL CYCLING

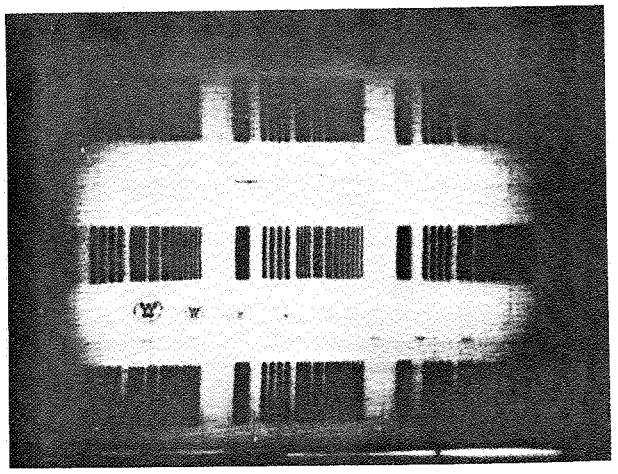

a. Monitor

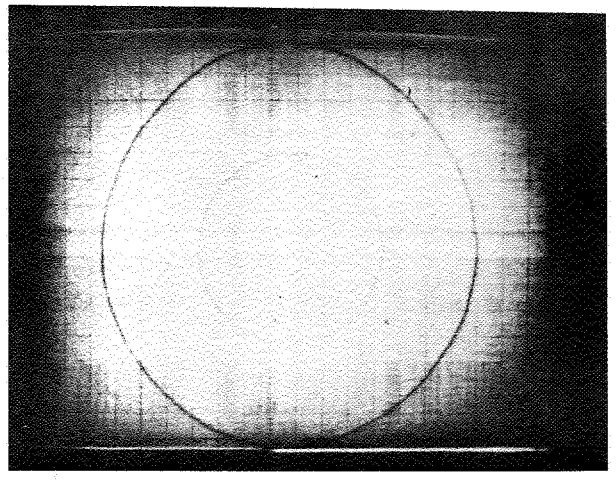

b. Spurious Signal

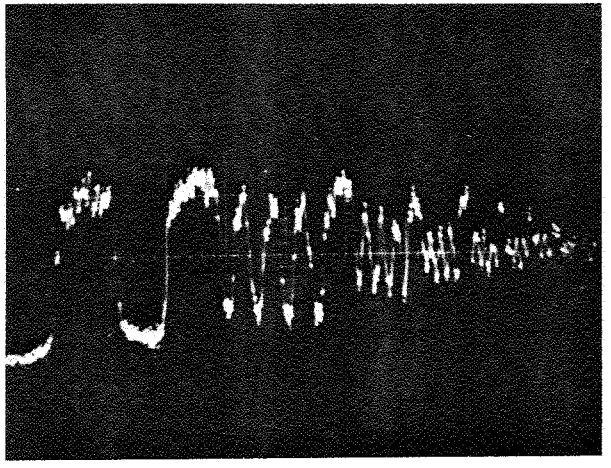

c. Center Resolution

88% at 30 l
65% at 100 l
37% at 200 l
21% at 300 l
7.5% at 400 l
4.5% at 500 l
2% at 600 l

6693D-PF-2

RESULTS FROM LCT NO. 411

(Elmira LCT Test Set Model E 154A)

1. Electrical Set Up Parameters For Photographs.

2. Electrical Tests Before Qualification Program (Photographs)

    a. Monitor
    b. Spurious Signal
    c. Center Resolution

3. List of Tests Performed on LCT Tube No. 411.

4. Post Humidity.

    a. Monitor
    b. Spurious Signal
    c. Center Resolution

1. TUBE #411

SET UP PARAMETERS FOR PHOTOGRAPHS

Eg_1 = -14 volts

Eg_{co} = -53 volts

Eg_2 = 300 volts

$Eg_{3,6}$ = 600 volts

Eg_4 = 98.5 volts

Eg_5 = 300 volts

Eg_7 = 25 volts

Esj = 25 volts

Epc = -8 KV

E_H = 1.5 volts

I_H = 144 ma.

I_{HAL} = 0 ma.

I_{VAL} = +8 ma.

Isj = 1×10^{-8} amp. at 1×10^{-3} ft-c. (10 f/s)

2. ELECTRICAL TESTS BEFORE QUALIFICATION PROGRAM

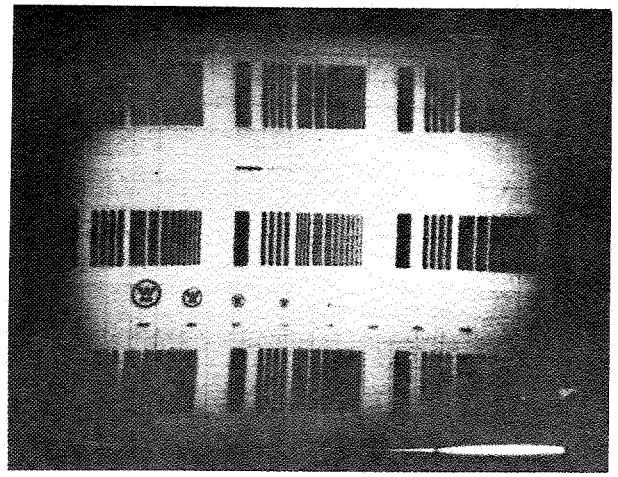

a. Monitor

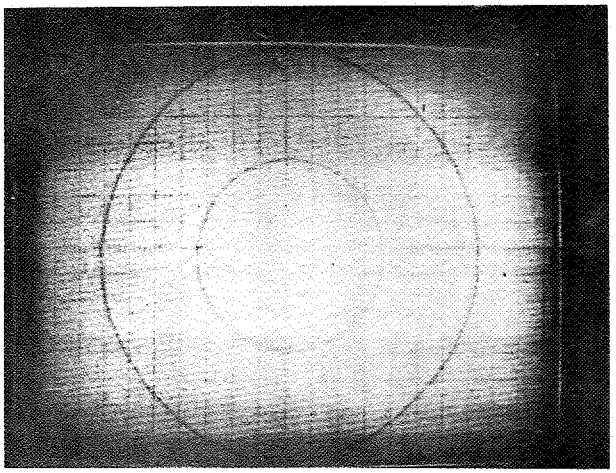

b. Spurious Signal

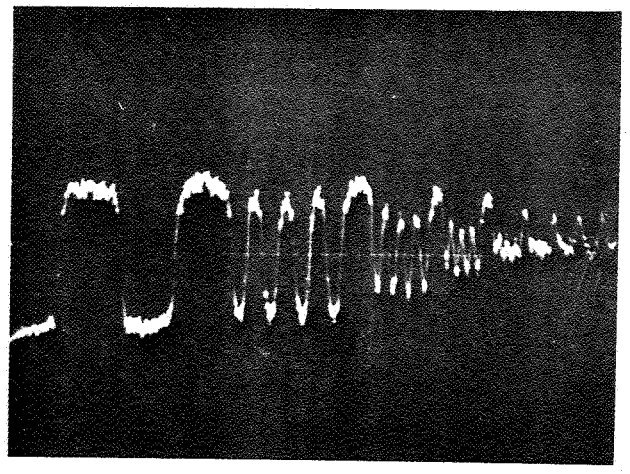

96% at 30 l
74% at 100 l
44% at 200 l
21% at 300 l
6% at 400 l

c. Center Resolution

6693D-PF-3

3. LIST OF TESTS PERFORMED ON LCT TUBE NO. 411

Test	Paragraph	Description	Performed by
Argon Hold	3.4.4	168 hrs. in 4 PSI Argon	D. Morehart
Glass Strain	3.4.5.11	Thermal Down Shock 100°C to 0°C	D. Morehart
Vibration I	3.4.5.1	2.5g Non-operating Sine Wave	D. Morehart
Vibration II	3.4.5.2	$.25g^2$/CPS Non-operating Random	D. Morehart A. Armstrong
Vibration III	3.4.5.3	$.02g^2$/CPS Non-operating Random	D. Morehart A. Armstrong
Mechanical Shock	3.4.5.4	18 - 30g Shocks	R. Fleming
Temperature Storage	3.4.5.10	15 days at -30°C and +60°C	D. Morehart
Humidity	3.4.5.13	Operating 95%+ Humidity See Eng. Memo #88 (Fig.2)	D. Morehart

4. POST HUMIDITY

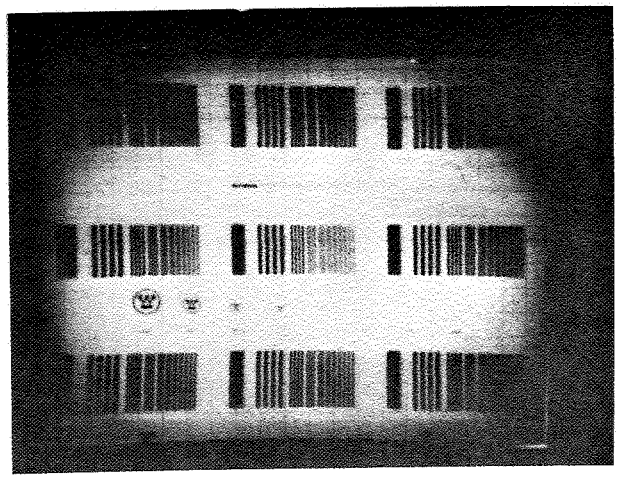

a. Monitor

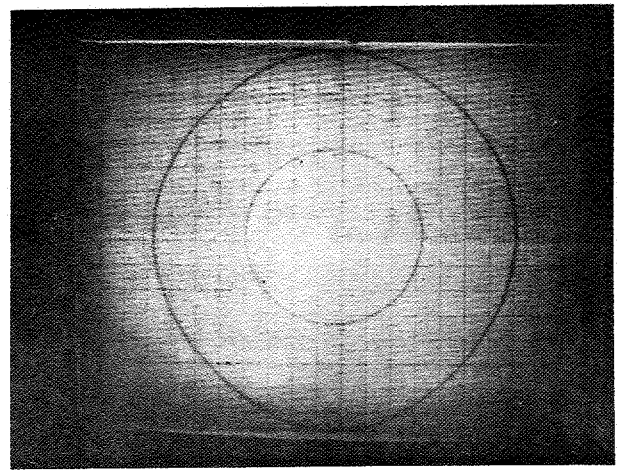

b. Spurious Signal

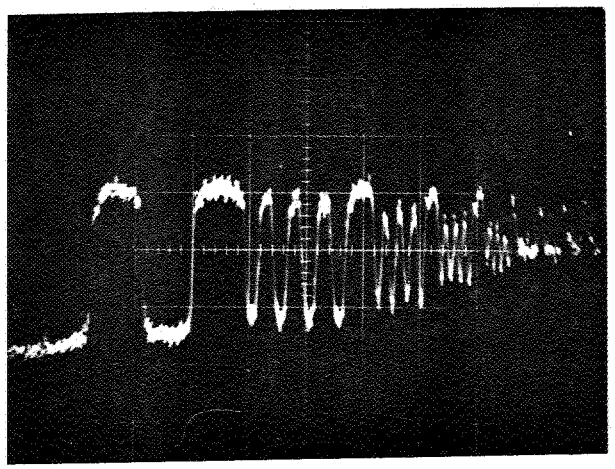

c. Center Resolution

96% at 30 lines
80% at 100 lines
49% at 200 lines
25% at 300 lines
9.5% at 400 lines
3% at 500 lines

6693D-PF-4

VIBRATION I (3.4.5.1)

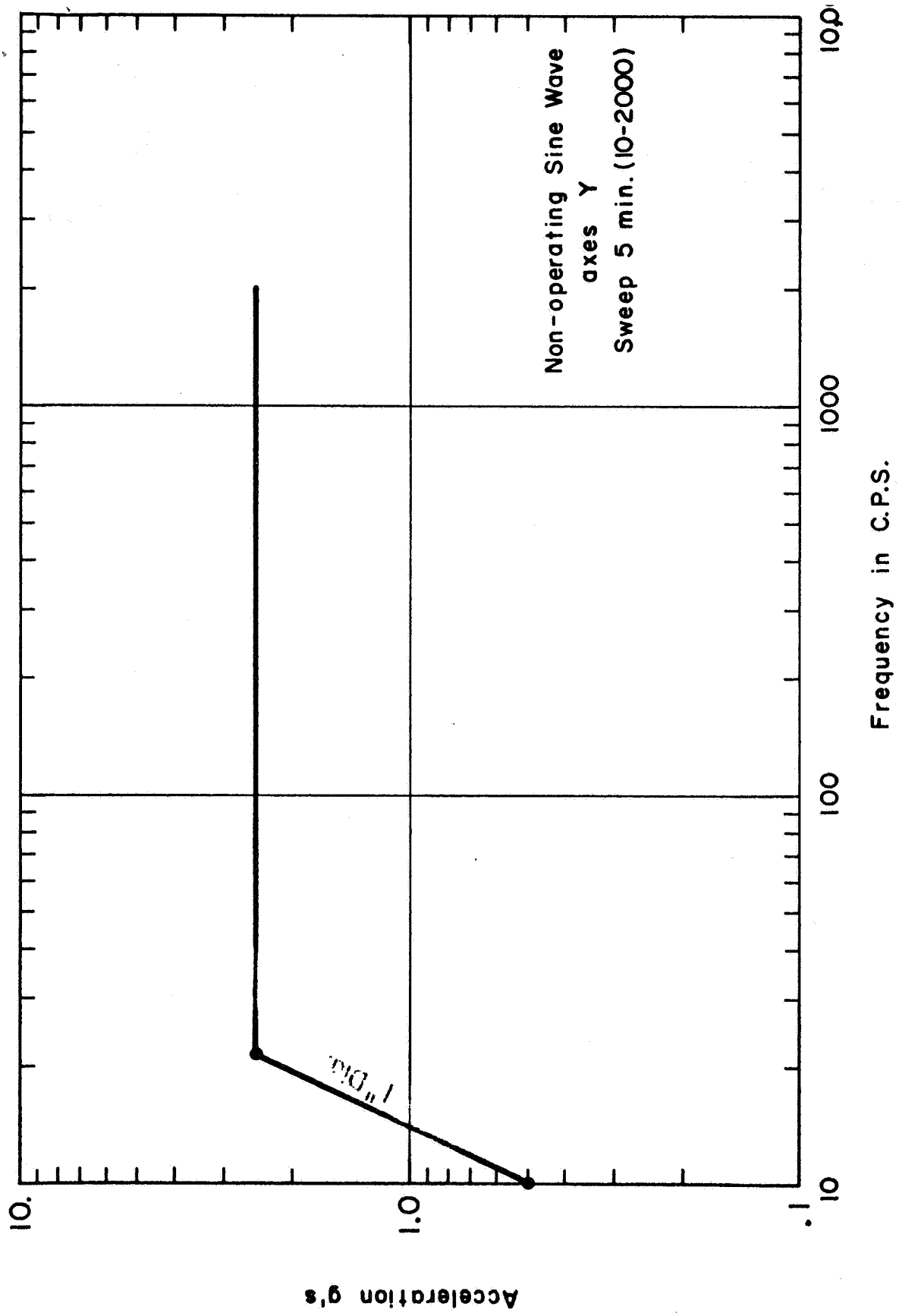
Non-operating Sine Wave
axes Y
Sweep 5 min. (10-2000)
1" Dia.
10
100
1000
10.0
Frequency in C.P.S.
10.
1.0
.1
Acceleration g's

Vibration I

Vibration I

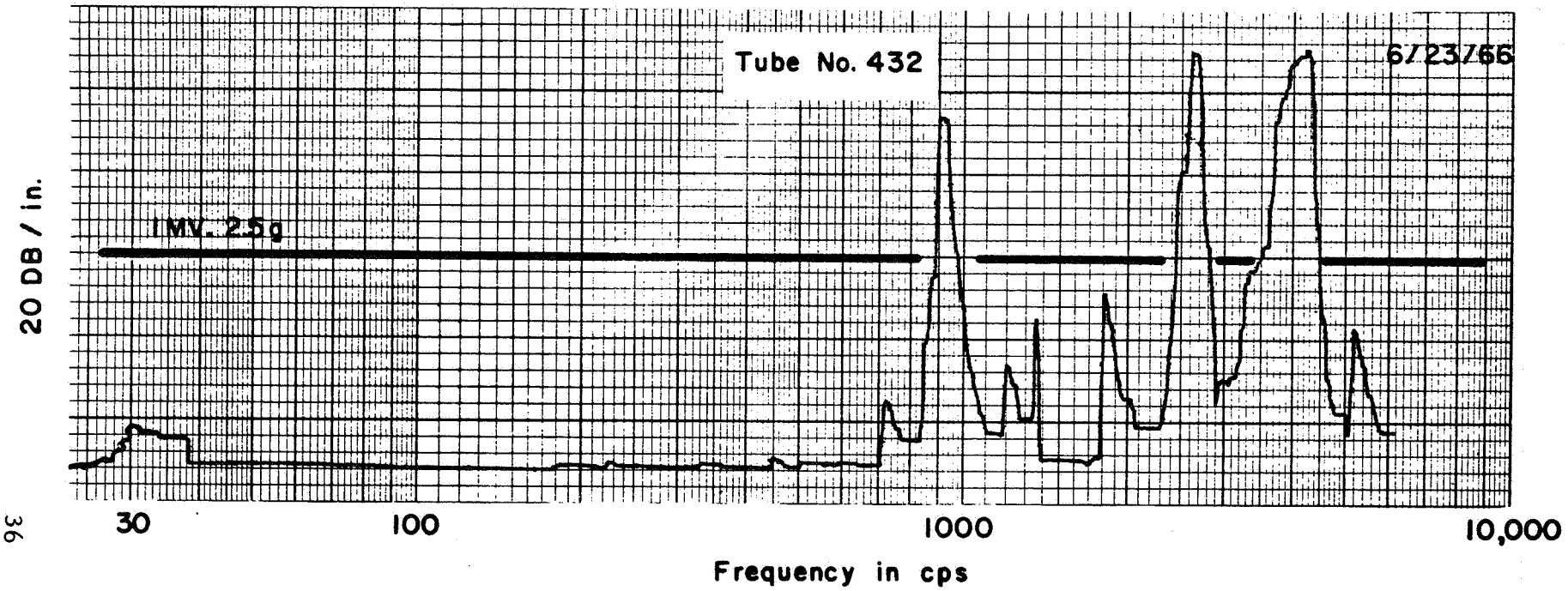

Frequency vs Relative Amplitude of Target-Mesh Resonances

Set-Up:

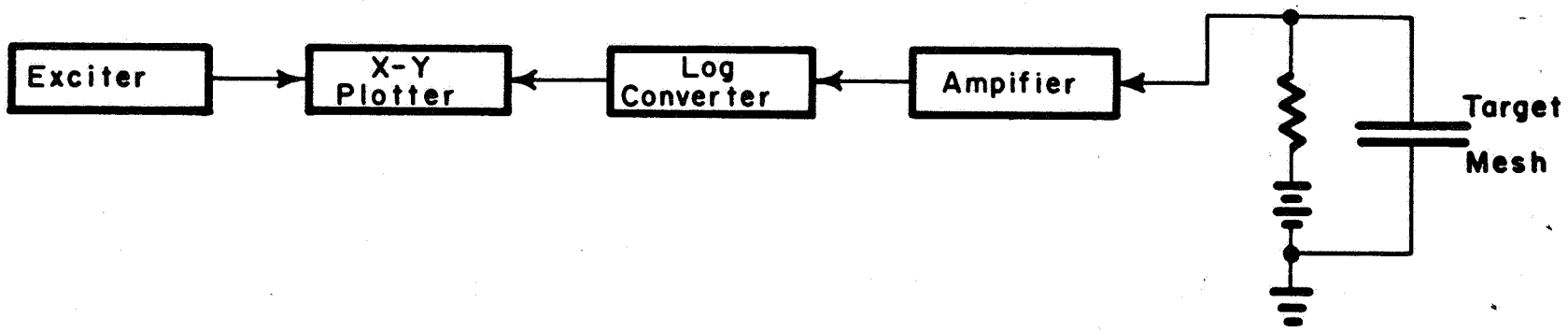

Vibration I

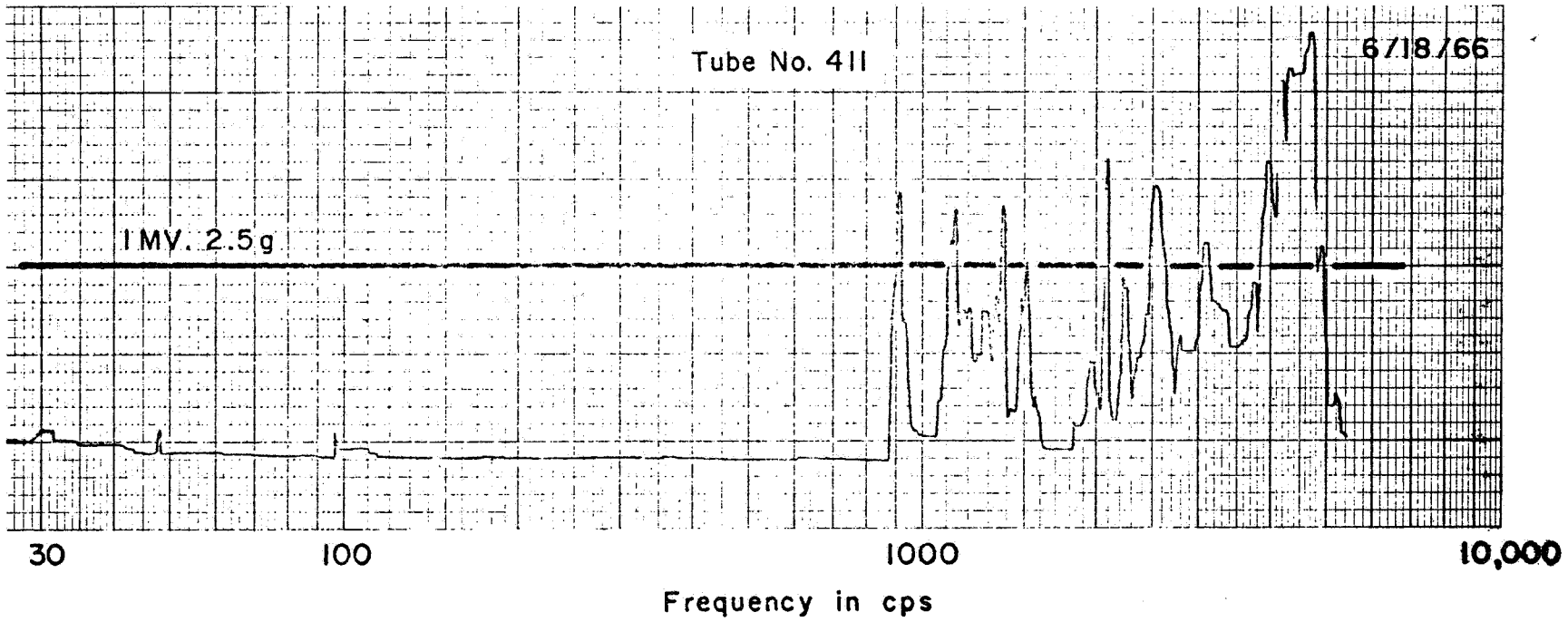

Frequency vs Relative Amplitude of Target-Mesh Resonances

Set-Up:

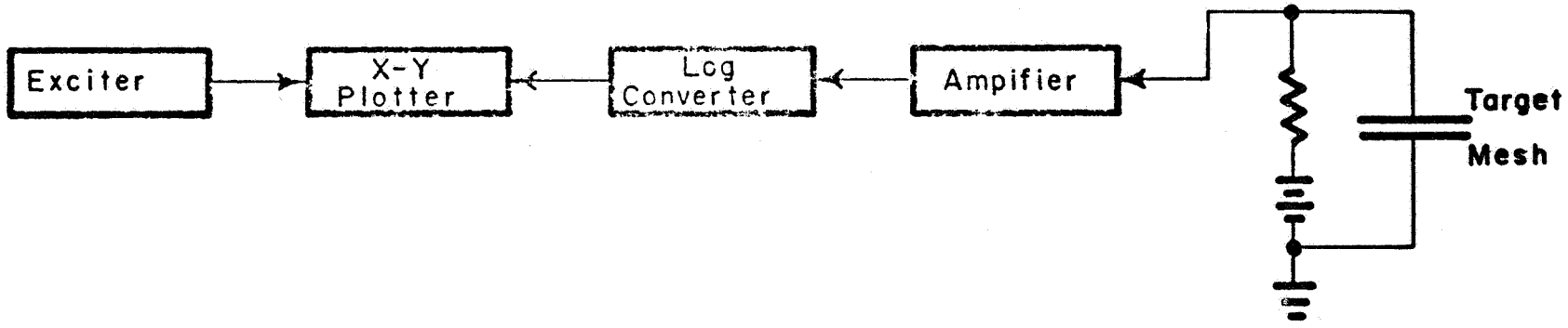

VIBRATION II (3.4.5.2)

(plot of Z axis and excerpt of notes)

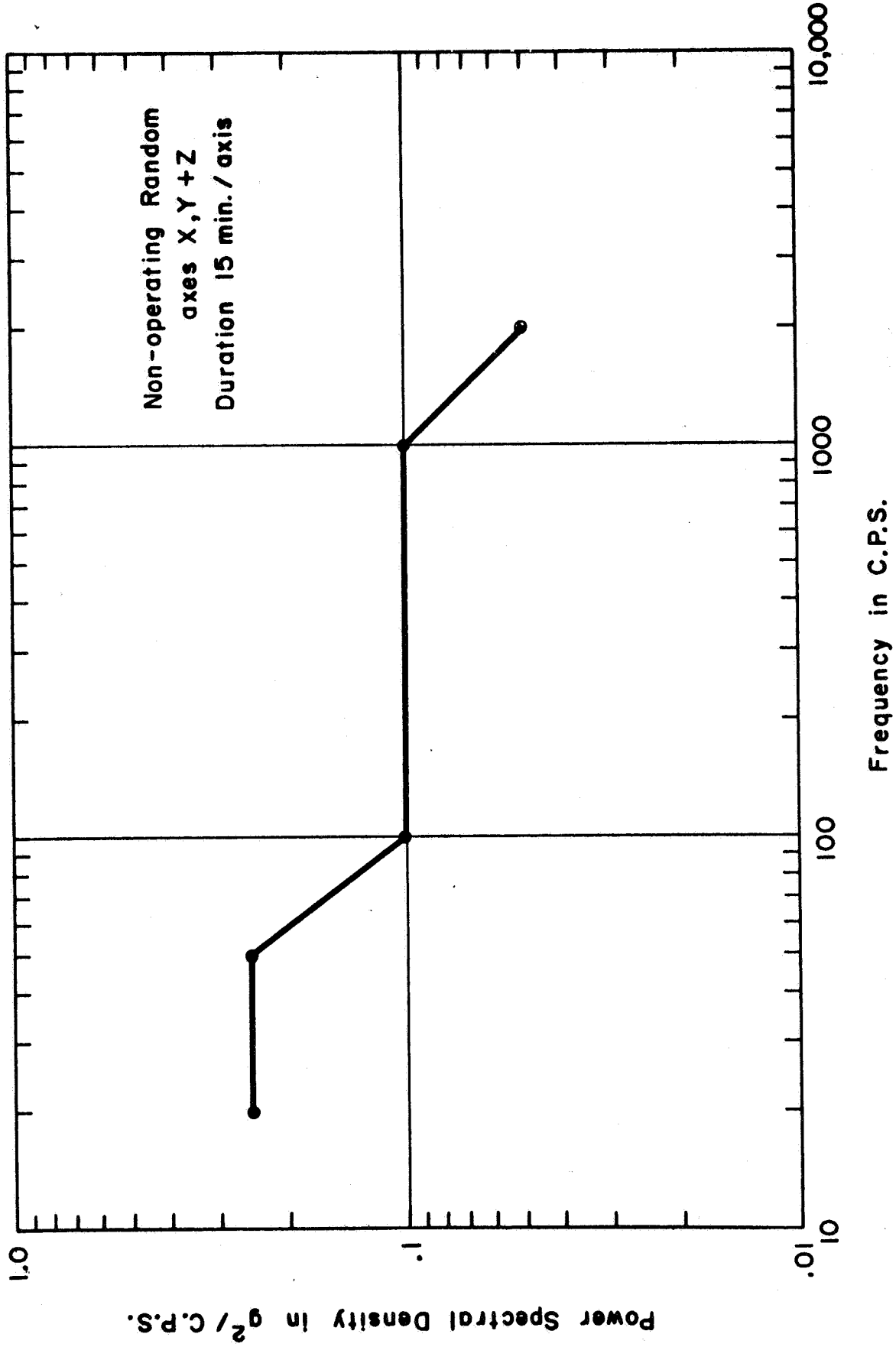

Vibration II

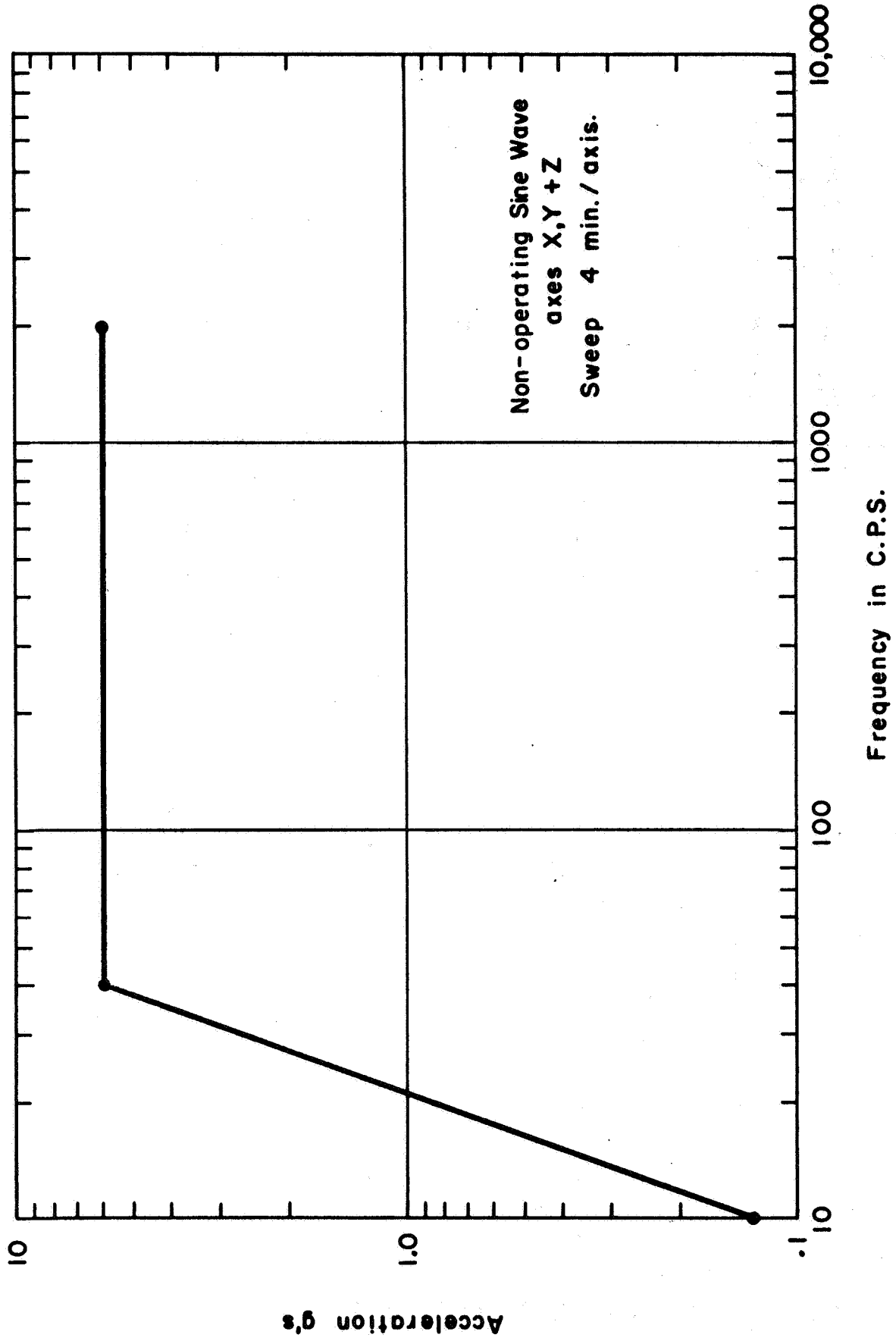

Vibration II

VIBRATION III (3.4.5.3)

(plot of Z axis and excerpt of notes)

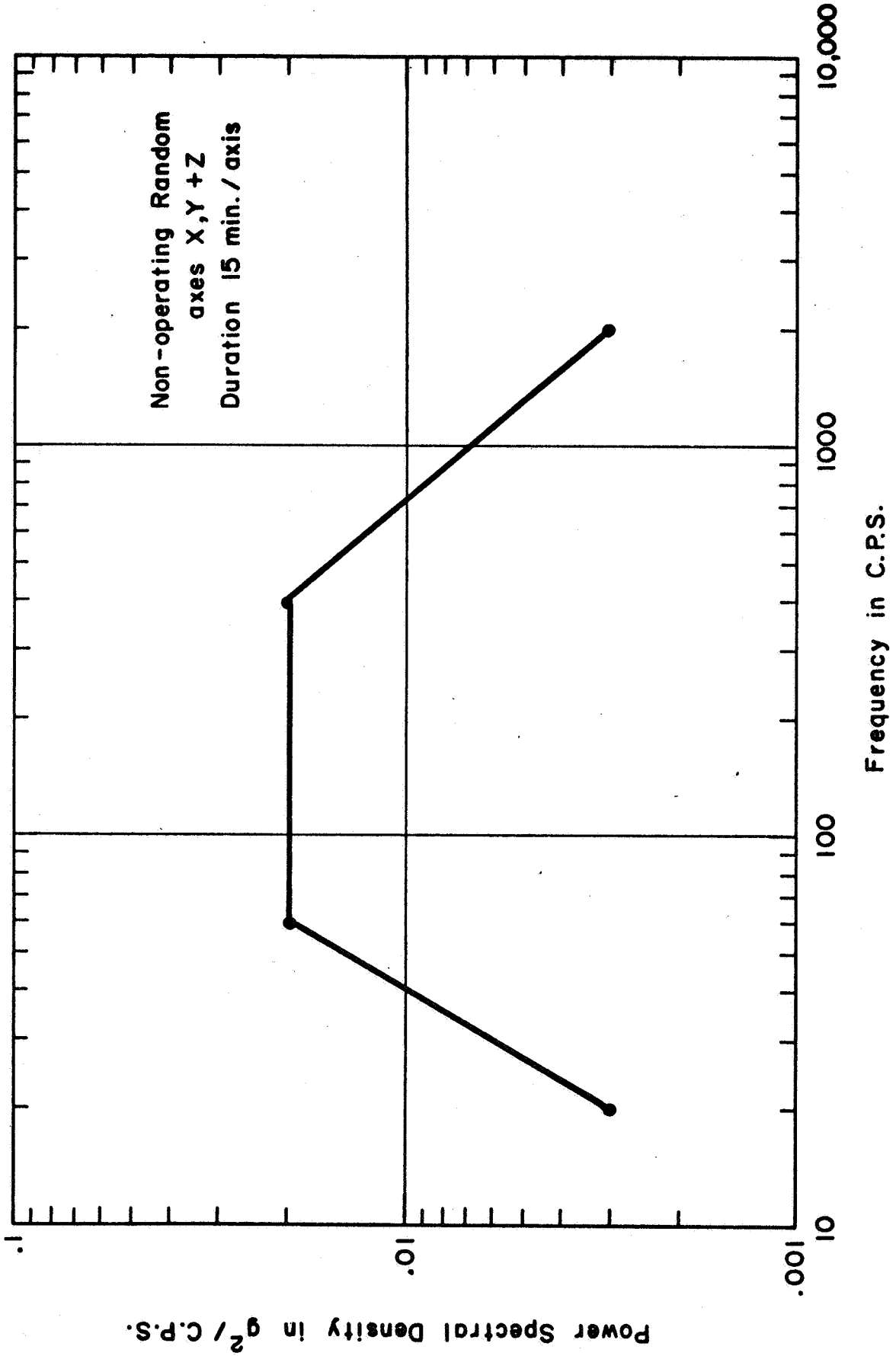

Vibration III

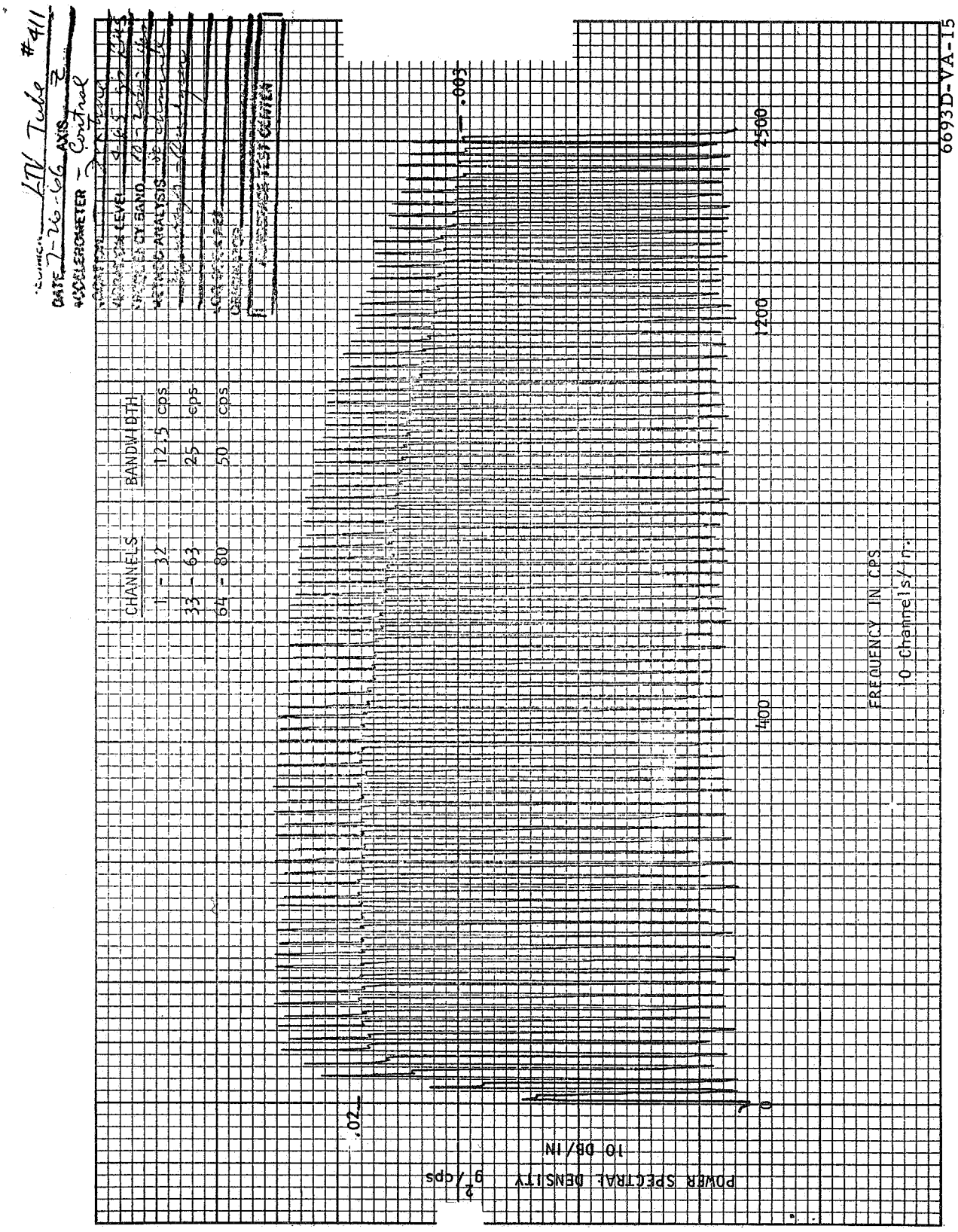
CHANNELS
BANDWIDTH
1 - 32
12.5 cps
33 - 63
25 cps
64 - 80
50 cps
.07
.003
0
400
1200
2500
POWER SPECTRAL DENSITY
10 DB/IN
FREQUENCY IN CPS
10 Channels/in.
6693D-VA-15

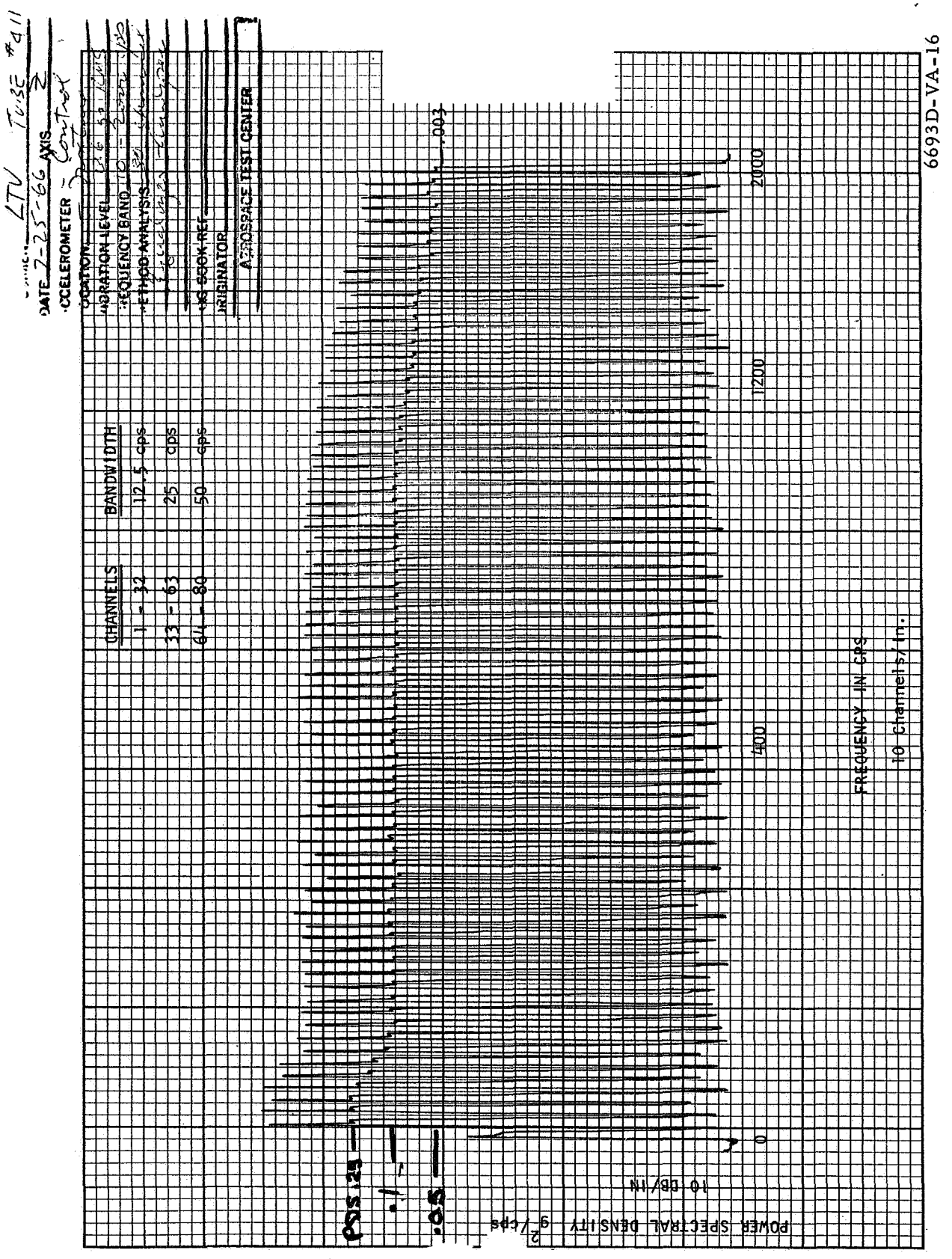
LTV TUBE #411
DATE 7-25-66 AXIS Z
ACCELEROMETER
LOCATION
VIBRATION LEVEL
FREQUENCY BAND
METHOD ANALYSIS
LOG BOOK REF
ORIGINATOR
AEROSPACE TEST CENTER
CHANNELS
BANDWIDTH
1 - 32
12.5 cps
33 - 63
25 cps
64 - 80
50 cps
.003
2000
1200
400
0
FREQUENCY IN CPS
10 Channels/In.
10 DB/IN
POWER SPECTRAL DENSITY g²/cps
PDS .25
.1
.05
6693D-VA-16

TEST RECORD
WESTINGHOUSE FORM [illegible]

THE SPACE ABOVE THIS LINE IS FOR FILING AND MUST NOT BE WRITTEN ON

K 2104839

SUBJECT Random and Sine Vibration of LTV Tube #411

CUSTOMER Elmira Tube Div. of Westinghouse SERIAL NO.

S. O. OR TEST NO. D. OR L. SPEC. NO. SHAFT NO. FRAME NO.

TO DETERMINE

7-25-66

Installed tube in yoke and front flange fixture supplied by Elmira #LCT-D31034-T23
Installed tube for X axis vibration (target pin is up and vibration is in horizontal minor direction. Will vibrate to spec level listed on p 2104838. Tube wrapped with layer of masking tape

2025	Started	Random	X axis	Filament 3 ohms
2043	Ended	"	"	
2046	Started	Sine	"	Filament 3 ohms
2050	Ended	"	"	
2105	Started	Random	Y axis	Filament 3 ohms
2120	Ended	"	"	
2124	Started	Sine	"	Filament 3 ohms
2128	Ended	Sine	"	
2134	Started	Random	Z axis	Filament 3 ohms
2149	Ended	"	"	
2152	Started	Sine	"	Filament 3 ohms
2156	Ended	"	"	
				Filament 3 ohms

No physical damage observable on tube.

2104838 PREVIOUS TEST PAGE 7-25-66 DATE A. Armstrong SIGNED ENGINEER IN CHARGE

TEST RECORD
WESTINGHOUSE FORM 2509 C BODY

THE SPACE ABOVE THIS LINE IS FOR FILING AND MUST NOT BE WRITTEN ON

K [illegible]

SUBJECT: Random Vibration of ATV Tube #411
CUSTOMER: Elmira Tube Div of Westinghouse
SERIAL NO.:
S. O. OR TEST NO.:
D. OR L. SPEC. NO.:
SHAFT NO.:
FRAME NO.:

TO DETERMINE:

7-26-66

Installed Elmira fixture LCT-D 31039-T23 on shaker for vibration in Z axis and performed random vibration equalization.
Installed Tube in fixture for vibration to the following specification.

20-60 cps linear increase from 0.005 g²/cps to 0.02 g²/cps
60-400 cps 0.02 g²/cps constant
400-2000 cps linear decrease from 0.02 g²/cps to 0.005 g²/cps

15 minute duration 4.65 g RMS.

1620	Started Z axis vibration			Target Pin Horizontal Filament 3 ohms
1635	Ended	"	"	Filament 3 ohms
1639	Started Y axis		"	Horizontal Mirror - Target Pin Horizontal
1654	Ended	"	"	Filament 3 ohms
1701	Started X axis		"	Target pin vertical - Horizontal Mirror axis
1716	Ended	"	"	Filament 3 ohms

Visual inspection of tube satisfactory

2104839 — PREVIOUS TEST PAGE
7-26-66 — DATE
R. Armstrong — SIGNED
ENGINEER IN CHARGE

MECHANICAL SHOCK (3.4.5.4)

SHOCK TEST

Tube Type 31034 Date 8-3-66

Tube No. 411

The tube shall be subjected to 30 g, half-sine, and duration of 11 milliseconds. Apply 3 shock (s) in each direction along each lateral axis. Apply 3 shock(s) in each direction along the longitudinal axis. Total of 18 shocks.

The tube shall be visually inspected and electrically tested after shock test.

Remarks:

1. Tube mounted in fixture WX-30152-T19 with wax.
2. Taft-Pierce Shock Test machine used.
   a. Hammer angle = 55°.
   b. Rubber pads (2) - 1/2" Thick each
3. DIAL-A-GAIN and LMD-250 filter used.

Performed by R. Fleming

Engineer " "

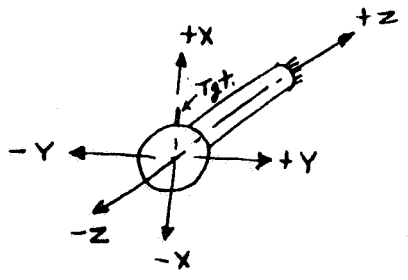

Accelerometer - BF-16 - (8.55 mv/g)

Oscilloscope sensitivity:

Horizontal - 2 ms/cm

Vertical - 5 V/cm

Shock amplitude:

DIAL-A-GAIN OUTPUT = 1 V/g

Filter gain = 0.25

$$g \text{ Amplitude} = \frac{\text{No. of cm } (5\text{V/cm})(1\text{ g/V})}{0.25}$$

TEST RECORD
WESTINGHOUSE FORM 2509E BODY

THE SPACE ABOVE THIS LINE IS FOR FILING AND MUST NOT BE WRITTEN ON

K

SUBJECT Acoustic Noise LTV Tube #432

CUSTOMER Elmira Tube Div. Westinghouse

SERIAL NO.

S. O. OR TEST NO. D. OR L. SPEC. NO. SHAFT NO. FRAME NO.

TO DETERMINE

6-30-66

Installed camera tube in acoustic noise chamber by means of vibration fixture which has yoke and front mount for tube.

Started test @ 1147 and 30 secs.
Stopped " @ 1153

	Required	Microphones #1	#2
Overall db	130 db min	132 db	133 db +1
90-180 cps	129 ± 3 db	~~123~~ 131 db	134 db +1
180-355 cps	124 ± 3 db	~~119~~ 123 db	121 db +1
355-710 cps	125 db min	~~127~~ 119 db	118 db +1
710-1400 cps	115 db min	~~105~~ 121 db	119 db +1
1400-2800 cps	107 db min	105 db	104 db +1
2800-5600 cps	99 db min	133 db	134 db +1
5600-11200 cps	90 db min	93 db	91 db +1

Calibration of #2 microphone against 124 db std source indicates only 123 db. Therefore 1 db should be added to the readings of microphone #2.
High energy on band 2800-5600 cps is an intermittent problem in the noise analyser electronics. Record of pre-test spectrum was very good. Repeated levels were:
131 db, 125 db, 123 db, 119 db, 107 db, 100 db, 93 db and 133 db overall.

2104834 PREVIOUS TEST PAGE 6-30-66 DATE [signature] SIGNED

MECHANICAL SHOCK WAVEFORMS

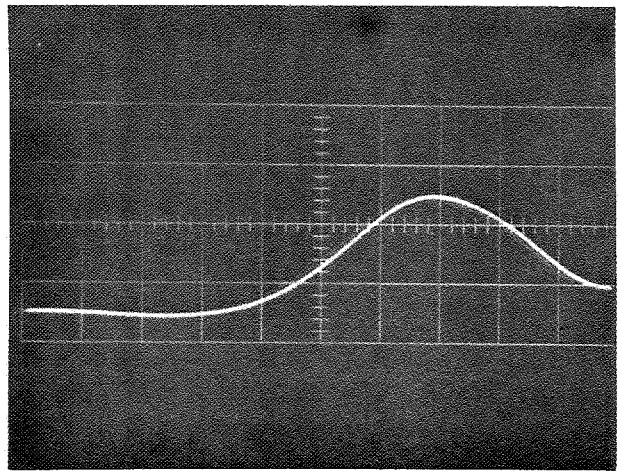

- X Axis

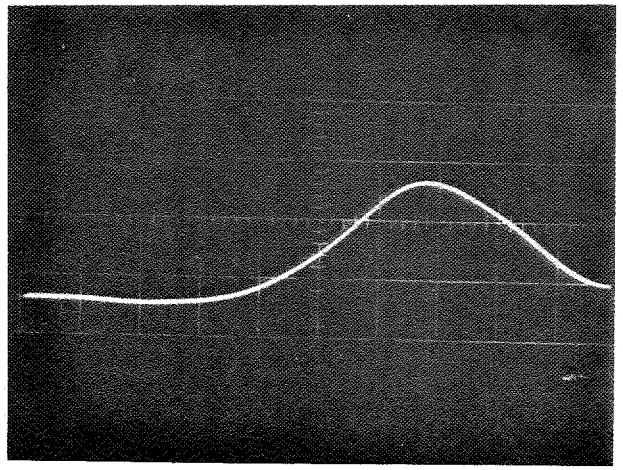

+ Y Axis

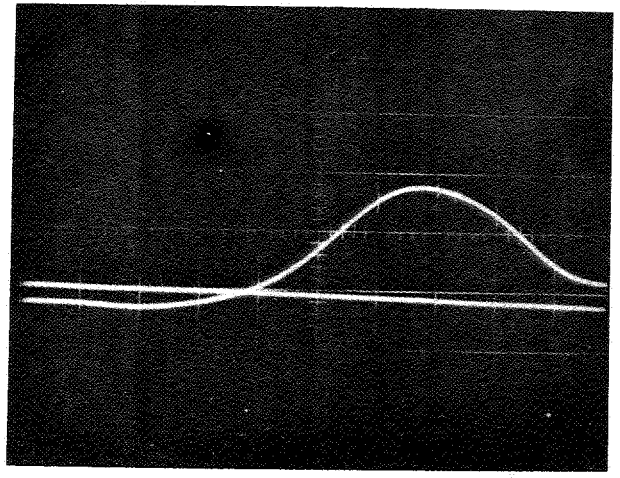

- Z Axis

Sensitivity

Horizontal - 2ms/cm
Vertical - 5 Volts/cm

6693D-PF-5

ACOUSTIC NOISE (3.4.5.5)

Acoustic Noise Plot and Excerpt of Notes

CONFIDENTIAL

Acoustic Noise

Pre-test Recording on Channels Alone

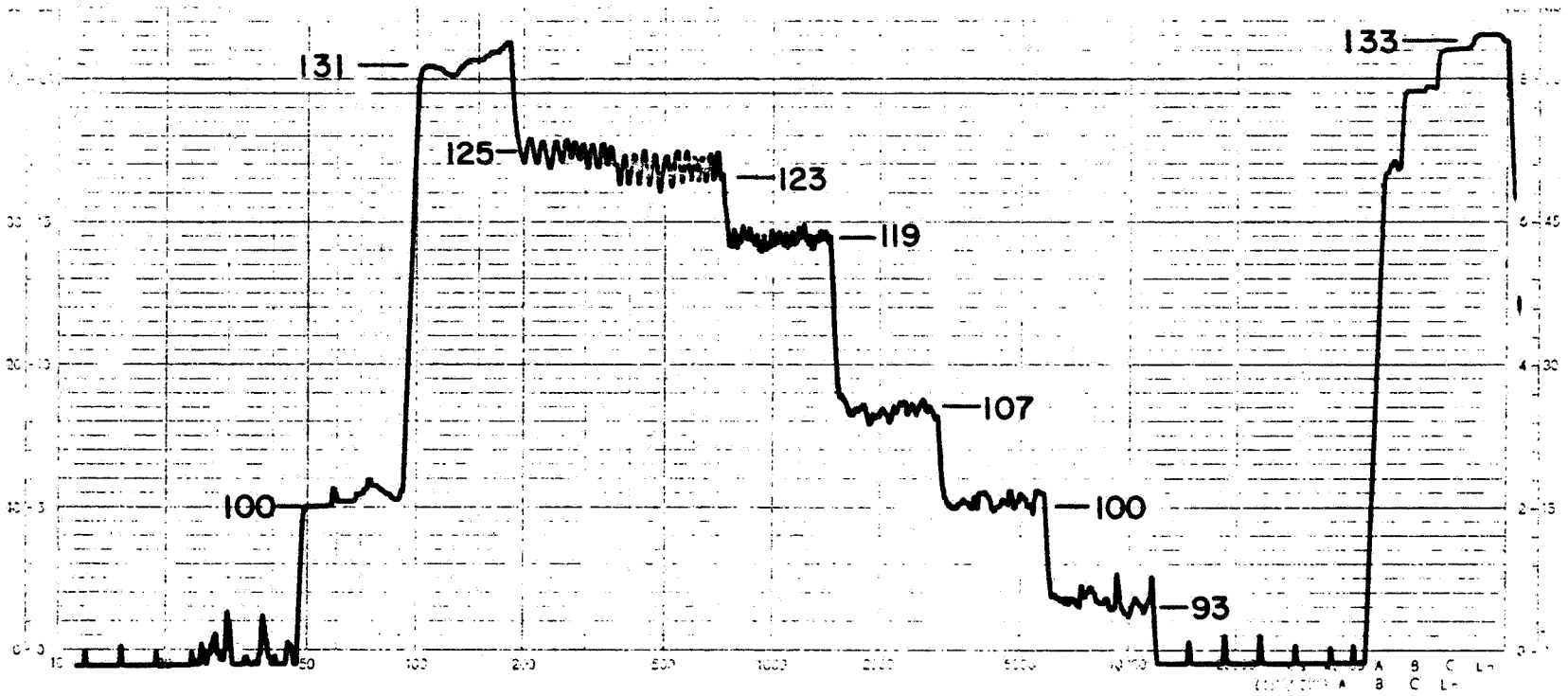

Rotor 1 - 600 rpm
Rotor 2 - 150 rpm
Rotor 3 - 0 rpm

Airflow - 31 Div. from Closed
No. 1 Microphone

Acoustic Noise vs Frequency Curve

CONFIDENTIAL

ACCELERATION (3.4.5.6)

ACCELERATION

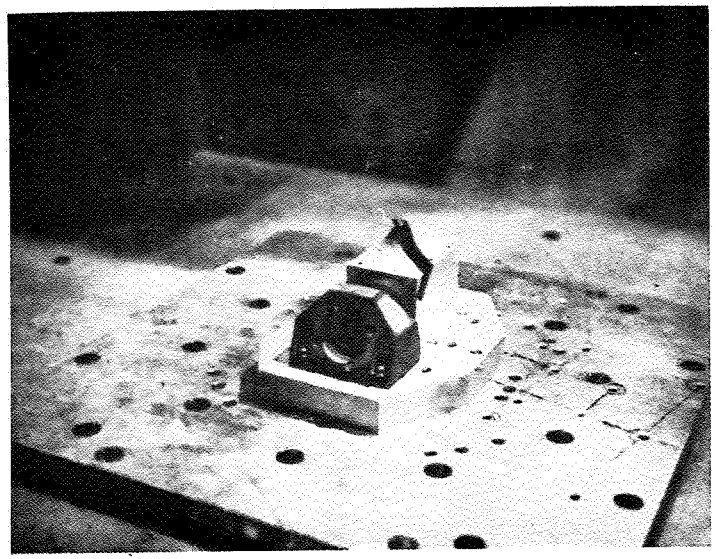

X and Y axis

Z axis

MOUNTING FIXTURE D31034-T23 IN POSITION
ON CENTRIFUGE FOR ACCELERATION TESTS

6693D-PF-6

TEST RECORD
WESTINGHOUSE FORM 2509 E BODY

THE SPACE ABOVE THIS LINE IS FOR FILING AND MUST NOT BE WRITTEN ON

SUBJECT Acceleration Test on LTV Tube #932 K[illegible]

CUSTOMER Elmira Tube Div. of Westinghouse SERIAL NO.

S. O. OR TEST NO. D. OR L. SPEC. NO. SHAFT NO. FRAME NO.

TO DETERMINE

Installed tube in vibration fixture and mounted fixture on arm of centrifuge. Center of fixture at 60 inches from center of rotation. For 7g acceleration RPM is 60.0

		Start	End	
1st direction	Z axis	1355	1400	Tube facing outward
2nd "	"	1413	1418	" " inward

Target Pin facing up - Center continuity checked at both directions

1st direction	X axis	1422	1427	

Target Pin facing up - Center continuity etc

Y axis - Center pin facing outward

Start 1440 end 1445 - Center continuity etc.

Shaevitz Rotary Accelerator Type T-16-A S/N 1

Potter Model 850 Counter

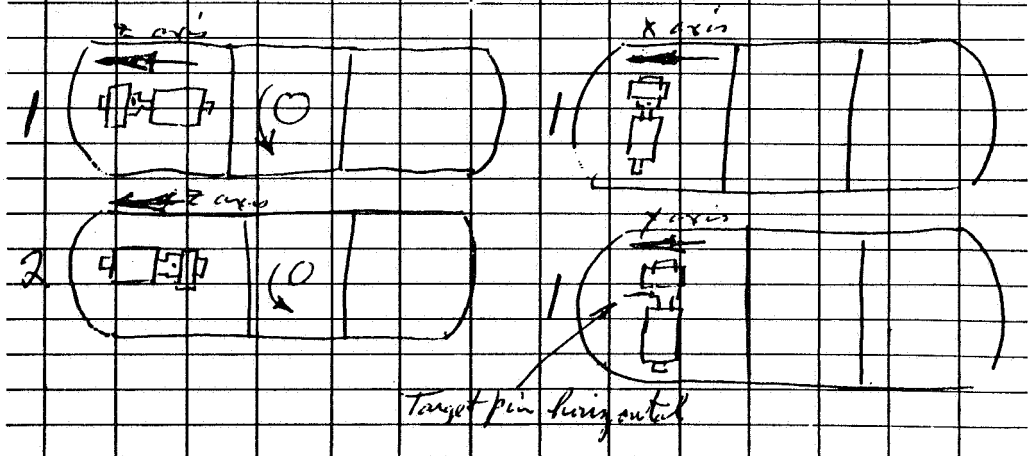

21C4533 PREVIOUS TEST PAGE 6-29-66 DATE C. Armstrong SIGNED ENGINEER IN CHARGE

THERMAL VACUUM (3.4.5.7)

THERMAL VACUUM

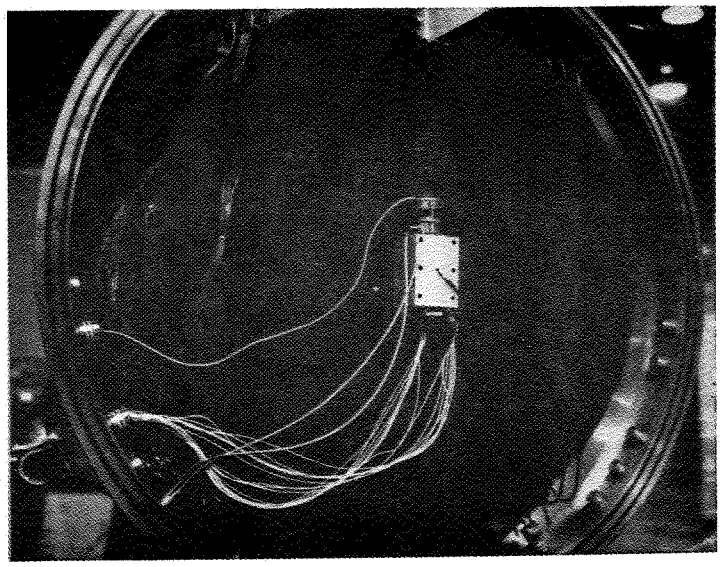

View of Controlled
Temperature Shroud

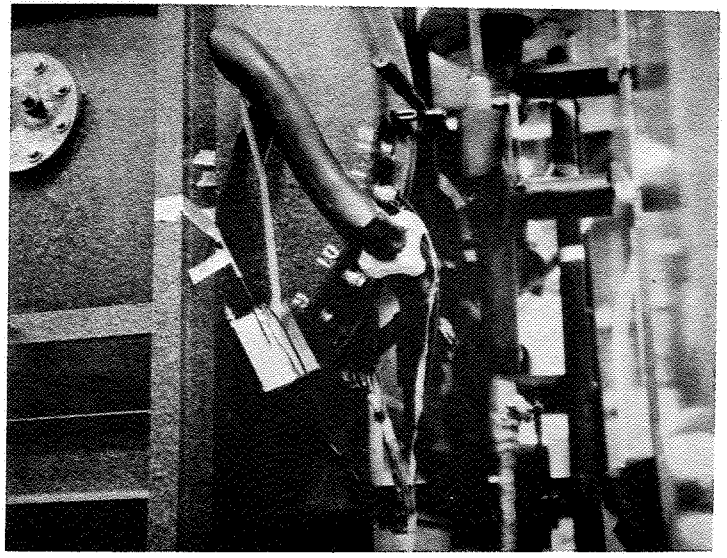

View of Pre-Amp
Location

6693D-PF-7

THERMAL VACUUM -54°C CYCLE

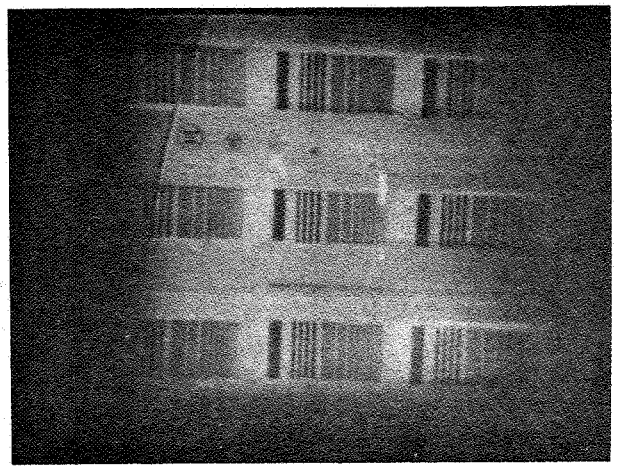

Monitor Display

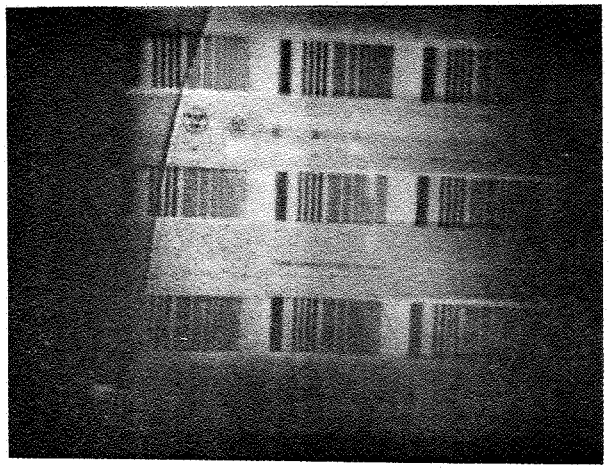

Set up Photos

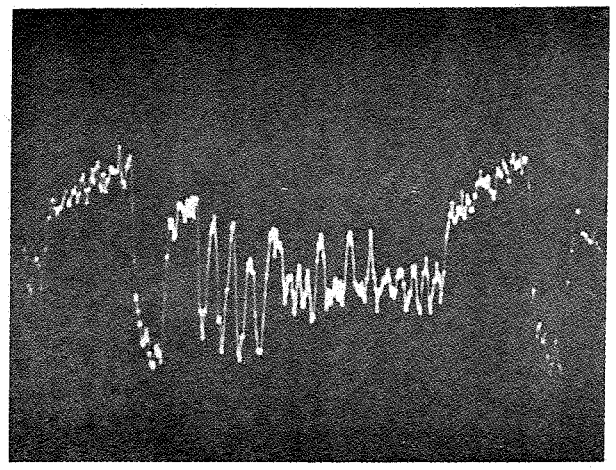

Selected Line

Toward End of Cycle

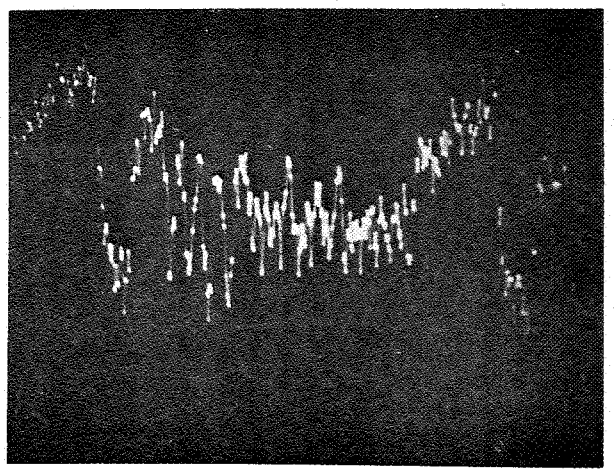

6693D-PF-8

THERMAL VACUUM +70°C CYCLE

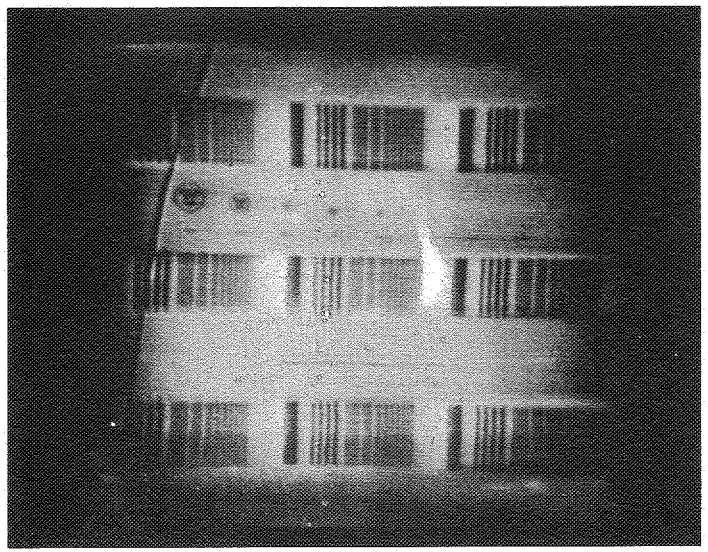

Monitor Display

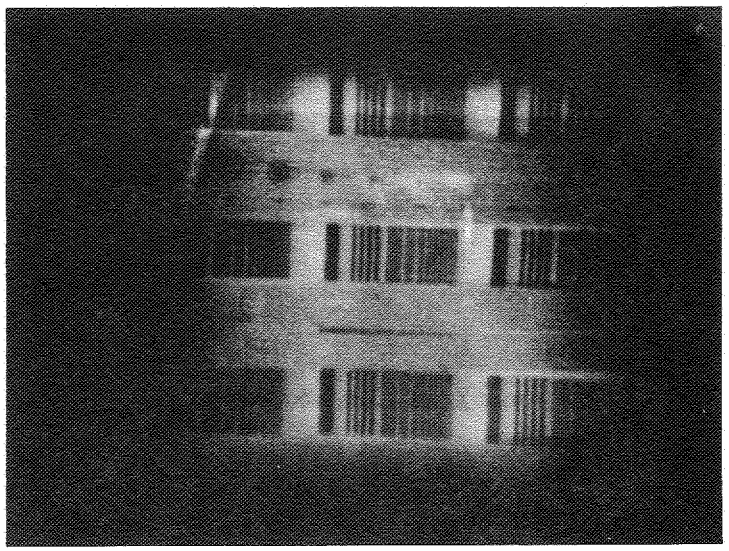

Set Up Photos

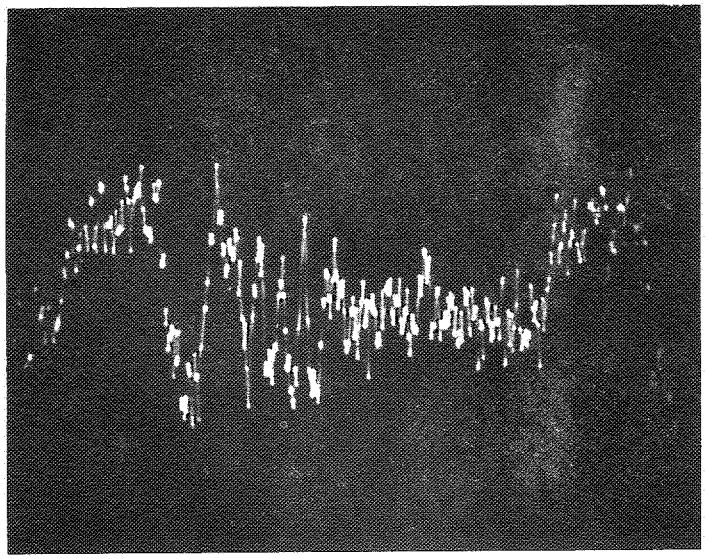

Selected Line

Toward End of Cycle

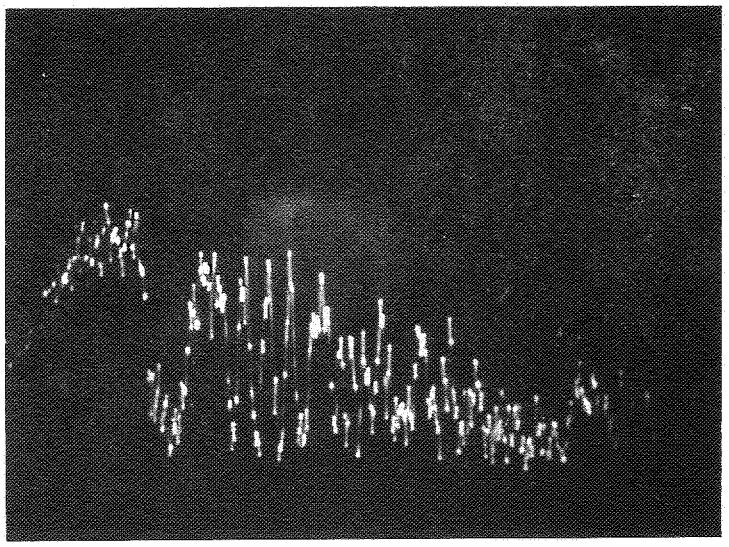

6693D-PF-9

TEST RECORD
WESTINGHOUSE FORM 2500 E 9657

THE SPACE ABOVE THIS LINE IS FOR FILING AND MUST NOT BE WRITTEN ON

SUBJECT Thermal Vacuum Test on LTV Tube #932

CUSTOMER Elmira Tube Division of Westinghouse

SERIAL NO.

S. O. OR TEST NO. D. OR L. SPEC. NO. SHAFT NO. FRAME NO.

TO DETERMINE

7-5-66

Mounted tube yoke to a flat copper plate and installed the plate on the end shroud of the vacuum chamber.

Electrical connections were completed and the tube installed in the yoke fixing upward. The preamplifier was connected just outside the chamber end bell.

Completed preliminary checks of tube and started evacuating chamber at 1710. At 1835 the chamber was at 7.6×10^{-5} mm Hg

7-6-66

0825 Chamber @ 2.9×10^{-6} mm Hg Room Temp conditions still remain in the chamber.

Checks of electrical operation of tube completed and shroud started to cool at 0915

1445 Yoke block reached −65 °F
Bristol Temp Recorder # 15,960 Calibrated 7-6-66
Veeco Ionization Gage + Power Supply # 31463 Cal. 6-23-66

Chamber at 4.9×10^{-7} mm Hg.

PREVIOUS TEST PAGE DATE 7-6-66 SIGNED Armstrong Jr.

TEST RECORD
WESTINGHOUSE FORM 2800 C 8007

THE SPACE ABOVE THIS LINE IS FOR FILING AND MUST NOT BE WRITTEN ON

K2104837

SUBJECT: THERMAL VACUUM TEST ON LTV TUBE #432

CUSTOMER: ELMIRA TUBE DIVISION OF WESTINGHOUSE — SERIAL NO.

S. O. OR TEST NO. — D. OR L. SPEC. NO. — SHAFT NO. — FRAME NO.

TO DETERMINE

7-7-66

0820 Tube continuing to operate with chamber at 3.7×10^{-7} mm Hg and yoke at $-65°F$.

1300 Electrical check of tube conducted by Elmira Representative H. Moreheart.

1545 Tube continuing to operate. Noted resolution chart pattern on monitor scope.
Chamber at 2.6×10^{-7} mm Hg. Yoke at $-65°F$

End of 25 hour cold temperature test

1550 Starting to warm chamber shroud.

1625 Chamber @ 9.0×10^{-7} mm Hg. Shroud @ $+75°F$
Yoke @ $-20°F$
Turned off the main power to the test set.

7-26-66
Completed troubleshooting of test set and corrected problems caused by corona on tube in chamber at about 300 μ.
Started pumping chamber at 1715. Yoke block temperature at 95°F will warm the shroud overnight.
7-27-66 0815 Yoke block @ 140°F Chamber @ 6.3×10^{-6}
In raising shroud temperature to stabilize yoke at 165°F the pressure in chamber went on the 10^{-5} side
7-28-66 @ 1300 test completed Pressure @ 1.1×10^{-6}

2104836 — PREVIOUS TEST PAGE
7-7-66 — DATE
A. Armstrong — SIGNED — ENGINEER IN CHARGE

HUMIDITY (3.4.5.13)

CONFIDENTIAL

HUMIDITY

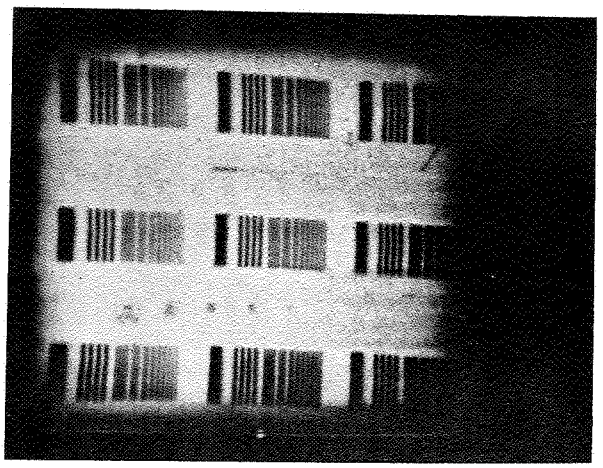

Monitor Display

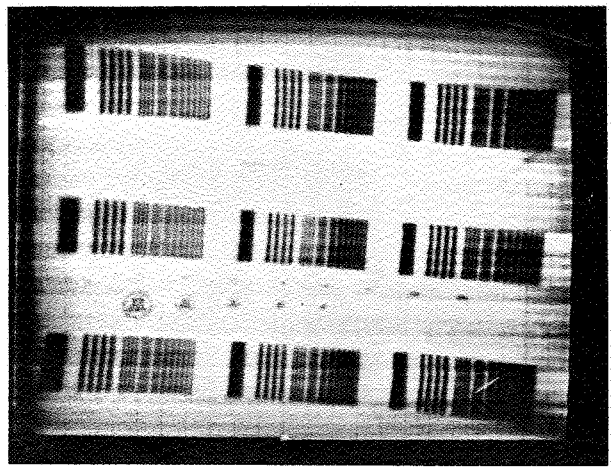

Set Up Photos

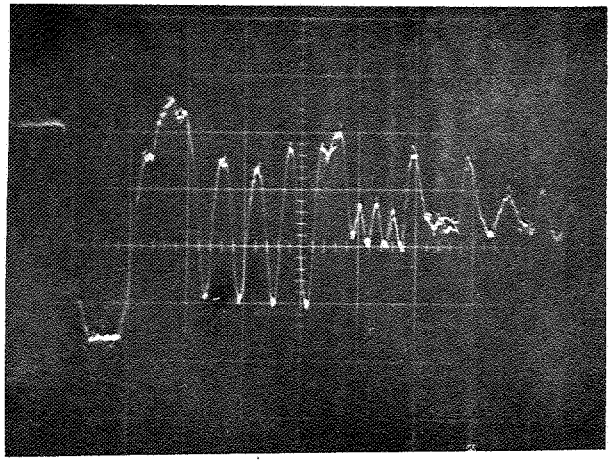

Selected Line

Photos at End of 10 Days

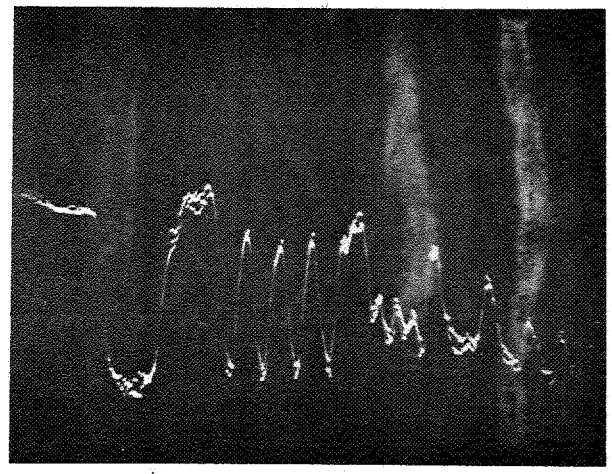

6693D-PF-10

CONFIDENTIAL

LEAD BEND (3.4.5.12)

LEAD BEND

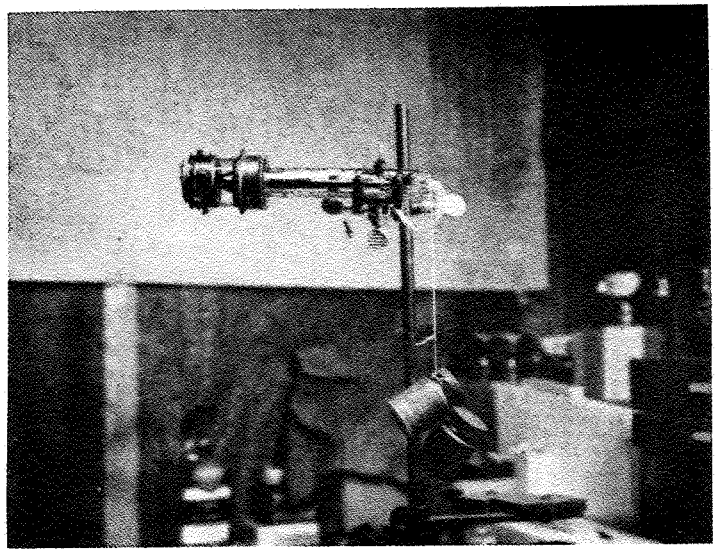

Photo of 32 oz. Weight

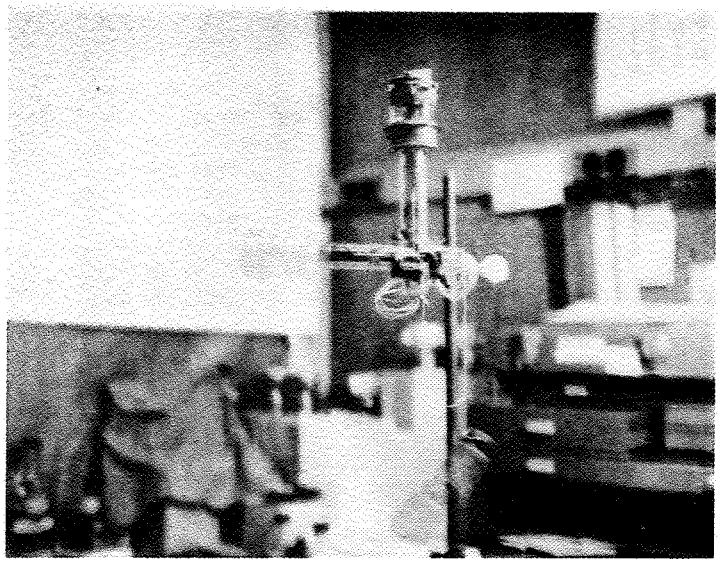

Photo showing 16 oz.
Weight and 90 arc

6693D-PF-11

CONFIDENTIAL

TEST EQUIPMENT USED

Test	Paragraph	Tube	Description	Mfg.	Model	Freq. Cal.
Electrical Tests	3.4.3.1 to 3.4.3.27	411 & 432	LCT Test Set	Westinghouse	E-154A	6 mo.
			Oscilloscope	Tektronix	RM 561A	6 mo.
			Ditital Voltmeter	Non-Linear Systems	4300	6 mo.
			Current Meter	Medistor	A-60C	6 mo.
Holding Period	3.4.4	411 & 432	Pressure Tank	Devilbiss	M 5744	-----
			Pressure Regulator	A.I.R.C.O.	9407	6 mo.
Vibration I	3.4.5.1	411 & 432	Exciter	MB Mfg. Co.	N570-71	6 mo.
			Amplifier	MB Mfg. Co.	T51MCG	6 mo.
			Vibrator	MB Mfg. Co.	C10	6 mo.
			Accelerometer	Endevco	2221C	6 mo.
			Accel. Amplifier	Dial-A-Gain	601	6 mo.
Vibration II	3.4.5.2	411	Exciter Analyzer System	MB Mfg. Co.	MBT-389	1 mo.
Vibration III	3.4.5.3		Vibrator	Caladyne	177	1 mo.
			Accelerometer	Endevco	2242	1 mo.
			Accel. Amplifier	Dyna-Monitor	2705	1 mo.
Shock	3.4.5.4	411	Shock Test Mach.	Taft-Pierce	E7855-A	-----
			Accelerometer	Endevco	2221C	6 mo.
			Filter	United Trans. Co.	LMD-250	6 mo.
			Oscilloscope	Tektronix	541	6 mo.
Acoustic Noise	3.4.5.5	432	Acoustic Noise Chamber	Noise Unlimited	---	1 mo.
			Level Recorder	Bruel & Kjaer	2305	1 mo.
Acceleration	3.4.5.6	432	Rotary Accelerator	Schaevitz	T 16-A	1 mo.
			Recorder & Counter	Potter Instruments	850F	1 mo.
Thermal Vacuum	3.4.5.7	432	Thermal Vacuum Chamber	Bethlehem Corp.	---	1 mo.
			Vacuum Gauge System	Veeco	RG-3A	3 mo.
			Temperature Recorder	Bristol	24P12 6570	3 mo.

CONFIDENTIAL

TEST EQUIPMENT (CONT'D.)

Test	Paragraph	Tube	Description	Mfg.	Model	Freq. Cal.
Temperature Cycling	3.4.5.9	432	Hot & Cold Chamber	Tenny Envir. Test Equip.	TMUF 1.5-100240	6 mo.
			-20°C to +120°C Thermometer	MB Co.	39686	6 mo.
			-100°C to +50°C Thermometer	Fisher Scientific Co.	15-035	6 mo.
Temperature Storage	3.4.5.10	411	Hot & Cold Chamber	Tenny Envir. Test Equip.	TMUF 1.5-100240	6 mo.
			-20°C to +120°C Thermometer	MB Co.	39686	6 mo.
			-100°C to +20°C Thermometer	Fisher Scientific Co.	15-035	6 mo.
Glass Strain	3.4.5.11	411 & 432	-20°C to +120°C Thermometer	MB Co.	39686	6 mo.
Humidity	3.4.5.13	411 & 432	Humidity Chamber	Environmental Equip. Co.		6 mo.
			Program Controller	Bristol	251A 500-G1	6 mo.

CONFIDENTIAL

CONFIDENTIAL

6.2 Target Breakdown Voltage

An experiment was conducted to determine the voltage that was required to cause a complete breakdown of the high capacity targets. A tube was set up at its normal operating point* with a faceplate illumination just below the maximum operating point. Without changing the beam, the suppressor voltage was increased to specific values, an observation made, and the beam turned off. The beam was then turned on again and another observation made. The following chart is a summary of observations.

EG7	Observation before beam turned off	Observation after beam turned on again
(A) 70	Target started to charge in from edge	Crossed over completely-after discharge, cross-over pattern remained
(B) 85	Charged in from edges Bright in center after 15-20 sec.	Crossed over completely-after discharge cross-over pattern remained
(C) 105	Extensive edge charging bright central area	Crossed over completely No pattern after discharge Target appeared grainy
(D) Repeat (A) (B)	Same as initial run	Crossed over completely NO crossover pattern after discharge
(E) 120	Extensive edge charging Bright central area	Crossed over completely No return after discharging
(F) 130	Same as (E)	Same as (E)
(G) 140	Breakdown	Not performed

* Faceplate illumination 9.5×10^{-3} ft-cdl
  Esj = 30V, EG7 = 28V

6.3 Shelf Life Considerations

Due to the nature of the Lunar TV Program, shelf life on the order of 3 years or more can be anticipated. Direct data for non-operating storage of Lunar tubes is not available, since the first tube having essentially the final design (.2 watt cathode) was not made until April, 1965 and the present high capacity target was not incorporated until August, 1965 - less than 18 months prior to the writing of this report.

We must draw on experience with image tubes in general to approach this problem:

(1) There are 4 general possibilities for on-shelf deterioration

(a) Loss of vacuum through leaks

(b) Deterioration of an unstable photocathode

(c) Outgassing of parts

(d) Deterioration of thermionic cathode

(2) These modes of failure manifest themselves as follows:

(a) Disappearance or change in appearance of getter flash from metallic shine to chalk white and low or no photoresponse are symptoms of loss of vacuum. There may also be a gas discharge glow with the application of high voltage to tube elements.

(b) Experience has shown that unstable photocathodes generally slump within a matter of a few days after exhaust processing which eliminates this as a probable cause of shelf life degradation. Photoresponse loss can also be symptomatic of poor vacuum as noted under (a) and serves as a valuable check.

(c) Outgassing of parts during non-operating storage to a small degree is not unexpected and should be absorbed by the getter flash. Outgassing would cause an ion spot (bright central area in picture) first. Should it be more severe, the getter flash would start to disappear, and gasses in the tube would glow with the application of high voltage.

(d) Degradation of the thermionic emission would be detected by:

(1) A drop in beam current (I_{G_2} max.)

(2) An inability to discharge highlights at moderate and high light levels

(3) Poorer resolution

(4) A lowering of the maximum operating point.

(3) Post exhaust testing, glass strain, and storage under a positive pressure of inert gas as specified are the best means of determining the integrity of the tube envelope as shipped.

Preship testing after all preceeding operations will detect any short term deterioration or incipient failure particularly with respect to photocathode or thermionic cathode instability. Forty-eight hour dynamic aging helps stabilize the SEC target. Subsequent testing in the assembly and final test of the camera unit further assures that there was no incipient failure built into the tube.

The remaining question then is to determine that the tube was not damaged or stressed during assembly into the camera unit. Since the tube at this point is not accessible and virtually impossible to see,

the only method of assuring that tube performance is unchanged is to operate the tube-camera system. Symptoms of tube failure or degradation at this point include:

(a) loss of sensitivity

(b) reduced resolution

(c) ion spot

(d) breakdown (noise) in picture

(e) inability to discharge highlights.

(4) Periodic operation is the only certain way of detecting deterioration of the tube. There is certain degradation of the tube with extended use as shown by life test results. This deterioration is associated with reduction in target with exposure to light while scanning.

Information on life test tubes indicates the possibility that high operating temperatures are partially responsible for deterioration in life test operation. Periodic short time operation, then, may not affect tube performance.

A suggested operating check schedule is 90 day intervals for the first year and six month intervals thereafter.

6.4 Life Tests

6.4.1. Introduction

As required in Purchasing Department Specification 21341 Revision C, Section 3.4.6, 7 WX-31034 Lunar Camera Tubes were operated on life test for a period of 1500 hours each. The tubes were operated under normal set up conditions as described in Section 3.4.2.1 of the P.D.S. and cycled at a rate of 50 minutes on, 10 minutes off. Tubes were checked at intervals of approximately 50 hours for the first 250 hours thereafter, for the following characteristics: target gain, signal current, photocathode sensitivity, thermionic cathode emission, center resolution, lag, and signal burn.

The internal construction of the tube includes a mask on the target which lies very close to the scanning raster. This results in excessive shading in that area, making raster burn measurements meaningless. Readings of signal current were taken and recorded rather than signal to noise ratio as specified, since the noise is primarily a function of the amplifier and remained constant throughout.

The tube was removed from the life test set for the periodic measurements and could not be reinstalled in perfect registration with the specified test pattern. This caused difficulty in trying to read resolution as the intensity of the burn approached the contrast of the test image and a pattern using large black and white areas was devised to eliminate this problem. With this new pattern we defined two areas: Area 1 is an area in which the target was exposed to photoelectrons as well as the scanning beam. Area 2 was exposed to only the scanning beam.

6.4.2 Test Conditions

It became apparent shortly after life test began that there was considerable degradation of target gain and signal burn under the specified conditions (50 $\pm$ 5°C ambient temperature, 3 x 10^{-2} ft-cdl faceplate illumination). We then varied conditions to determine, if possible, whether ambient temperature or faceplate illumination were causal factors.

As a result, we tested 3 tubes at specified conditions, 2 tubes at specified temperature and reduced light level, and 2 tubes with both ambient temperature and light level reduced.

6.4.3 Results

The attached curves and tabulations show the results of tubes tested and are grouped to show the various results under conditions described in 6.4.2. Readings of thermionic cathode emission, center resolution, and lag were not reduced to a chart since they showed no significant change for any tube in any of the three test conditions with respect to time. It is interesting to note, however, that in all seven tubes the maximum G_2 current and the aperture response at 200 lines was equal to or better than the initial readings after 1500 hours operation.

6.4.4 Conclusions

This is a very small sample from which to draw conclusions, but it appears to be necessary if only to give some indication to the direction of further investigation. The data suggests the following statements:

a) Operation of the tube with the standard setup conditions causes degradation of target gain and produces a permanent "burn" of the target.

b) The degradation is greater where the target is exposed to the photoelectrons as well as the scanning beam.

c) Reduction of faceplate illumination to approximately one tenth the specified illumination had no significant effect on degradation of gain.

d) Reduction of ambient temperature from 50°C to 30°C had a marked effect on loss of gain, reducing this loss to about 1/2 that experienced on the standard tubes.

e) Lag, aperture response, and maximum G_2 current, were not noticeably affected by operation under any of the life test conditions.

Tube No.	Ambient Temp.	F.P. Illum.	Change 1500 Hrs. *			
			Photok	Area 1	Area 2	Burn
	^{o}C	Ftc	%	%	%	%
386	50 ± 5	3×10^{-2}	25	52	27	29
421			10	69	49	38
428			7	45	29	22
384	50 ± 5	4×10^{-3}	+1 *	65	50	26
398		1×10^{-2}	+5	45	25	26
517	30 ± 5	4×10^{-3}	2	17	11	6
522	30 ± 5	1×10^{-2}	0	26	12	16

* Degradation except where Indicated

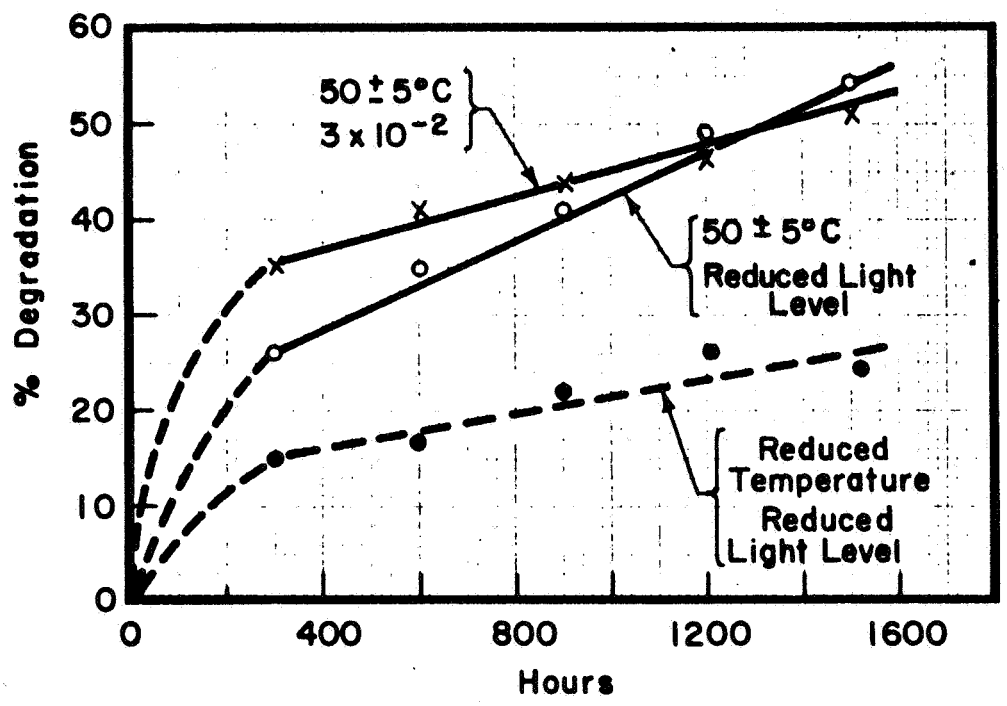

Decrease in Target Gain of Area Exposed to Primary & Scanning Electrons (Area 1)

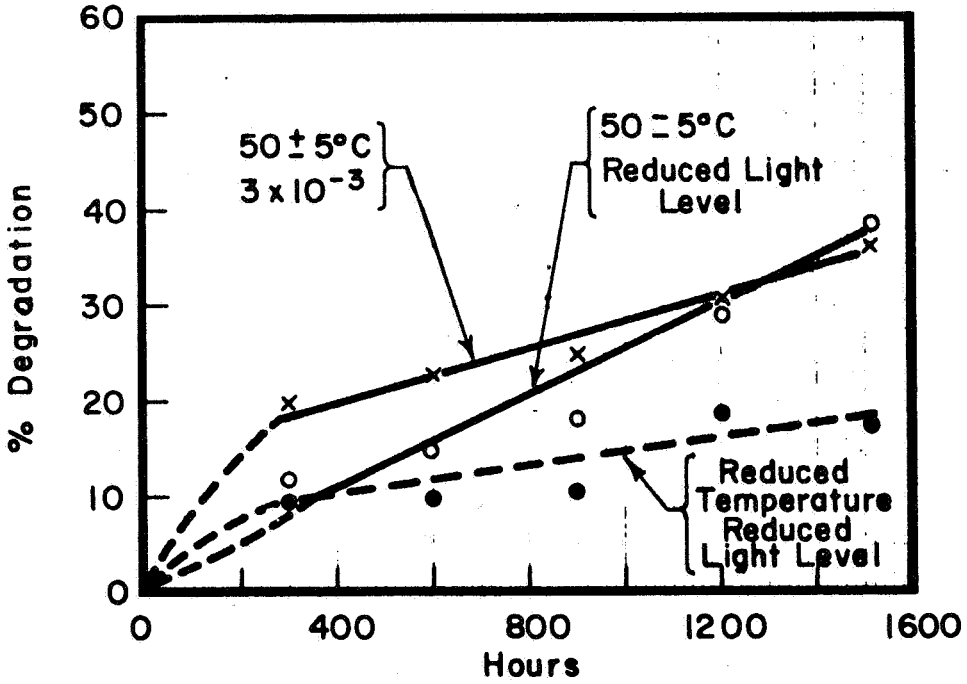

Decrease in Target Gain of Area Exposed
Only to Scanning Beam (Area 2)

LCT LIFE TEST REPORT

TUBE NO. 517

4×10^{-3} ft-c

30°C

Elapsed Time	Target Gain	P.C. Sensitivity	I_{G2}	200 L Resolution	Lag	Raster Burn
0	50	121	1.55	46	11	0
63.9	46	121	1.5	38	10	0
128.2	47.5	119	1.6	39	4	0
192	43.7	118	1.6	40	0	0
283.7	42.3	118	1.6	46	0	0
540.7	42.3	118	1.6	42	6	7
787.5	41.6	118	1.63	43	10	8.5
1068.7	39.1	117	1.62	47	0	7.2
1401	25.9	114	1.65	40	7.6	9.6
1561.5	41.6	118	1.65	46	11	6

Elapsed Time	Tgt.Gain Area 1	Tgt.Gain Area 2	%Gain Loss Area 1	%Gain Loss Area 2	% PR Change	I_{si} (nA)
0	50	50	0	0	0	12.2
63.9	46	46	8	8	0	11.2
128.2	47.5	47.5	5	5	-1.7	11.2
192	43.7	43.7	12.6	12.6	2.5	10.2
283.7	42.3	42.3	15.4	15.4	2.5	9.9
540.7	42.3	45.5	15.4	9	2.5	9.9
787.5	41.6	45.5	16.8	9	2.5	9.9
1068.7	39.1	42.2	21.8	15.6	3.3	9.24
1401	25.9	28.7	48.2	42.6	5.8	5.94
1561.5	41.6	44.3	16.8	11.4	2.5	9.9

LCT LIFE TEST REPORT

TUBE NO. 522

1×10^{-2} ft-c

30°C

Elapsed Time	Target Gain	P.C. Sensitivity	I_{G2}	200 L Resolution	Lag	Raster Burn
0	52.8	138	2.15	44	0	0
63.9	47	138	2.15	41	0	0
128.2	49.3	138	2.15	41	0	0
192	47	138	2.15	41	0	0
283.7	45.7	138	2.15	45	0	5
540.7	45.7	138	2.1	41	0	13.0
787.5	41.3	138	2.1	44	0	13.7
1068.7	37.5	138	2.15	41	0	15
1401	22.9	136	2.15	30	0	12.8
1561.5	38.9	138	2.15	46	0	16

Elapsed Time	Tgt.Gain Area 1	Tgt.Gain Area 2	%Gain Loss Area 1	%Gain Loss Area 2	% PR Change	I_{si} (nA)
0	52.8	52.8	0	0	0	14.8
63.9	47	47	11	11	0	13.2
128.2	49.3	49.3	6.6	6.6	0	13.8
192	47	47	11	11	0	13.2
283.7	45.7	48	13.5	9.2	0	12.8
540.7	45.7	52.5	13.5	0	0	12.8
787.5	41.3	48	21.8	9.1	0	11.6
1068.7	37.5	44.2	29	16.3	0	10.5
1401	22.9	26.3	56.7	50.8	1.5	6.3
1561.5	38.9	46.3	26.4	12.3	0	10.9

LCT LIFE TEST REPORT

TUBE NO. 398

Area 1 - Area covered by beam and primary signal at 50°C ambient.

Area 2 - Area covered by beam only at 50°C ambient.

Illumination = 1×10^{-2} Ft-C.

Elapsed Time	Target Gain	P.C. Sensitivity	I_{G2}	200 L Resolution	Lag	Raster Burn
0	111	79.3	1.25	34	0	0
49	118	80	1.25	33	0	0
115.3	100	80	1.2	32	0	7
374.5	95.8	81.5	1.2	32	0	13
630.7	81	82.3	1.2	36	0	21.7
888.6	75	82.3	1.15	35	0	24.6
1192.7	63	82.3	1.1	34	0	25.7
1478	61.4	84.7	1.1	36	0	25.7

Elapsed Time	Tgt.Gain Area 1	Tgt.Gain Area 2	%Gain Loss Area 1	%Gain Loss Area 2	% PR Change	I_{si} (nA)
0	111	111	0	0	0	17.8
49	118	118	0	0	0	19.1
115.3	100	108	9.9	2.7	0	16.2
374.5	95.8	110	13.7	.9	0	15.8
630.7	81	103	27	7.2	0	13.5
888.6	75	99.4	32.4	10.5	0	12.5
1192.7	63	84.8	43.2	23.6	0	10.5
1478	61.4	82.8	44.7	25.4	0	10.5

LCT LIFE TEST REPORT

TUBE NO. 384

Area 1 - Area covered by beam and primary signal at 50°C ambient.

Area 2 - Area covered by beam only at 50°C ambient.

Illumination = 4×10^{-3} Ft-C.

Elapsed Time	Target Gain	P.C. Sensitivity	I_{G2}	200 L Resolution	Lag	Raster Burn
0	91.5	115	1.1	44	0	0
51.8	70.6	115	1.1	48	0	11
141.7	59	115	1.1	45	0	20.5
400.9	53.5	115	1.2	51	0	24.7
657.1	50	117	1.2	49	0	27.9
915	47.3	117	1.2	48	0	31.1
1219.1	41.8	117	1.2	51	0	28.4
1478.5	33.5	117	1.2	48	0	26.2

"END OF LIFE"

Elapsed Time	Tgt.Gain Area 1	Tgt.Gain Area 2	%Gain Loss Area 1	%Gain Loss Area 2	% PR Change	I_{si} (nA)
0	91.5	91.5	0	0	0	21.4
51.8	70.6	79.3	22.9	12.8	0	16.5
141.7	59	74.3	35.6	18.8	0	13.8
400.9	53.5	71	41.6	22.4	0	12.5
657.1	50	69.3	45.3	24.3	0	11.8
915	47.3	68.7	48.3	25	0	11.2
1219.1	41.8	58.4	54.3	36.1	0	9.9
1478.5	33.5	45.4	63.4	50.4	0	7.9

LCT LIFE TEST REPORT

TUBE NO. 428

Area 1 - Area covered by beam and primary signal at 50°C ambient.

Area 2 - Area covered by beam only at 50°C ambient.

Elapsed Time	Target Gain	P.C. Sensitivity	I_{G2}	200 L Resolution	Lag	Raster Burn
0	59	72	1.5	41	0	0
283	49.5	69	1.4	38	0	14.5
537.5	43	68.5	1.5	48	0	22
796.6	43	68.5	1.5	52	0	23
1075.5	43	68.5	1.3	53	0	28
1290.5	35.7	68.5	1.3	51	0	20.2
1571.3	32.5	67.7	1.6	41	0	22

"END OF LIFE"

Elapsed Time	Tgt.Gain Area 1	Tgt.Gain Area 2	%Gain Loss Area 1	%Gain Loss Area 2	% PR Change	I_{si} (nA)
0	59	59	0	0	0	9.4
283	49.5	58	16	1.7	5.5	6.9
537.5	43	55.2	27.1	6.4	6.2	5.9
796.6	43	55.9	27.1	5.2	6.2	5.9
1075.5	43	59.6	27.1	0	6.2	5.9
1290.5	35.7	44.8	39.5	24.1	6.2	5
1571.3	32.5	41.7	45	29.3	7.3	4.6

LCT LIFE TEST REPORT

TUBE NO. 421

Area 1 - Area covered by beam and primary signal at 50°C ambient.

Area 2 - Area covered by beam only at 50°C ambient.

Elapsed Time	Target Gain	P.C. Sensitivity	I_{G2}	200 L Resolution	Lag	Raster Burn
0	91	69	1.6	41	0	0
50	70	65	1.6	37	0	13
101	50	65	1.65	41	0	18.5
261	44	63	1.65	43	0	28.5
512.6	42	62.3	1.65	38	0	27.4
771.8	36.7	62.3	1.7	40	0	33.3
1027.3	28.8	62.3	1.7	40	0	35
1242.3	28.8	62.3	1.7	43	0	41.2
1523.1	28.8	62.3	1.6	44	0	38

"END OF LIFE"

Elapsed Time	Tgt.Gain Area 1	Tgt.Gain Area 2	%Gain Loss Area 1	%Gain Loss Area 2	% PR Change	I_{si} (nA)
0	91	91	0	0	0	11.5
50	70	80.5	23	11.5	6	9.2
101	50	61.3	45	32.7	6	6.6
261	44	61.5	51.7	33.5	9	5.6
512.6	42	57.8	53.8	36.5	9.7	5.3
771.8	36.7	55	59.7	39.6	9.7	4.6
1027.3	28.8	44.3	68.3	51.3	9.7	3.6
1242.3	28.8	49	68.3	46.2	9.7	3.6
1523.1	28.8	46.5	68.3	48.9	9.7	3.6

LCT LIFE TEST REPORT

TUBE NO. 386

Area 1 - Area covered by beam and primary signal at 50°C ambient.

Area 2 - Area covered by beam only at 50°C ambient.

Elapsed Time	Target Gain	P.C. Sensitivity	I_{G2}	200 L Resolution	Lag	Raster Burn
0	69.2	82.3	1.8	43	0	0
41	68.8	83.1	1.8	46	3	5
93.7	61.2	82.3	1.8	40	0	9
183	50	81.7	1.9	38	0	17
444.3	41.2	79.3	2.05	44	0	18
679.7	40	73	2	46	0	18
934.2	40.2	73.2	2.1	41	0	24
1193.3	40.4	73.2	2.15	37	0	22
1497.6	35.7	73.2	2.1	45	0	29

"END OF LIFE"

Elapsed Time	Tgt.Gain Area 1	Tgt.Gain Area 2	%Gain Loss Area 1	%Gain Loss Area 2	% PR Change	I_{si} (nA)
0	69.2	69.2	0	0	0	11.2
41	68.8	69.2	6	0	+1	11.2
93.7	61.2	67.3	11.5	2.8	0	9.9
183	50	60	27.7	15.4	-.7	8.25
444.3	41.2	50.3	40.5	27.3	-4	6.6
679.7	40	48.7	42.2	29.6	-11.3	5.9
934.2	40.2	527	42	23.8	-11	5.9
1193.3	40.4	51.7	43.1	26.8	-11	5.9
1497.6	35.7	50.3	48.4	27.3	-11	5.3

Reverse page intentionally left blank

APPENDIX A

INVESTIGATION OF ELECTRICAL LEAKAGE THROUGH FIBER OPTIC FACEPLATES

From: ELMIRA WORKS

Date: MARCH 21, 1966

Subject: LCTTM - 66-001

TO: R. A. WHITE

cc: A. Szilasi
G. R. Feaster
R. A. Shaffer
V. J. Santilli
A. H. Boerio
M. Green
R. B. Randels

INVESTIGATION OF ELECTRICAL LEAKAGE THROUGH FIBER OPTIC FACEPLATES

INTRODUCTION

The fiber optic faceplate as used on the Lunar Camera Tube is subjected to a -8 kV potential on the inner or photocathode surface, while the outer surface is at ground potential. In this condition, a spurious signal was noted in the monitor display which was ultimately traced to some sort of discharge phenomenon in the fiber optic. The purpose of this experiment was to investigate fiber optics of various manufacturers to see if this was peculiar to a particular product, or a characteristic of all fiber optics.

SET-UP

An experimental set up was constructed to test several types of faceplates in the as-received condition. The circuit consisted of an 8 kV D.C. supply, an astrodata manovoltmeter and two resistors arranged as shown in the attached figure.

PROCEDURE

The faceplate to be tested was cleaned in blacosolv, rinsed in isopropyl alcohol and placed (outside surface) on a paper towel saturated with boric acid solution. The towel was on an aluminum plate which was connected to the positive side of the 8 kV supply through the nanovoltmeter. A small amount of

mercury (7.9 grams) was placed on the photocathode surface to serve as the contact leading to the negative or ground side of the power supply through a 100 megohm resistor. The voltage was then slowly applied across the fiber optic faceplate while observing the meter and the fiber optic itself for indications of a discharge.

RESULTS

Mosaic fiber optics were the first to be tested, it was found that the average leakage current was approximately one nanoampere and that an erratic discharge was present in all five Mosaics tested.

Corning fiber optics showed no evidence of a discharge and had an average leakage of about .5 nanoamperes.

American Optics and Optics Technology were also tested and it was found that both had a leakage of a little less than .5 nanoamperes, with no discharge characteristic.

As a final test, two complete processed tubes of both Mosaic and Corning were tested (Mosaic (229 and 147) and Corning (216 and a WX-30152)). It was found that both Mosaic fiber optics had leakages above 10,000 nanoamperes, and that the Cornings had only 50 nanoamperes leakage.

CONCLUSION

Since the two fiber optics most extensively used in the SEC Camera Tubes and other tubes requiring fiber optics are either Corning or Mosaic. Corning would be a better choice between the two considering the main trouble to be erratic discharges.

Dennis E. Morehart
D. E. Morehart
LCT Department

/cah

Approved by:

Herbert S. Wilcox
H. S. Wilcox
Engineering Director, LCT

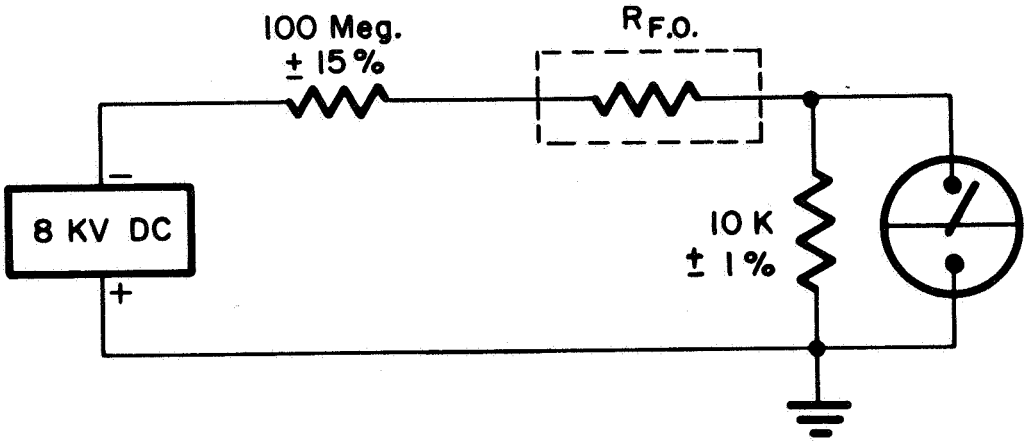

FIGURE 1

APPENDIX B

THERMIONIC CATHODE EMISSION

From: IMAGE TUBE E & M DEPT.

Date: JULY 26, 1966

Subject: THERMIONIC CATHODE EMISSION

1. Description: The thermionic cathode used in the Lunar Camera Tube is an indirectly heated .2 watt cathode consisting of a sintered "pill" suspended on a coiled heater. The heater leads pass through a ceramic and are fastened down with "sauereisen" high temperature cement.

2. Ruggedization: The cathode as manufactured by Sylvania is not designed for environmental use and must be ruggedized prior to assembly. The ruggedized structure consists of another ceramic similar to the support ceramic which has supports brazed into it adjacent to the holes through which the filament leads pass. These are welded to the supports to restrict their movement. Many of the cathode assemblies as received and more after ruggedization have the "sauereisen" chipped and cracked. In order to restrict the movement it was necessary to "repair" the cathodes by applying a high temperature cement to replace the "sauereisen" which was chipped off. At a later period, an additional layer of cement was placed between the two ceramics to arrest any possible shifting of the two ceramics.

3. The cathode emission is given a numerical value by recording maximum G_2 current with $G_1 = 0$. Specified minimum is 1.2 ma, average was 1.5 ma. Starting with tube #423, the control charts show a significant difference. At the same time, a new lot of cathodes was put into production.

4. Readjustment of activation and aging schedules appeared to give temporary improvement; however, emission dropped again after tube #459 and did not yield to any other efforts.

5. We then made up 9 dummy triodes as follows:

   Lot (A) - 3 from new lot as received;
   Lot (B) - 3 taken from guns in production;
   Lot (C) - 3 made up from new lot and ruggedized in normal manner.

   The results were that the 3 dummies in lot (A) met or exceeded spec limits, while no dummy in lot (B) or (C) exceeded 1 ma, and 3 showed no emission whatever.

   Lots (A) and (C) were from the same cathode. Lot (B) was from a different lot. Lots (B) and (C) both had a layer of high temperature cement between the ceramics. Lot (A) had none.

6. Conclusions: The cement is highly suspect and mounts are now being made without this layer between ceramics.

Herbert S Wilcox

/cah

H. S. Wilcox

APPENDIX C

RIBBON CATHODE DEVELOPMENT

ET-20

August 10, 1966

The Ribbon Cathode Development for the Lunar Camera Tube

by

Anton van der Jagt

This work was supported by the Manned Spacecraft Center of the National Aeronautical and Space Administration on Contract No. NAS9-3548. This report is issued as a special technical report as required by contract.

Approved by:

R. A. White
Program Manager
Lunar Camera Tube

WESTINGHOUSE ELECTRONIC TUBE DIVISION
ELMIRA, NEW YORK

ET-20 The Ribbon Cathode Development for the Lunar Camera Tube

A. van der Jagt August 10, 1966

I Introduction

One of the requirements for the Lunar Camera Tube, WX 31034, is low heater wattage. Therefore, this tube type has been designed with the well-known Sylvania .2 Watt powdered nickel cathode. However, since this cathode is periodically of poor quality, a decision was made in September, 1965, to design and develop a directly heated cathode as a back-up. Although the use of such a cathode necessitates changes in the camera circuit, it was felt at that time that these changes would be justified if the design would give a better performance.

II The Heater Wattage-Temperature Characteristic

A very important requirement for this newly designed cathode is a low heater wattage which, however, should give the proper emission current.

K. Cooper had previously done some work on filamentary cathodes. (A report: "50 mW Filamentary Cathode for Cathode Ray Tubes" is available.) It was decided to use this work as the starting point of the new design. Due to the low current density of the filamentary cathode, it was necessary to use a ribbon cathode, as advised in his report.

Most of the following tests have been made with a Cobanic ribbon with dimensions .0005 x .025" except as otherwise noted. All tubes were measured for brightness temperature and heater wattage.

The first test, made by Mr. A. Hanna, contained a ribbon cathode supported by micas and kept under tension by a single spring of .005" nickel clad molybdenum (similar to the construction used by Mr. Cooper). The distance between the support micas was .150". The ribbon had been cataphoretically coated with emission coating.

The emission of the tubes was good, i. e., comparable with the Sylvania cathode.

Wattage versus temperature curves were measured. (See Fig. 1, Curve 1.) In order to get a ribbon temperature of 800°C, a wattage of .4 Watt was necessary. This was far too high since we were aiming at .2 Watt (the same as for the Sylvania cathode).

The test had also the disadvantage that micas were used, which we would rather avoid since it is always possible that mica particles may come loose and ruin the performance of the tube.

In the next test the ribbon had been mounted on a ceramic disk, again supported by a single spring. The wattage-temperature curve is shown in Fig. 1, Curve 2. For a temperature of 800°C a wattage of .38 Watts is needed. This construction has the disadvantage that the support of the ribbon by a single tension spring is mechanically unreliable. Therefore, a new construction had to be designed (the same construction as in Fig. 6 but with the ribbon welded to the springs and not to the support rods). The ribbon is, in this construction, supported by two specially formed springs. Each spring has a flat surface which will keep the ribbon flat. Since the springs are coiled on each end around a .020" Nilvar rod, the tension is equally divided in each leg; and, due to the relatively large distance between the legs, the springs are rather stable for vibration in a perpendicular plane through the ribbon. The use of a spring on either end of the ribbon has the effect that, during vibration, either each spring has a damping effect on the other spring (the spring amplitude during vibration not in same direction) or that the tension on the ribbon is maintained during vibration (spring amplitude in same direction during vibration).

The wattage-temperature curve is shown in Fig. 1, Curve 3. For a temperature of 800°C, a power of .56 Watts is needed.

Although it is evident that the wattage should be higher than for a single spring design, this construction is necessary to warrant good performance during environmental testing. Therefore, steps were taken to reduce the wattage by changing the spring design, as well as the dimensions of the ribbon. A series of tests were made with different spring dimensions, ribbon length and spring material. The ribbons were not coated with emission coating in order to speed up the processing of the test tubes. The wattage-temperature curves are given in Fig. 2. In Table I the characteristics of the test tubes corresponding to the curves are listed.

TABLE I

SPRING		RIBBON	WATTAGE FOR	CURVE #
MATERIAL	HEIGHT	LENGTH	T = 800°C	IN FIG. 2
NiCr	.080	.200	.415	1
NiCr	.110	.200	.42	2
NiCr	.080	.150	.44	3
NiCr	.110	.150	.445	4
NiCr	.080	.110	.48	5
NiCr	.110	.110	.495	6
W	.080	.110	.56	7

The lowest wattage for 800°C was achieved by using a long ribbon and a small spring height. However, the maximum ribbon length is defined by the diameter of the ceramic and by the vibration performance. It is not advisable to use a longer ribbon than .200". The spring height is mainly defined by the characteristics of the spring in view of environmental testing. A spring height

less than .080" would give a higher tension but less amplitude during vibration. The thermal conductance of NiCr spring wire is significantly lower than tungsten wire so that the necessary wattage could be reduced drastically by using NiCr.

Approximately at the same time a new test had been made with the same ribbon cathode but etched till the ribbon thickness decreased approximately 30%. The wattage-temperature curve is shown in Fig. 3, Curve 2. In the same figure, Curve 1 of Fig. 2 has been drawn (this tube had the same dimensions, except the thickness of the ribbon). The wattage decreased approximately .04 Watts at 800°C.

The etching did not improve the reliability of the design. The burrs and roughness on the sides of the ribbon, caused by cutting the ribbon to the proper width became ragged due to the etching and weakened the ribbon. Therefore, the spring tension in this test had to be reduced to less than 5 grams (in all other tests the tension was at least 12 grams). A rough calculation revealed that the cathode wattage was approximately equally divided between the ribbon and the springs. Consequently, a reduction in the electrical resistance of the springs would reduce the total wattage. It was not possible to increase the spring wire diameter (too much tension on the ribbon). Therefore, a test was made with the ribbon supported by the top of the spring but with the ribbon ends welded to the Nilvar support rods (Fig. 6). By doing this the total electrical resistance of the springs was reduced because the resistance of part of the ribbon was in parallel with the resistances of the spring legs.

Fig. 4, Curve 2 shows the wattage-temperature curve of this test. Curve 1 of the same figure shows a parallel test, run as the test of Curve 1, Fig. 2. The latter curve does not agree very well with the other curves. This is very likely due to processing (residual air in the tube). The construction of Curve 2 seems to reduce the wattage approximately .05 Watts for T = 800°C.

The wattage-temperature curve, given in Fig. 5, shows the latest construction with all improvements combined. We used .005" NiCr springs with .080" height and mounted on .020" nilvar rods. The tension on the springs is approximately 10 gram. The ribbon material was cobanic nickel (dimension, .0005" x .015"). The distance between the springs is .200". The ribbon is guided across the springs and welded to the nilvar support rods. The result shows .18 Watts for a temperature of 800°C or .16 Watts for 750°C. The emission was quite satisfactory (comparable with the total current of a Sylvania cathode).

III Environmental Testing

Three tubes of the tests shown in Fig. 2 were environmental tested by D. Morehart. The purpose of the test was to determine the resonance frequency of the ribbon and to determine whether the ribbon cathode would fatigue when subjected to 15 g's for 5 minutes at the resonance frequency of the ribbon.

The equipment was set up as shown in Fig. 7. In Fig. 8 the heater is drawn schematically and the axis of vibration indicated.

The three tubes had very similar test results. Fig. 9, 10, and 11 show the measurement results for one of these tubes.

The resonance frequency of the ribbon cathode was approximately 1800 c/s. The cathodes were able to stand the vibration with 15 g's during 5 minutes without any difficulty.

IV Emission and Life Tests

All previously mentioned tubes which were coated with emission coating were measured for emission characteristics. The emission quality of the ribbon cathodes was, in general, satisfactory. The level of the emission current was at least as good as for the Sylvania .2 Watt cathode.

One tube was life tested under static conditions. After 600 hours the emission level was still satisfactory; the slump in emission was not significant.

One tube has been cycled at a heater voltage equal to 1.5 x nominal heater voltage. After 38000 cycles the tube was still operable, and the emission level of the cathode was very good.

V Conclusion

The design of the ribbon cathode is satisfactory. Some more work is necessary if the design has to be produced in large quantities.

A. van der Jagt

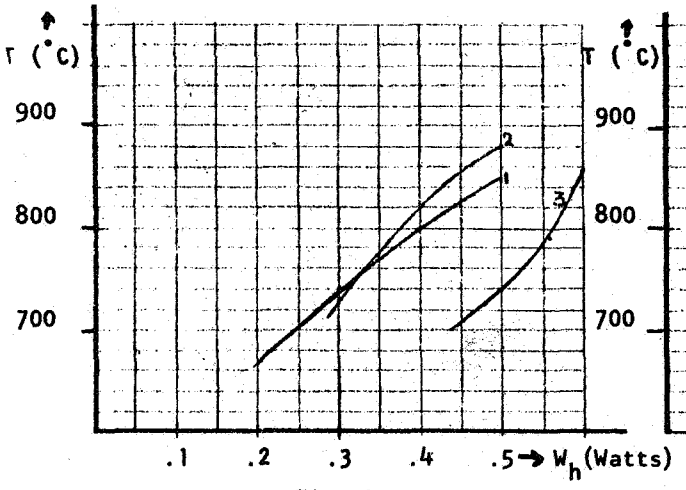

Fig. 1

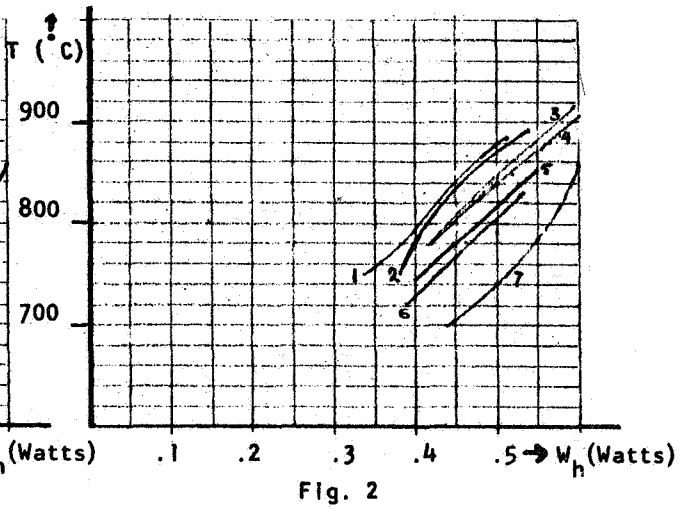

Fig. 2

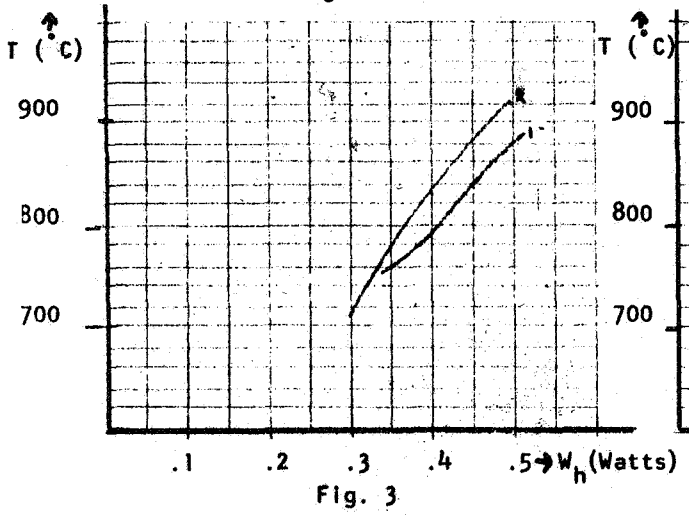

Fig. 3

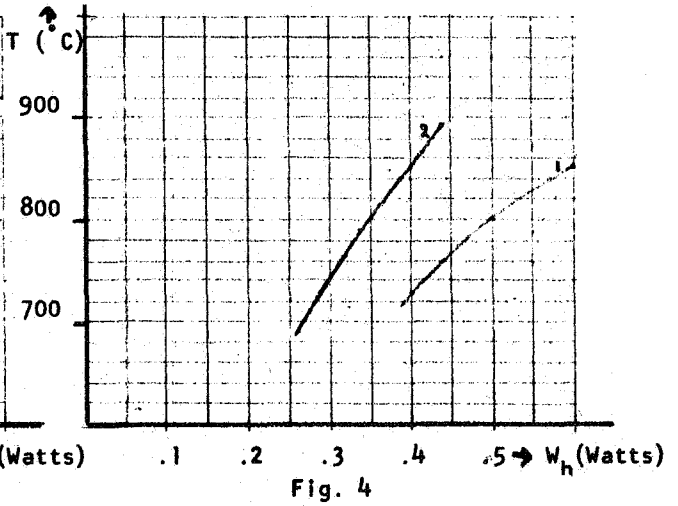

Fig. 4

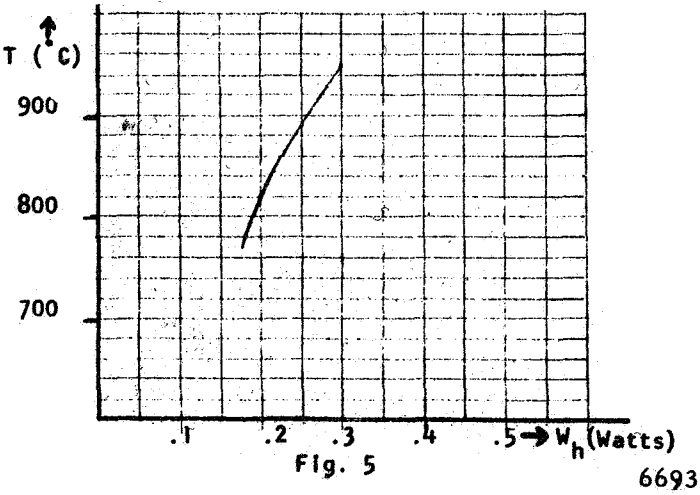

Fig. 5

6693D-VA-17

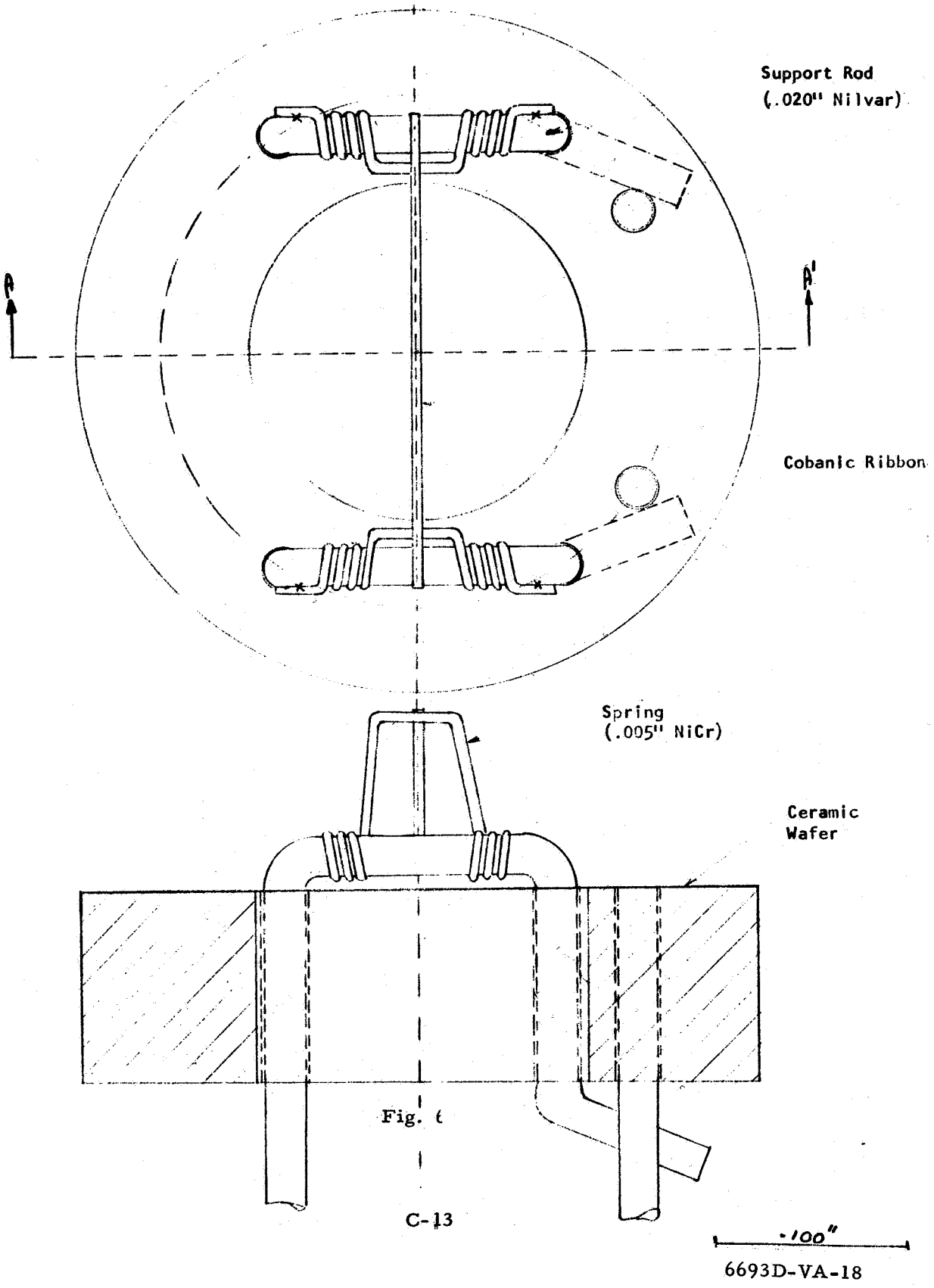
Support Rod
(.020" Nilvar)
A
A'
Cobanic Ribbon
Spring
(.005" NiCr)
Ceramic
Wafer
.100"
6693D-VA-18

Fig. 6

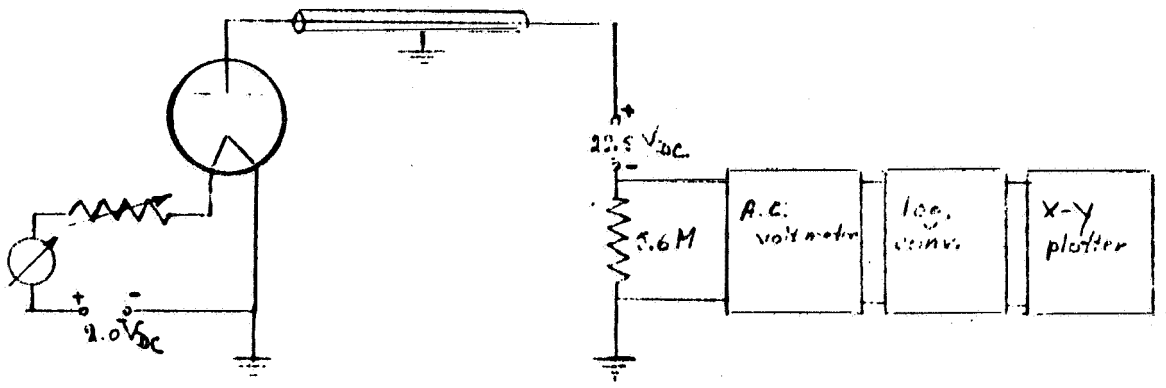

Fig. 7

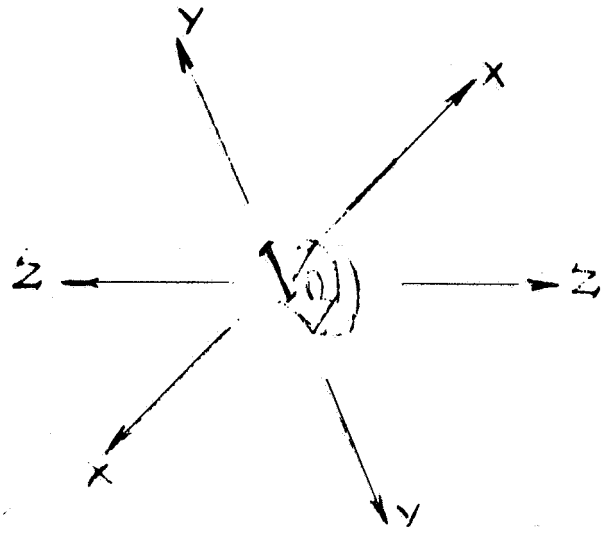

Fig. 8

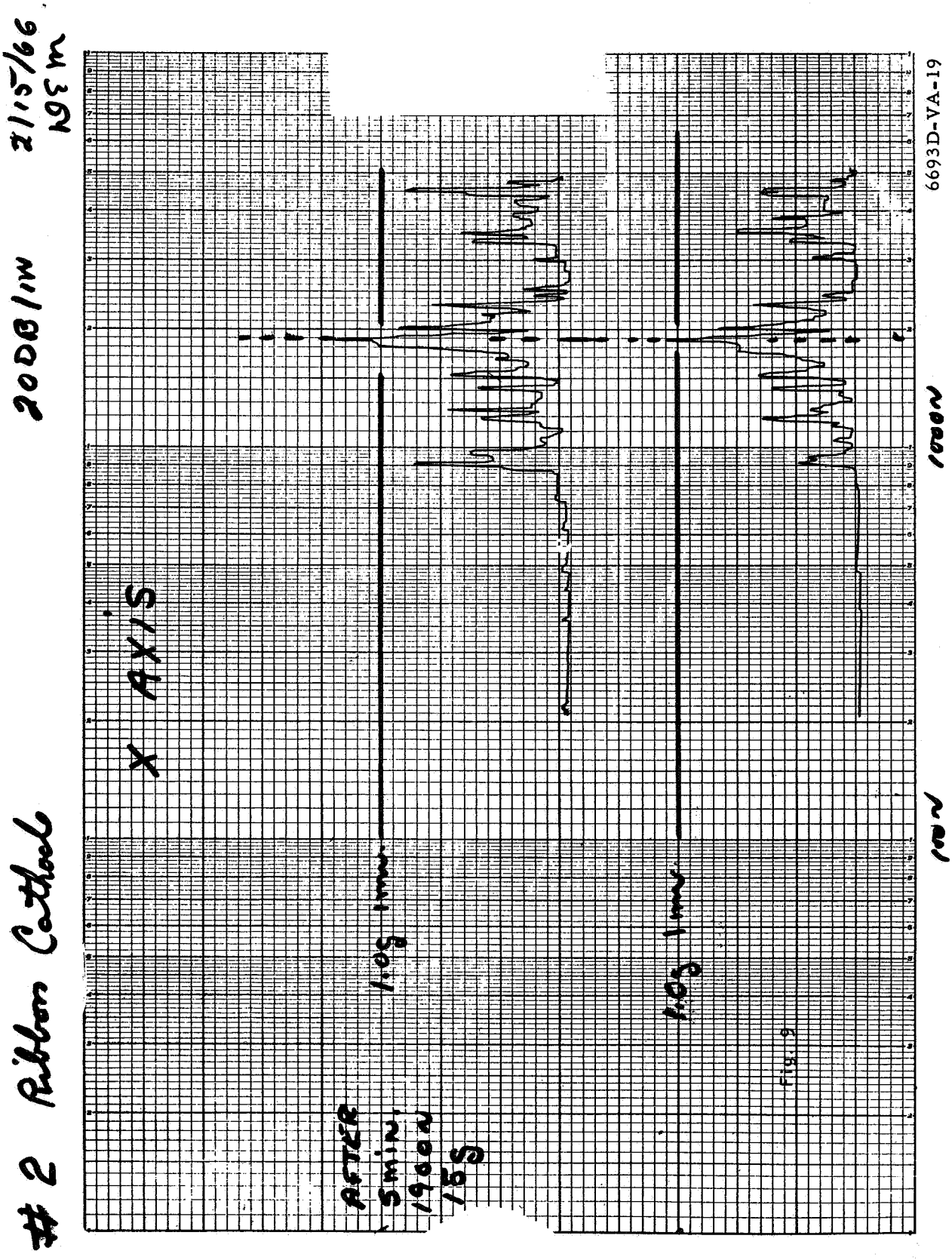
#2 Ribbon Cathode
X AXIS
20DB/IN
2/15/66
1.0g 1mv
1.0g 1mv
AFTER 5min. 1900N 15g
1000N
100N
6693D-VA-19

Fig. 9

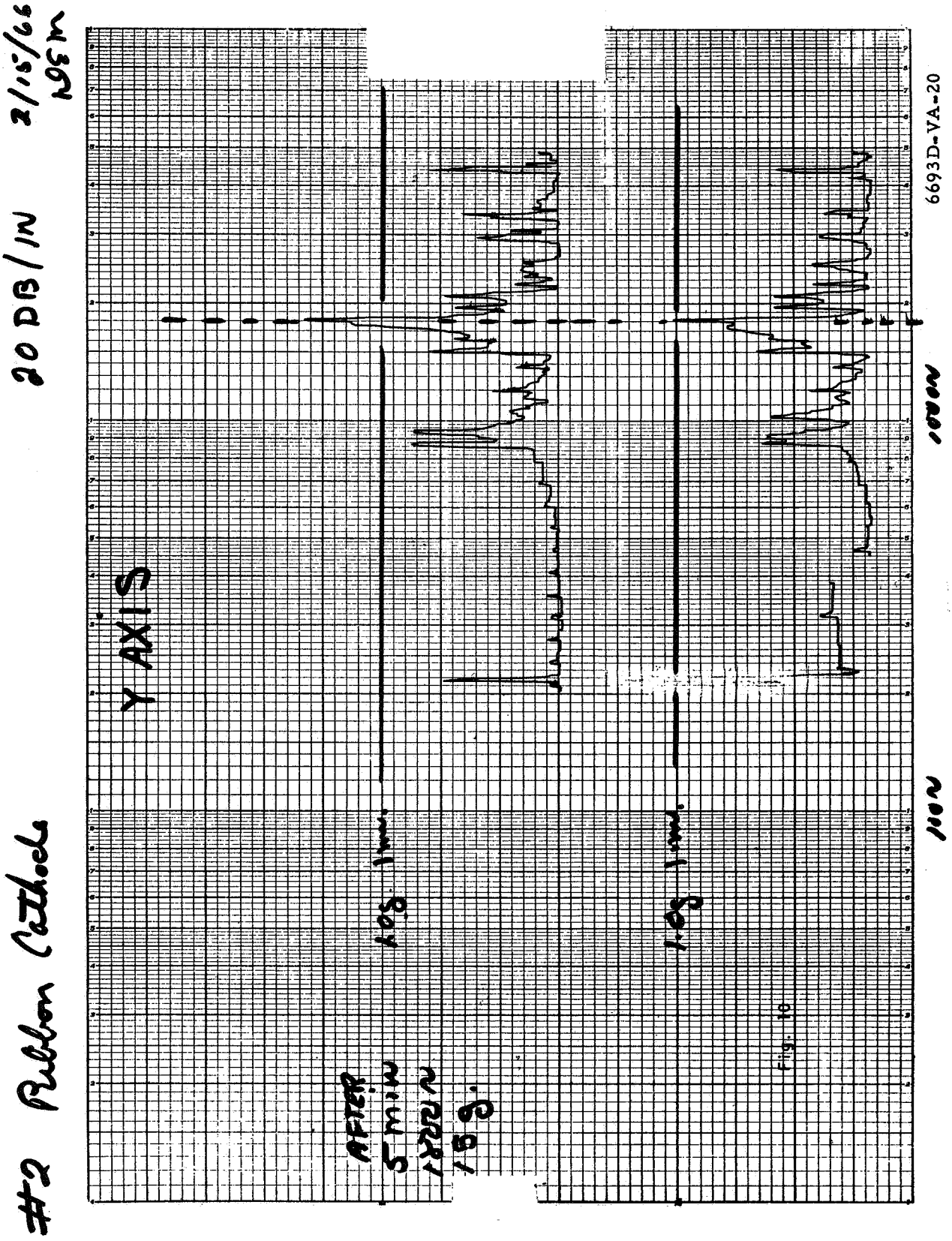

Fig. 10

6693D-VA-20

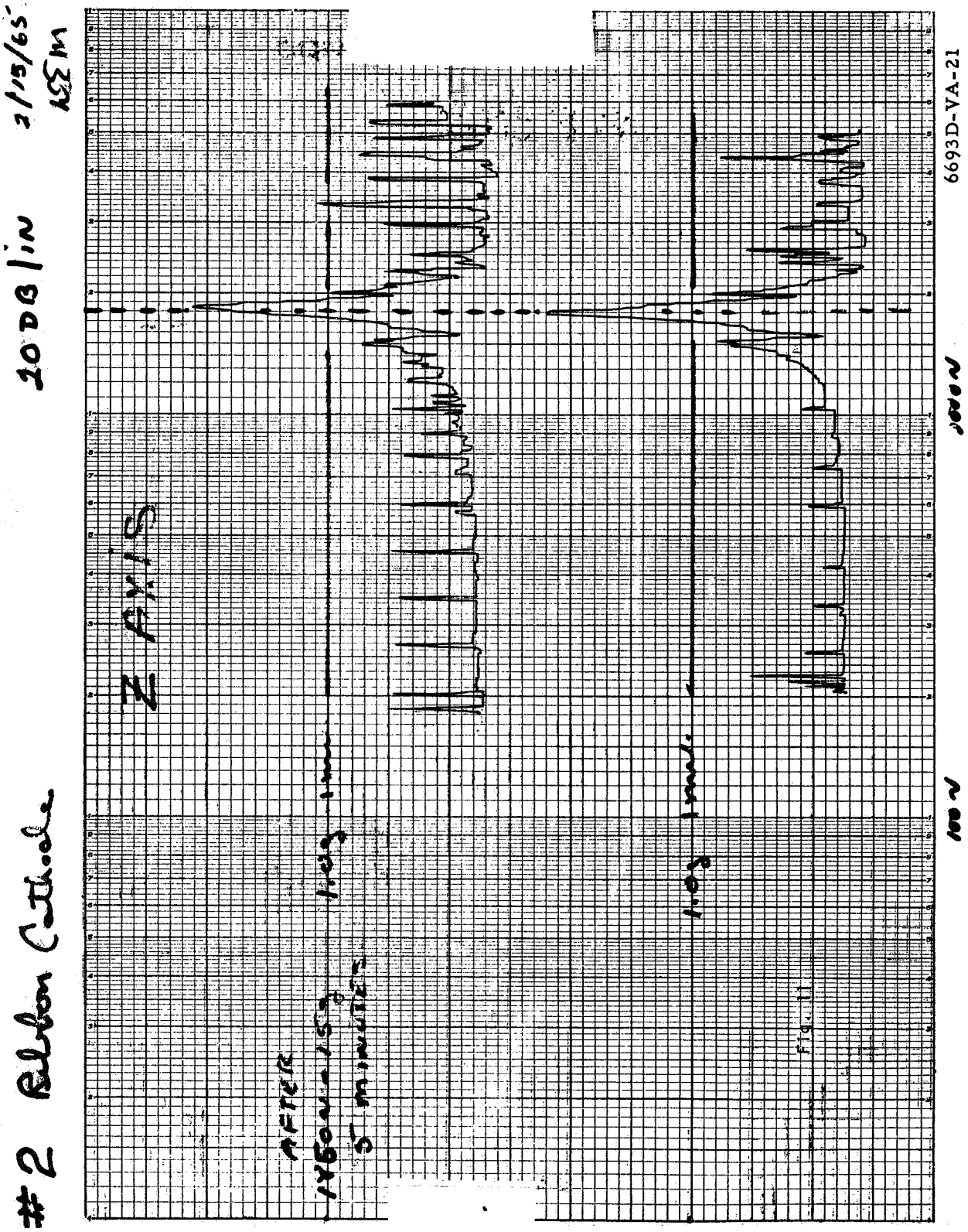
#2 Ribbon Cathode
10 DB/in
2/15/65
Z AXIS
AFTER
1.0g 1mv
5 MINUTES
1.0g 1mv
100 V
1000 V
6693D-VA-21

Fig. 11

APPENDIX D

TARGET BURN-IN INVESTIGATION

TARGET BURN-IN INVESTIGATION

Introduction

The use of the Lunar Camera tube involves a situation in which intense, small lights may be in the field of view of the camera for considerable length of time. Consequently, the tube may be subjected to small area highlight illumination imaged on the faceplate. If the area is not large enough, the automatic light control circuit may not be activated and damage to the tube is likely. The purpose of this investigation is to study the effects of such exposures and to determine, if possible, the limits of safe operation. There were four parts to the study:

a) Investigation of photocathode damage

b) Damage to target at normal (-8kv) photocathode voltages

c) Damage at reduced photocathode voltages

d) Determination of on-set of damage

Set-Up

a) The tube non-operating except for -8kv between photocathode and anode was exposed to small area illumination with exposures in excess of 500 ft-cdl for 30 minutes. The photocathode was masked off except for the small area exposed and measurements of photocurrent were made before and after exposure.

b) The tube was set up in the test set in normal operating configuration imaging a resolution pattern that produced an illumination of approximately 1×10^{-2} ft-cdl on the photocathode. A microscope light was then placed in

the field of view and its voltage adjusted to give the desired intensity. Illumination was determined by selecting a line of the display that included the light and measuring its signal relative to the 1×10^{-2} ft-cdl background. Other exposures were made by varying the f-stop of the lens and adjusting the background illumination. The light was moved about in the field of view to expose various areas of the target.

c), d) The set-up was identical with b) except the photocathode voltage was varied to determine the effect of different primary energies.

Procedures

After the exposures were made, a line was selected from display and the change in signal of the exposed area from the unexposed area was determined. In the case of temporary damage, measurements were made periodically to determine the rate of decay.

Results

a) No apparent change was detected from exposure of the photocathode to the 500 ft-cdl illumination and after several repetitions of the exposures, that part of the investigation was terminated.

b) This second series of tests was made with moderate photocathode illumination and full (-8kv) photocathode voltage for periods up to 30 minutes. In this mode, permanent damage resulted in all cases. The illumination was reduced to 1 ft-cdl while the photocathode was run at -6kv for a 40 minute exposure. This resulted in temporary damage that recovered within a few hours of normal operation.

c) In this series the photocathode was run at considerably reduced voltage (33.5 kv) while illumination was increased to 12-1/2, 25, 50, and 100 ft-cdl for various exposures on the target. At the end of the exposures, the camera and tube was focused on a white screen for 1 hour before the "burned" areas were evaluated. Target degradation consisted of darker areas (less sensitive) where the light had been imaged. This degradation was, in the worst case, a decrease in signal of 25% although it apparently did not degrade resolution. In some instances, as when the filament of the light was imaged, the damaged area produced a white signal and a complete loss of information.

Not all exposures resulted in damage to the target, but no correlation of illumination, time, or the product of illumination and time to degree of degradation was apparent. Tests were also performed with photocathode voltages ranging from 2 - 2.5 kv and small area illumination of 200 ft-cdl during exposure. After exposure, the photocathode voltage was raised to -8 kv and the photocathode uniformly flooded with 6×10^{-3} ft-cdl during the recovery period. No damage was observed for any exposure (up to 200 ft-cdl) with photocathode voltages less than -2.5 kv. At -2.5 kv target damage appeared, however, this was not permanent damage and recovered.

d) The final series of tests were performed to determine the onset points of permanent damage in the 2.5-3 kv range, and determine if there is correlation between the A.L.C. and damage onset. Results show that non-recoverable damage occurs when the tube is operated at any point equal to or

greater than the A.L.C. curve. The A.L.C. curve is defined as the constant signal current curve which begins at the maximum operating point (or the point just below which the picture starts to lose resolution as illumination is increased) and maintains constant signal output as photocathode voltage is reduced while light input is increased.

Summary

1) The photocathode is not the limiting factor to survival from exposure to high intensity small area illumination.

2) High primary energy (photocathode voltage) appears to be a necessary condition for permanent damage to the target.

3) Onset of damage can be expected where illumination-photocathode parameters exceed those defined by the A.L.C. curve.

4) Temporary, recoverable damage can occur at exposures below that defined by the A.L.C. curve.

5) It is not known whether there is a time-brightness reciprocity for either permanent or temporary damage or recovery from temporary damage.

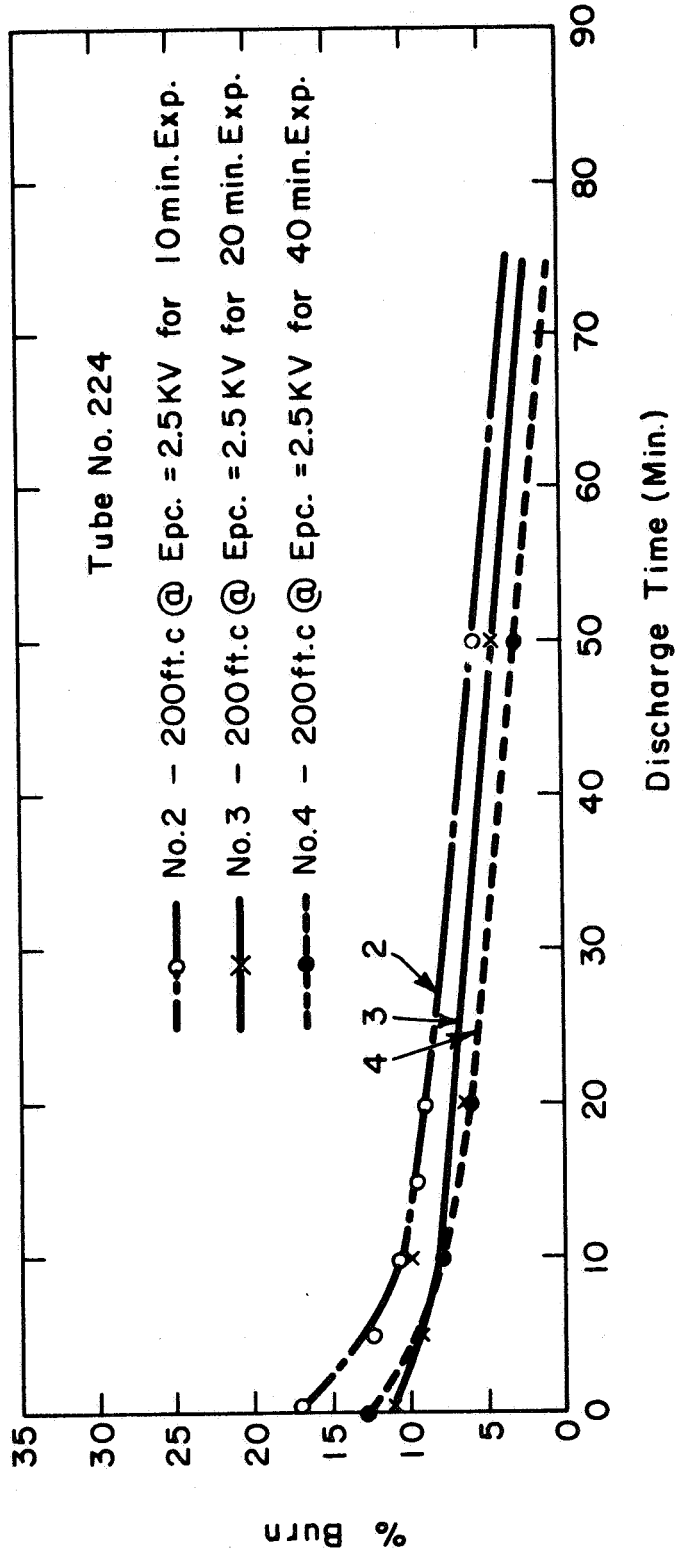

Fig. 1

Per Cent Degradation vs Time

APPENDIX E

THE EFFECT OF INTENSE EXPOSURES ON SEC TARGETS

Report No. ET-5

THE EFFECT OF INTENSE EXPOSURES ON SEC TARGETS

by

A. H. Boerio

April 13, 1965

WESTINGHOUSE ELECTRIC CORPORATION

ELECTRONIC TUBE DIVISION

ELMIRA, NEW YORK

Approval:

G. W. Goetze

G. W. Goetze, Manager
R & D Department

Purpose

The SEC target is normally operated with a suppressor mesh adjacent to the scanning surface of the target. This mesh is used to limit the voltage excursion of the target which, for intense signals, could exceed safe levels. However, even with the presence of this mesh, the target can be damaged due to exposure to intense signals. If a signal great enough to drive the target well into saturation is impressed for some time, a temporary and perhaps permanent reduction in gain is observed in the exposed area. Since in some applications intense exposures are inevitable, quantitative data is needed. Thus, the purpose of this investigation was to determine:

1. The illumination levels an SEC camera tube can be exposed to before first, a temporary loss, and second, a permanent reduction in gain results.
2. The effect of the duration of such signals.
3. Whether or not an initial loss in gain "ages" the target so that much more intense exposures are required to cause a further loss in gain.

Method

Two WX-5419A SEC camera tubes were used for these experiments. Both tubes employ a suppressor mesh spaced 10 mils from the target. In all cases, this mesh was operated at 15 volts so that no matter how intense the exposure, the target could not cross over. A 0.1 cm^2 rectangular aperture was focused one-to-one on the photocathode and the resulting photocurrent was measured. The effective light level was then calculated on the basis of a 100 uamp/lumen photocathode response. All light levels specified in this memo were determined in this manner.

In all cases, the signal current from the area to be exposed was measured at a photocathode illumination of 10^{-3} foot-candles. Then the appropriate exposure was made and the signal current was re-measured under the same conditions of the initial measurement. During the exposure only a 0.1 cm^2 area was illuminated. After the exposure, a somewhat larger area was illuminated such that the exposed area was contained in the larger area. In this way, gain differences of a few percent could be observed on the monitor. The absolute value of the signal current was measured by comparing it with a reference signal which was generated by applying a variable voltage pulse across the video load resistor. This pulse was applied to each video line so that a vertical bar was generated on the monitor. The amplitude of the pulse was adjusted to match the amplitude of the signal current by comparing the two on a line selector oscilloscope. This absolute measurement was accurate to ± 0.5 db.

Results

A series of experiments was conducted with the gain of the tube adjusted to give a signal current of 2.8×10^{-8} amps at a photocathode illumination of 10^{-3} foot-candles. Without changing any of the tube operating parameters, progressively longer time exposures were made at a given light level. After each exposure, the signal current was re-measured under uniform illumination at 10^{-3} foot-candles. Figure 1 shows the results for exposures at 10 foot-candles. Each of these exposures was made on the same target area. As indicated in the figure, the signal current was noted immediately after the exposure and again some time later. The measurements made immediately after the exposure are rather inaccurate since the gain of the target began to recover. The approximate recovery time in minutes is indicated for each exposure.

In general, the recovery rate was rapid at first, then decreased roughly exponentially. The total time required for recovery increased with the intensity of the exposure, however, in no case did it exceed 5 minutes. Uniform illumination at 10^{-3} foot-candles for further periods of up to an hour were not successful in improving the situation that existed after 5 minutes.

Figures 2, 3 and 4 show the results obtained for exposures at 1, 10^{-1} and 10^{-2} foot-candles respectively. These curves, along with several others, each measured on a different area of the target, were used to construct Figure 5. Exposures in region 1 of Figure 5 have no harmful

effects on the target while those in region 2 result in a temporary "after image". Exposures in region 3 result in a permanent loss in gain.

All the data presented in Figures 1 through 5 was taken from the same WX-5419A (6444036) operated in all cases at a primary voltage of 6 kV. Target voltages of from 14 to 17 volts were used, corresponding to target gains of from 35 to 50. These variations in gain required to give a constant signal current were due to inadvertant changes in the area scanned. As we shall see later, the permanent "burn in" characteristic is essentially independent of target voltage so that combining the data taken at slightly different voltages is justified.

The transfer curve for this target was measured and is shown in Figure 6. In order to further characterize the target, primary penetration measurements were attempted with limited success. Instability in the image section limited measurements to 5 kV where 6% penetration was measured. This measurement along with a measured capacity of about 110 pF/cm^2 indicates a "thin" target.

Additional exposure studies were made on a second WX-5419A camera tube in order to determine whether the results described above are typical for SEC targets or whether they are peculiar to that target only. Figure 7 shows the results of a series of exposures made with this tube.

The conditions and procedures were identical to those used in obtaining the curves in Figure 3 except that the target voltage was 10 volts in this case. The target gain at 10 volts was 90, corresponding to a signal current of 4.0×10^{-8} amps.

In order to determine the effect of reducing either the target voltage or the primary voltage during the exposure, two additional curves were measured with this tube. For both of these curves, the target gain was reduced by a factor of 10 during the exposure only. Otherwise, the conditions were the same as those of Figure 7. In the first case, the gain was reduced to 9 by lowering the target voltage to 1 volt and maintaining the primary voltage at 6 kV. The results are shown in Figure 8. A comparison of Figures 7 and 8 shows that the permanent "burn in" characteristic is essentially unchanged. While the temporary reduction in gain was significant at a target voltage of 10 volts, none was detected at 1 volt for exposures up to 10 minutes.

The second curve made at reduced gain during exposure was accomplished by maintaining the target voltage at 10 volts and reducing the primary voltage to 3.25 kV corresponding to a gain of 9. In this case, no "burn in", either temporary or permanent, was observed for even the longest exposure time, 60 minutes.

Conclusions

The two targets used for these measurements are fairly representative of SEC targets in general. The results obtained with exposures at 10^{-1} foot-candles and 6 kV primary voltages for each target, Figures 3 and 7, do not differ from each other by an amount significantly greater than the experimental accuracy. Thus, within an order of magnitude, the exposures to which a typical SEC target can be subjected without suffering a loss in gain are given in Figure 5. The permanent "burn in", essentially independent of target voltage, is a strong function of primary voltage. It has been measured only at 6 kV. The temporary "burn in" characteristic, shown in Figure 5 for a target voltage of about 15 volts, varies with target voltage. This dependence as well as that on primary voltage has not been measured.

The curve in Figure 1 shows that an initial loss in gain due to an intense exposure does not enhance the ability of the target to withstand future exposures. This fact and the fact that the permanent loss in gain depends on the bombarding energy indicates that "burn in" is an appropriate term. It seems likely that the heat generated in the exposed area causes a damaging structure change. Further exposures producing the same or higher temperatures would then cause further damage and an associated loss in gain. The lack of reciprocity in exposures causing permanent damage also indicates that the effect is a thermal one.

An interesting phenomenon was observed during the course of the experiments. Tube #6444036 initially showed a very pronounced pattern of coarse blemishes. After each successive exposure in a given area, the blemishes in that area grew less and less pronounced. Since only relatively small areas of the target were illuminated, the rest of the target was generally unobserved. However, at one point the whole target was illuminated and the entire pattern of blemishes was gone, even those in the unexposed areas. The finer "grain" structure was not affected. Unfortunately, no photographic record of these observations was made. Since the tube was operated continuously for quite lengthy periods of time, it is possible that the heat generated by the focus and deflection coils subjected the target to a mild bake.

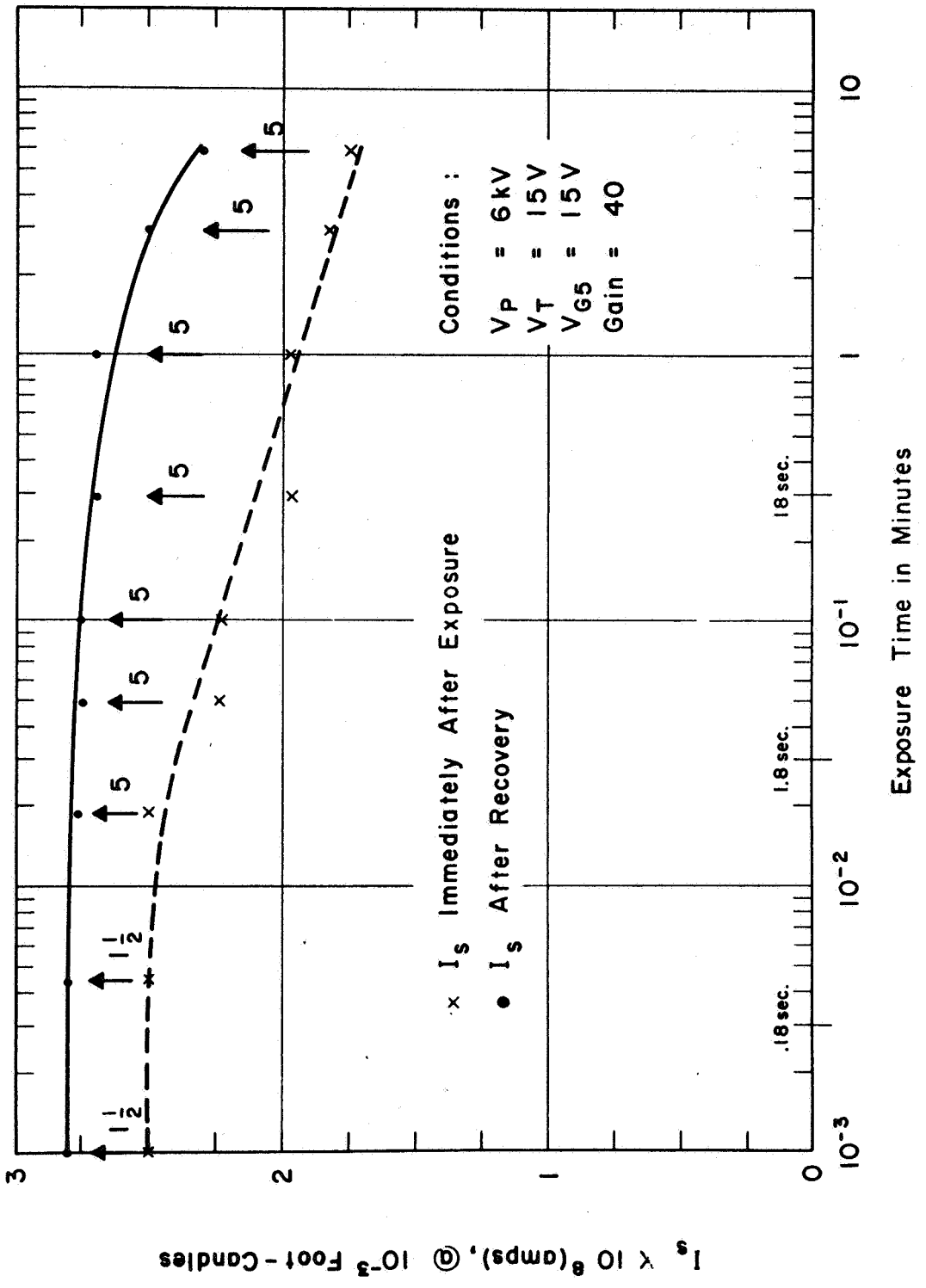

FIG. 1 : I_s vs Exposure Time @ 10 Foot-Candles

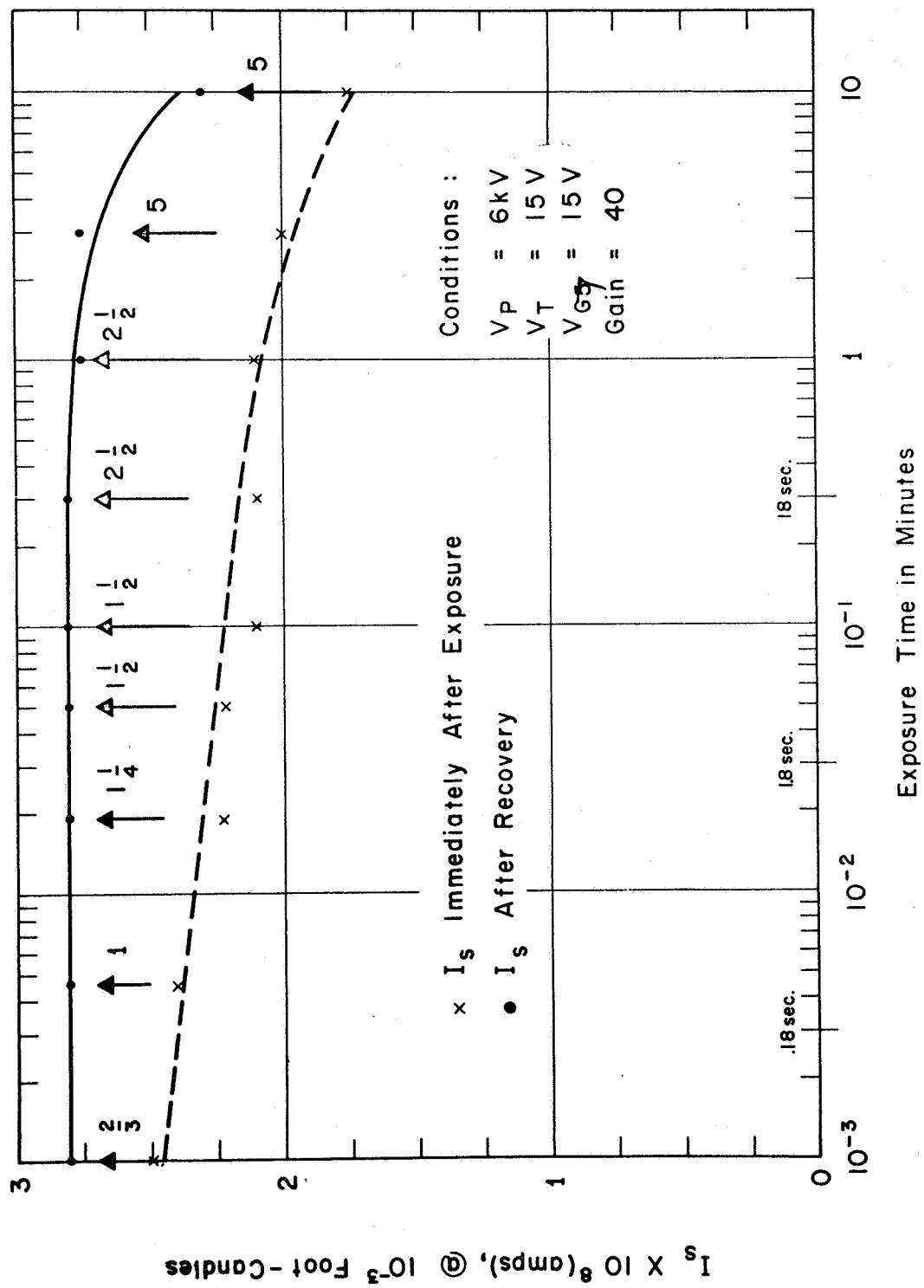

FIG. 2 : I_s vs Exposure Time @ 1 Foot-Candle

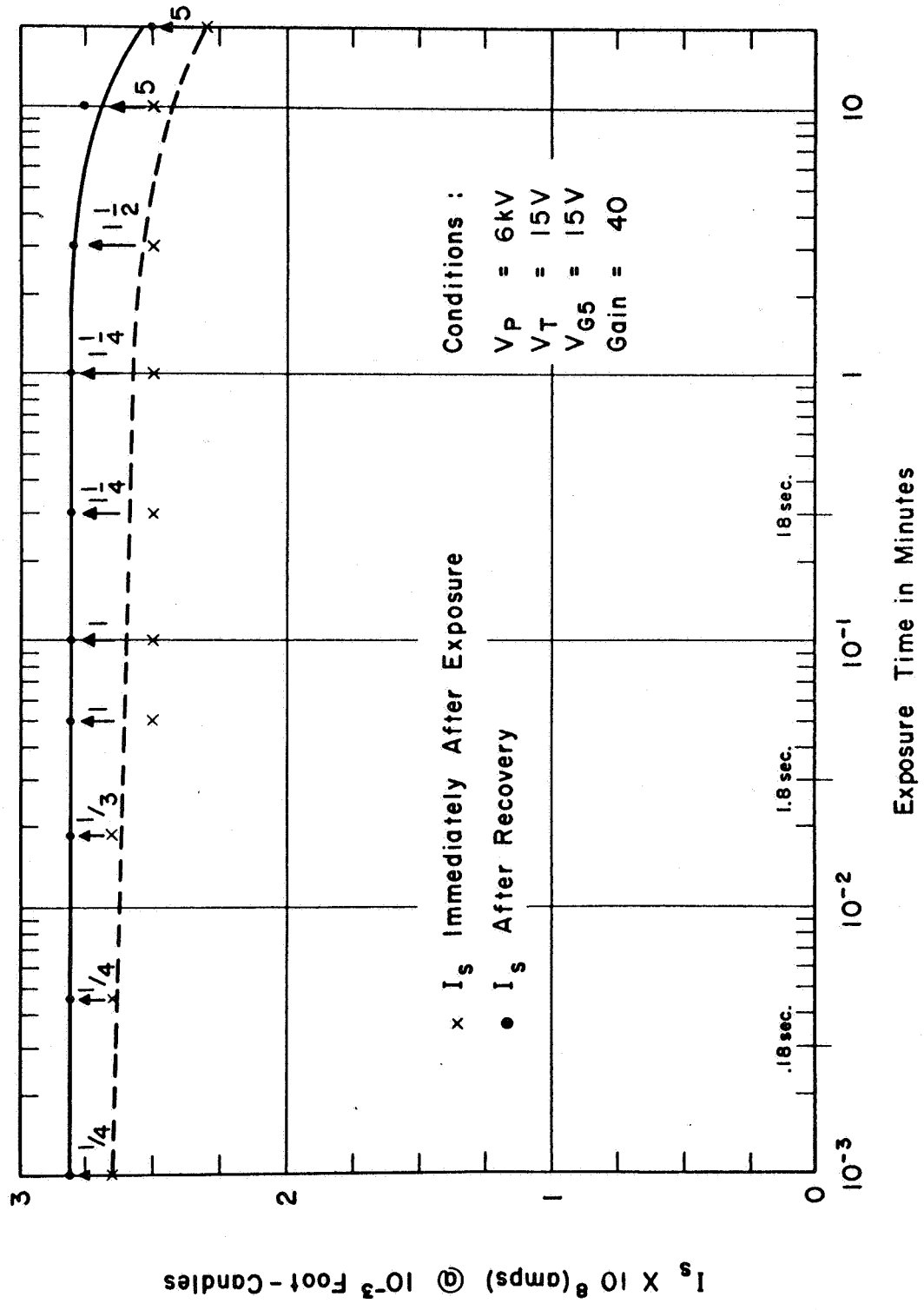

FIG. 3 : I_s vs Exposure Time @ 10^{-1} Foot-Candles

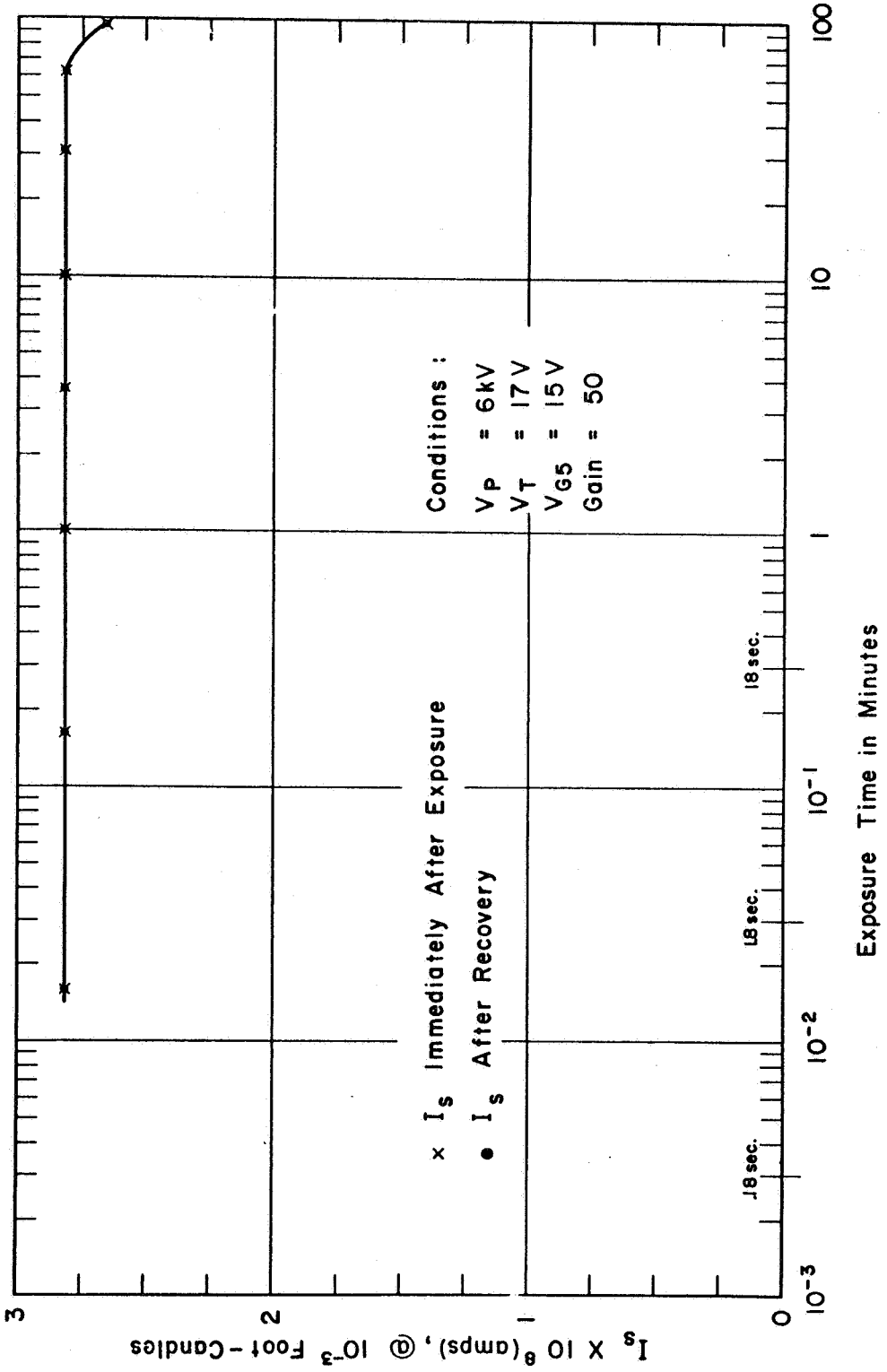

FIG. 4: I_s vs Exposure Time @ 10^{-2} Foot-Candles

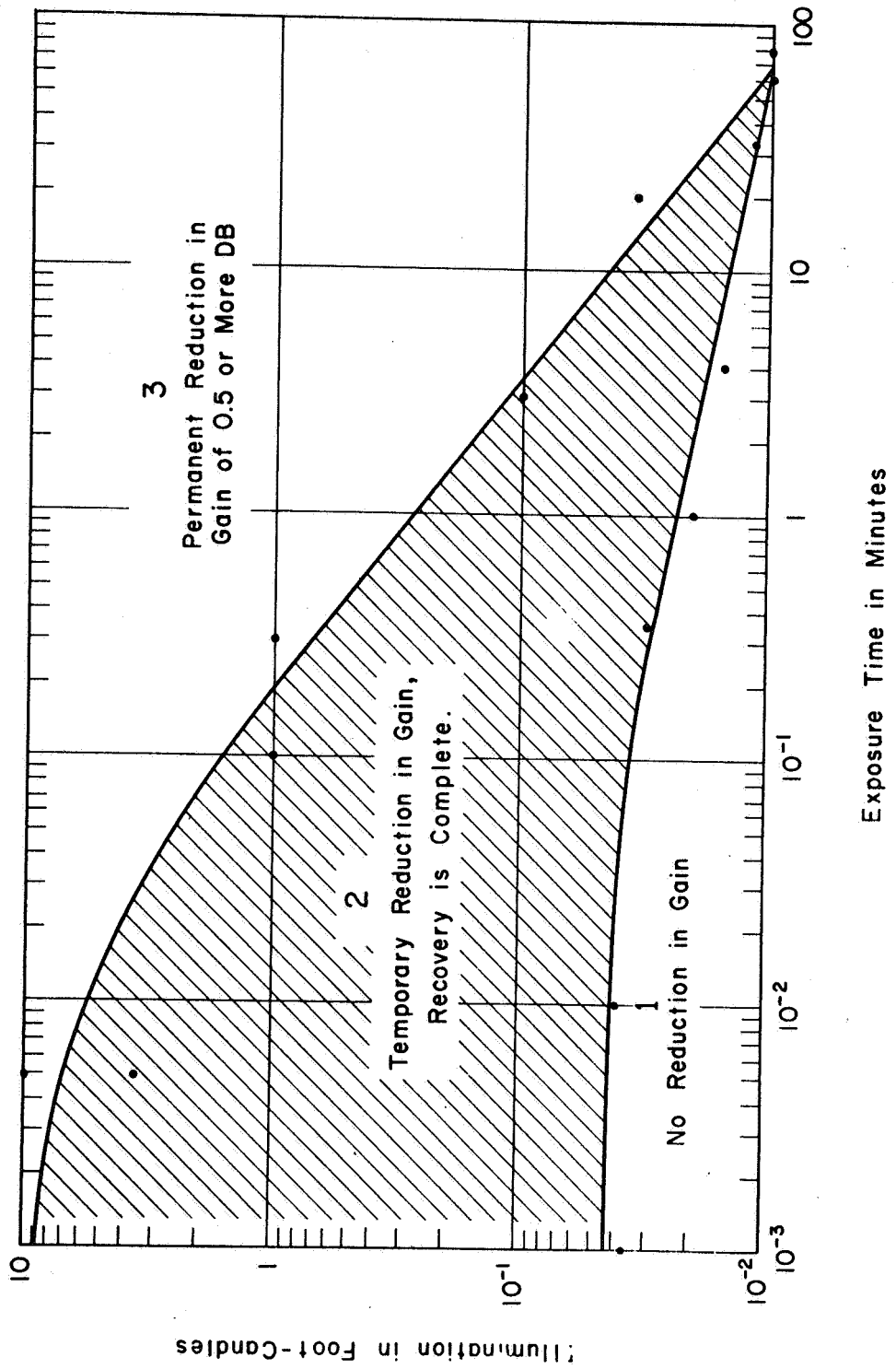

FIG. 5 : Target Behavior For Various Exposures

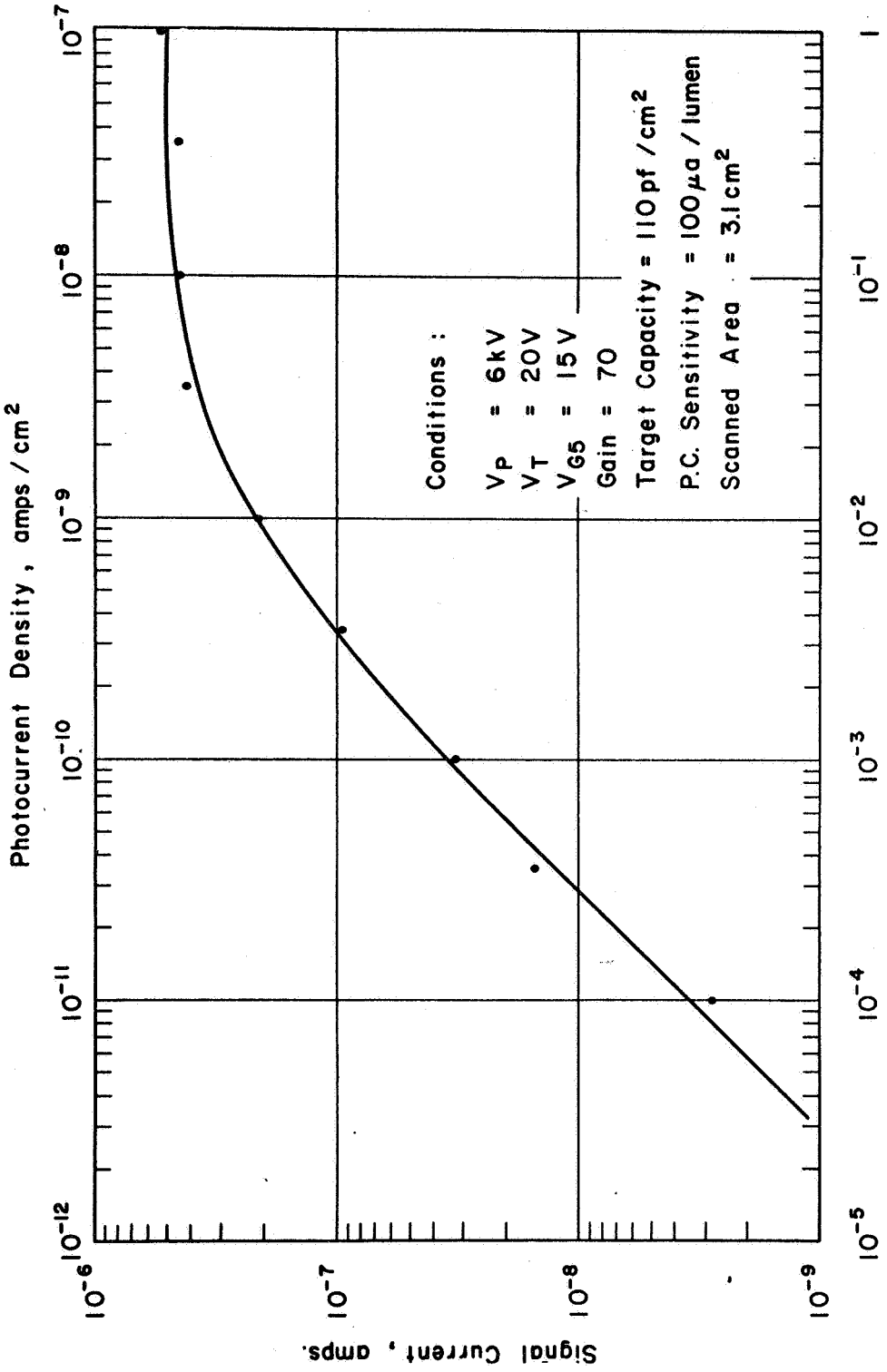

FIG. 6 : Transfer Curve of Tube #6444036

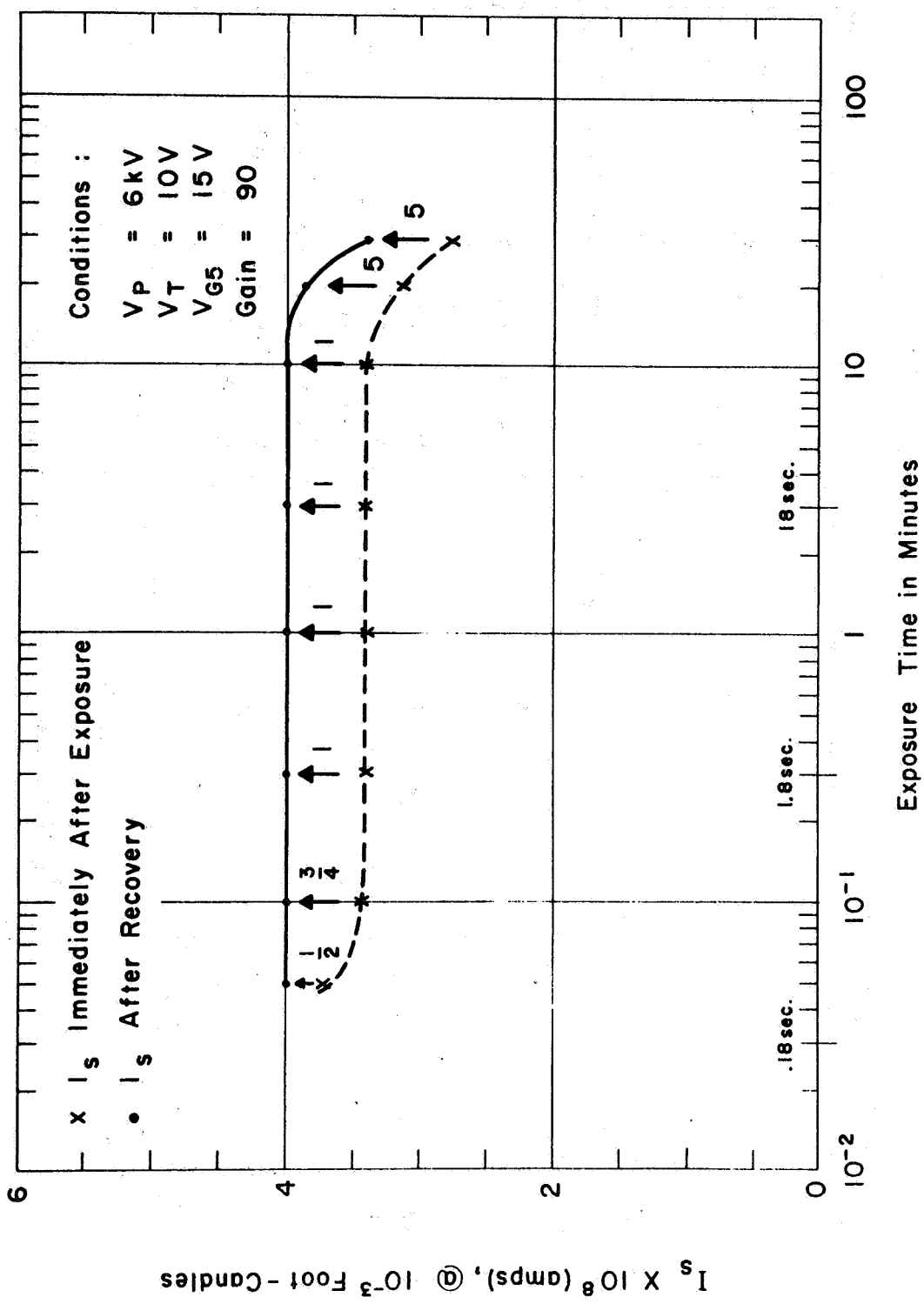

FIG. 7 : I_s vs Exposure Time @ 10 Foot-Candles

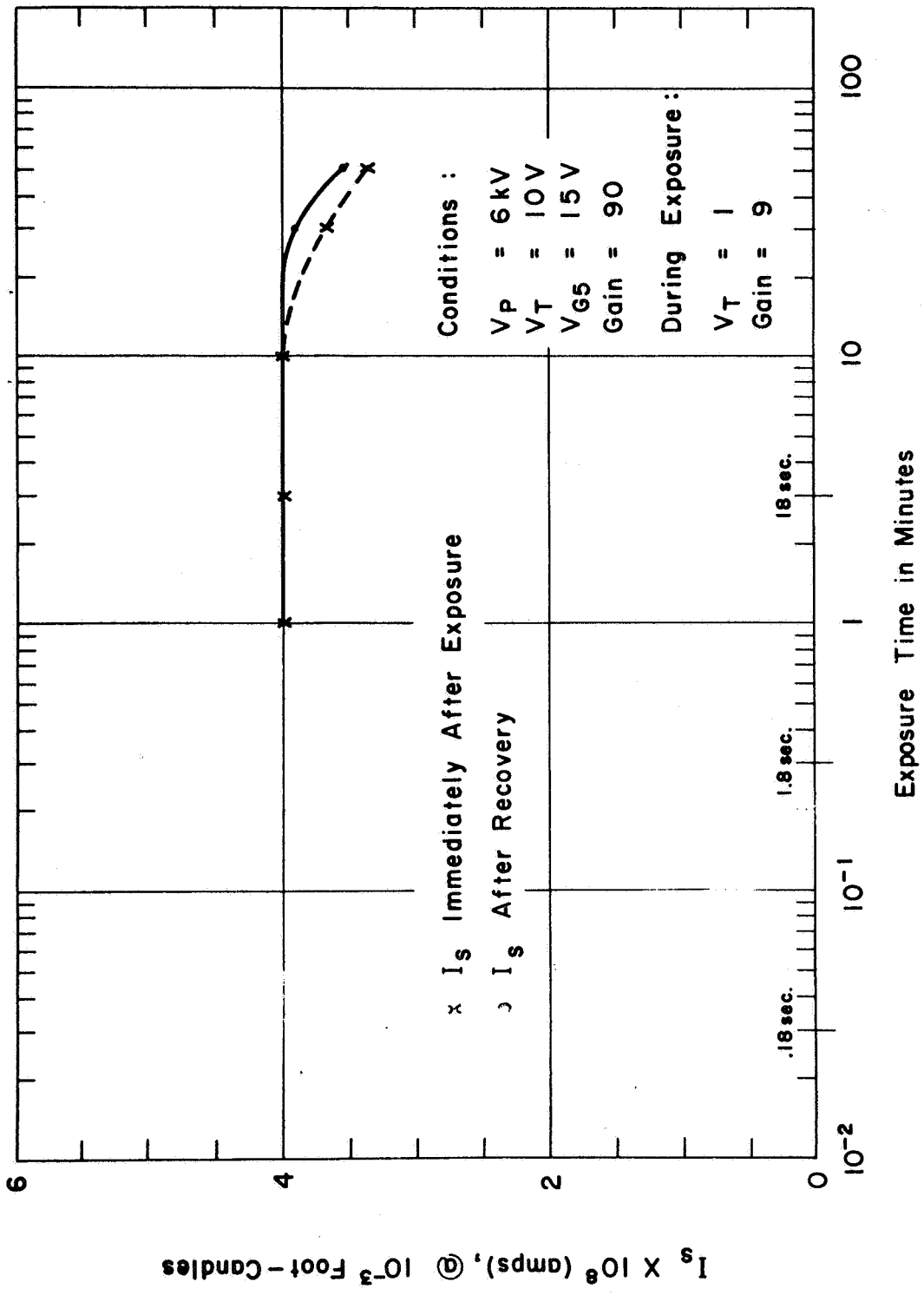

FIG. 8 : I_s vs Exposure Time @ 10 Foot-Candles

APPENDIX F

MOISTURE DAMAGE TO THE SEC TARGET

From: ELMIRA WORKS

Date: March 1, 1965

Subject: Blemishes In The SEC Target

TO: G. W. GOETZE, MANAGER
Image Tube R & D

PURPOSE:

The purpose of the investigation was to determine if blemishes are produced in an SEC target by exposure to moist air.

EXPERIMENTS:

An SEC target was evaporated under standard conditions and placed into a demountable camera tube with the least possible handling time. The camera tube was pumped continuously with a Vac Ion pump and kept at a typical pressure of 10^{-7} Torr. The target was operated in a standard manner, the video signal displayed on a monitor and photographs taken from the monitor with an exposure time of 0.5 - 1 sec. The system was opened and the target placed in a humidity chamber for a given time. The chamber was kept at a relative humidity of 30% by a saturated solution of aqueous $CaCl_2$ in equilibrium with solid $CaCl_2$. The target was retested and then exposed in the humidity chamber for a further period.

RESULTS:

Figure 1 shows a series of photographs of the same target. Photograph A shows the target with no previous exposure to moist air at a target voltage of 20 V with no input illumination. The target was overscanned and the white and black rings are the result of beamlanding on the target mount. Photograph B was taken after a 15 minute exposure to a relative humidity of 30%. The target was operated under the same conditions as for Photograph A. Photograph C was obtained after a second exposure, this time for one hour at 30% relative humidity. Photographs D through F show the same target operated at a target voltage of 10 V but with a uniform input illumination. The exposure of the target to humidity in the pairs of photographs A and D, B and E, and C and F are the same. It should be noted that the slight nonuniformities and the dark areas in photographs E and F are caused by variations in photocathode emission and are not relevant to the present discussion.

As can be seen, an SEC target once exposed to moist air develops white blemishes and grain.

The extent of the damage to the target depends on the level of humidity and the exposure time. It is also observed that the target readout speed becomes progressively slower and the TSE gain falls under these circumstances.[1]

It should be noted that a relative humidity of 30% can be produced by inserting 1 mg water into a volume equal to that of the LCT at 25°C.

R. R. Beyer

mlr
Attach.

REFERENCE:

(1) M. Green, R.R.Beyer Second Interim Engineering Report Contract No. AF 33 (615)-1271 (February 1965)

Figure 1 MONITOR PHOTOGRAPHS OF AN SEC TARGET

A: V_T : 20 V
No illumination
No exposure

D: V_T : 10 V
Illumination
No exposure

B: V_T : 20 V
No illumination
1. Exposure: 15 min.
30% relative humidity

E: V_T : 10 V
Illumination
1. Exposure: 15 min.
30% relative humidity

C: V_T : 20 V
No illumination
2. Exposure: 1 hour
30% relative humidity

F: V_T : 10 V
Illumination
2. Exposure: 1 hour
30% relative humidity

A

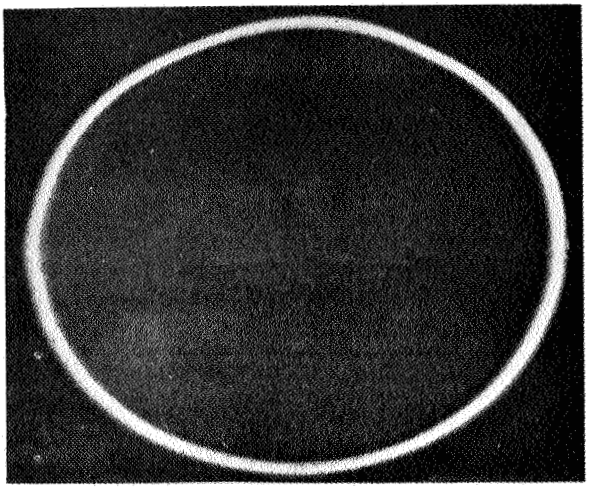

D

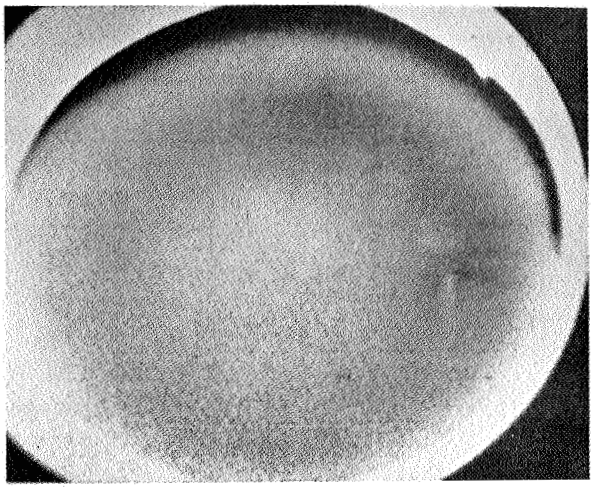

B

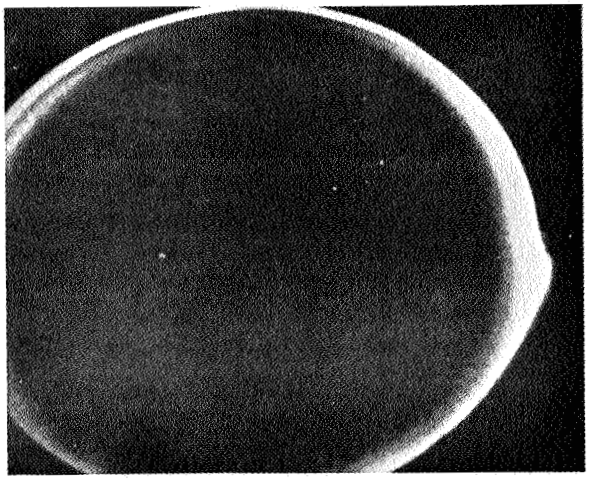

E

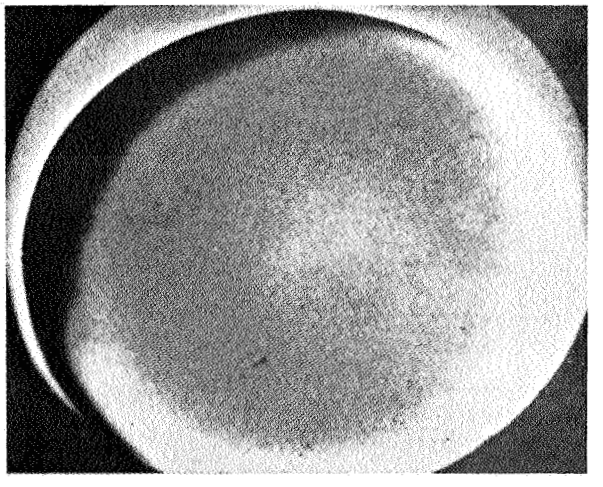

C

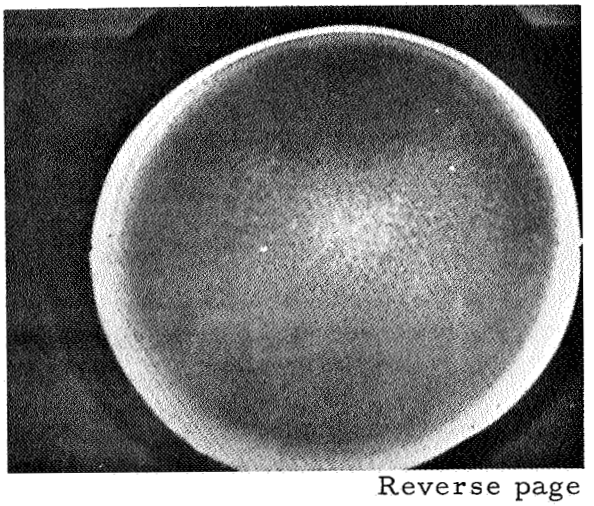

F

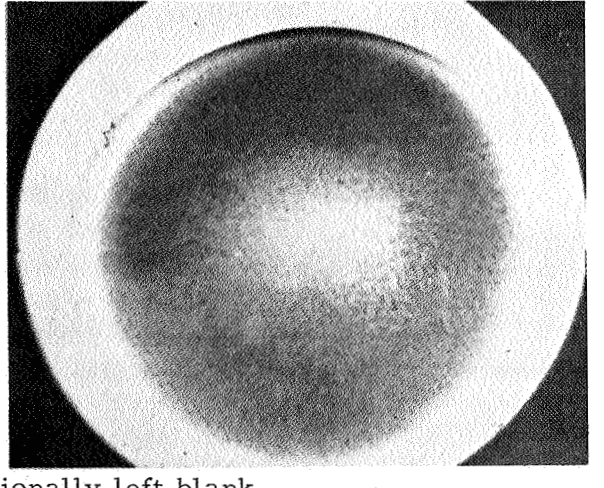

Reverse page intentionally left blank

6693D-PF-12

APPENDIX G

A RESOLUTION STUDY PROGRAM FOR THE LUNAR CAMERA TUBE

ET-21
August 26, 1966

FINAL REPORT ON THE RESOLUTION STUDY PROGRAM FOR THE LUNAR CAMERA TUBE

J. Vine

Lunar Camera Tube Program
Purchase Order No. 86KP-87-96641-OS
from Westinghouse Aerospace Division
Prime Contract NAS9-3548
from NASA Manned Space Craft
Center, Houston, Texas

This report is prepared to cover a specific technical phase of the program as required by contract.

Approved by

R. A. White
Program Manager
Lunar Camera Tube

M. Green
Engineering Manager
Image Tube Department

The work reported here was performed in the Image Tube Department of the Westinghouse Electronic Tube Division, Elmira, New York, under the direction of Dr. G. W. Goetze.

CONTENTS

1. INTRODUCTION

2. VIDICON STUDY

2.1 Operating Potential

2.2 Field-Mesh Target Spacing

2.3 Beam Limiting Aperture

2.4 Focusing Mode

2.4.1 Alternative G3 Connections

2.4.2 "Inverted" Focus Lens

2.4.3 Bipotential Lens Operation

2.5 Field Mesh Pitch

3. SUPPRESSOR-MESH VIDICONS

3.1 Variation of Suppressor Potential

3.2 Field-Mesh Target Spacing

3.3 Suppressor Mesh Pitch and Spacing

3.4 Focusing Mode

3.5 Magnetic Focus

3.6 Single Mesh Tube

4. IMAGE SECTION

4.1 Image Section Construction

4.1.1 Image Diode

4.1.2 Bellows Diode

4.1.3 Triode Image Section

4.2 Determination of Design Centers

4.3 Resolution Measurements

4.4 Computational Analysis

5. LCT RESOLUTION

6. CONCLUSIONS

ABSTRACT

This study program was undertaken to improve understanding of the electron optical properties of the Lunar Camera Tube and to determine the feasibility of extending the resolution of the tube beyond the level of the original specification. Separate studies of the reading section and the image section were carried out by the construction and testing of experimental hybrid vidicons and image intensifiers. Work on the reading section was concerned particularly with the effects of the suppressor mesh. The results of these experiments are discussed in detail, and conclusions are drawn regarding design changes favorable to resolution. Some of the suggestions made have already been incorporated into the Lunar Camera Tube. The original resolution specification is shown to be very close to the limiting performance that can be attained in this tube, without some basic improvement to the triode gun, or without a modification to the SEC target that will permit it to operate without a low voltage suppressor mesh.

FOREWORD

The author of this report was the project leader on the study program described, under the supervision of Mr. R. A. White, Lunar Camera Tube program manager. The help of many colleagues, both within and outside the Lunar Camera Tube team, is gratefully acknowledged. In particular, Mr. R. P. Carpentier was responsible for the construction and testing of all the experimental vidicons, and many of the graphs presented in Sections 2 and 3 are reproduced directly from his results. The meticulous work of Mr. W. E. Merritt in the construction and measurement of the experimental image sections was instrumental in clearing up difficulties in that area of the tube. Dr. G. R. Feaster contributed significantly in the early stages of that work. Specific contributions from several other people are mentioned in the text.

1. INTRODUCTION

The resolution study program on the Lunar Camera Tube was started in July, 1965, as a result of disappointment with the performance of early tubes. The original resolution specification called for a 40% aperture response at 250 TV lines/picture height and 5% at 400 TV lines/picture height, these figures having been based on data available on the image section and the 1" hybrid vidicon. The deficiency of the early tubes appeared to be attributable to two factors that had not been fully appreciated. One of these factors was the critical dependence of the image section resolution on the precise shaping of the anode cone tip, and the other was the degrading effect of the suppressor mesh on the resolution of the reading section. The objective of the study program was to improve our understanding of these and other factors, and so to re-assess the potentialities of the tube. We wished to consolidate the performance of production tubes at the level of the original specification and to determine the feasibility of going beyond that level. The TV systems group had indicated a desire to raise the resolution specification to a 40% response at 300 TV lines/picture height and 5% at 600 TV lines/picture height.

Work was started on the electron optics of the image section and the reading section. The resolution capability of the image section being inherently high, effort in that area was directed towards establishing the correct dimensions and the constructional accuracy necessary to realize

the full potential in production tubes. The reading section was recognized as the prime limitation to resolution in the complete tube, and in this area the possibility of basic redesign was contemplated if an advantageous electron optical configuration could be determined. Work on this section included a study of the effects of various parameters on the performance of hybrid vidicons both with and without suppressor meshes.

No study of the SEC target resolution capability was made, that being the subject of other research programs in progress. At the present stage of development the target does not appear to be an important limitation to resolution in the Lunar Camera Tube.

2. VIDICON STUDY

A diagram of the electron-optical components of an orthodox 1.0" vidicon is shown in Fig. 1. This diagram shows schematically the action on the electron beam of the focus lens (G3-G4-G5), the deflection yoke, and the collimation lens (G5-G6). The table shows the nominal operating voltages for three cases which will be referred to as low, medium, and high voltage operation. Normally the tube is operated with G3 connected directly to G6 and carrying the highest potential in the tube. Other methods of operation are possible and some of them will be discussed in the following pages.

In principle, the electron optical action of the tube may be described as an imaging, with approximately unit magnification, of the small source of electrons represented by the beam-limiting aperture, onto the target. In detail, the action is rather complex and it is not well established whether the beam-limiting aperture acts simply as a small object, or partly as an aperture-stop as well. Apart from the aperture size and the magnification factor, the size of the spot at the target is affected by spherical aberration in the focus lens, and possibly by chromatic aberration (spreading effects due to the variable emission energies of the electrons). Practical evaluation of these details is greatly complicated by the poor mechanical alignment that is achieved with existing constructional techniques, due to which it is necessary to employ electrical

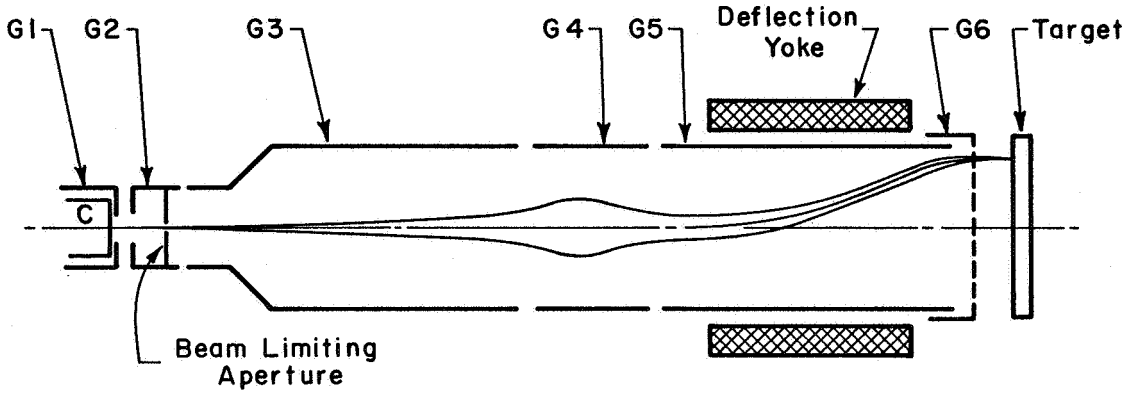

OPERATING POTENTIALS

Voltages	C	G1 (Typical)	G2	G3	G4 (Approx.)	G5	G6	Target (Typical)
Low Voltage	0	-40	300	300	50	180	300	15
Medium Voltage	0	-40	300	600	90	300	600	15
High Voltage	0	-40	300	1000	150	500	1000	15

6693D-VA-22

FIG. 1 ELECTRON OPTICS OF THE VIDICON

alignment of the beam during operation. This is done by means of small coils in the vicinity of the G1-G2 gap. Ideally, the beam needs to be centered on the limiting aperture for maximum transmission of current. It should travel centrally through the focus lens for nonastigmatic focusing and emerge centered along the axis of the collimation lens for good landing uniformity. Since only one alignment adjustment is available for each of two perpendicular directions, some compromise between these various objectives has to be accepted. Optimum adjustment of the alignment currents is probably the most critical single factor affecting resolution performance of the tube. This has an important bearing on the study described here because mechanical alignment represents an uncontrolled variable which may be responsible for appreciable resolution differences between tubes.

The principal geometrical parameters that are electron-optically significant can be listed, together with what will be referred to as their standard values:

beam-limiting-aperture diameter	0.0018"
G6 - target spacing	about 0.100"
field mesh (G6) pitch	750 line/inch

During the program variations of these parameters were studied, together with variations of operating potentials and electrode interconnections. A total of 25 orthodox vidicons were built, details of which are summarized in Table 1. Also included are tubes 264 and 265 which, although built for a special experiment in the suppressor mesh study (see Section 3.6), were capable of operation as orthodox vidicons with very small G6-target spacing.

TABLE 1 VIDICON DETAILS

Tube No.	Internal Conn.	Aperture	Heater-Cath Type	Special Features	Field Mesh Lines/Inch	G6-Target Spacing	Normal Response at 300 Lines
32	G3-G6	.0018"	1 watt	Sb_2S_3 photoconductor	750	.205"	34%
33	-----	.0018"	"	" "	750	.140"	38
34	-----	.0008"	"	" "	750	.135"	44
35	G3-G6	.0018"	"	----------	750	.080	44
36	"	.0018"	"	----------	750	.115	47
37	"	.0018"	"	----------	750	.050	44
38	"	.0018"	"	----------	750	.075	46
39	"	.0018"	"	----------	750	.190	44
40	-----	.0018"	"	----------	750	.080	45
41	-----	.0010"	"	----------	750	.085	52
6540012	-----	.0018"	"	.040" aperture stop	750	.130"	48
6540013	-----	.0018"	"	.100 " "	750	.130"	48
6540040	G3-G6	.0018"	"	----------	750	.210"	44
6540046	"	.0018"	"	----------	750	.310"	39
6540050	"	.0006"	"	"precision" triode	750	.105"	62
6540058	"	.0018"	"	" "	750	.100"	38
199	"	.0018"	0.2 watt	----------	750	.125"	52
228	"	.0007"	1 watt	"precision" triode	750	.100"	60
229	"	.0007"	"	----------	750	.105"	62
264	G3-G5	.0018"	0.2 watt	special experiment	1000	.010"	41
265	"	.0018"	"	see Sect. 3.6	1000	.030"	49
255	G3-G6	.0018"	"	----------	2000	.105"	43
259	"	.0018"	"	----------	750	.125"	48
6608091	"	.0018"	1 watt	----------	500	.135"	39
6608009	"	.0018"	"	cat. coated cathode	500	.115"	30
297	"	.0018"	0.2 watt	----------	500	.125"	44
304	"	.0018"	"	----------	750	.130"	47

Se target unless Sb_2S_3 specified.
Standard triode unless precision specified.

6693D-VA-23

2.1 Operating Potential

It is well known that vidicon resolution improves with increasing tube voltages, and this effect has been observed consistently on all vidicons tested. Examples are shown in Fig. 2, which gives aperture response curves for vidicons 35 and 36. Their performance is typical. A steady improvement in resolution is obtained with increasing voltage and a considerable further improvement when magnetic focusing is employed. Both these facts are consistent with the theory that sperhical aberration of the main focusing lens is a prime limitation to resolution of the hybrid vidicon. At high voltage operation the lens effect bewteen G2 and G3 is increased (because the G2 voltage remains fixed at 300 while G3 voltage increases). This has the effect of reducing the beam angle into the main focusing lens, which can explain, at least qualitatively, the improved perfomrance as due to reduction of the aberration disc. It should be realized that this reasoning is rather superficial, because the conjugates of the multiple lens system change, as well as the beam angle. A full explanation of the effects of voltage changes would therefore require a much deeper analysis.

2.2 Field-Mesh Target Spacing

A number of tubes have provided evidence on the effect of varying target-G6 spacing. Results from 12 tubes, identical except for this parameter, are summarized in Fig. 3. The three graphs correspond to three different operating voltages; 300, 600, and 1000 volts. Each curve connects aperture response values at a fixed line number for tubes with various

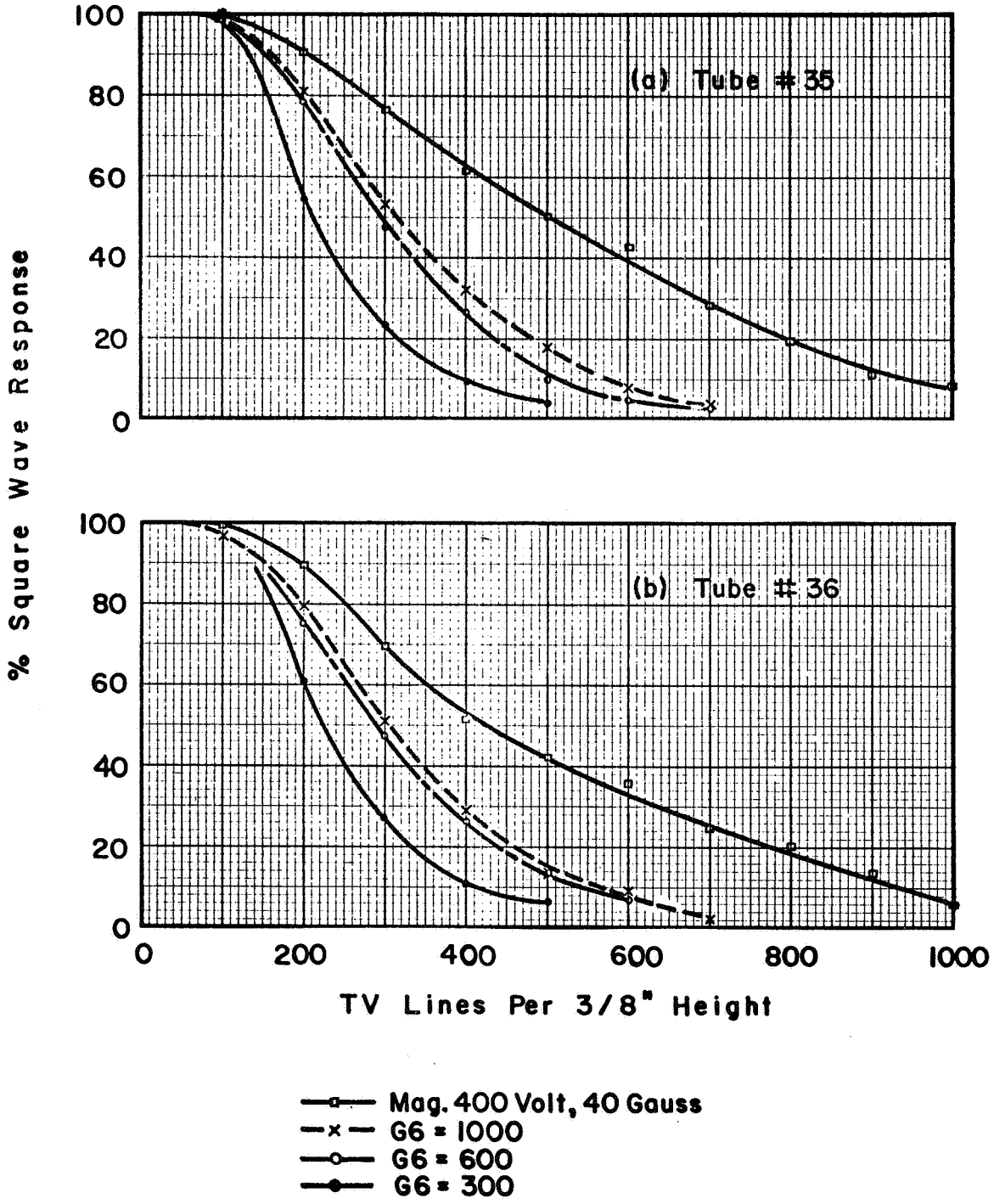

FIG. 2 STANDARD VIDICON - VARIATION OF APERTURE RESPONSE WITH OPERATING VOLTAGE

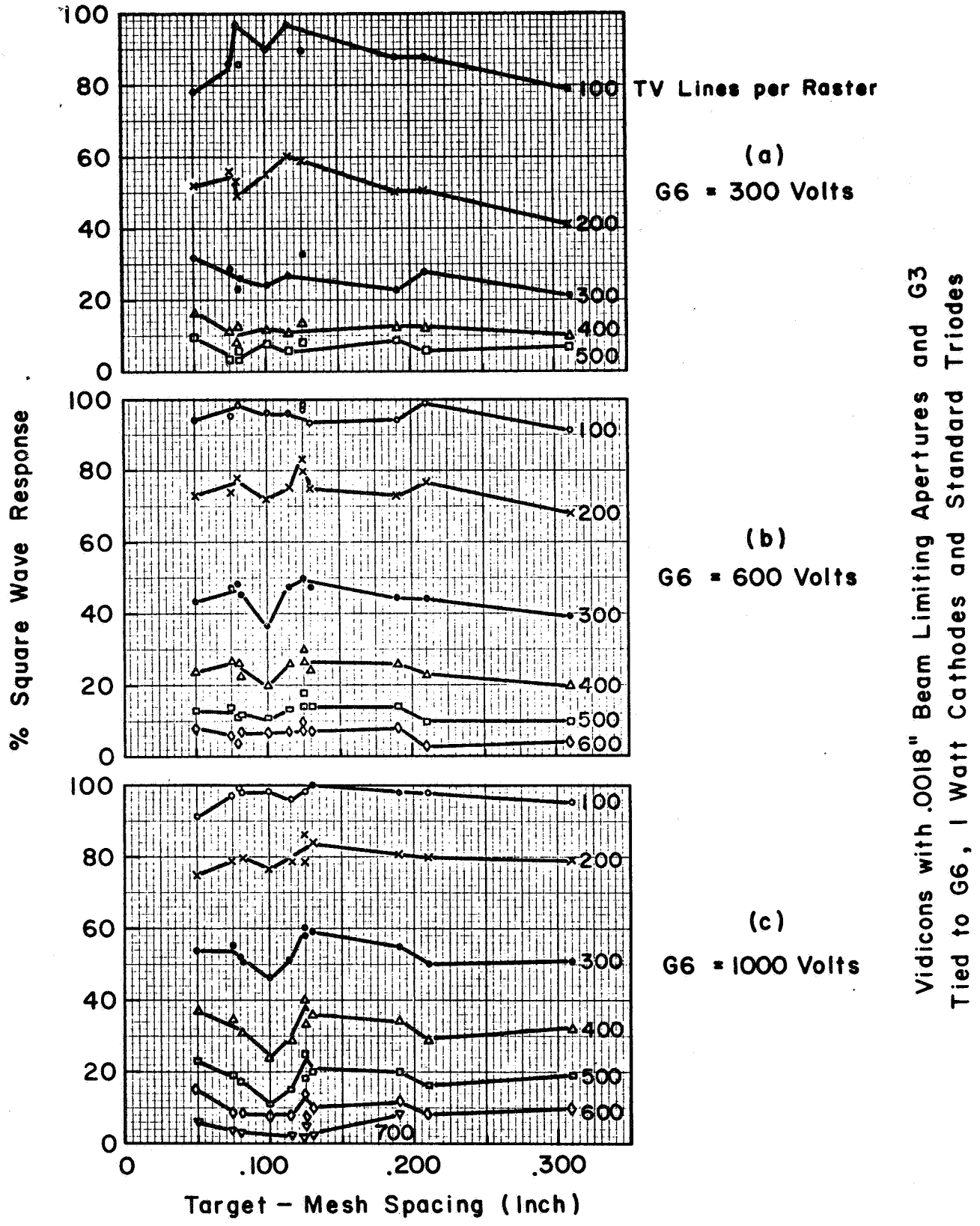

FIG. 3 APERTURE RESPONSE AS FUNCTION OF TARGET-MESH SPACING

spacings. Curves for 100, 200, etc. TV lines per raster height are shown. No clear cut trend is indicated by these results. The tube with .310 spacing is a little worse than other tubes at low voltages, but at 1000 volts, its performance is about average. The spread in response is quite large - as much as 15% in the 300 TV line region. This results from small uncontrolled variations in the tubes, and the inaccuracies inherent in the test procedure. One tube with 0.125" spacing (tube 199) is particularly good, while the tube with 0.100" spacing (tube 6540058) is rather poor.

Tubes 32 and 33, which have the correct geometrical properties for inclusion in this graph, were omitted. These two tubes, the first constructed in this study, have Sb_2S_3 photoconductors instead of the selenium type used in the other tubes, and both show poor resolution. It seems doubtful that the poor resolution can be attributed to the photoconductor, but it does not seem wise to include the tubes in Fig. 3. Together with tube 34, which also has an Sb_2S_3 photoconductor, they can be considered as a separate group (see Section 2.4).

From the data in Fig. 3, we conclude that resolution is not sensibly dependent on target-G6 spacing over the range 0.050" to 0.300". It should however be realized that uniformity problems might arise with very large spacings, due to possible non-uniformity of the decelerating field. This would depend on the location of other tube members outside the large gap. Such effects were not observed in this study, but they were not specifically sought.

The range of permissible spacings can be extended down to 0.010" as a result of experiments on tubes 264 and 265. These two tubes were built for a special experiment which will be described in Section 3.6 but were capable of operation as orthodox vidicons with very small target-G6 spacing, in which mode they gave resolution comparable to other vidicons with 0.001" beam limiting apertures.

The conclusion reached here implies that there is no significant chromatic aberration effect in the tube. Spot-spreading due to emission energies should be dependent on transit time which, for a given voltage, increases with target-G6 spacing. This further supports the suggestion made in Section 2.1 that resolution improvement with increasing operating voltage is due to reduction of spherical aberration. In an attempt to study further the spherical aberration effect, tubes 6540012 and 6540013 were built (See Table 1). These tubes have aperture stops located in field-free space in the G3 cylinder, such as to limit the incident beam total angle to 0.04 and 0.10 radians respectively. The results from these tubes are not included in Fig. 3. Both showed good but not exceptional resolution. It is likely that neither aperture stop was really effective in restricting the incident beam angle, although the smaller of the two appeared to intercept the beam to some extent, making alignment difficult and requiring large grid drive voltage. The alignment difficulty would probably vitiate any experiment with still smaller aperture stops with which effective beam-angle limitation might be obtained, and so this approach was not pursued further.

2.3 Beam Limiting Aperture

All results given in Figs. 2 and 3 are for vidicons with beam limiting apertures of approximately .0018" diameter. Several vidicons have been built with smaller apertures. Three vidicons with different aperture sizes are compared in Fig. 4. Each graph corresponds to a different mode of operation. In the hybrid mode, at all operating voltages, there is a clear substantial resolution improvement with decreasing aperture size. Tube 40 is typical of vidicons with .0018" apertures (see Fig. 3). It was constructed at the same time as tube 41, the aperture sizes being the only intended difference between the two. Tube 6540050 was made at a later date and differs from the others in having a slightly larger target-G6 spacing, and a precision triode instead of the standard triode. Neither of these factors is thought to influence resolution.

Fig. 4(c) compares the performance of the tubes when magnetically focused. There does not appear to be any clear trend. It seem likely that the important action of the smaller aperture is reduction of the beam angle into the focusing lens, resulting in improvement in the hybrid mode through reduction of the spherical aberration disc.

Tubes 228 and 229 provide further evidence on the effect of smaller apertures. These tubes have apertures of 0.0007" diameter and show resolution similar to tube 6540050. A further comparison is made in Fig. 5, between tubes 33 and 34 which have beam limiting apertures of 0.0018" and 0.0008" respectively. Superiority of the smaller aperture is less marked in this case. As mentioned earlier, these tubes and tube 32,

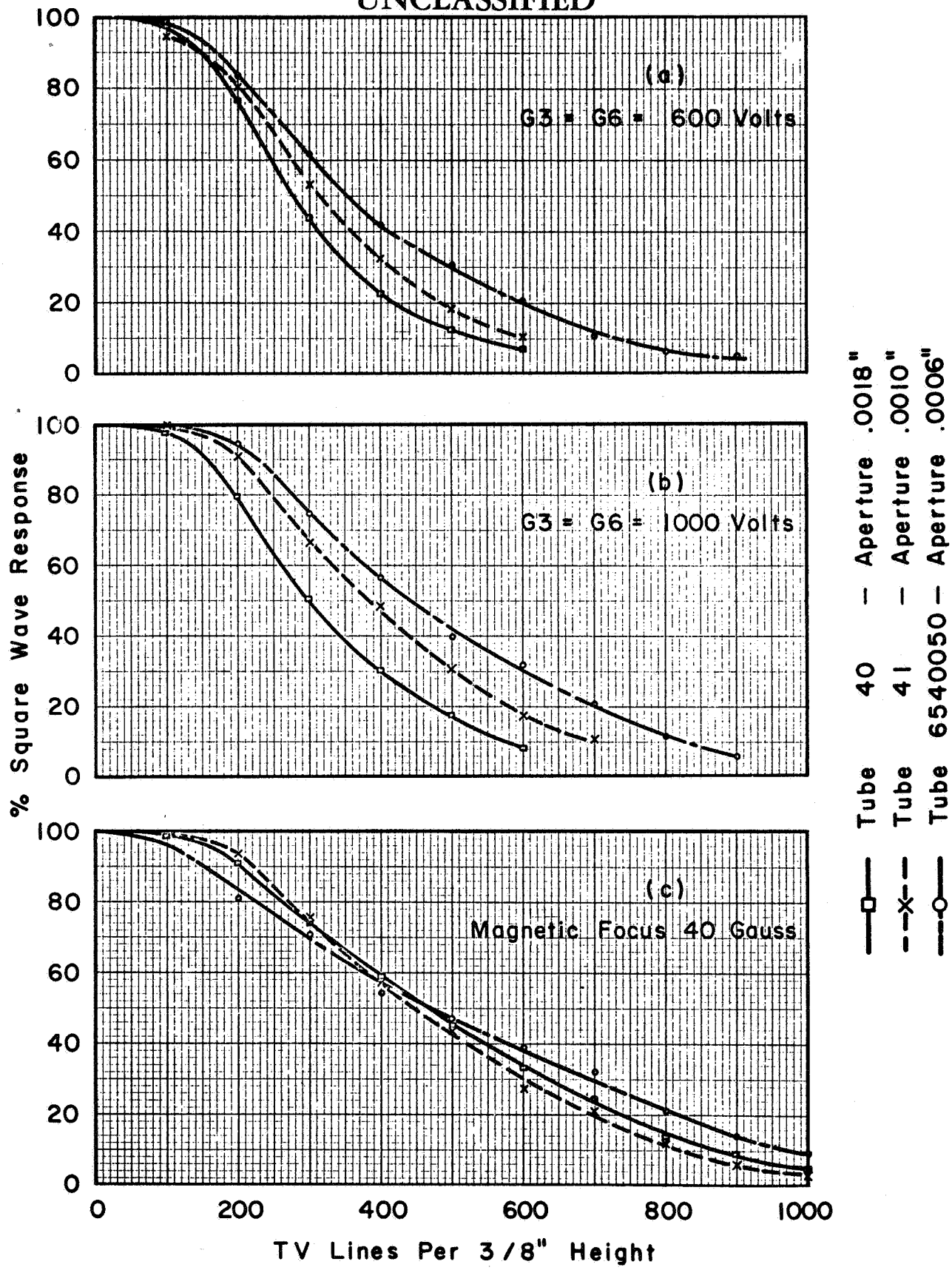

FIG. 4 RESOLUTION VARIATION WITH BEAM LIMITING APERTURE

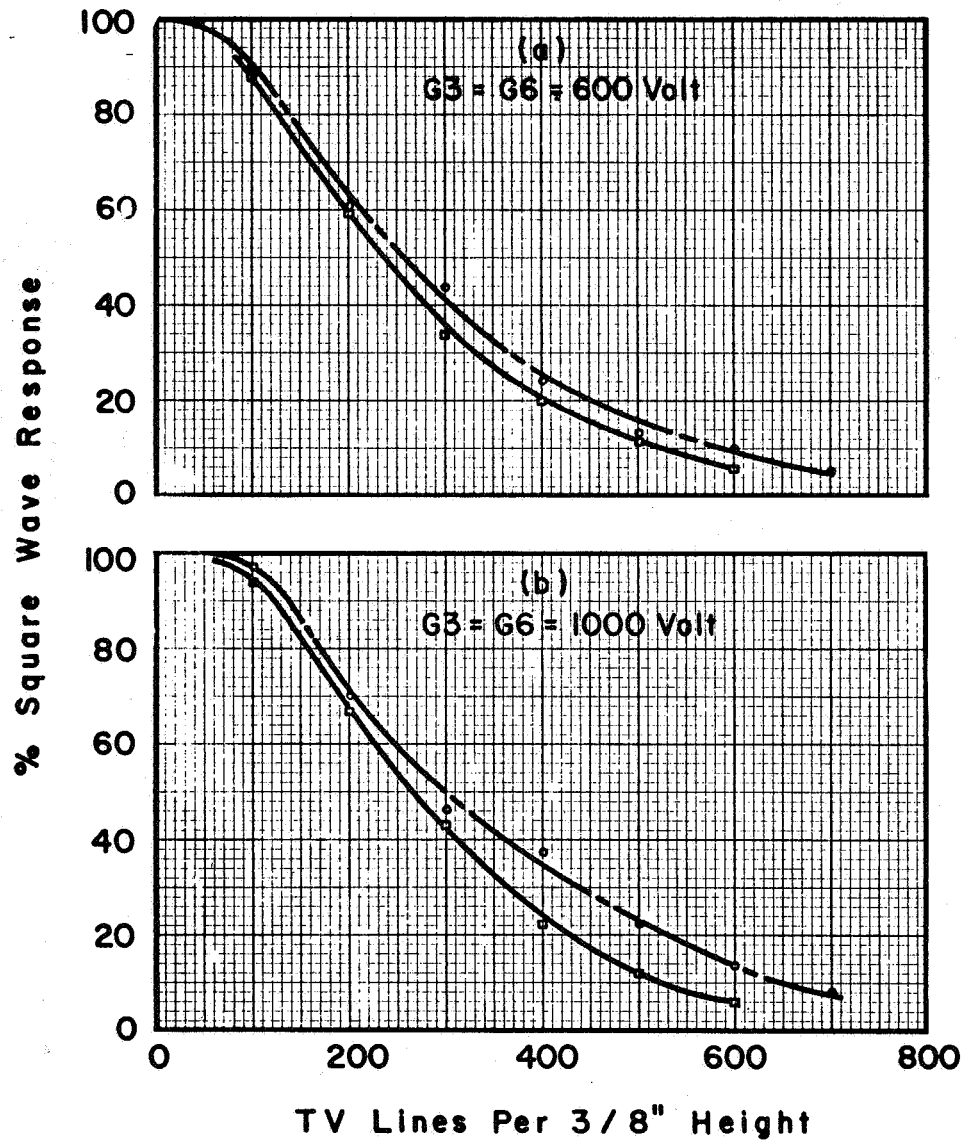

FIG. 5 RESOLUTION VARIATION WITH BEAM-LIMITING APERTURE

—□— Tube 33 Aperture .0018"
—o— Tube 34 Aperture .0008"

as a group, exhibit relatively low resolution, possibly due to use of an Sb_2S_3 photoconductor instead of the standard selenium.

A disadvantage of the smaller aperture is the need to drive the cathode harder in order to maintain the required beam current at the target. This is evidenced by the G1 voltages of 38 and 18 on tubes 41 and 6540050 respectively, compared with the more typical value of 55 on tube 40. These tubes had 1 watt cathodes, which were able to supply the additional total current without difficulty.

2.4 Focusing Mode

The potential values listed in Fig. 1 are those used in the standard method of focusing a vidicon. In this condition the main focusing lens, G3-G4-G5, is an unsymmetrical three-cylinder lens. Various other possible arrangements exist and some study was made of their relative merits.

2.4.1 Alternative G3 Connections

In the past vidicons have been constructed alternatively with G3 internally connected to G5 or to G6. In this program tubes were built with all three of these electrodes isolated on separate pins so that the merits of the two alternative connections of G3 could be examined. This study was inconclusive. Of six tubes, three showed systematically slightly better resolution with G3 connected to G5, and one was better with G3 connected to G6. The other two performed almost identically in the two modes. With G3 connected to G5, the focus lens becomes a symmetrical three-cylinder lens.

Typical operating voltages are:

	G2	G3	G4	G5	G6
Low voltage	300	180	40	180	300
Medium voltage	300	300	60	300	600
High voltage	300	500	100	500	1000

A point which may have some bearing on this question concerns the motion of positive ions. With the G3-G6 connection, ions formed in the main volume of the tube will tend to be trapped, whereas with G3 at the lower G5 potential, some ions formed in the G6 region would be capable of penetrating to the thermionic cathode.

2.4.2 "Inverted" Focus Lens

The orthodox operation of the three-cylinder lens sets the central cylinder G4 at lower potential than its neighboring cylinders G3 and G5. Operation with G4 at higher potential than G3 and G5 ("inverted" mode) is thought to result in lower spherical aberration. Fig. 6 shows results of an investigation of this effect in tube 40, an orthodox vidicon with .0018" beam limiting aperture and .080" target-G6 spacing. Fig. 6(a) is a striking illustration of the improved performance of the focus lens in the inverted mode. The lower curve is for ordinary low voltage operation, for which it represents typical performance. The upper curve was obtained immediately after the lower, simply by raising the G4 potential until the tube was refocused. This curve is comparable to that obtained in orthodox high voltage operation, as can be seen from the direct comparison made in Fig. 6(b). However, it is to be noted that in the inverted mode the improved resolution is obtained without increased scanning power, since the G5 and G6 potentials remain low. Scanning power requirement is roughly

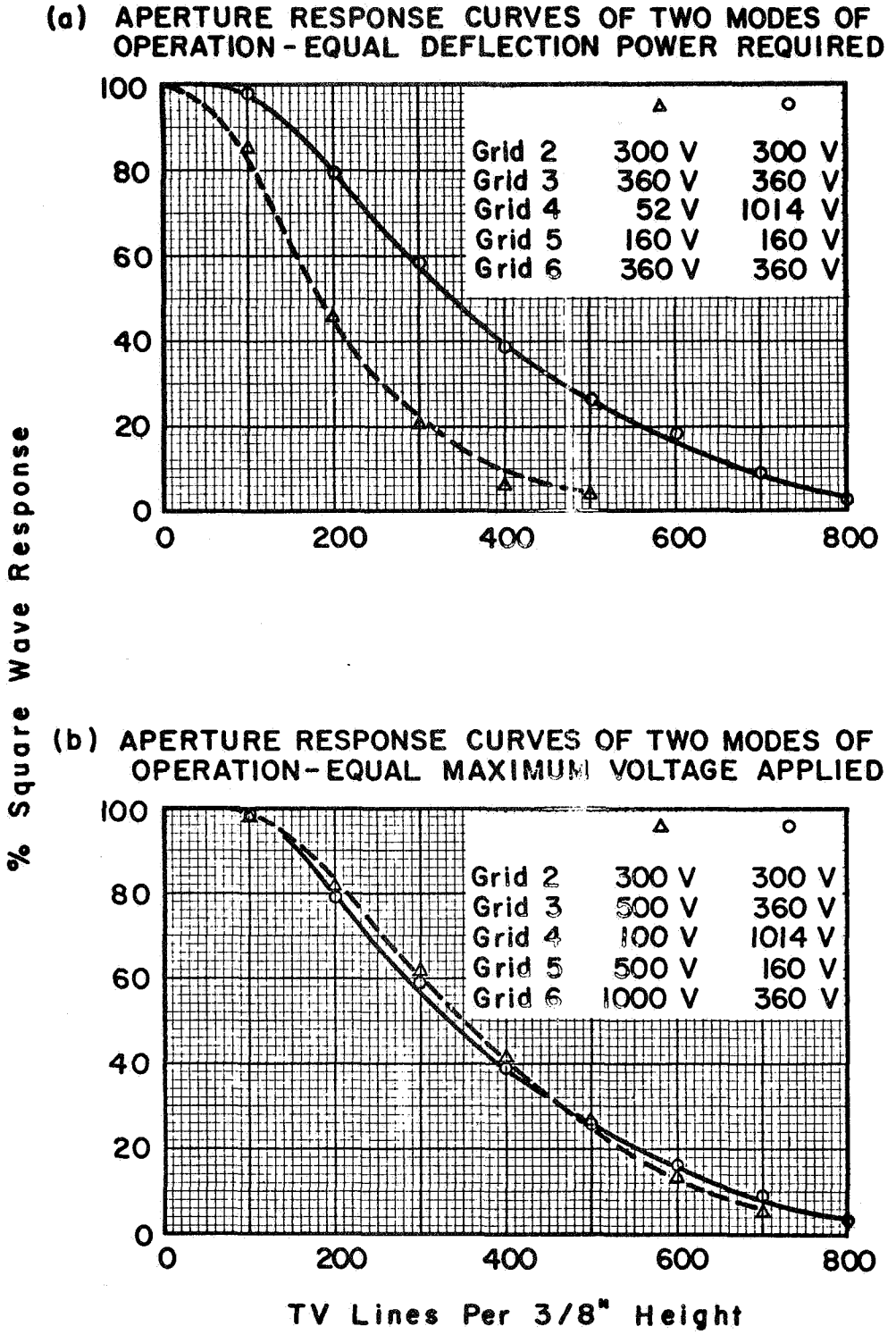

FIG. 6 TUBE 40 COMPARISON OF ORTHODOX AND INVERTED OPERATION OF FOCUS LENS

proportional to the G5 and G6 potentials and so is normally increased by a factor of 3 in changing to high voltage operation, Fig. 6(b) shows that orthodox and inverted lens operation offer about the same resolution for a given maximum voltage in the tube. In the inverted mode apart from the reduction in scanning power, the fact that G6 is set at a low potential has additional significance in tubes having a suppressor mesh, as will be discussed in Section 3. The electrode voltages used in this experiment are listed in Fig. 6.

Tests on other tubes largely confirmed the conclusions drawn from Fig. 6. Tubes 255, 259, 6608091 and 6608009 all performed in the inverted mode as well as, or slightly better than, in the normal mode for a given maximum applied voltage. The last two vidicons built, 297 and 304, performed less well in the inverted mode.

2.4.3 Bipotential Lens Operation

The focus lens of the vidicon can be made into a bipotential lens by connecting G4 either to G3 or to G5. Focusing can be achieved either with the accelerating or with the decelerating form of lens. Four different types of bipotential focusing are thus possible. No extensive study of these operating modes was made in this program. Some results obtained from tube 41 are shown in Fig. 7. Fig. 7(a) shows the results of decelerating bipotential operation at three voltage levels, with G4 connected to G3. The curves are quite similar to those for normal operation at the equivalent voltages. A direct comparison between normal, inverted and bipotential modes of operation is made in Fig. 7(b) for the

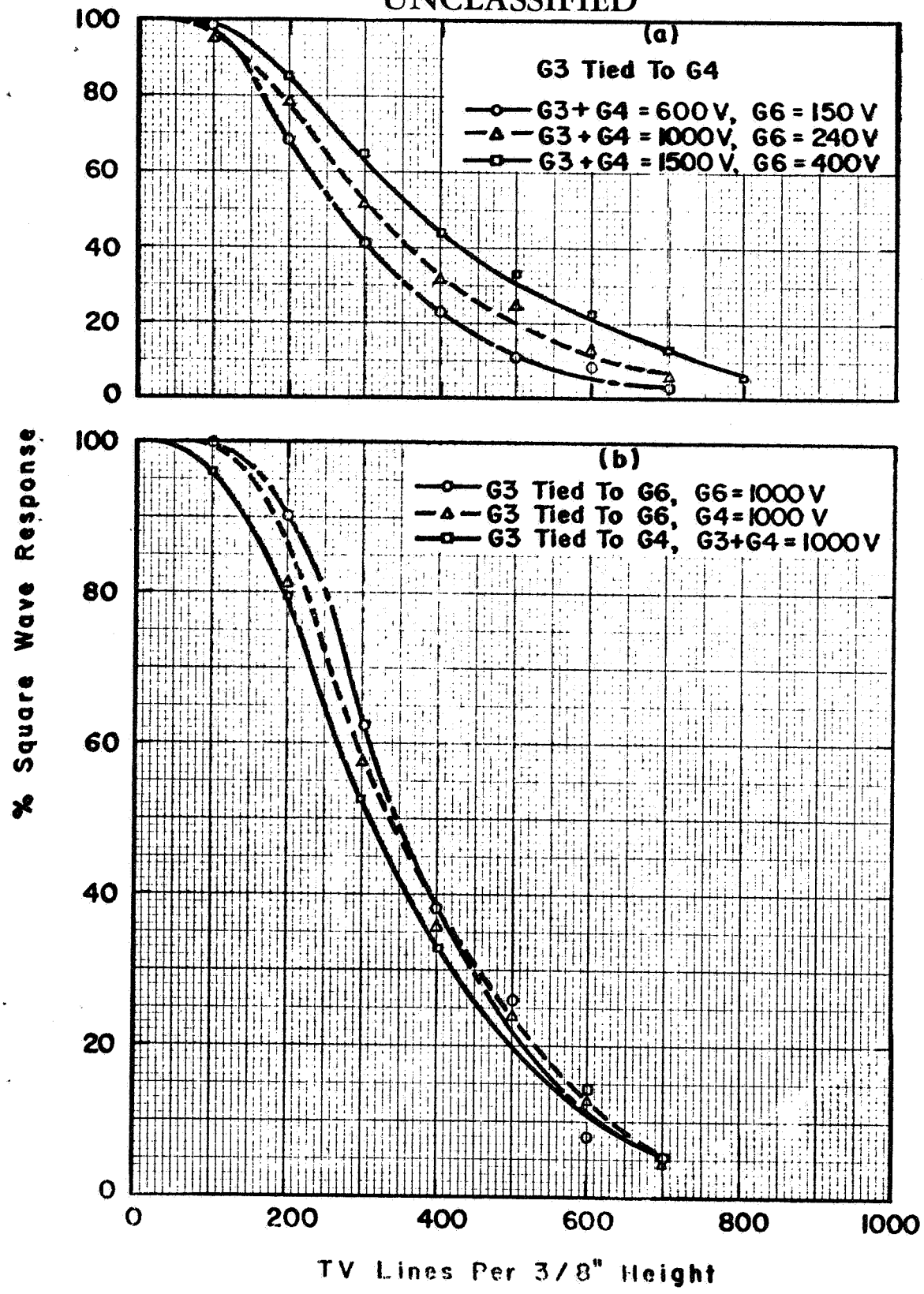

(a) DECELERATING DIPOTENTIAL OPERATION
(b) COMPARISON OF THREE 1000 VOLT MODES OF OPERATION

FIG.7 Tube 41

1000 volt case. Bipotential operation appears slightly worse than the other two, although limiting resolution is about the same in all three cases. The main operating potentials used for the bipotential mode are shown in Fig. 7(a). The G3 potential was held at 300 volts in all cases, and G5 was maintained at about half the G6 potential for normal action of the collimation lens. A test was also made on tube 41 with G4 connected to G5, which has the effect of moving the bipotential lens further from the target. Resolution in this case appeared to be considerably degraded.

2.5 Field-Mesh Pitch

Towards the end of the study some orthodox vidicons were built with non-standard field meshes. It was hoped that a coarser field mesh could be used without affecting resolution. This would provide higher transmission of the beam, which is beneficial. In a suppressor mesh tube, for example, it would permit the use of a finer suppressor mesh to improve resolution without reduction in overall transmission of the two meshes

The six tubes involved in this experiment were Nos. 6608091, 6608009 and 297 with 500 line mesh, Nos. 259 and 304 with 750 line mesh, and No. 255 with 2000 line mesh. Further details of the tubes can be found in Table 1. All have .0018" beam limiting apertures and target-mesh spacings in the range .105" to .135". Apart from field-mesh pitch, therefore, they do not differ in any respect that is thought to influence resolution. Tube 6608009 differs from all others involved in this work in having a cataphoretically deposited cathode.

Table 2 compares the aperture response figures obtained from these tubes in normal operation at (a) 600 volts and (b) 1000 volts on G6. The 500-line mesh tubes show wide differences--19% in the 300-line figures at 1000 volts. Tube 6608009 looks particularly bad (it does not seem reasonable to attribute this in any way to the cataphoretic cathode). The two 750-line mesh tubes are similar to each other, and comparison with Fig. 3 shows that they can be regarded as fairly typical standard vidicons. It is not easy to draw any firm conclusions from these results. Tube 297 is the best of the 500-line mesh tubes. At higher line numbers it falls somewhat short of the 750-line mesh tubes (both in Table 2 and Fig. 3) and so there is some suggestion that the coarser field mesh degrades resolution. The suggestion is not supported by tube 255 with 2000-line mesh, which shows results similar to typical 750-line mesh tubes. This experiment is therefore rather inconclusive, but change to mesh coarser than 750 lines/inch does not appear advisable. Improvement in resolution by use of finer field mesh, as has been claimed[1], seems unlikely.

Neither does it appear likely from these results that improved resolution is obtainable by the use of smoothed cathodes[2]. The cataphoretically deposited cathode used in tube 6608009 was probably as smooth as any cathode obtainable, but this tube showed unusually poor resolution, although its performance was normal in other respects. We cannot, of course, draw firm conclusions on the basis of results from only one tube.

TABLE 2

Variation of Field Mesh Pitch. Aperture Response.

600 Volt Operation

	TV lines	100	200	300	400	500	600
500 line mesh	6608091	96	70	39	18	7	3
	6608009*	97	65	30	11	5	
	297	98	79	44	21	8	3
750 line mesh	259	98	80	49	26	14	8
	304	93	75	47	25	13	7
2000 line mesh	255	95	70	41	22	11	5

1000 Volt Operation

		100	200	300	400	500	600
500 line mesh	6608091	99	81	48	24	12	5
	6608009*	99	67	33	15	6	2
	297	99	84	52	27	12	5
750 line mesh	259	98	80	58	34	18	8
	304	99	84	59	36	20	10
2000 line mesh	255	99	83	53	33	19	8

*Cataphoretic cathode

3. SUPRESSOR MESH VIDICON

The typical effect of introducing a suppressor mesh is illustrated in Fig. 8, which compares aperture response curves from tube 207 at two different suppressor mesh voltages with a curve from tube 36, which is representative of orthodox vidicon performance. The two tubes are nominally the same apart from the suppressor mesh, which is placed at the standard .010" from the target. It is seen that over 20% response is lost at 200 to 300 lines with the suppressor mesh at 30 volts, a normal operating value in the Lunar Camera Tube. Limiting resolution is reduced by about a hundred and fifty lines. This degradation is serious, and it can be seen why the original estimates of LCT resolution, which were based on knowledge of orthodox hybrid vidicon performance at that time, were rather optimistic. The surprisingly severe effect of the suppressor mesh is revealed as the primary cause of disappointment in the resolution performance of the early Lunar Camera Tubes. Since confirmation of this fact, the suppressor mesh effect has been the main object of investigation in this study.

Fig. 9 shows the construction adopted for suppressor mesh vidicons. The additional mesh is mounted on top of the standard G6 by means of a ceramic ring with metal tabs (spider). The required separation of the meshes is set by the introduction of ceramic spacers. Insulation of the suppressor mesh from the target is provided by a mica washer, which automatically sets the spacing between the two electrodes when the complete mount is inserted into the tube envelope. A washer thickness of 0.002" is required to achieve the standard target-G7 spacing of 0.010".

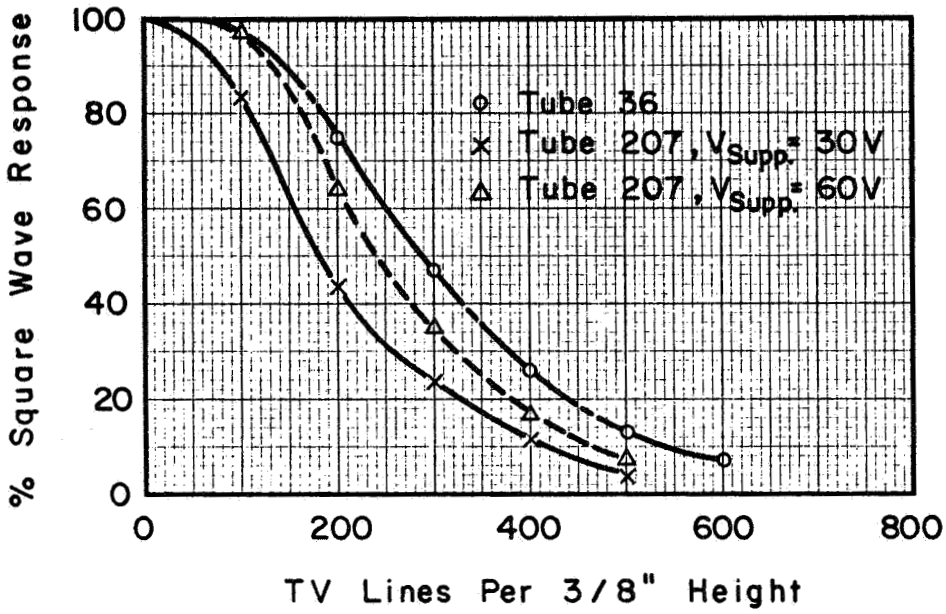

FIG. 8 COMPARISON OF VIDICONS WITH AND WITHOUT SUPPRESSOR MESH (600 VOLT OPERATION)

Target Field-Mesh Spacing 0.110" (Approx.)

Beam Limiting Aperture — .0018"

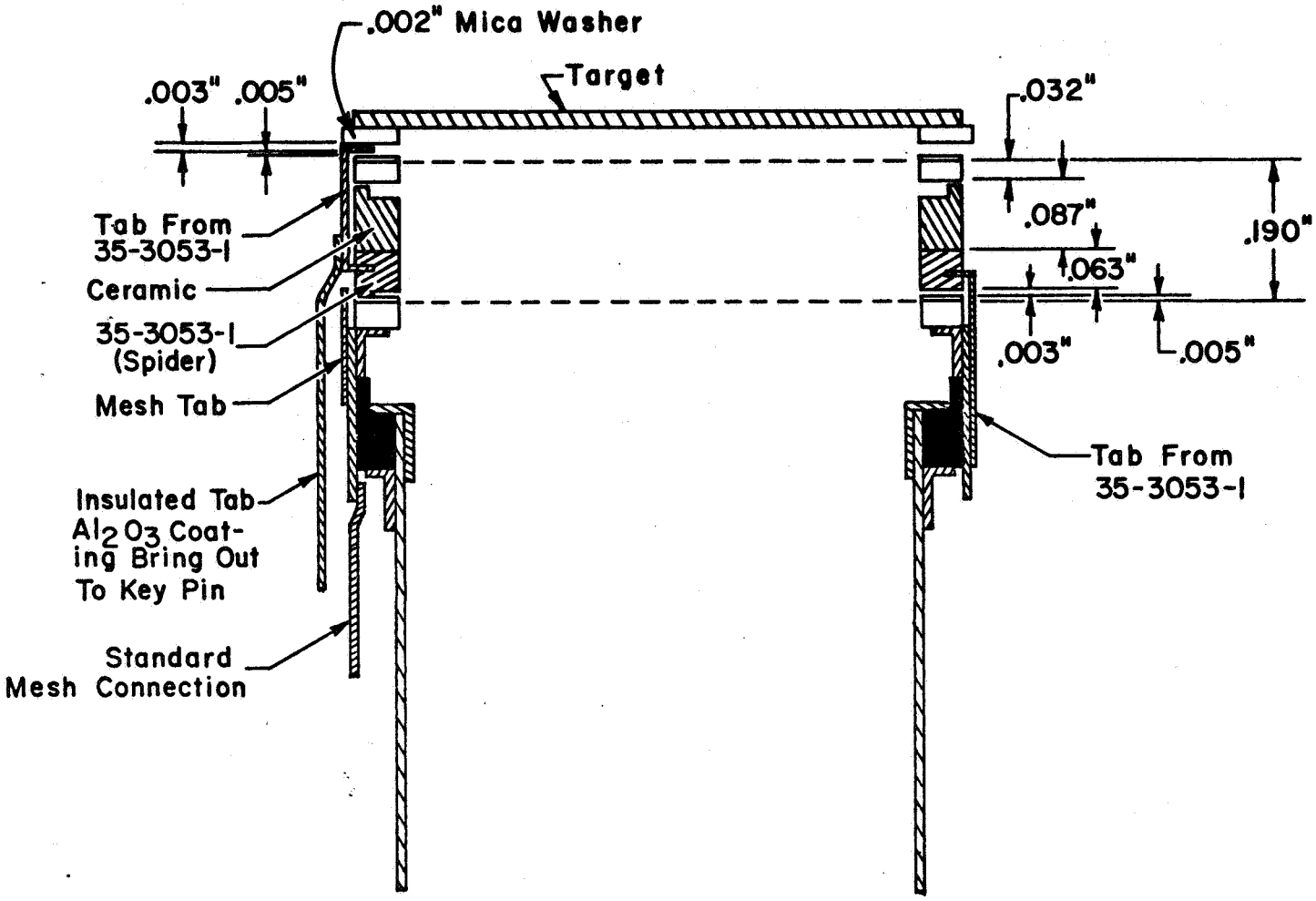

FIG. 9 CONSTRUCTION OF SUPPRESSOR MESH VIDICON

3.1 Variation of Suppressor Potential

To some extent, the degradation produced by the suppressor mesh can be explained by the lenslet action that occurs at the mesh openings when the field strengths on the two sides of the mesh differ. This effect has been analyzed quantitatively elsewhere[3]. It is not the full story, however. The lenslet action can be eliminated by adjusting the suppressor mesh to such a potential that the field strengths on either side are equalized. This field-equalization point may be too high for satisfactory operation of an SEC camera tube, but it can always be attained in the vidicon tubes being described here. Invariably it is found that resolution, although improved, still falls short of that of an equivalent vidicon without suppressor mesh. The curve for V_{supp} = 60 volts shown in Fig. 8 illustrates this point.

Surprisingly, it is found that resolution continues to improve as the suppressor mesh voltage is raised above the equalization point. This effect is illustrated in Fig. 10 which shows, still for tube 207, how the response at 300 TV lines increases with suppressor mesh potential. The two curves correspond to 600 and 1000 volt operation, and the suppressor mesh voltages for field-equalization in the two cases are marked with corresponding symbols. For 600 volt operation resolution improves as the suppressor mesh potential is raised to 80 volts, where it still is not equal to the resolution of a vidicon without suppressor mesh. The curves appear to be leveling off at the upper end. The crossing of the two curves is an interesting feature. It appears that at low suppressor mesh voltages

the resolution improvement normally observed in the 1000 volt operation mode is more than cancelled out by aggravation of the lenslet effect. The advantages of the 1000 volt mode can be realized at higher suppressor mesh potentials, and at V_{supp} = 80 volts the response is approaching that of a vidicon without suppressor mesh (typically about 55%--see Fig. 3).

Complete aperture response curves for various suppressor voltages at two different field mesh potentials are given in Fig. 11.

The salient features illustrated in Figs. 8, 10, and 11 are not peculiar to tube 207. They are observed in all the suppressor mesh tubes constructed, to a degree which depends on some of the tube parameters, as will be further discussed in following sections. The lenslet effect already mentioned is not adequate to explain these features, although it undoubtedly contributes to them. Additional contributing effects may be electron scattering or secondary emission at the suppressor mesh, either of which would contribute to reduction of contrast. However, it seems unlikely that these effects would reduce as the suppressor mesh potential is increased. Fig. 12 shows schematically how the field tends to direct more electrons to the mesh bars the higher the mesh potential so that scattering effects could be expected to get worse. It might be argued that the improvement with increasing suppressor mesh potential is simply the result of increasing the field in front of the target and hence reducing electron transit time. However, experiments with ordinary vidicons, already described in Section 2.2, tended to show that this effect is not as influential as is sometimes claimed. At the present time, therefore, there is no satisfactory explanation of the suppressor mesh effects on resolution described here.

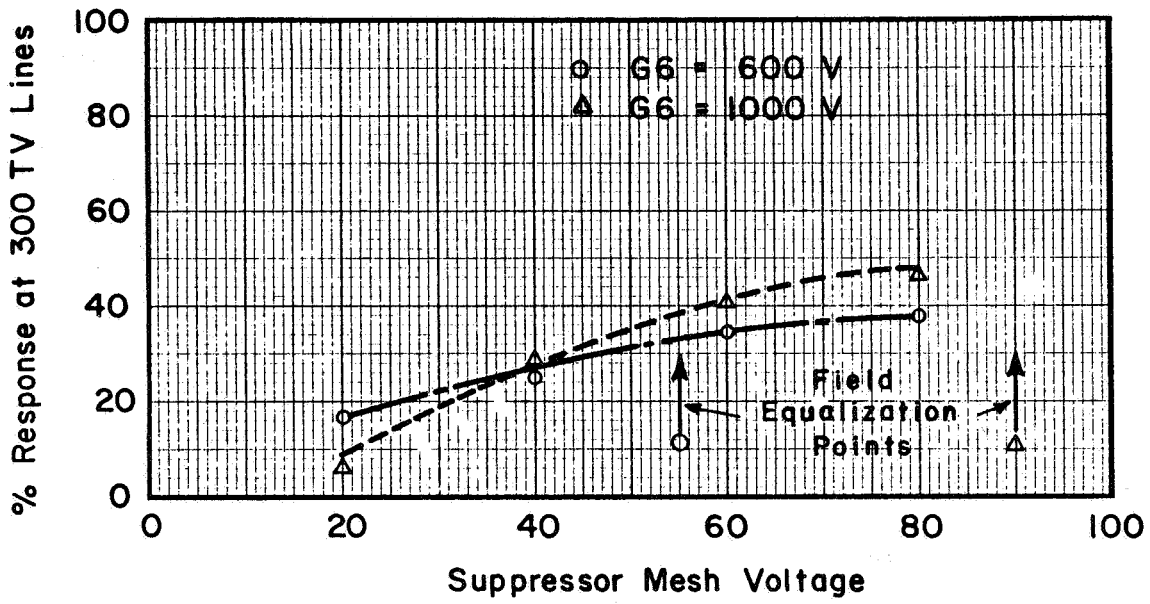

FIG. 10 APERTURE RESPONSE VARIATION WITH SUPPRESSOR MESH POTENTIAL

Tube 207 Target Field-Mesh Spacing 0.112"

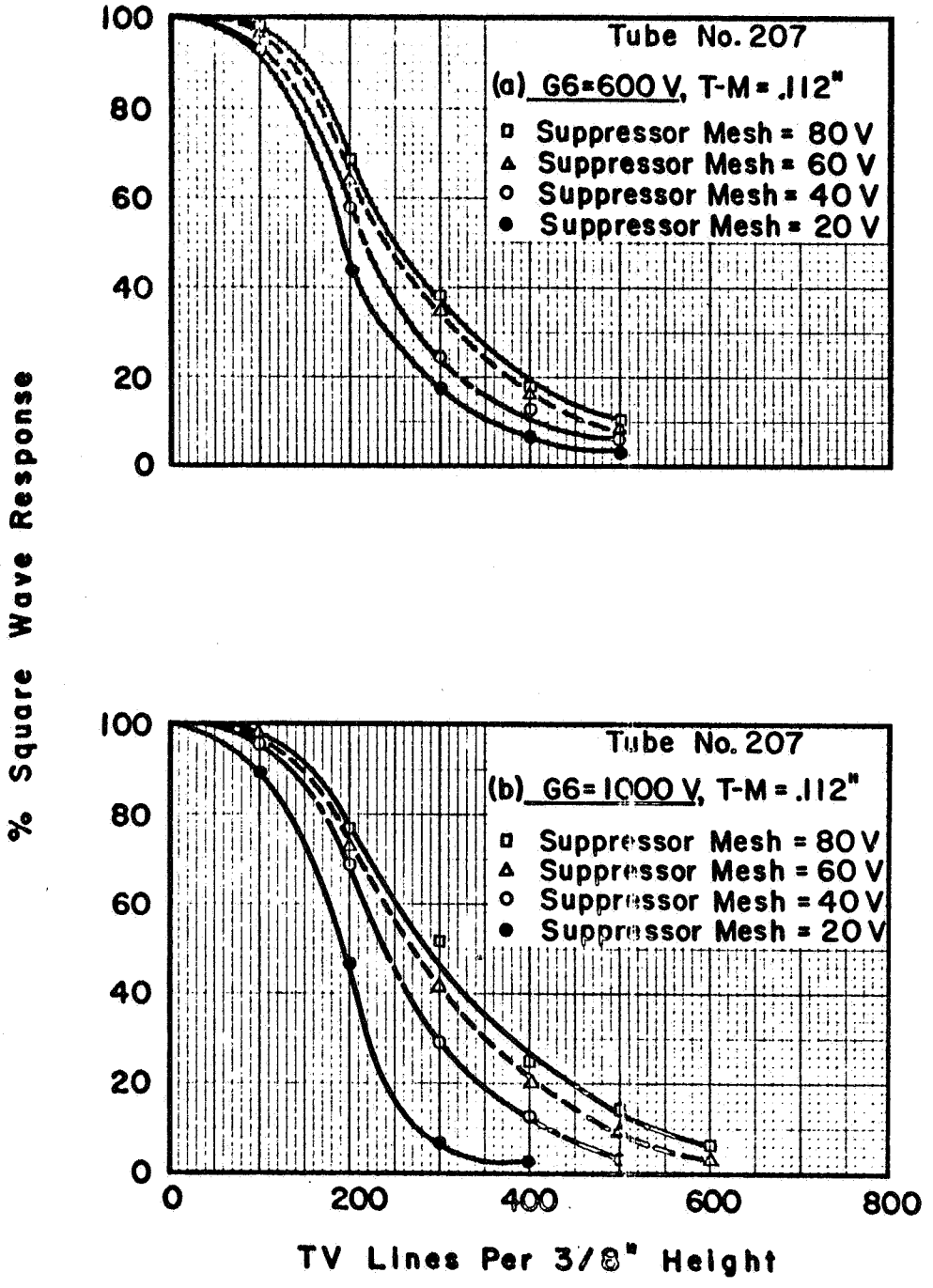

FIG. 11 APERTURE RESPONSE VARIATION WITH SUPPRESSOR VOLTAGE

Tube 207 Field-Mesh Target Spacing = 0.112"

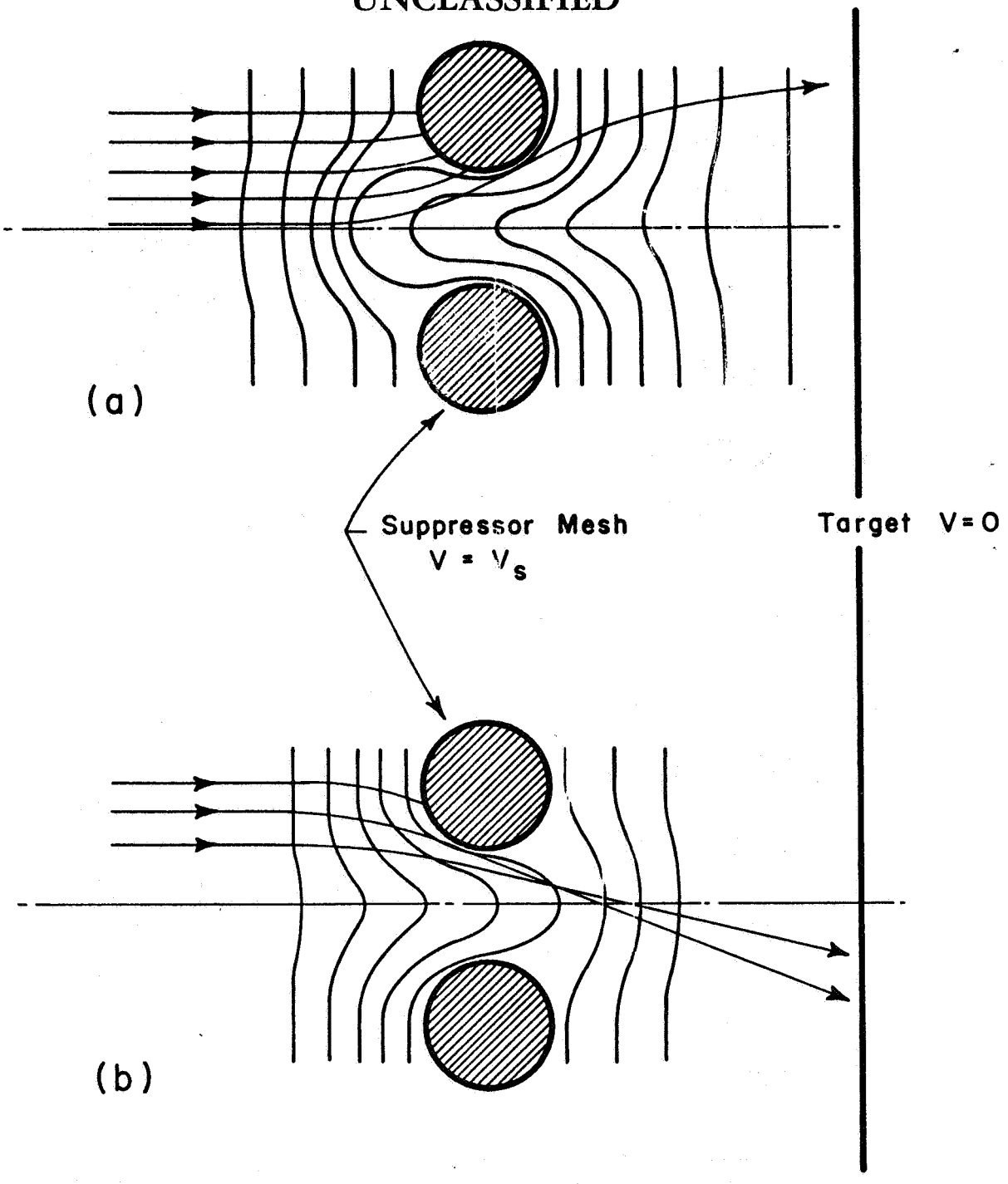

FIG. 12 INTERCEPTION OF ELECTRONS BY SUPPRESSOR MESH

(a) High Suppressor Potential

(b) Low Suppressor Potential

The most important details of all the suppressor mesh vidicons built during this program are listed in Table 3.

3.2 Field-Mesh Target Spacing

Variation of the separation of field-mesh and target is closely related to the question of suppressor mesh potential. Experiments described in Section 2.2 have suggested that field-mesh spacing ordinarily has no significant influence on vidicon resolution. In suppressor-mesh vidicons, therefore, the field-mesh position would be expected to affect resolution only through its influence on the lenslet effect at the suppressor mesh. On this basis spacings that tend to equalize the field strengths on the two sides of the suppressor mesh should provide best resolution.

Tube 207 discussed in the preceding section has a target field-mesh spacing of 0.112" and so, in normal 600 volt operation, requires a suppressor mesh potential of 54 volts for field-equalization. To reduce the field-equalization potential, larger field mesh spacing is required. To investigate this, tubes 6544010 and 206 were built, nominally identical with 207 except for field mesh spacings of .200" and .296" respectively. Resolution performances of the three tubes are compared in Fig. 13 for operation with 30 volts on the suppressor mesh. There appears to be a steady improvement with increasing spacing. The improvement is more pronounced in the high voltage mode of operation, which is consistent with the fact that the lenslet effect is stronger in that case. For 600 volt operation the field-equalization spacing is .200", corresponding exactly to tube 6544010. However, there is further improvement in performance

TABLE 3 SUPPRESSOR MESH VIDICONS

Tube No.	Aperture	Heater-cath type	Special Features	Field Mesh Lines/Inch	G6-Target	Suppressor Lines/Inch
6544009	.0018"	1 watt		750	.200"	1000
6544010	.0018"	"		750	.200	750
206	.0018"	0.2 watt		750	.296	1000
207	.0018"	"		750	.112	1000
250	.0007"	1 watt		750	.232	2000
251	.0007"	"		750	.232	1000
268	.0010"	"		750	.108	1000
269	.0010"	"		750	.197	1000
266	.0010"	"		750	.293	1000
6608026	.0010"	"		500	.233	1500
6608110	.0010"	"		750	.232	1500
6608101	.0010"	"		500	.298	1500
6608109	.0010"	"		500	.389	1500
6608012	.0010"	"	.030" suppressor spacing	500	.253	1500
264	.0018"	0.2 watt	single mesh .010" spac	---	----	1000
265	.0018"	"	single mesh .030"	---	----	1000

All have Se targets and standard triode assemblies.

All have .010" nominal supp. mesh spacing unless other specified.

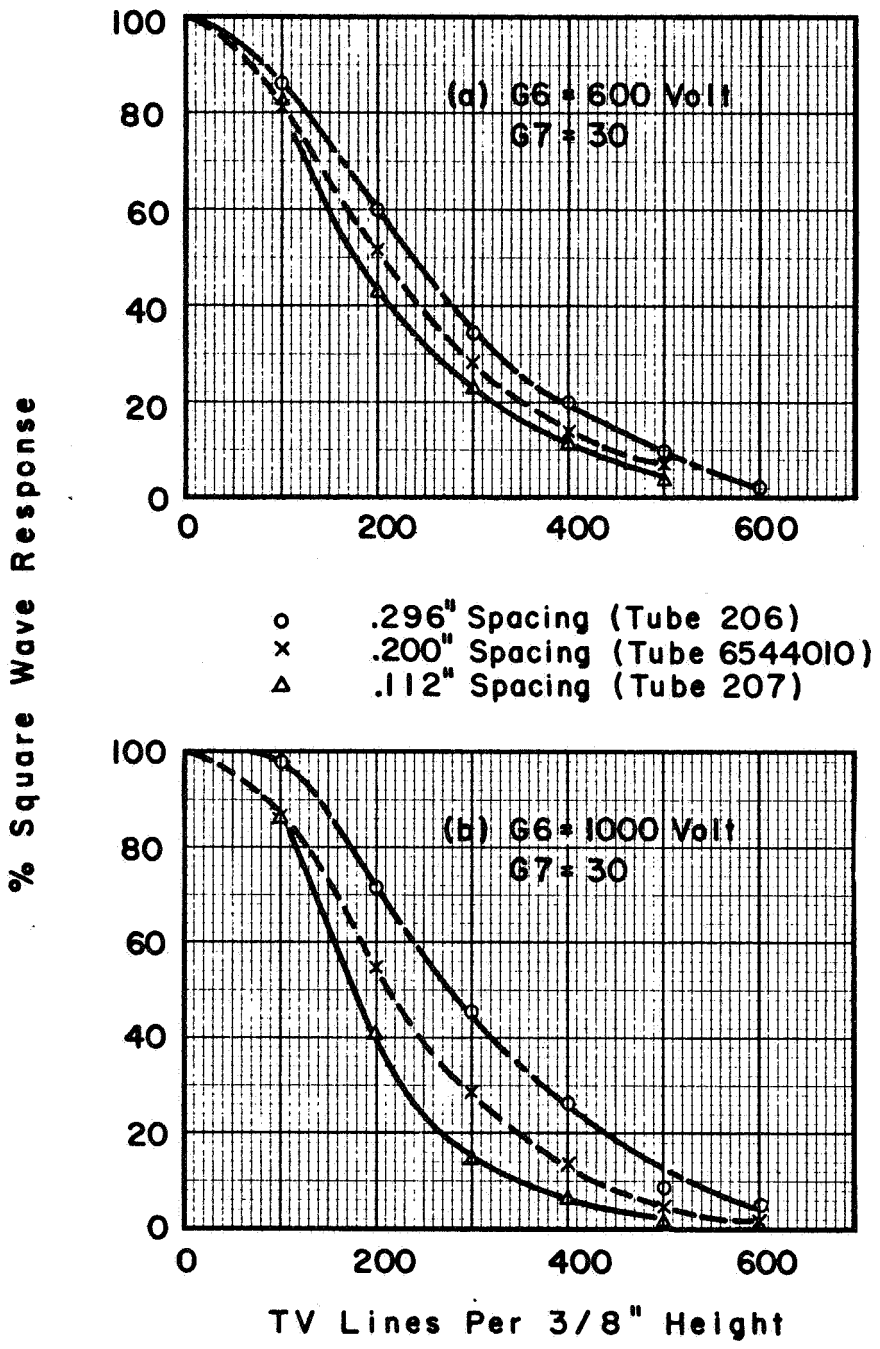

FIG. 13 APERTURE RESPONSE VARIATION WITH FIELD-MESH TARGET SPACING

.0018" Beam Limiting Aperture
750 Line/Inch Field Mesh
1000 Line / Inch Suppressor

with still larger spacing such that the field on the target side of the suppressor becomes stronger than the field on the G6 side. This effect may be analogous to the improvement obtained by operating the suppressor at potentials above the equalization value. A possible explanation of both effects is that the target surface is not at zero potential, as assumed in this discussion, but at some positive potential of perhaps 10 to 30 volts.

Fig. 14 compares three further tubes which again are nominally identical except for field-mesh target spacing. The same trends are evident. Tube 6608109 has a spacing of .389", considerably greater than that needed for field-equalization even in the 1000 volt operation mode, yet it shows higher resolution than the other two tubes. These three tubes differ from the three represented in Fig. 13 in having smaller beam limiting aperture, coarser field mesh, and finer suppressor mesh. Tube 6608026, with .233" spacing, seems to have surprisingly poor resolution compared with the other tubes and is regarded with some suspicion. It has to be borne in mind throughout this work that vidicon performance can vary quite noticeably from one tube to another for reasons that are not well understood. The difficulty is to see through these random variations and detect any trends that may be due to intentionally varied parameters. Sometimes the trend may be masked to the extent that it could be detected only by statistical analysis of the results from a large number of tubes. In the case of Fig. 13, on the other hand, it may well be that the trend is accentuated by unaccountably poor performance of tube 6608026.

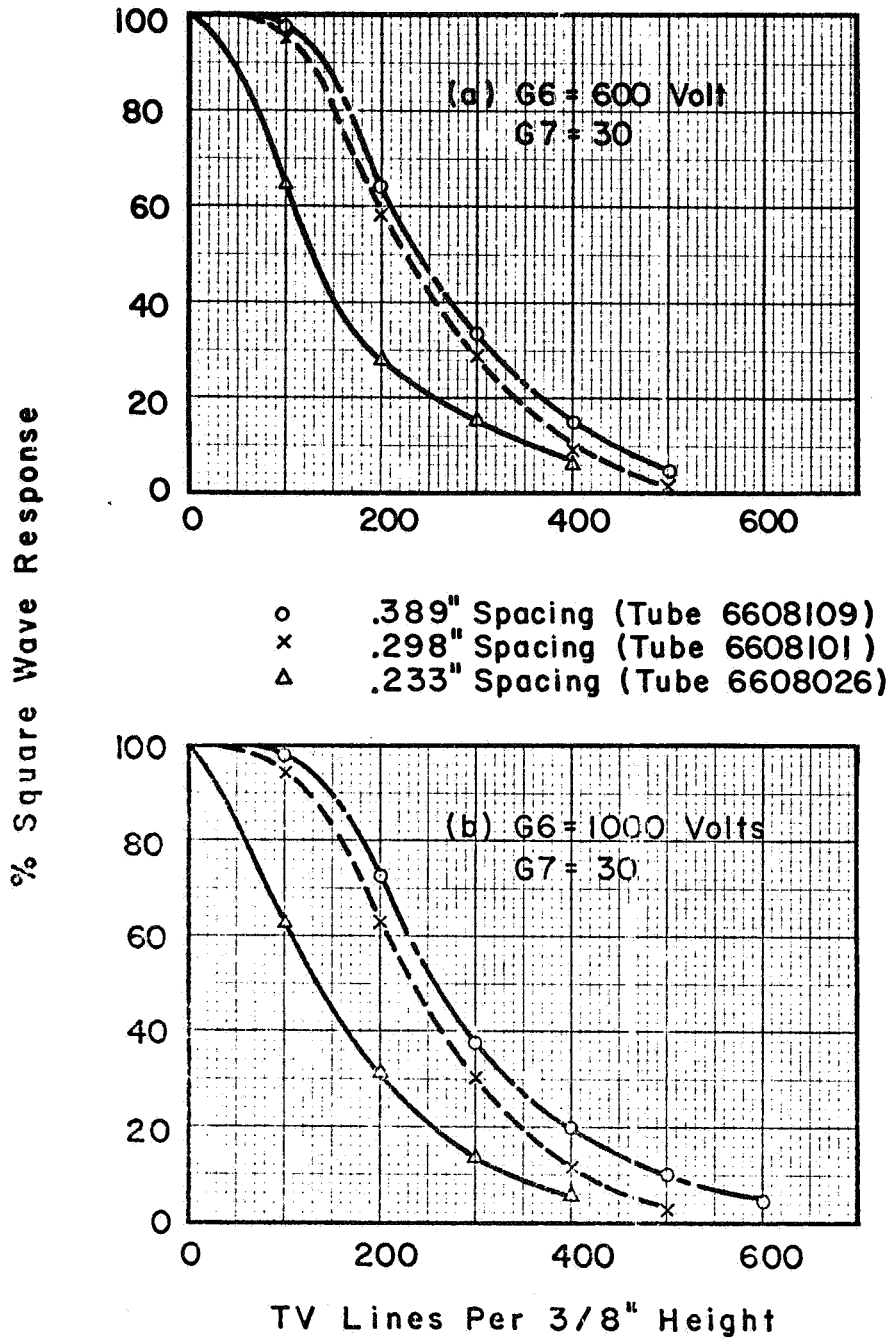

FIG. 14 APERTURE RESPONSE VARIATION WITH FIELD-MESH TARGET SPACING

0.001" Beam Limiting Aperture
500 Line / Inch Field-Mesh
1500 Line / Inch Suppressor

Further evidence on field mesh target spacing is given in Fig. 15. The three tubes compared there are similar to those of Fig. 13 except that they have smaller beam-limiting apertures. Because of this, each tube in Fig. 15 would be expected to be better than its counterpart in Fig. 13. This is true of tubes 268 and 289 but not of tube 266, which has the largest spacing of the three. Tube 266 therefore looks like a bad tube, and we are inclined to discount it. The remaining two tubes of Fig. 15 conform satisfactorily to the pattern of improving resolution with increasing field-mesh target spacing.

3.3 Suppressor-Mesh Pitch and Spacing

Several tubes provide evidence on the effect of varying suppressor mesh pitch. The first two suppressor mesh vidicons made, tube nos. 6544009 and 6544010, were nominally identical except for their suppressor meshes, which were 1000 and 750 lines/inch respectively. Some of the results from these tubes are shown in Fig. 16. Fig. 16(a) compares the 300 TV line response of the two tubes in normal 600 volt operation as the suppressor mesh potential is varied. The tube with the finer mesh is clearly superior. Both tubes show improvement in resolution beyond the field-equalization point, the characteristic already discussed in Section 3.1. Fig. 16(b) compares the complete aperture response curves for the case of 20 volt suppressor potential. Observation of limiting resolution on the test monitor showed tube 6544009 to be generally the better tube by about 100 TV lines.

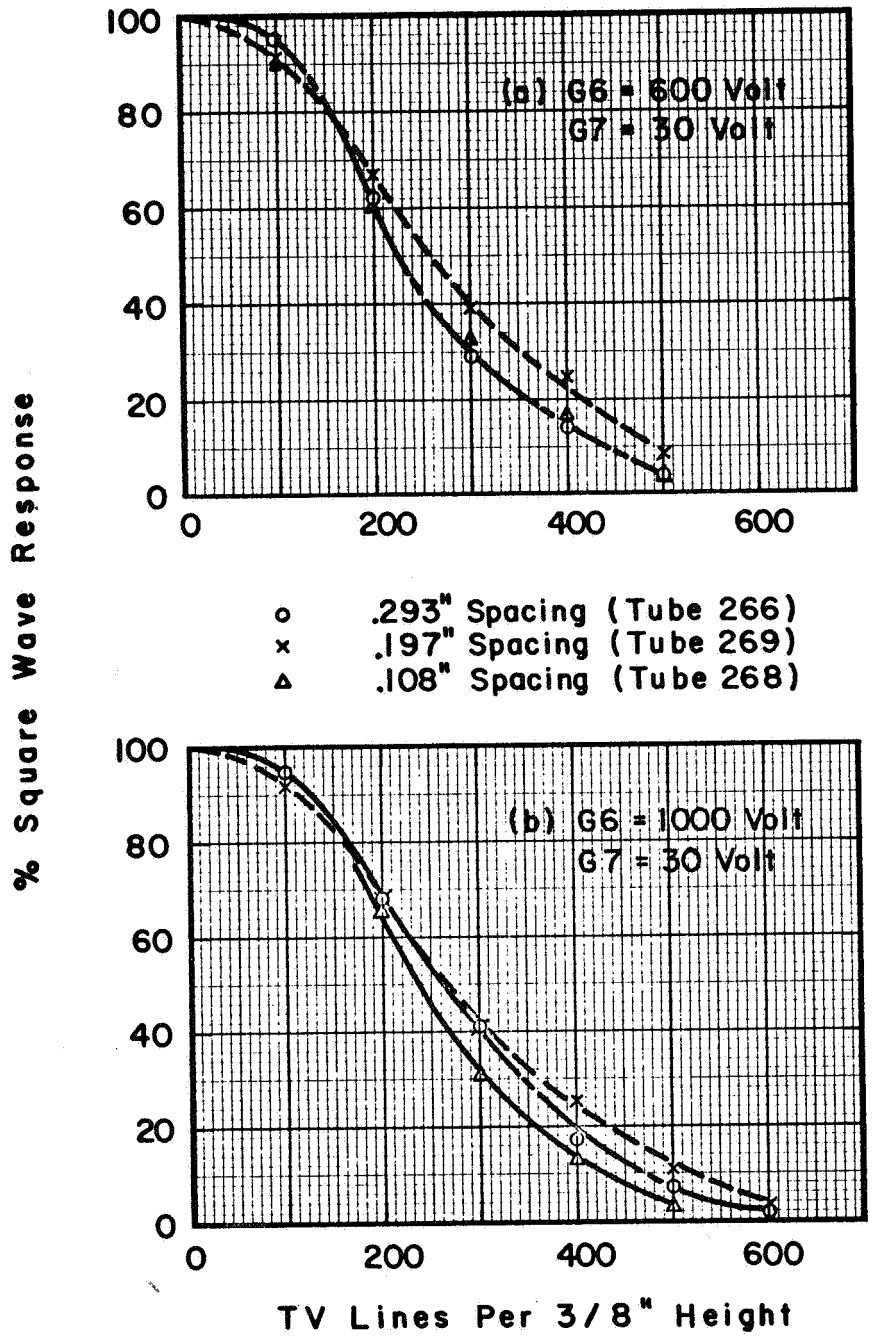

FIG. 15 APERTURE RESPONSE VARIATION WITH FIELD MESH TARGET SPACING

0.001" Beam Limiting Aperture
750 Line / Inch Field Mesh
1000 Line / Inch Suppressor

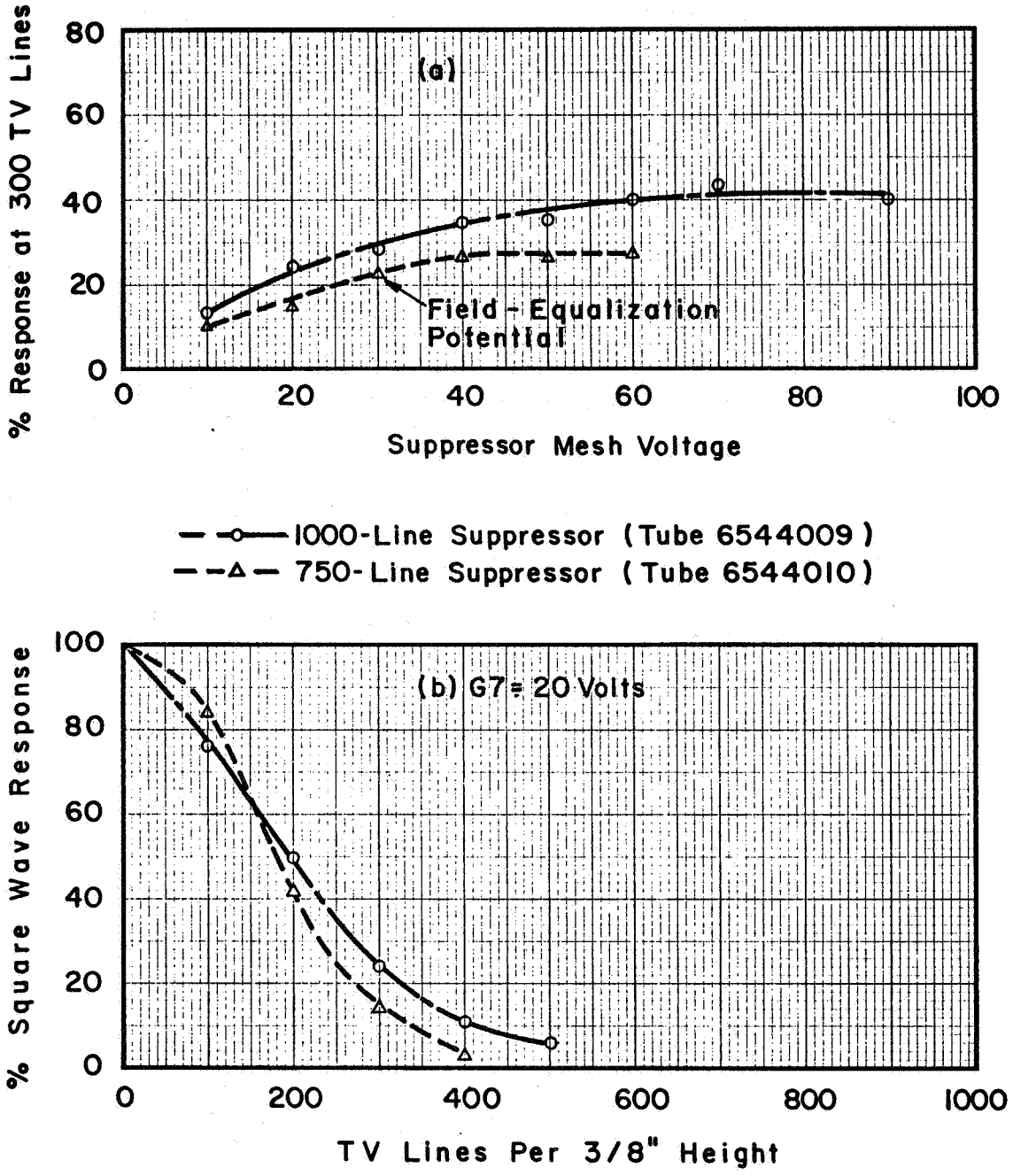

FIG. 16 VARIATION OF SUPPRESSOR PITCH G6 = 600 Volt

.0018" Beam Limiting Aperature
750-Line Field Mesh
.200" Field-Mesh Target Spacing

Shown in Fig. 17 are results from another pair of tubes, also identical except for suppressor mesh pitch. Again the tube with the finer mesh has somewhat better resolution. These tubes have better resolution than the previous pair because of the very small limiting aperture used (.0007" diameter). Tube 250 has the highest resolution of all the suppressor mesh vidicons constructed, due to its combination of small beam limiting aperture, very fine suppressor mesh, and large field-mesh target spacing. It is in fact slightly superior to the orthodox vidicons represented in Fig. 3. However, the 2000 line mesh used in tube 250 has a transmission rating of only 22% which, in conjunction with the small beam limiting aperture, severely reduces the beam current available to discharge the target. Because of this, it was necessary to operate the tube at near-zero bias voltages and low light levels. The signal currents possible were about half those for a more normal tube. These limitations weigh against the introduction of the features of this tube into the LCT.

From our results it seems reasonable to conclude that some resolution improvement is obtained by use of finer suppressor meshes. This conclusion is in agreement with predictions made on the basis of an analysis of the lenslet effect given elsewhere[3]. It should however be mentioned that tubes 6608110 and 269, which essentially differ only in suppressor mesh pitch (1500 and 1000 lines/inch respectively) show very closely similar aperture response curves.

Consideration of the lenslet effect suggests that resolution should be a quite sensitive function of suppressor-target spacing. As a

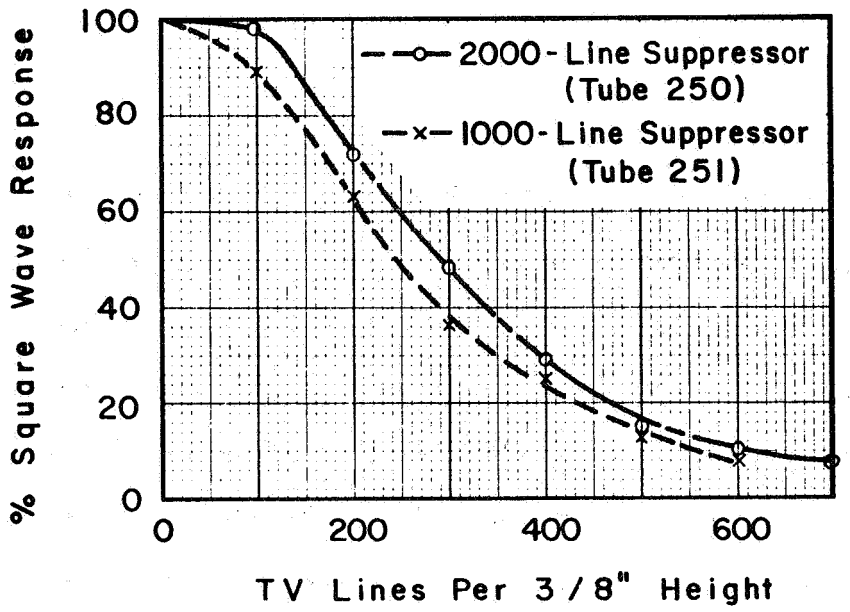

FIG. 17 VARIATION OF SUPPRESSOR PITCH
G6 = 600 Volt, G7 = 30 Volt

.0007" Beam Limiting Aperture
750-Line Field Mesh
.232" Field-Mesh Target Spacing

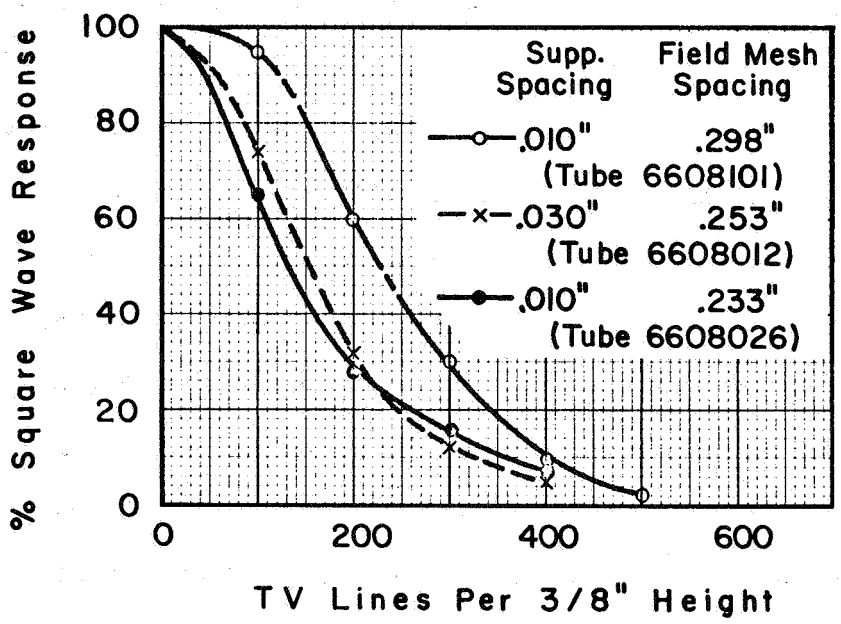

FIG. 18 VARIATION OF SUPPRESSOR-TARGET SPACING
G6 = 300 Volt, G7 = 30 Volt

.001" Beam Limiting Aperture
500 Line/Inch Field Mesh
1500 Line/Inch Suppressor

result of the lenslet analysis[3] and some early work on SEC camera tubes, it now seems to be generally assumed that the smallest possible spacing is desirable. This assumption influenced the present study to the extent that nearly all the suppressor mesh vidicons were built with the standard .010" suppressor target spacing. However, towards the end of the work, tube 6608012 was made with a .030" spacing. A typical comparison of it with two other tubes is shown in Fig. 18. The other two tubes have standard .010" suppressor spacing and slightly different field mesh spacings; they have already been considered in Section 3.2. As mentioned there, one of them, tube 6608026, seems to have unaccountably poor resolution. If we discount this tube and compare the remaining two, it appears that the .030" suppressor spacing may be responsible for quite a large degradation. However, firm conclusions cannot be drawn from this evidence.

3.4 Focusing Mode

Results presented in Section 2.4.2 indicated that a vidicon performs as well in the "inverted" focus lens mode as in the normal mode, for a given maximum voltage in the tube. In the inverted operation the maximum voltage is applied to the G4, and the G6 is held at a relatively low potential compared with that in the normal focusing mode. One would expect this to be beneficial in a suppressor mesh vidicon since the lenslet effect should be reduced. Tests carried out on the earliest suppressor-mesh vidicons built confirmed this expectation. Fig. 19(a) shows results obtained from tube 6544009 when operated in two alternative high voltage modes, compared with performance in the normal low voltage mode. The

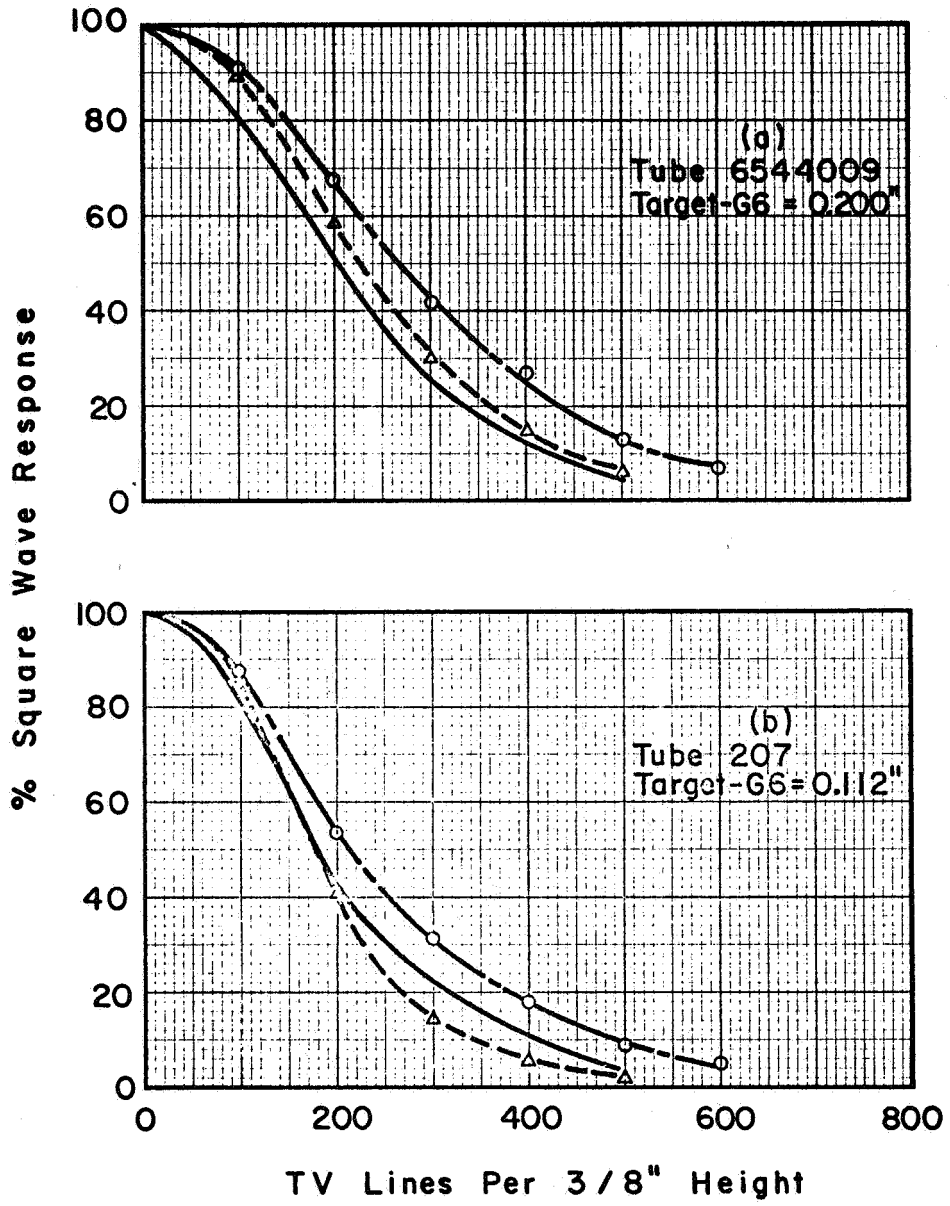

FIG. 19 SUPPRESSOR MESH VIDICONS.
ALTERNATIVE HIGH VOLTAGE MODES.

——— Normal Operation G6 = 600 Volt.

— —△— — G6 = 1000 Volt

—— —o—— G6 = 360 Volt, G4 = 1000 Volt.

suppressor mesh potential was held fixed at 30 volts for all three cases. Application of the 1000 volt potential to G4 rather than to G6 is seen to be beneficial, providing over 10% increase in response and an additional 100 lines on the limiting resolution. As with the ordinary vidicon, the inverted focus mode also reduces the scanning power requirement.

In tube 207, results for which are shown in Fig. 19(b), the advantage of the inverted lens is slightly greater. This tube has a smaller target-G6 spacing of 0.112", which apparently accentuates the lenslet effect to the point where the normal high voltage mode actually degrades resolution. Tube 268, which also has a rather small target-G6 spacing, shows similar effects. On the other hand, tubes with very large target-G6 spacing, such as tube 206 (0.296"), display very little difference between normal and inverted modes of operation.

The majority of suppressor mesh vidicons built conform reasonably to the patterns described above. However, three tubes built late in the program, Nos. 6608110, 6608109, and 6608012, did not. These tubes performed worse in the inverted mode than in the normal mode, the reasons for which are not known.

Tubes 6608101 and 6608109 were built with all electrodes connected to separate pins to provide complete flexibility of operation. In addition to the normal and inverted modes, these tubes were operated in both accelerating and decelerating bipotential modes, with G3 connected to G4. For a given maximum voltage in the tube, very little distinction in performance was found among these various methods of focusing. In

tube 6608101 the normal focusing mode was slightly worse than the others, while in tube 6608109 it was slightly better. The decelerating and accelerating bipotential modes provided identical performances withintthe limits of experimental error.

We conclude from these experiments that the "inverted" focus lens with G4 at high potential provides better resolution than the normal method of focusing in suppressor mesh tubes with target-G6 spacings less than about 0.200". At larger spacings the two methods are practically the same. It should be mentioned that the non-standard focusing methods appeared to be more generally troubled by extraneous problems. For example, ion bombardment of the target becomes more pronounced when the field mesh potential is low, as in the "inverted" mode or the decelerating bipotential mode. Also, problems with tube alignment and astigmatism are often increased with non-standard focusing.

3.5 Magnetic Focus

Tube 6544009 was tested with magnetic focusing to provide information on the possible advantages of that mode for SEC camera tubes generally. Fig. 20(a) shows results for suppressor mesh potentials of 30 and 40 volts in comparison with normal electrostatic focusing. As with orthodox vidicons, a marked resolution improvement results from magnetic focusing. In Fig. 20(b) the curve for G7 = 40 volts is compared with results from an equivalent tube without a suppressor mesh. The resolution degradation due to the suppressor mesh is not so marked here as that shown in Fig. 8 for electrostatic focusing. The tubes concerned here, however, have larger target-G6 spacing than those of Fig. 8.

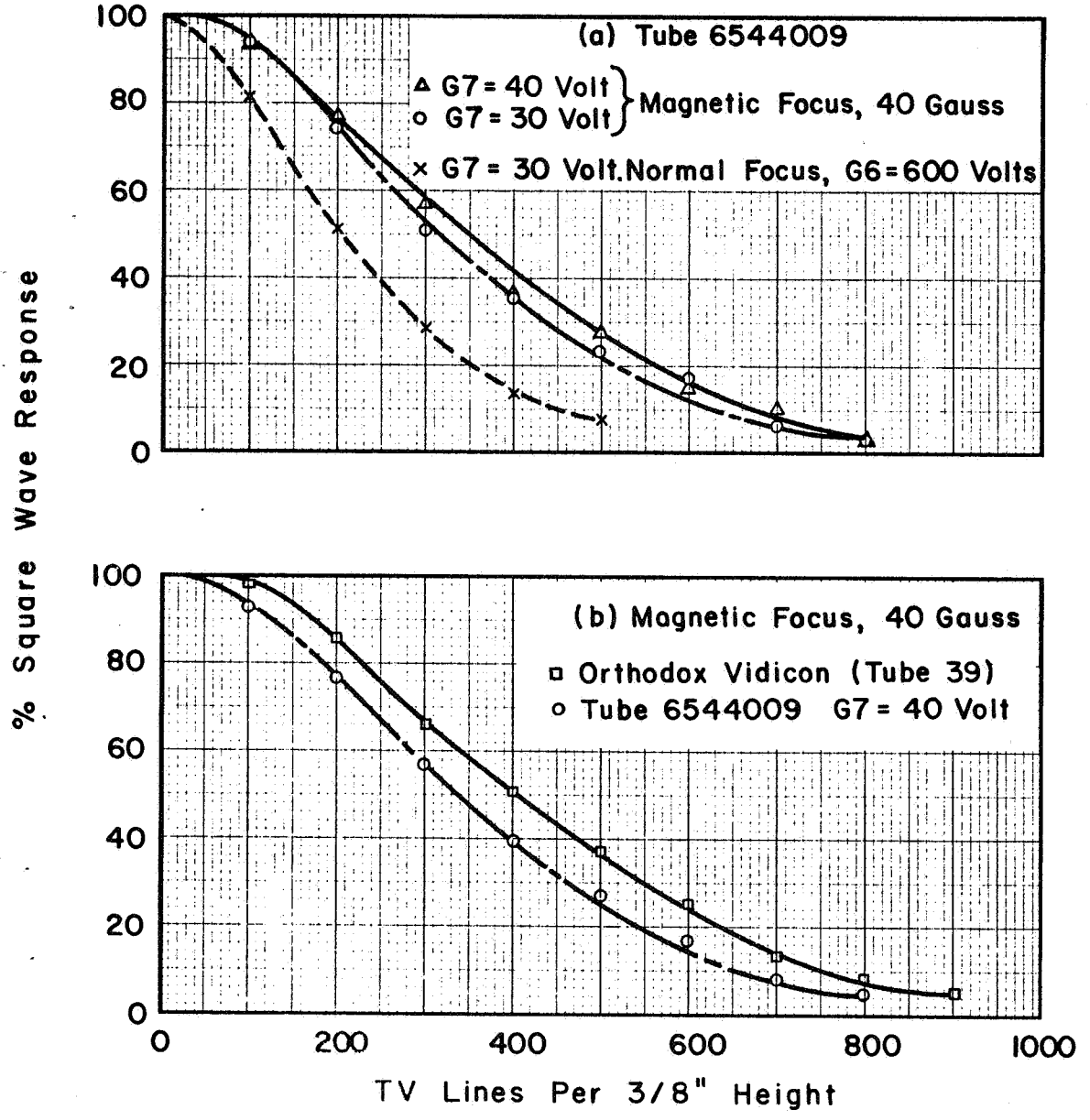

FIG. 20 MAGNETIC FOCUSING OF SUPPRESSOR MESH VIDICON

It appears from these results that magnetic focusing can provide a substantial resolution improvement in tubes with a suppressor mesh. The results were obtained with a magnetic field of about 40 gauss and a potential of 450 volts applied to G3, G4, G5, and G6. Possibly better results could be obtained from a tube in which the field mesh (G6) could be operated at an independent voltage as is normally done in magnetically focused tubes.

3.6 Single Mesh Tube

It is generally accepted that meshes degrade resolution and their use in tubes is to be avoided wherever possible. Since the SEC target does not at present permit satisfactory operation without a low voltage suppressor mesh, it is logical to inquire whether that mesh can simultaneously perform the function of the field mesh in a standard vidicon. Apart from expected resolution advantage, such a single mesh tube would provide superior utilization of beam current. The objective was achieved in this study by redesign of the collimation lens, and although results obtained were disappointing, a brief description of the experiment is appropriate at this point.

Since the beam leaves the focusing lens at high potential and is decelerated to a potential of about 30 volts at the suppressor mesh, the basic requirement is a positive decelerating electron lens. The standard collimation lens of a vidicon, as depicted in Fig. 21(a), is positive only if the beam is accelerated as it passes from G5 to G6. If G6 is placed at a potential lower than G5, the lens becomes negative and so accentuates

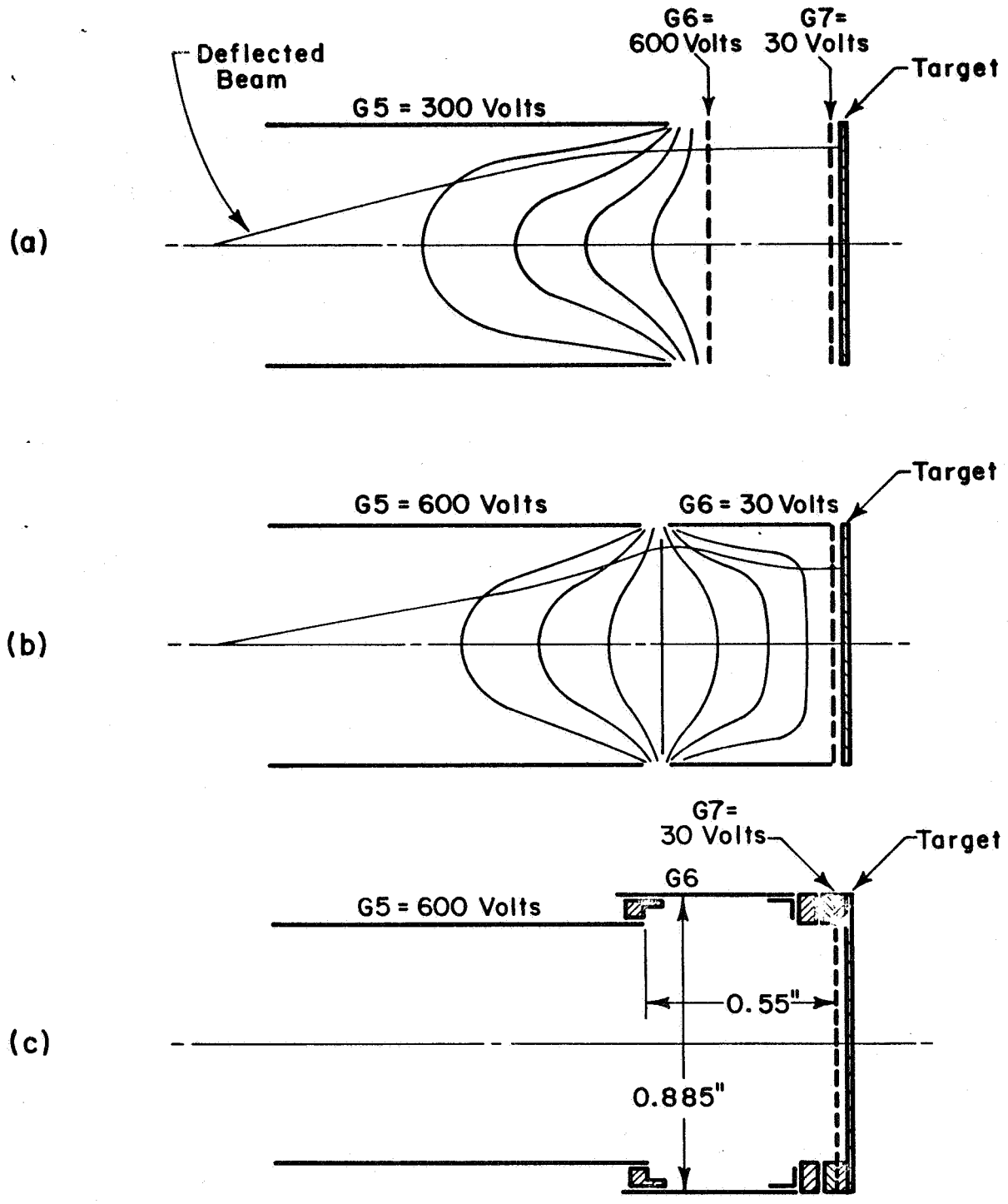

(a) Standard Accelerating Type
(b) Decelerating Type
(c) Practical Form of (b)

FIG. 21 COLLIMATION LENS OPERATION (SCHEMATIC)

the scanning angle instead of reducing it to zero. To get a positive lens effect in the decelerating condition, it is necessary to attach a short cylindrical section to the G6, as shown in Fig. 21(b). The lens becomes a modified two-cylinder lens. With this configuration the mesh part of G6 could become the suppressor mesh, and an operable single-mesh SEC camera tube could be made. However, the cylinder length chosen for G6 would dictate the voltage ratio required for best collimation, and the ratio of G5 potential to suppressor mesh potential would thus be set. To overcome this inflexibility, it is better to separate the cylindrical G6 from the mesh. Fig. 21(c) shows the practical form of decelerating collimation lens that was used in vidicons 264 and 265. In this form, adjustment of the G6 potential for best beam landing can be made independently of the G5 and G7 potentials. The G6 cylinder length of 0.55" was chosen to provide approximately the required strength of lens when set at a potential close to that of the suppressor mesh. This design work was done with the aid of the ray-tracing computer program. No attempt was made to be very precise since it was only desired initially to obtain a working tube on which the resolution could be observed. The cylinder length chosen is therefore not necessarily optimum for beam landing uniformity.

As stated above, the results of the experiment were disappointing. Vidicons 264 and 265 differed only in respect of their target-G7 spacings, which were respectively .010" and .030". Both tubes showed satisfactory beam collimation but resolution was very poor. Aperture response curves for the two tubes are shown in Fig. 22. Both are rather worse than the

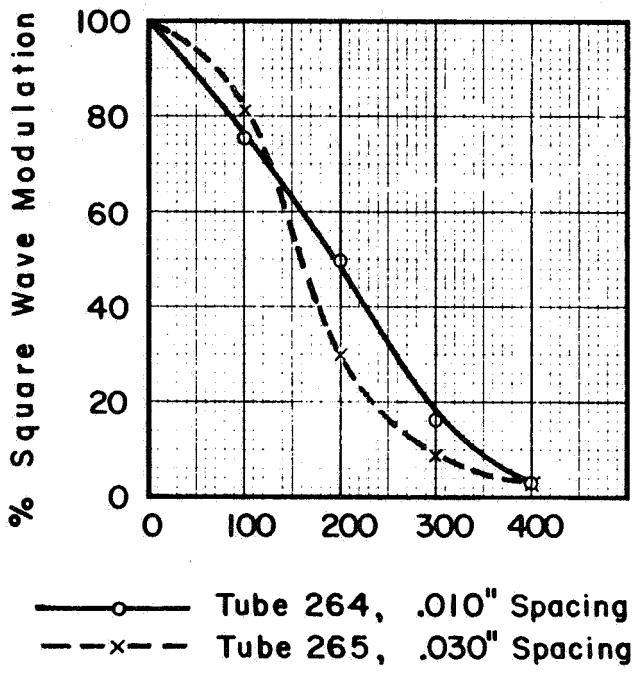

FIG. 22 SINGLE MESH TUBES G7 = 30 VOLTS

orthodox suppressor mesh vidicon such as tube 6544009, the curve for which is shown in Fig. 16. Because of this, the single mesh approach was not pursued further. The operating voltages employed in obtaining the results shown in Fig. 22 were G2 = 300, G3 = G5 = 600, G4 = 140, G6 = 65, G7 = 30. The G6 potential of 65 volts, at which best beam landing was obtained, was somewhat higher than had been predicted from the design computations.

Both tubes 264 and 265 were operated also as orthodox vidicons by connecting G5 to G6 and running the mesh at high potential, in which condition they performed satisfactorily.

4. IMAGE SECTION

Three lines of investigation were followed in the image section study, as follows:

(i) Construction of a series of diodes with dimensions controlled as closely as possible.

(ii) Construction of a diode with a bellows permitting the phosphor position to be varied.

(iii) Conversion of the image section design to a triode, the third electrode to allow individual focusing of each tube.

It was intended that the bellows tube should provide information on the correct positioning of the output surface (i. e. target in the lunar camera tube), while the diode work would determine the dimensional tolerances on the image section construction and our ability to achieve them consistently in production. The triode study was essentially a back-up program intended to provide a ready alternative if the accuracy requirements on the diode proved too stringent.

Because of constructional problems experienced with the bellows diode, the program did not develop quite as it had been foreseen. In fact, satsfactory design centers for the image section were determined quite early in the program from the diode study, and it proved to be not difficult to maintain the constructional tolerances required for good resolution. Results subsequently obtained from the bellows diode work

and the triode work confirmed conclusions drawn from the diode study and provided useful additional information regarding tolerance requirements.

4.1 Image Section Construction

4.1.1 Image Diode

A sketch of the image diode is given in Fig. 23. It is basically a lunar camera tube image section with the signal flange cut to a suitable length for mounting a plain glass output window as shown. The output window flange was brazed to the signal flange prior to the frit sealing of the output window. Final steps in the tube construction were the two heliarc welds which fix the input and output window assemblies to the main tube body. The output windows were mostly of lime glass which was of poor quality, inhomogeneities being clearly visible. Tube performance did not suffer to any detectable extent due to this. Later tubes were provided with output windows of 1045 polished crown glass of considerably better quality. Both types of window were mounted to flanges of Carpenter 49 steel with standard frit-sealing techniques.

4.1.2 Bellows Diode

As shown in Fig. 24, construction of the bellows diode is similar to that of the ordinary diode except that the signal flange is considerably shortened to permit insertion of the bellows between it and the anode support flange. Complications arose here because the readily available vacuum bellows were made of stainless steel and were of too small a diameter for easy connection to the other members of the tube. The signal flange diameter was simply reduced to that of the bellows flange for direct heliarc welding.

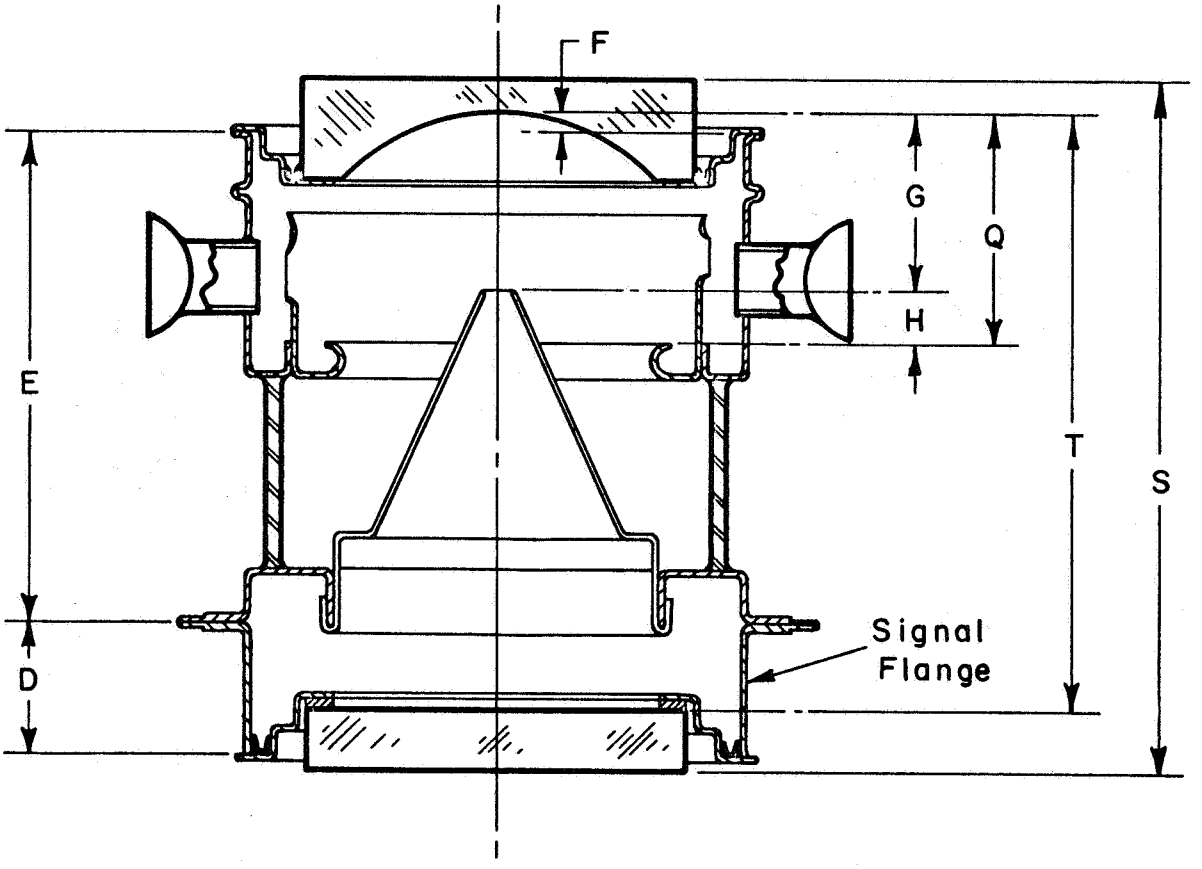

FIG. 23 IMAGE DIODE WX 31235

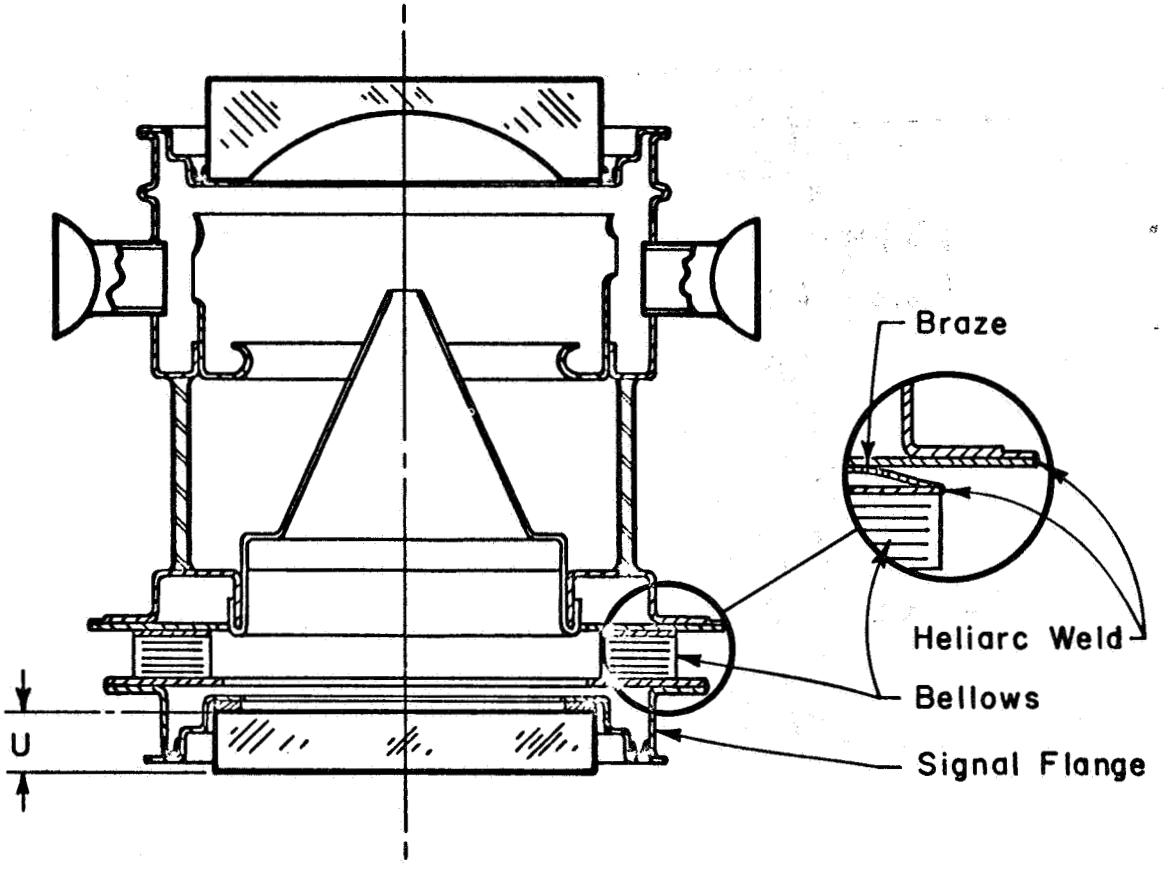

FIG. 24 BELLOWS IMAGE TUBE WX 31242

The anode support flange could not be similarly reduced because of the close proximity of the glass seal of the tube body, and so it was necessary to build up the diameter of the bellows flange at this joint. This diameter increase was achieved by first heliarc welding to the bellows flange a kovar washer of the same outside diameter. To that washer a second kovar washer was brazed of outside diameter equal to that of the anode support flange to which it was then heliarc welded. The detail of this connection is shown in the inset in Fig. 24.

This construction was not satisfactory, and out of several attempts only one properly operable bellows tube was obtained and a second that was operable for a short period. The main trouble experienced was failure of the output window frit-seal during heliarc welding of the output assembly to the bellows, which occurred on 4 tubes. This may have been due to a stiffening of the output flange resulting from braze material between it and the signal flange. A deliberate reduction of the quantity of braze material in this joint did result in the single successful tube. However, an attempt to repeat this failed just as had the earlier tubes.

It should be emphasized that the failures experienced in these tubes were due to design modifications incidental to the introduction of the bellows and not in any way to the bellows themselves. The bellows components appeared to be completely satisfactory, and the single successful tube confirmed entirely the value of this method of electron optical investigation. It should certainly be possible to devise a detailed design different from that described here that would provide a more satisfactory

yield of successful tubes. Difficulties with parts procurement prohibited such a redesign within the scope of the resolution study program.

For accurate adjustment of the phosphor screen position in the bellows tube, a special fixture was designed. Fig. 25 shows a bellows diode mounted in the fixture. The two heavy plates of the fixture have fine inner edges that fit between the flanges of the bellows. The plates are pulled apart by means of the three micrometer screws. A total movement of about 0.150" was possible.

4.1.3 Triode Image Section

Three different methods of construction were developed during the program for electrical isolation of the cathode shield from the cathode itself. The original design due to H. Glaser is shown in Fig. 26(a). The outer cathode shield was cut down to the small ridge, leaving a lip which could be brazed to the metalized ceramic ring. To the other side of the ceramic and to the input-window flange were brazed metal washers of equal outside diameter, between which the final heliarc weld was made. This construction was satisfactory and was used in 4 triode tubes.

A rather neater design due to W. Merrit is shown in Fig. 26(b). Here the outer shield is divided into two parts, between which is inserted a thin ceramic ring. With this design the final tube is almost identical with a diode tube, dimensionally and in appearance. This form of construction was employed successfully on 2 triode image sections on experimental lunar camera tubes.

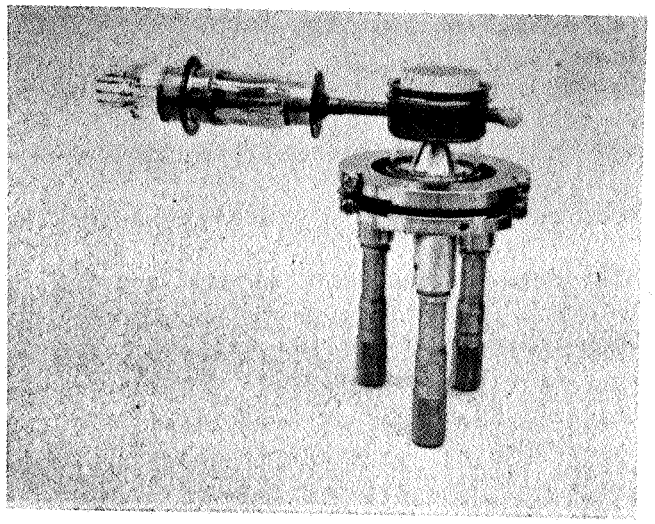

6693D-PF-13

FIG. 25 BELLOWS DIODE MOUNTED IN MICROMETER ADJUSTED FIXTURE

A third design due to R. Nelson was used on a single image triode. As shown in Fig. 26(c), this design insulated the cathode from the input flange by means of a ceramic insert, to which the input window is frit-sealed. Electrical contact from the cathode to the metalized surface of the ceramic is achieved by silver painting across the frit. The metalizing runs under the frit to the inner cylindrical surface of the ceramic for external contact. This construction was satisfactory, and results in a tube dimensionally identical to a diode. Ideally, a special connector would be designed to fit between the input window and the ceramic for contact to the photocathode which is otherwise difficult to achieve.

4.2 Determination of Design Centers

A summary of the important details of all the experimental image sections built is given in Table 4. In the column headed "tube" symbols D, T, and B are used for diode, triode, and bellows tubes. The list is in chronological order. The three dimensions given are those labeled G, Q, and T in Fig. 23. If the shapes of the tube components are assumed not to vary significantly, then these three dimensions are the most important electron optical parameters in the design. All three of them can be adjusted during assembly of the tube. The original design specification for this image section gave the following values for the dimensions:

dimension G	0.769"
dimension Q	0.882"
dimension T	2.169"

During the LCT program some difficulty had been experienced in obtaining anode cones of the correct shape, and variation of the above

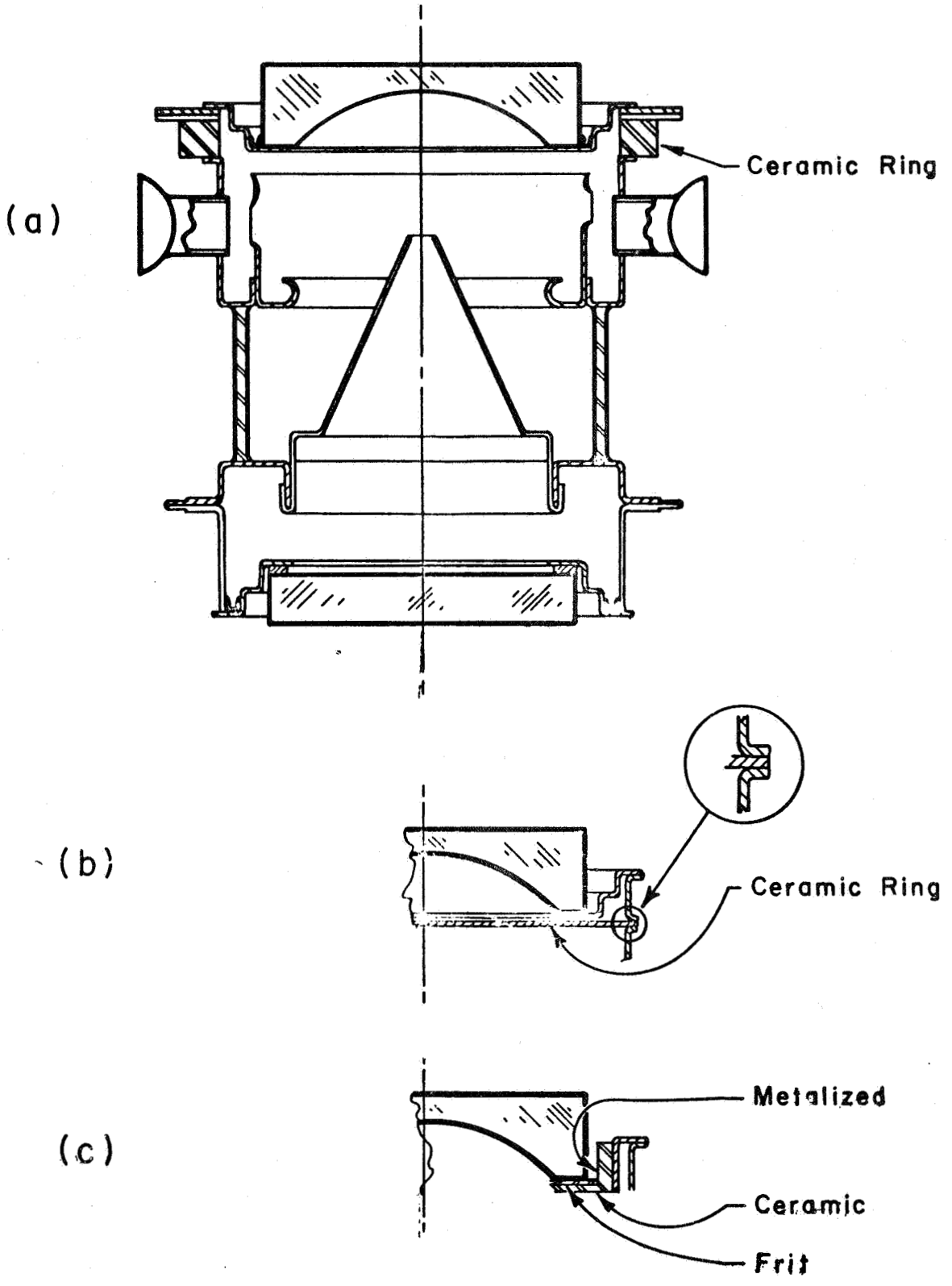

FIG. 26 TRIODE IMAGE TUBE WX 31245

dimensions had been tried in an attempt to compensate for inaccurate cone shaping. Earlier experiences on the PIP program had indicated that the electron optical performance of the design is quite sensitive to slight variation of the formation of the anode tip. From the start of this study, therefore, great attention was paid to this component. A number of anode cones were selected for their similarity by close inspection on a shadowgraph comparator. This ensured control over this important electron optical factor. The selected components were very close to the design specification requirement, and so they are referred to as "spec" in the column headed "anode cone" in Table 4. During the study only two tubes were constructed with anodes intentionally different from the specification; tubes B1 and D3 had anodes with rather rounded tips.

The dimensions recorded in Table 4 are those measured before the two final heliarc welds that complete assembly. By measuring the tube overall dimension before and after weld, the changes occurring due to the weld can be recorded. This was done on all but the first two tubes. The most important change was found to occur on welding the input window assembly since this affects the cathode anode spacing G, the most critical dimension. This change is therefore recorded in Table 4, and it affects all three listed dimensions. Dimension T is also affected by welding of the output window assembly, but this was found to produce only very small changes which can be ignored. Dimension T is rather less critical than G.

Amongst the first 7 tubes, diodes 1, 2, and 4 and triode 2 were reasonably successful attempts to achieve the previously specified design

centers. Of these 4, only diode 2 showed center resolution of less than 80 line pairs per mm. In diode 2 this peak resolution was observed at a radius of 5 mm, approximately half way to the edge of the tube, which indicates too small a value for dimension G. This tube does have the smallest recorded value for G out of the 4 tubes, and it is likely that the dimension was further reduced by a rather large shrinkage on welding. Triode 2 has a similar pre-weld figure, but because of the different construction of the triode (see Fig. 26(a)), the shrinkage at weld in this case is negligible. For the triode tubes Table 4 shows two values of center resolution, one with the shield at cathode potential (unfocused) and one with the shield adjusted to the optimum potential V_f for center resolution (focused). For triode 2 these two conditions are the same, confirming the correctness of the dimensions in this tube. The results from these four tubes seemed to establish that the originally specified dimensions were satisfactory, provided care was taken to ensure proper shaping of the anode. Results from diode 5 subsequently provided further confirmation of this. The trouble with diode 2 suggested that the pre-weld value for dimension G could advantageously be increased a little so as to place the final dimension achieved nearer to the center of its permitted range of variation. Chances of reject tubes due to unusually high dimensional changes during welding should thus be reduced.

The importance of the anode shape had been illustrated at this stage by tubes B1 and D3. There were available a large number of anode cones which, although slightly different from the specified shape, were

all very similar. It was thought expedient to utilize these components, provided a compatible set of dimensions could be determined. Two of the cones were therefore used in tubes B1 and D3. In the bellows tube dimension G was deliberately increased by about 0.015" in an attempt to compensate for the different anode configuration. The effect of the latter was underestimated, however, and the focal length finally determined for this tube was still nearly 0.200" longer than specification. This tube actually had a slight leak at the output frit seal, which largely destroyed the photocathode, but it was operable just long enough for the focal length determination to be made. Unfortunately, diode 3 had already been assembled at this point, or a larger dimensional compensation could have been tried. Inevitably, very poor center resolution was obtained in diode 3. These results indicated the sensitivity of the design to changes in the anode configuration. Because of the excessive dimensional adjustments necessary to compensate for this effect, it was decided not to pursure further study of non-standard anode cones. Rather, steps were taken to facilitate the procurement of correctly shaped anodes. The anode design was changed slightly to simplify accurate specification of its shape. The manufacturers were then supplied with accurately drawn comparator charts of the new design, and the correct inspection procedure to be followed was detailed to them by Mr. C. Beristain. Subsequent supplies of anode cones have proved satisfactory.

Anode cones conforming to the changed specification are indicated as "new spec" in Table 4. The slight change of shape from the original

TABLE 4 EXPERIMENTAL IMAGE SECTIONS

SUMMARY

Tube	Before Weld Dimension Cath. to Anode "G"	Shield "Q"	Output Surface "T"	Change on Weld	Anode Cone	Center lp/mm Unfoc.	Focused	Focus V_f/V_a	Comment
D1	.767	.880	2.171	Not rec.	Spec.	80			
D2	.766	.880	2.166	" "	"	50			
T1	.769	.885	2.188	-.001	"	64	72	.010	Triode design (a)
B1	.7835	.8805	(2.366)	-.005	Blunt .023"		80		Long focus due to anode shape
T2	.766	.880	2.175	-.0005	Spec.	90	90	0	Triode design (a)
D3	.788	.880	2.167	-.0045	Blunt .023"	30			Low resolution due to anode shape
D4	.775	.8775	2.172	-.008	Spec.	80			
T3	.7675	.8785	2.193	-.002	New spec.	50	75	-.009	Triode design (a)
T4	.7765	.8795	(2.156)	-.013	" "			-.008	Triode design (b) LCT 277
D5	.773	.880	2.173	-.009	Spec.	80			
T5	.780	.880	2.194	-.0035	New spec.	64	90	.010	Triode design (a)
T6	.774	.881	Not rec.	-.0095	" "			-.008	Triode design (b) LCT 282
T7	.767	.880	2.175	-.004	" "	45	90	-.012	Triode design (c)
B2	.775	.880	(2.191)	-.006	" "		100		
D6	.776	.880	2.178	-.0045	" "	60			Resolution severely phosphor limited
D7	.772	.875	2.179	-.0065	" "	100			Production assembly
D8	.775	.868	2.169	-.0075	" "	100			Production assembly

specification was not expected to have much effect on the electron optics. Subsequent experimental results and a computational analysis which will be described in a following section have confirmed this. The results from the second bellows tube suggest that the focal length is somewhat greater than is implied by the original design centers. However, excellent performance was obtained from diodes 7 and 8 with rather smaller dimension "T" than is suggested by the bellows tube. The latter results were particularly pleasing since the tubes were constructed from image section assemblies taken at random from the camera tube production line. Diode 6 should have yielded similar results, but the phosphor in this tube was spoiled during photocathode processing and limited the resolution to 60 line pairs per mm so that no judgment of the focusing in this tube was possible. On the basis of these results the appropriate design centers for use with the new anode cones are established as:

dimension G	0.775" ± .003"
dimension Q	0.880" ± .010"
dimension T	2.180" ± .020"

These are pre-weld target values, a shrinkage of about .005" in dimension G being anticipated during weld.

4.3 Resolution Measurements

Resolution measurements made on image sections included both observation of limiting resolution with a standard USAF test pattern and recording of the modulation transfer function. The limiting resolution observation was made at nine points for each of two perpendicular directions.

Fig. 27 shows some typical results. These observations were made on bellows diode 2 operating at 6 kV, the three diagrams corresponding to three different positions of the phosphor screen. Diagram (b) corresponds to the screen location that was judged to give best center resolution, while (a) and (c) correspond to positions .050" either side of that optimum. In (a) the focal surfaces fall short of the screen and resolution is degraded at all points. In (c) the focal surfaces intersect the screen, resulting in improved resolution in some off-axis regions. At the maximum resolution of 100 line pairs per mm, it is probable that the main limitation is set by the fiber optic input window. The phosphor, and probably the electron optics also, are of rather higher resolution capability. Limiting resolutions up to about 200 line pairs per mm have been observed on specimens of the phosphor screens used in these tubes when ultraviolet excitation is used. In diagram (b) it can be seen that resolution of radial lines is consistently better than resolution of tangential lines. This is typical of such tubes with flat output screens, and results from astigmatism, the curvature of the tangential image surface being rather sharper than curvature of the sagittal surface.

The modulation transfer functions of the experimental image tubes were measured with the aid of a scanning microdensitometer in the experimental arrangement depicted in Fig. 28. Although this is a less subjective procedure than the observation of limiting resolution, it is nevertheless a rather vague measurement due to the very complicated dependence of the performance of each component upon the manner in which it is used. For

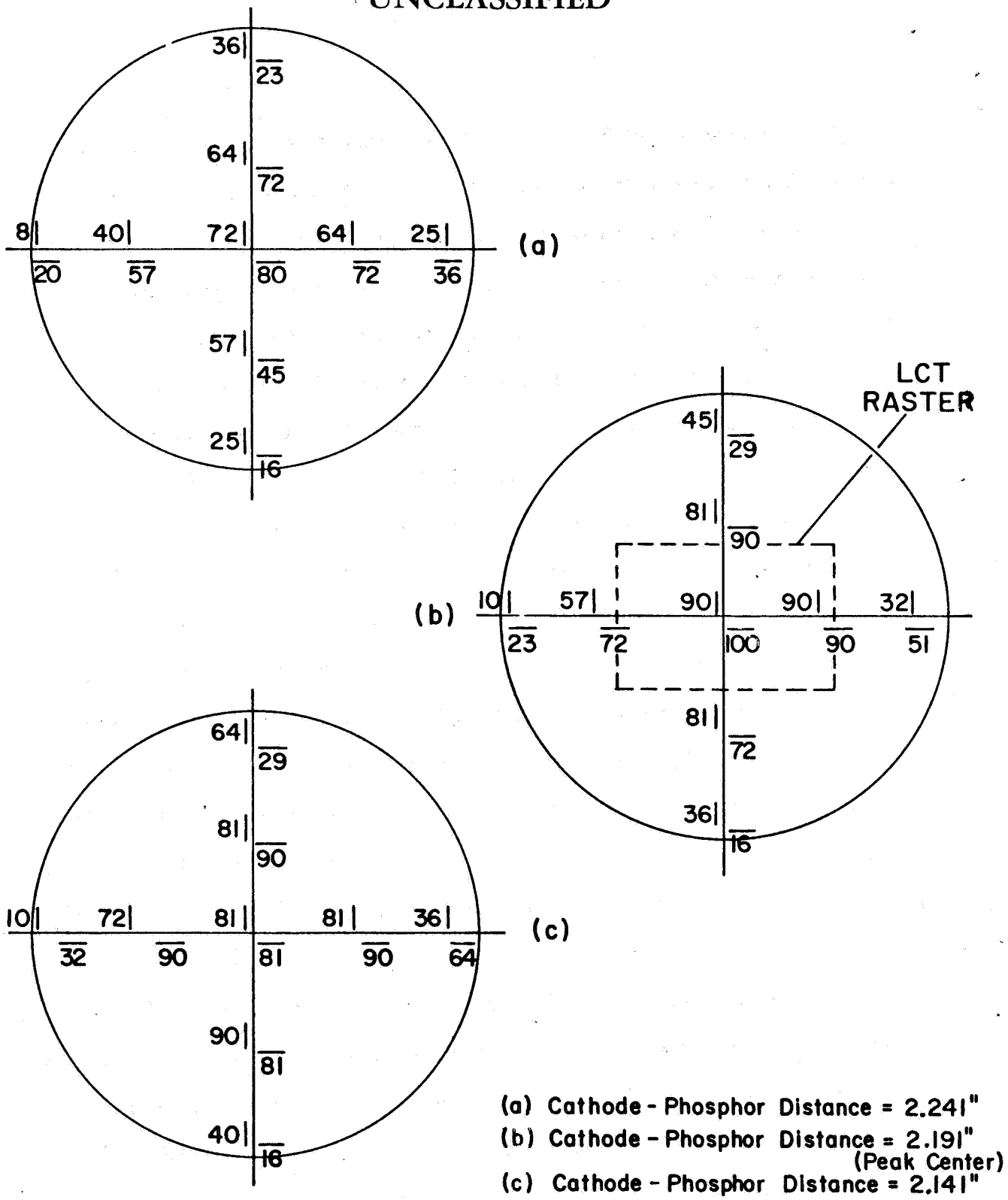

(a) Cathode - Phosphor Distance = 2.241"
(b) Cathode - Phosphor Distance = 2.191" (Peak Center)
(c) Cathode - Phosphor Distance = 2.141"

FIG. 27 BELLOWS DIODE 2. LIMITING RESOLUTION 6 KV
(Line Pairs/mm)

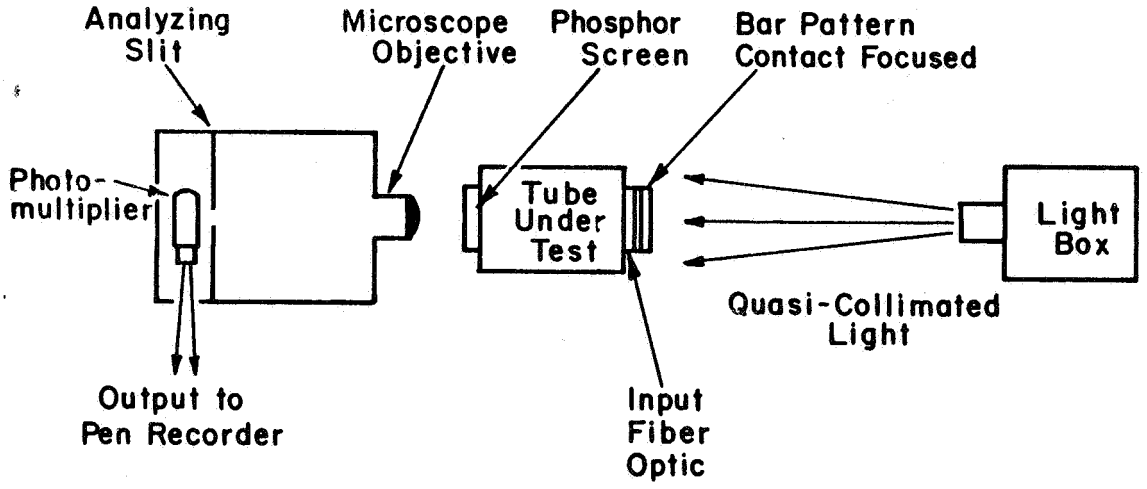

FIG. 28 EXPERIMENTAL ARRANGEMENT FOR MEASUREMENT OF MODULATION TRANSFER FUNCTION.

example, the angular distribution and the spectral distribution of the light affect the performance of the fiber optic and of the microdensitometer optics. The spectral distribution also affects the image tube performance since it determines the energy distribution of the photoelectrons. To minimize the variables in the system no optical focusing need be employed on the input side of a tube with a fiber optic input window. In the present study a Westinghouse diminishing-bar pattern was placed in direct contact with the window, presenting an essentially 100% contrast square wave input of spatial frequency varying from 5 to 50 lp/mm. This was illuminated by a light box placed about 30 inches away. The incident light is thus restricted to fairly small angles (quasi-collimated) as it is when the input picture is imaged by a lens. This corresponds to normal operating conditions for a lunar camera tube. Performance of the input fiber optic is significantly better under these conditions than it would be with diffuse light.

The output of the image tube is scanned by the microdensitometer, which registers the intensity variations by means of a photomultiplier placed behind a fine analyzing slit. To determine the performance of the image tube alone, some correction of the results should be made to allow for the degradation introduced by the optics of the microdensitometer. In determining the performance of the latter, care should be taken to ensure that the operating conditions are the same as during the tube test. This was done simply by moving the bar pattern from the input of the image tube to the output. The microscope objective was thus presented with a

100% contrast pattern illuminated by the phosphor of the image tube. The modulation transfer curve obtained in this way was used to correct those obtained in the tube tests. Only curves corrected in this way are presented in this report.

Fig. 29 shows some modulation transfer functions taken from the second bellows tube for three different positions of the phosphor screen. The top curve corresponds to the center focus position determined by limiting resolution observation, while the other two curves are for positions .100" on either side of that. The focus curve is typical of those measured on good tubes during this program, showing about 20% response at 50 line pairs/mm. The curve has a very long tail, since limiting resolution in the region of 90 to 100 line pairs/mm was observed in this condition. Fig. 30 shows how the response at various spatial frequencies varied with screen position. These curves suggest a focal length about 0.025" longer than that determined from limiting resolution observations. There is no known reason why the curves should be other than symmetrical about the focus position. This graph indicates a safe depth of focus of ± 0.025" on either side of true focus. In the lunar camera tube, where overall resolution performace is limited to 25 line pairs/mm, a tolerance of ± 0.050" would probably be reasonable on dimension "T", although the recommended figure is reduced to ± 0.020" in recognition of the fact that other dimensions also will vary.

Variation of resolution with anode potential was found to be quite slow. In a properly focused tube a potential change from 7 kV to

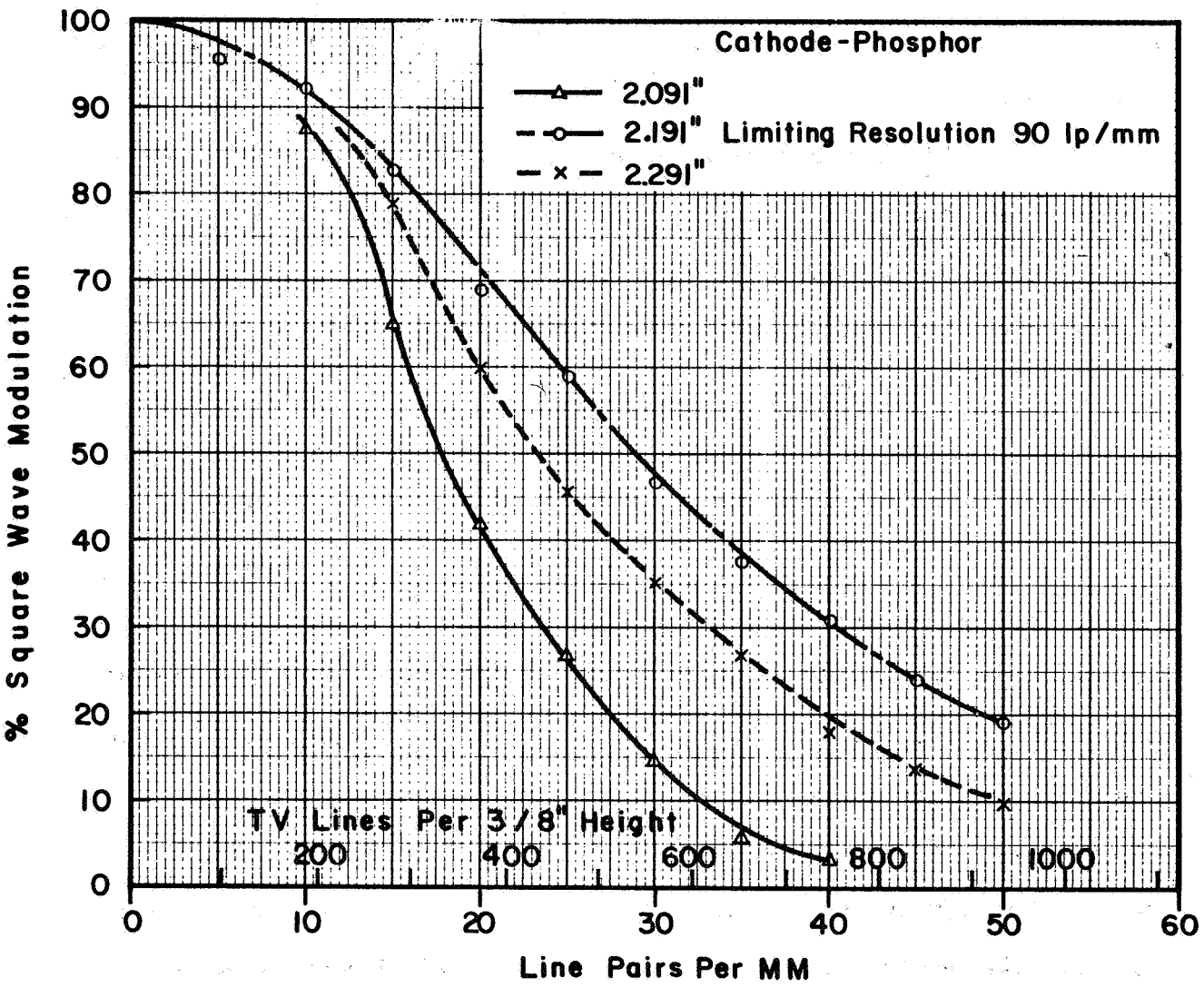

FIG. 29 BELLOWS DIODE 2. MODULATION TRANSFER FUNCTION

V_A = 7 KV

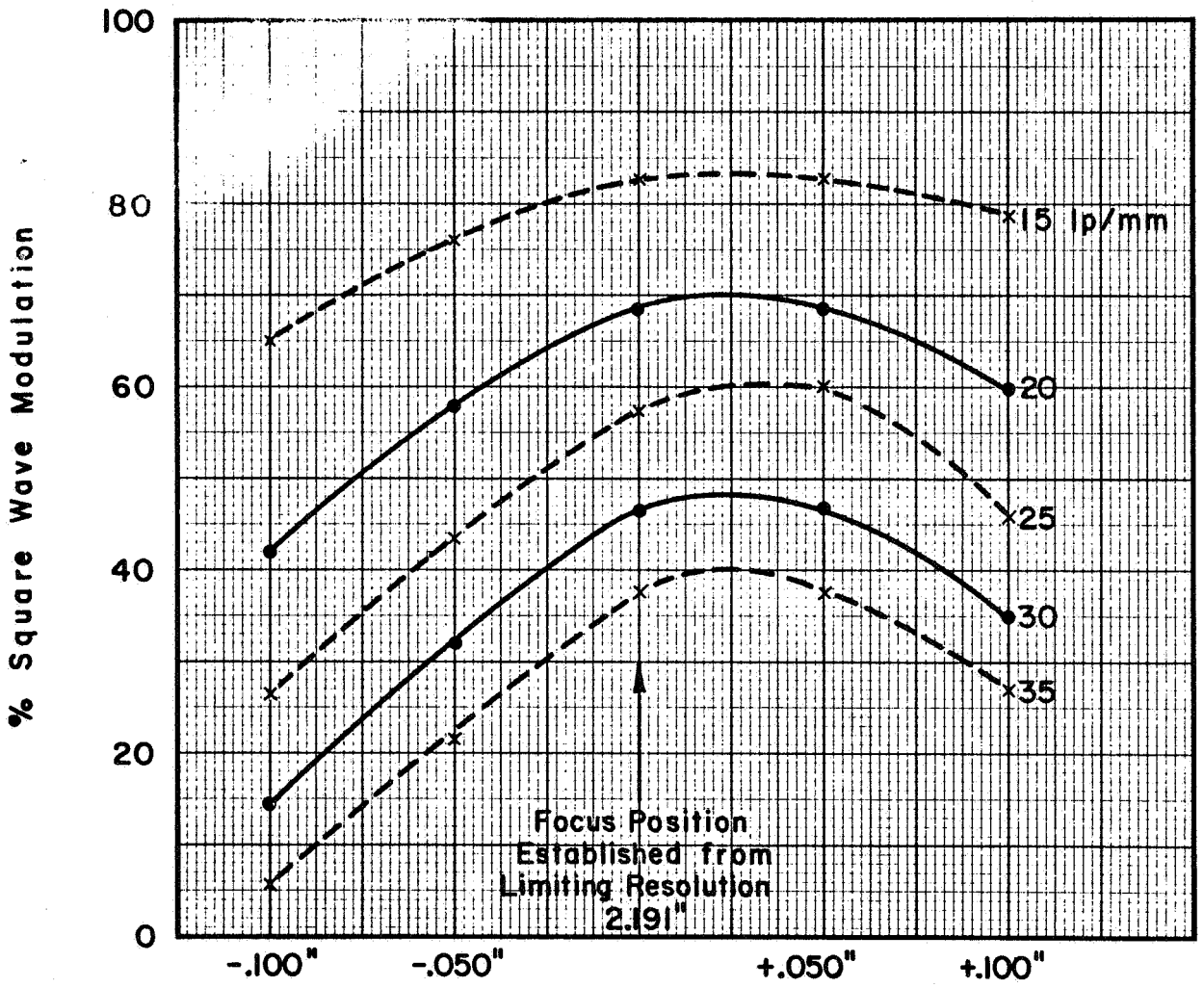

FIG. 30 BELLOWS DIODE 2. RESPONSE VS. SCREEN POSITION
(V_A = 7KV)

15 kV typically results in a limiting resolution improvement of one or two elements on the USAF chart, e.g. from 90 to 100 or 110 line pairs/mm. In this focused condition the electron optical resolution is limited by chromatic aberration and so should be directly proportional to the voltage gradient at the cathode. The slow variation observed is thus an indication that the tube resolution capability is still a lot short of the electron optical limit. Fig. 31 shows modulation transfer curves measured on diode 1 at three different anode potentials. At low resolution the variation is even less noticeable than it is near the limiting resolution. In the lunar camera tube, where response is limited by the read-out section to below 10% at 25 line pairs/mm, it is evident that no detectable resolution variations will occur with changes in the image section potential, at least in the range 5 to 15 kV.

In the triode image section variation of the shield potential produces effects similar to movement of the screen of a bellows tube. Some results from triode 2 are shown in Figs. 32 and 33. The dimensions of this triode were such that center focus occurred when the shield was connected to the cathode. The highest curve in Fig. 32 corresponds to this condition, while the other curves illustrate the degradation as the shield is made negative with respect to cathode. Similar degradation occurs with positive shield voltages, as can be seen from the curves in Fig. 33. Comparison of Fig. 33 with Fig. 30 is made difficult because the peak response values do not match. They are nearly the same at 15 line pairs/mm, however, and comparison of the separations of the 80% points

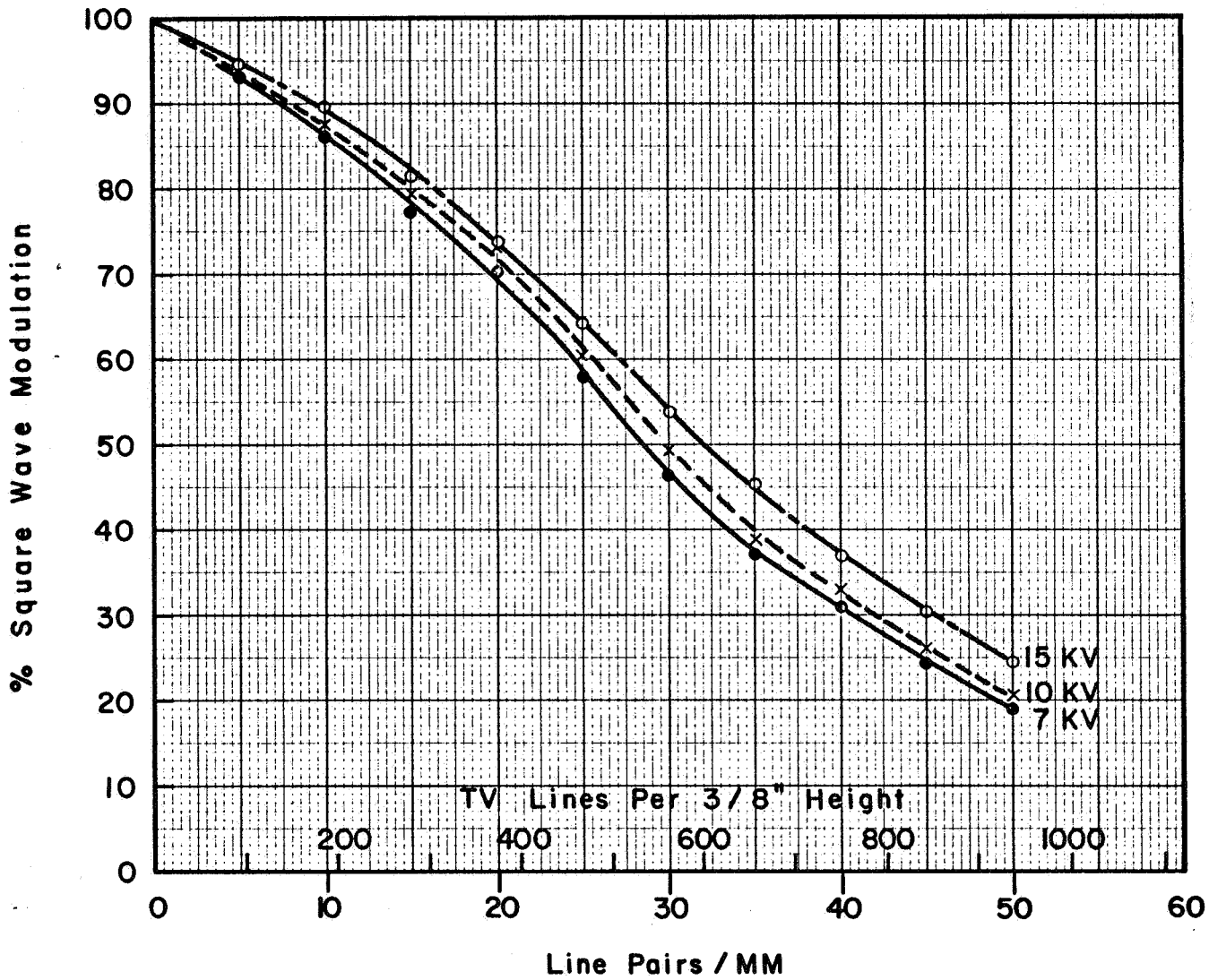

FIG. 31 DIODE I. MODULATION TRANSFER FUNCTION AT DIFFERENT VOLTAGES (Limiting Resolution 80 to 90 lp/mm)

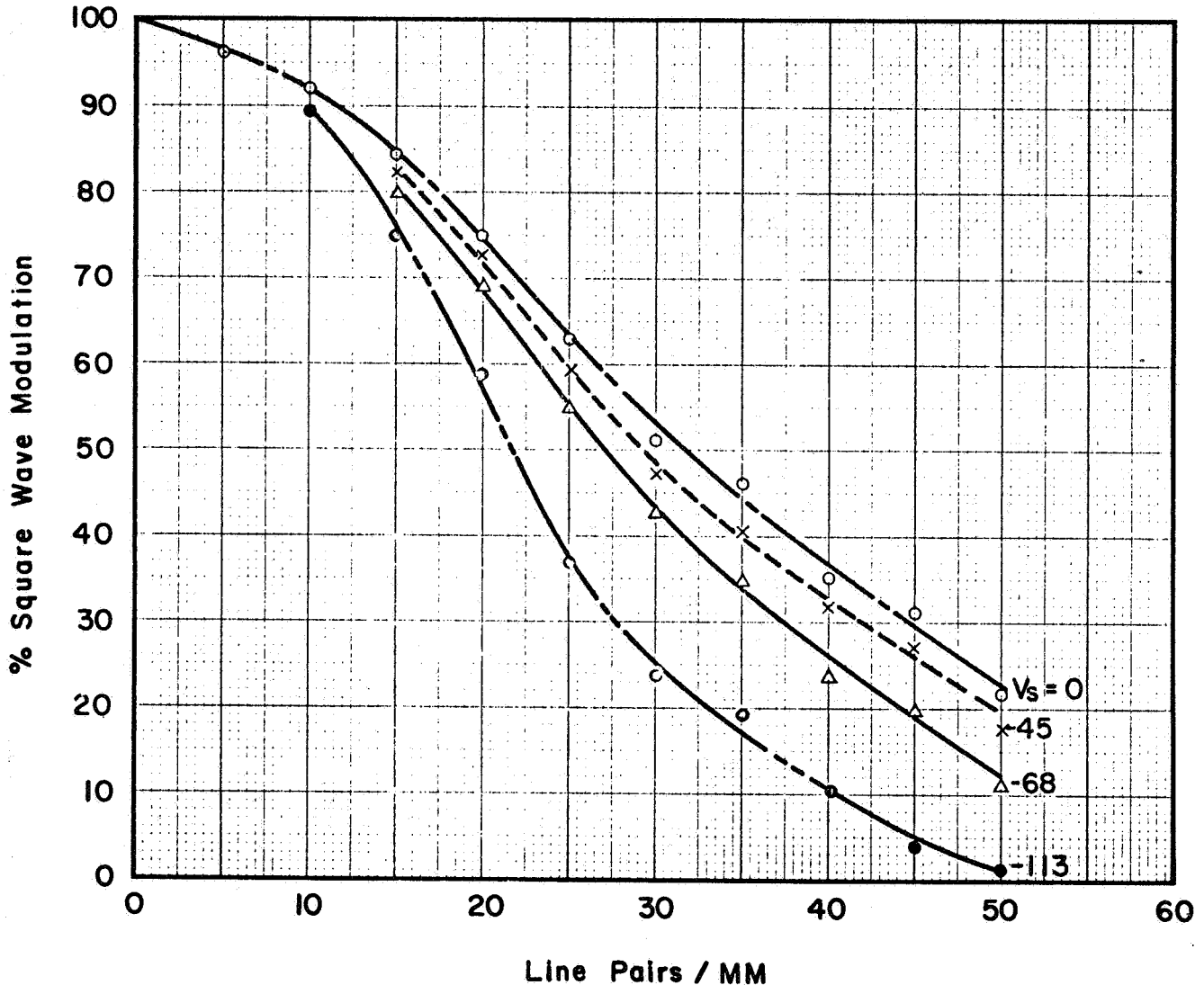

FIG. 32 TRIODE 2. MODULATION TRANSFER FUNCTION AT CENTER FOR VARIOUS SHIELD VOLTAGES V_A = 10 KV

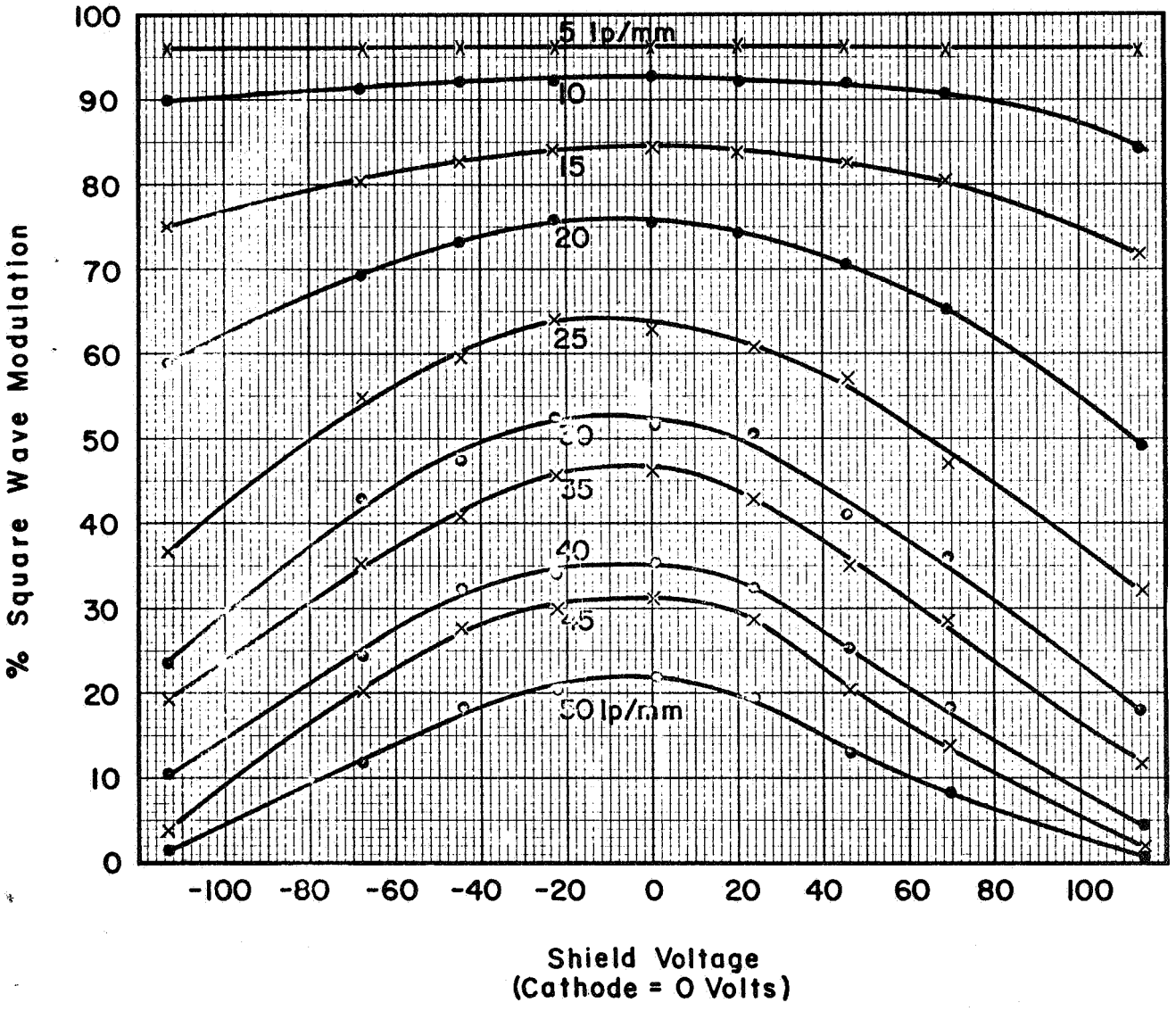

FIG.33 TRIODE 2. SQUARE WAVE RESPONSE AT CENTER AS A FUNCTION OF SHIELD POTENTIAL, AT VARIOUS LP/MM

$V_A = 10KV$

indicates that a change of shield potential of 138 volts is equivalent to a screen movement of 0.110". For the triode design, therefore, the movement of the image surfaces is slightly less than 0.001" per volt change in shield potential at 10 kV anode potential.

4.4 Computational Analysis

The ray tracing computer program was applied to the image section to evaluate the effect of the anode-tip configuration. The general imaging characteristics of the design are fairly well known from earlier work on the PIP program. Some difficulty is experienced in computing the properties of this particular design because of the small size of the anode aperture and the very high fields in the vicinity of it. Fig. 34 shows the electrode model superimposed on the relaxation net (73.5 mesh/inch) and some computed principal rays on which are marked the tangential and sagittal focal points. The scatter of the focal points reflects computational errors incurred in the high field region near the anode tip. However, it is thought that the axial focal point is probably more reliable than the others, and since the curvature and astigmatism properties are well known from earlier studies, we will not be concerned here with accurate determination of the complete image surfaces. The axial focal length determined from this computation is 2.124", about 0.045" shorter than the specified cathode to target dimension. The computation was repeated with a larger scale model (100 mesh/inch) and the value 2.141" was obtained. Agreement between these two computations is satisfactory.

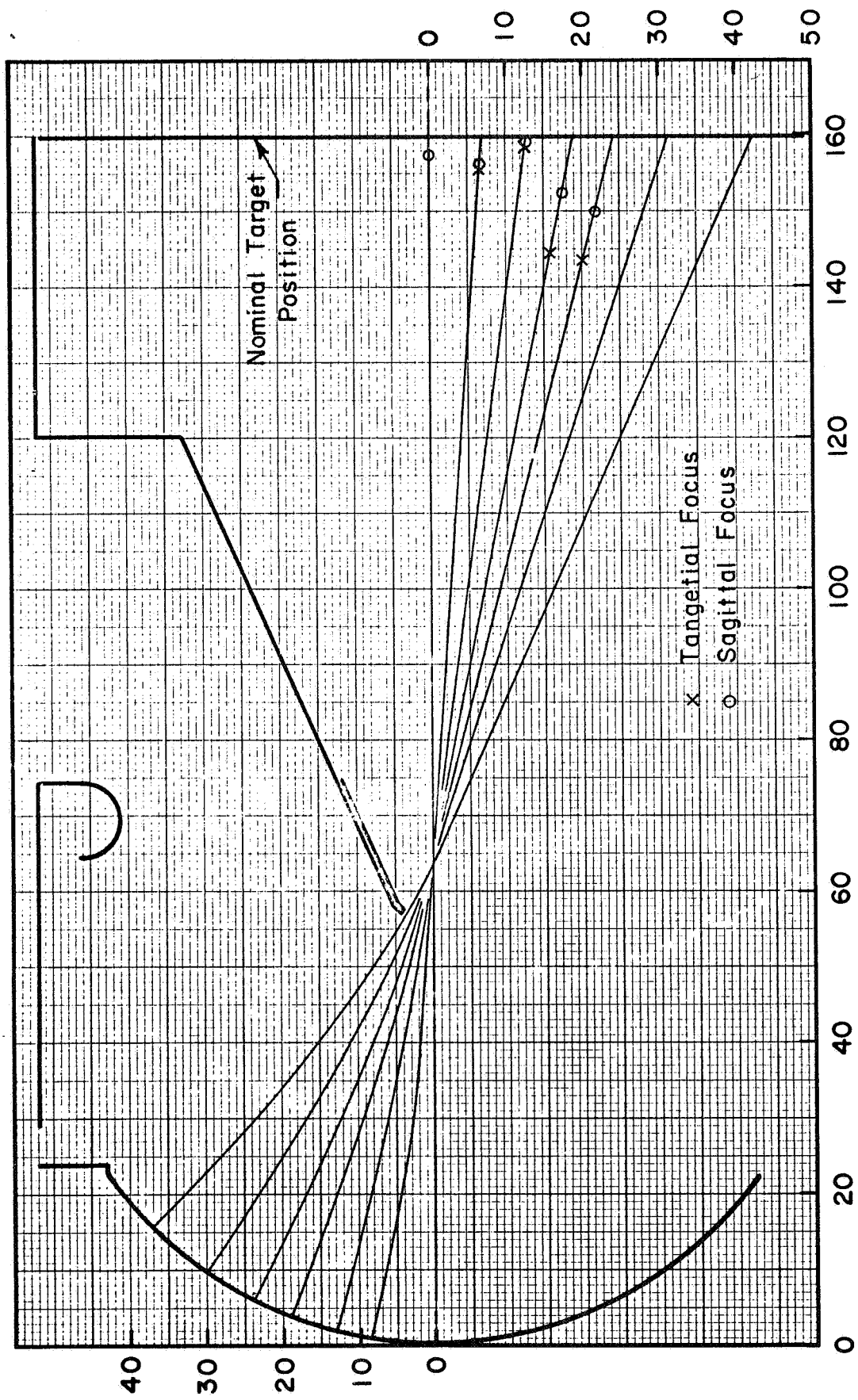

FIG. 34 IMAGE SECTION COMPUTATION
ORIGINAL SPEC. ANODE. 73.5 MESH / INCH
Cathode Shield (Dimension Q) 0.875"
Cathode Anode (Dimension G) 0.770"

With the same dimensions the computation for the new anode specification (scale 73.5 mesh/inch) showed a focal length of 2.157", i.e about 0.030" longer than with the original anode. This increase agrees with the findings of the experimental study discussed in Section 4.2. The focal length value itself is about 0.025" shorter than that indicated by bellows diode 2, which had dimensions almost identical to those used in the computation. In view of the computational difficulty the agreement with practice is very satisfactory.

To examine the action of the triode form of the image tube, computations were also made with small potential differences between shield and cathode. The results are summarized in Table 5.

TABLE 5

Triode image section. Original spec. anode, 10 kV

Cathode to anode 0.770"

Cathode to shield 0.875"

Shield voltage	- 150	0	150	300
Focal length	2.005"	2.124"	2.257"	2.407"
Magnification	.842	.917	1.002	1.098

Movement of the image surfaces is 0.00084" per volt change in shield potential, which agrees closely with the value deduced from practical results in Section 4.3.

The distortion of the image section can be determined from computed results such as those of Fig. 34. Distortion is the variation of

magnification with position in the field of view. With a flat output surface, as is of interest here, electrostatic image sections almost invariably display pincushion distortion--magnification increases steadily with radius r from the axis. Fig. 35 shows the relationship of r_{out} to r_{in} for principal rays in the LCT image section. The slope of this curve is the magnification, and in the absence of distortion the curve would be a straight line. The second curve plotted shows the slope $M = \frac{dr_{out}}{dr_{in}}$ as a function of r_{in}. Severe distortion is evident, particularly at the edges of the field. The maximum radius used in the LCT is 0.31" within which distortion does not appear to be objectionable.

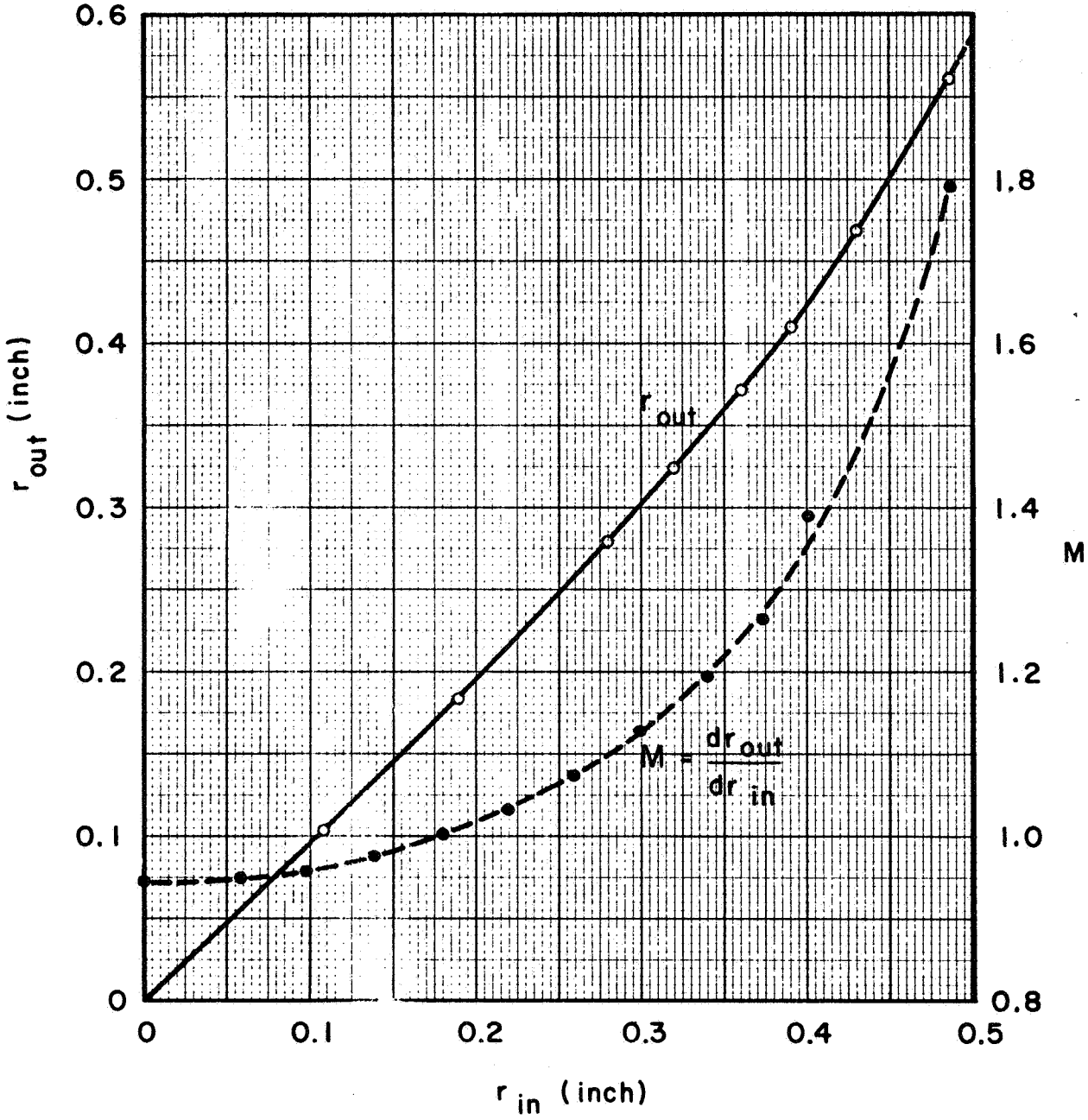

FIG. 35 MAGNIFICATION CURVE FOR THE IMAGE SECTION

(Computed Data)

5. LCT RESOLUTION

On the basis of the work on the readout section and the image section, reported in Sections 3 and 4, the resolution performance to be expected from the lunar camera tube can be estimated. Fig. 36 illustrates the procedure for the case of a standard LCT operated normally, with 30 volts on the suppressor mesh. The dashed curve represents the performance of a good image section, as given by the bellows diode results in Fig. 29. The broken curve for the readout section is taken from suppressor mesh vidicon 6544009, which has a 0.0018" beam-limiting aperture and 0.200" target-G6 spacing as are now standard in the LCT. The full curve in Fig. 36 is the point-by-point product of the other two curves, which indicates the performance to be expected from a LCT. Strictly speaking, the multiplication procedure should be applied only to sine wave response curves, but the errors involved in applying it to square wave responses are quite small and will here be ignored. For comparison is shown the performance of LCT 239, which is a fairly typical good tube. Agreement is satisfactory, being within experimental error. It appears that because of the high resolution of the image section, the resolution of the LCT is essentially that of the readout section. Within experimental error the results presented for suppressor mesh vidicons in Section 3 should indicate directly the variation of LCT performance with changes in the various parameters considered. From Fig. 36 the assumption that

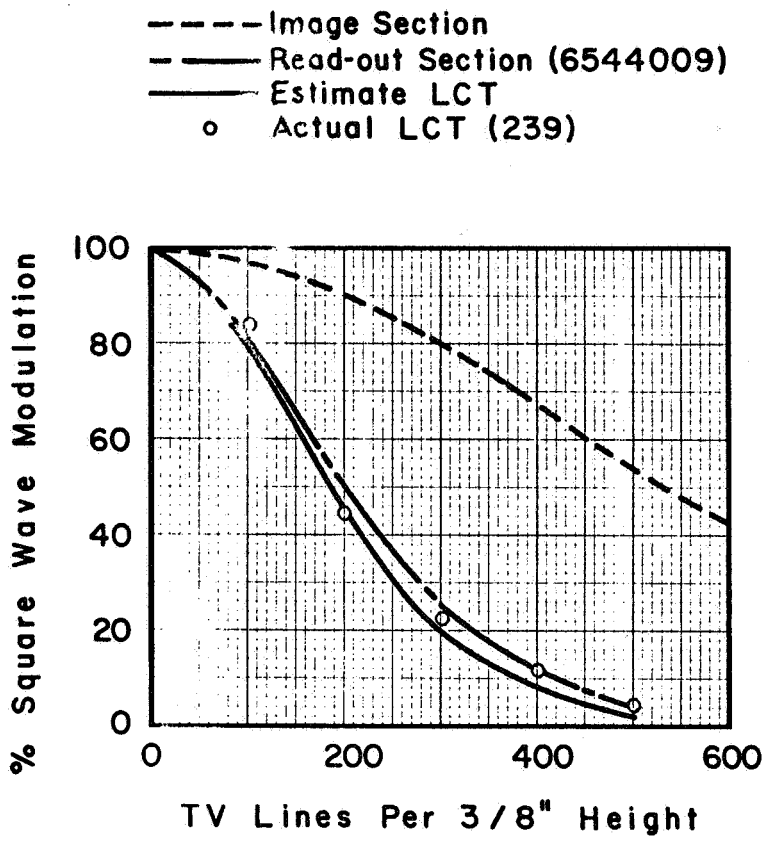

FIG.36 ESTIMATE FOR STANDARD LCT, NORMAL OPERATION (SUPPRESSOR MESH = 30 VOLTS)

the SEC target is not an important factor limiting the resolution appears to be reasonable. Further, it appears that the requirement in the LCT specification for 40% response at 250 lines is difficult to achieve even with the design improvements that have already been made. The limiting resolution requirement for 5% at 400 lines should be readily attainable, however.

The two most promising ways to improve resolution, according to results in Section 3, are reduction of beam-limiting aperture and refinement of suppressor mesh. Unfortunately, because of beam limitations and the poor quality of available 2000 line/inch mesh, neither procedure was considered practical in the LCT. However, one LCT was constructed with a 0.0007" beam-limiting aperture. This was tube 282, which also had increased target-G6 spacing of 0.264", and a triode image section (T6 in Table 4, Section 4.2). The image section was found to focus with the shield at approximately -65 volts with respect to photocathode. Depth of focus is so large that it was difficult to locate the focus potential by observing the monitor. Fig. 37(a) shows aperture response curves taken with the shield at the determined focus voltage and then at 50 volts on either side of it. It appears that the image section defocusing is just about detectable. In Section 4,4 the image surface movement was established to be slightly less than 0.001" per volt change in shield potential at 10 kV anode potential. Fig. 37 corresponds to anode potential of 8 kV, so that a tolerance of ±0.050" on placement of the target with respect to the focal point is suggested by these results. This experiment was

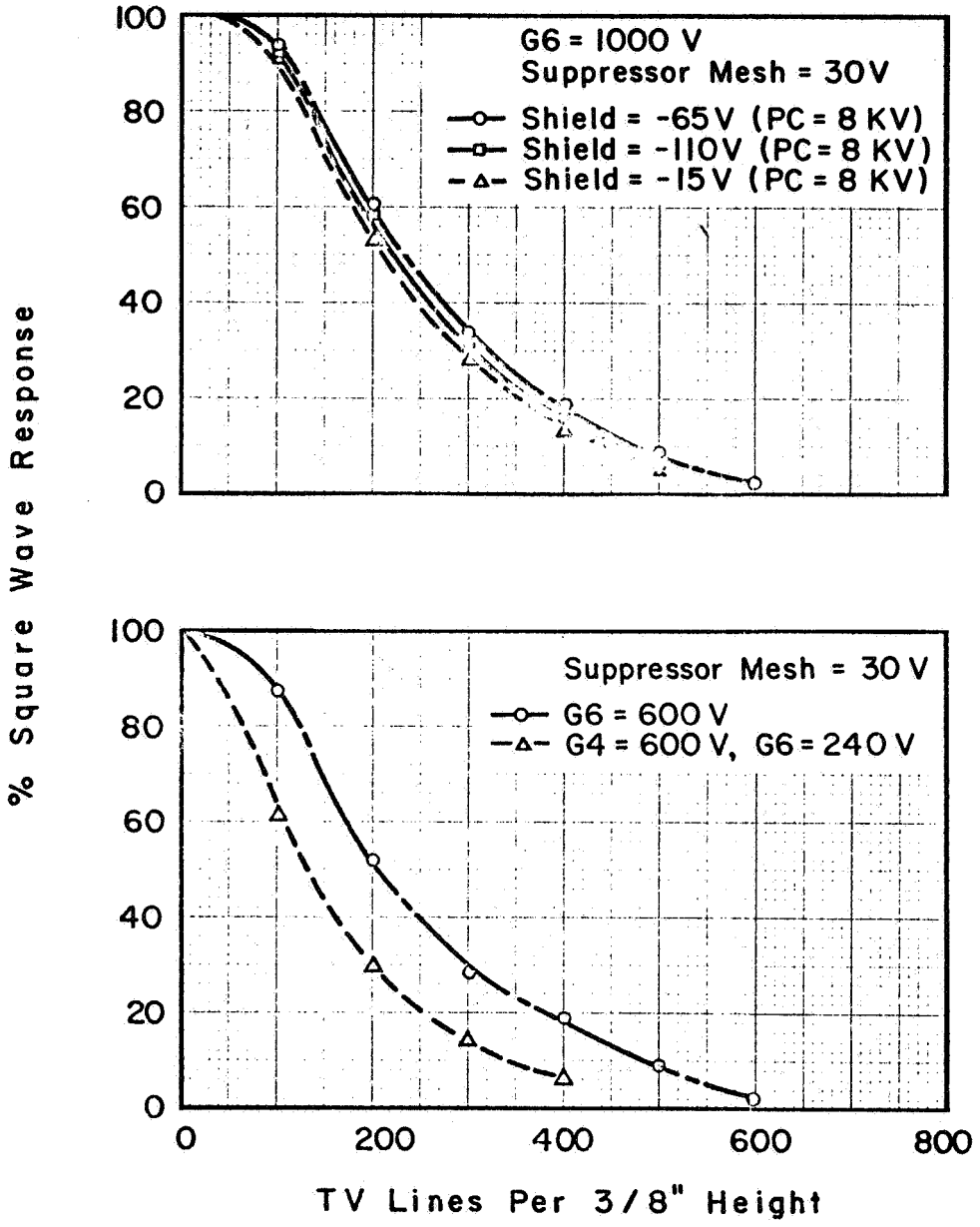

(a) Variation of Image Section Focus
(b) Normal and "Inverted" Focus of Read-out Section

FIG. 37 LCT 282 BEAM LIMITING APERTURE .0007"
TARGET-G6 SPACING 0.264"
TRIODE IMAGE SECTION

carried out with high voltage operation of the readout section in order to maximize the sensitivity of the performance to changes in the image section. Performance of the tube in the normal 600 volt operation mode is shown in Fig. 37(b). In normal operation the tube resolution is very close to that of suppressor mesh vidicon 251, which has very similar physical properties (see Table 3, Section 3.1). With the readout section operated in the inverted focus mode, the resolution of the tube was found to be comparatively poor, as shown by the lower curve in Fig. 37(b). No explanation is known for this. The same effect was noted in some suppressor mesh vidicons in Section 3.4.

Another LCT with a triode image section was no. 277. This was a standard tube in other respects, having a .0018" beam-limiting aperture and a 0.200" target-G6 spacing. In spite of the larger aperture this tube performed very nearly as well as tube 282. Similar conclusions regarding the image section focusing were drawn. This tube showed that 40% response at 250 lines is just about possible with the present tube configuration.

Further studies of the relative merits of normal and inverted focusing of the readout section were made on a number of tubes, with varying results. Tube 277, like 282, showed the inverted mode to be considerably worse, while tube 222 showed it to be only slightly worse. Tube 220 showed no detectable difference between the two modes, and tubes 227, 239 and 258 all showed some improvement in the inverted mode. Apart from 282, all the tubes had standard readout sections, and so, no explanation

of their differing performances can be given. As with the suppressor mesh vidicons some difficulties were experienced in the inverted focus mode with alignment and ion spots, and it is possible that these factors may have a bearing on the results obtained.

An unexpected observation was a significant variation of resolution with G5 potential in the normal mode of operation. The standard potential for the G5 electrode is 300 volts, which provides satisfactory scan linearity and beam landing uniformity. It was found that reduction of the potential below 300 volts (with, of course, accompanying adjustment of focus) produces a steady improvement in resolution. Fig. 38 shows aperture response curves from LCT 258 illustrating this effect. At G5 = 200 volts limiting resolution improved by over 100 lines. Unfortunately, this resolution gain is accompanied by loss of scan linearity, resulting in severe distortion of the monitor picture, and the effect therefore cannot be exploited in practice. It can, however, be recommended that the G5 potential be held at as low a value as is consistent with a geometrically satisfactory picture, perhaps in the vicinity of 250 to 275 volts.

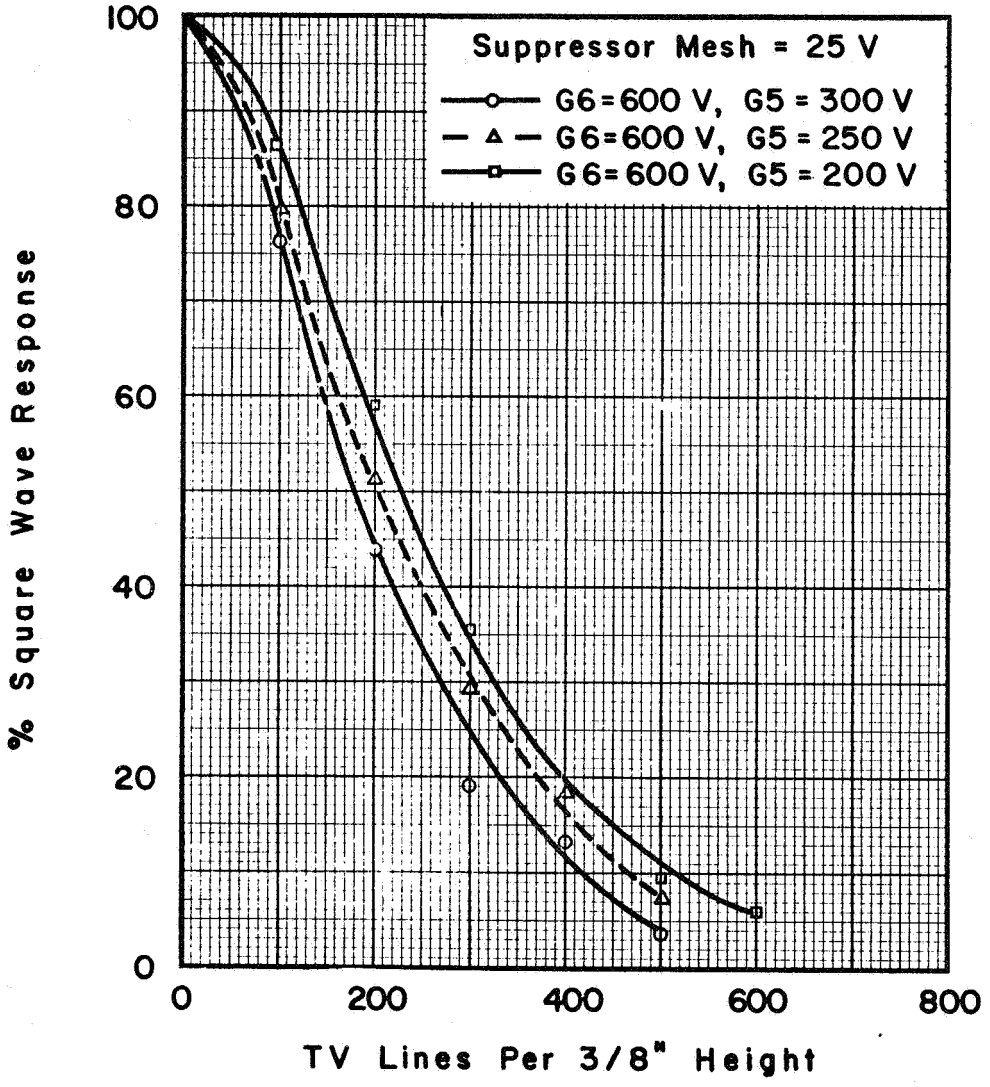

FIG. 38 LCT 258 VARIATION OF G5 VOLTAGE

6. CONCLUSIONS

This study has enabled the image section of the LCT to be closely specified. The importance of the anode shaping was demonstrated, and satisfactory sources of supply of well shaped components were established. Proper design centers for the image section and the important tolerances associated with them have been determined. Our ability to meet the tolerance requirements consistently in production assembly has been confirmed. Doubts about the image section should therefore be eliminated, it is hoped permanently, and the question of conversion to a triode no longer arises. It is worth remarking, however, that this position could have been reached much earlier had the original tube design been such as to permit triode operation of the image section.

The main contribution from the study of the readout section was confirmation of the correctness of changes recommended earlier in the LCT program, namely, refinement of the suppressor mesh from 750 to 1000 lines/inch and increase of the target-G6 spacing from 0.100" to 0.200". The modified values are now standard in the LCT. Results suggested that still finer meshes may be advantageous, but the difficulty of obtaining them with reasonable transmission and good quality prohibits their incorporation into the LCT. Also, it seems likely that the target-G6 spacing has now been increased to a point of diminishing returns. A value of 0.250" would probably be a reasonable value at which to settle, although it is questionable if the advantage offered justifies the change at this stage of the program.

Because of the troubles experienced with alignment and ion spots in some tubes, non-standard focusing modes in the readout section cannot be generally recommended. The "inverted" focus mode may provide improved resolution in particular tubes, however. In the normal mode of operation, resolution can be improved slightly by reducing the operating potential of G5 below the normal value of 300 volts at some sacrifice of geometrical uniformity.

Reduction of the beam-limiting aperture appeared to be the most promising method of improving resolution in electrostatically focused vidicons, but, because of accompanying reduction of beam current, such a modification could not be made in the lunar camera tube. The finding may be useful in connection with other SEC camera tubes, however. This result suggests that further studies of the triode gun design should be made with the objective of achieving higher currents through the small diameter apertures, if possible without increasing the beam angle. Higher resolution tubes with undiminished signal level could then be designed. This kind of work on triode guns is difficult and probably requires the construction of special demountable apparatus. The setting up of such apparatus being initially costly and time consuming, no study of triode gun modifications was considered within the scope of the present program.

The main objective of the resolution study program has been achieved in that the original resolution specification has been shown to be realizible, although only in a fairly small percentage of tubes. The limiting resolution requirement for 5% response at 400 lines is more

readily attainable than the requirement for 40% response at 250 lines. To improve the yield of such tubes would require modifications that will reduce beam current and so restrict the signal capability of the tube. Without further research along the lines suggested above it would be unrealistic to accept the improved resolution specification requested by the systems group.

REFERENCES

1. O. H Schade, B. H. Vine, and A. Rotow, "Applied Research on High Resolution Camera Tubes," AD602425.

2. S. Gray, P. C. Murray, and O. J. Ziemelis, "Improved High Resolution Electron Gun for Television Cameras," J.S.M.P.T.E., 72, 792 (1963).

3. M. Green, R. R. Beyer, and H. de Vries, "Exploratory Development of High Resolution Television Camera Tubes," Westinghouse Report No. ET-12, 87 (Nov. 29, 1965).

APPENDIX H

THE INFLUENCE OF THE READING BEAM DIAMETER ON RESOLUTION

ET 13

December 15,1965

THE INFLUENCE OF THE READING BEAM DIAMETER ON THE TRANSFER FUNCTION OF AN SEC CAMERA TUBE

M. Green

Approved by

R. A. Shaffer
Engineering Section Manager
R & D Department

WESTINGHOUSE ELECTRONIC TUBE DIVISION
ELMIRA, NEW YORK

Table of Contents

		Page
1.	Introduction	1
2.	Theoretical Analysis	
	2.1 Charging of the target during the frame period - normal signal current	6
	2.2 Charging of the target during the line period - the first component of the supersaturation signal current	9
	2.3 Charging of the target during the elemental dwell time - the second component of the supersaturation current	15
3.	Comparison With Experiment	
	3.1 Simultaneous and sequential read and write	17
	3.2 Estimates of beam diameter	18
	3.3 Frame rates	20
4.	Conclusion	25
5.	Acknowledgements	26
6.	References	27

1. INTRODUCTION

Elementary considerations suggest that the transfer function of an SEC camera tube (the relation between signal current and photocathode illumination or primary current density at the target) should show two distinct regions. At a low primary current density the signal current will be proportional to the primary current density. At a high primary current density the signal current will be substantially independent of the primary current density. These two regions will be linked by a transition region where the gradient of the transfer function will fall from unity to zero on a log-log plot.

The above characteristics have been observed in the measured transfer functions of SEC camera tubes such as the WX-5419 (see Figure 1). However, measurements made more recently on other types of SEC camera tubes have shown significantly different behavior. In particular, the region where the signal current is independent of the primary current density has been found to be small or even non-existent, and is often followed by a further upward swing in the signal current (see Figure 2). This "supersaturation" region of the transfer function is also observed in image orthicons with a wide-spaced target mesh. Here it is produced by "line" storage in the interelement capacity of the orthicon target[1,2]. However, interelement capacity effects do not appear to be large enough to account for the supersaturation regions of the SEC camera tube transfer functions shown in this report. From measurements on image orthicons it is known that interelement capacity effects are

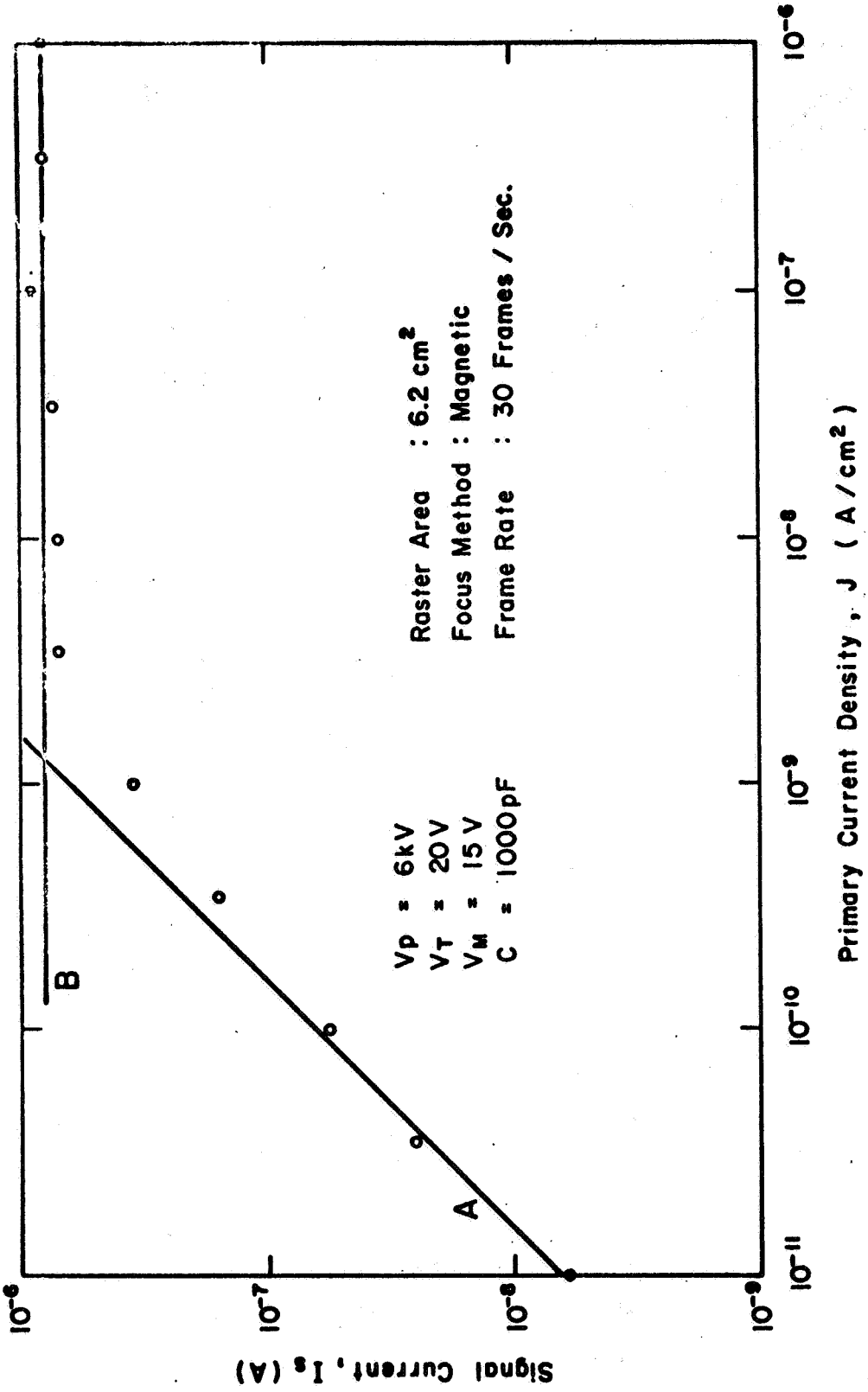

Figure 1

Transfer Function Of A Magnetically Focused SEC Camera Tube With A 25mm Diameter Target

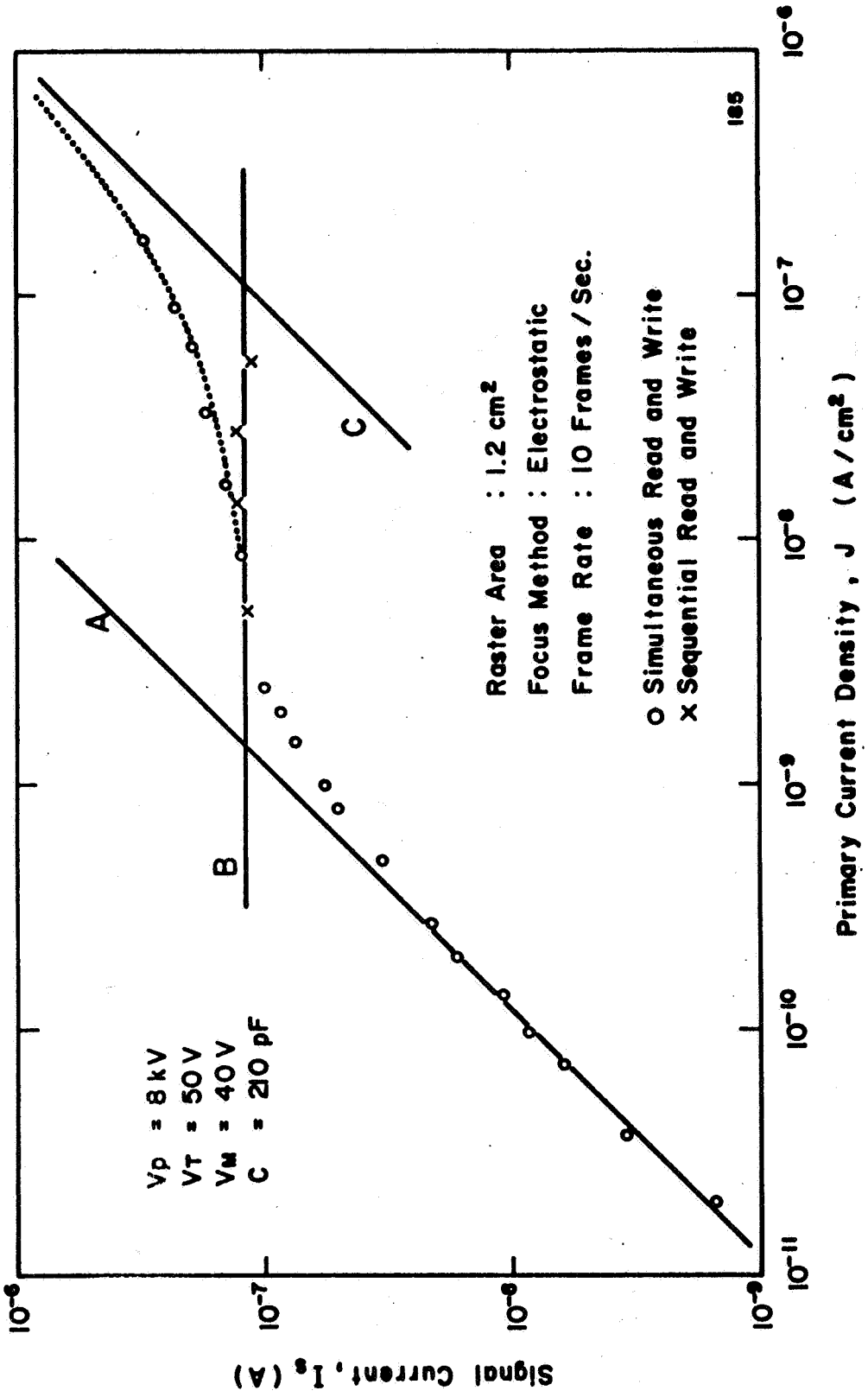

Figure 2

Transfer Function of an Electrostatically Focused SEC Camera Tube With a 16mm Diameter Target - Tube 1

negligible (with 250 to 525 scanning lines) when the storage capacity per raster is greater than 400 pF. This is the case for the SEC camera tube whose transfer function is illustrated in Figure 6 (storage capacity per raster 650 pF) yet the supersaturation region is clearly present.

Figure 3 demonstrates that the supersaturation region is controlled by factors other than interelement capacity. With a G_1 bias of -10V, a "normal" transfer curve (circles) with a flat plateau is obtained showing that interelement capacity effects are negligible. However, if the bias is reduced to 0V, a supersaturation region develops (crosses). The reduction of the G_1 bias produces an increase in beam diameter, and this increase is a likely cause for the appearance of a further upward swing in the signal current. In this report the effects of beam diameter variations on the transfer function of an SEC camera tube are studied in some detail and are, in fact, shown to be responsible for the behavior of the signal current in the supersaturation region.

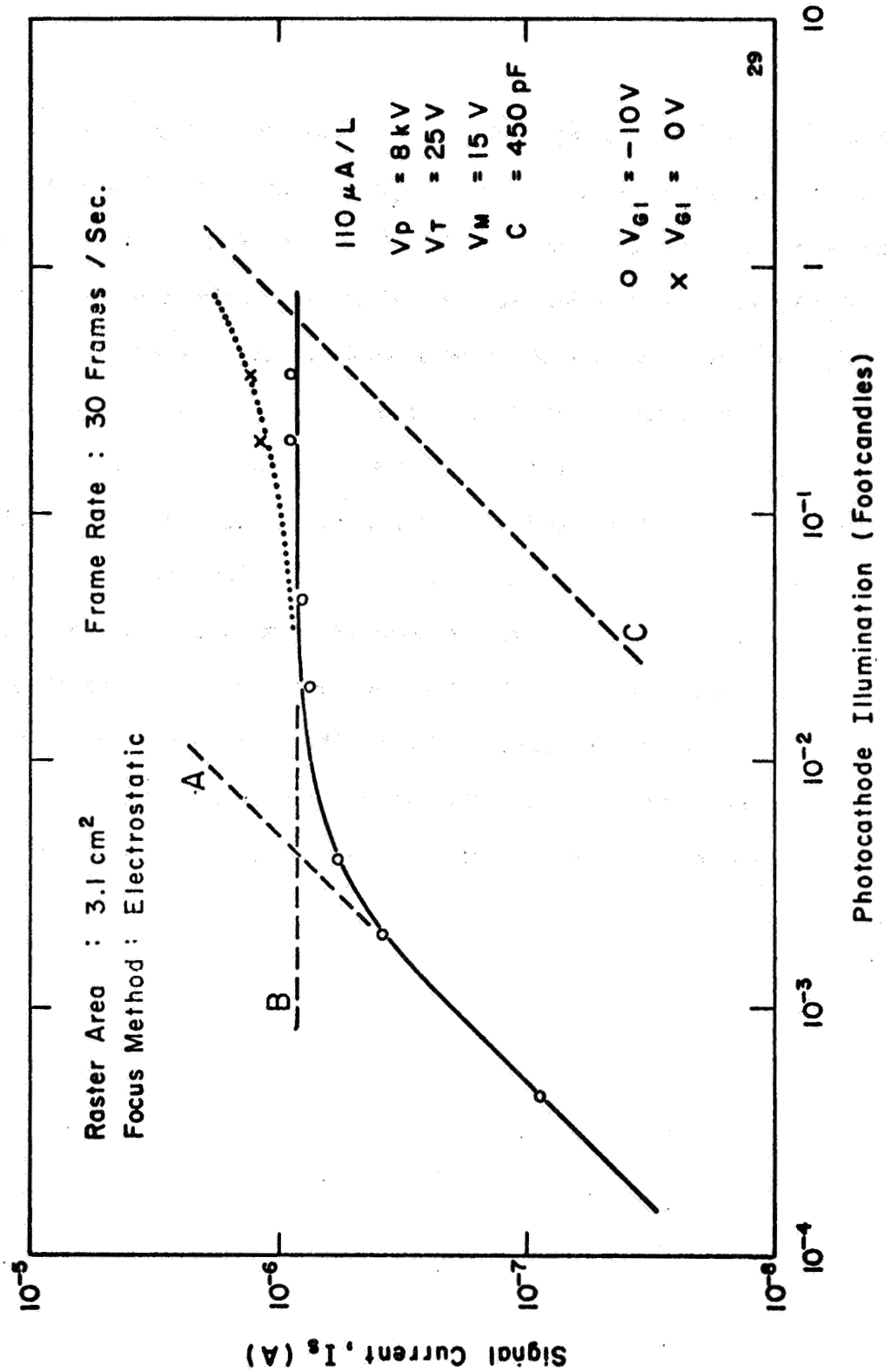

Figure 3

Transfer Function of an Electrostatically Focused SEC Camera Tube with a 25mm Diameter Target

2. THEORETICAL ANALYSIS

2.1 CHARGING OF THE TARGET DURING THE FRAME PERIOD - NORMAL SIGNAL CURRENT

We will review first the mechanism responsible for the 'normal' response curve. Let the frame period be T and the charge built up on unit area of the target during this period be Q. Then, if E_H and E_V are the horizontal and vertical scanning efficiencies, the reading time will be $E_H E_V T$. The signal current, I_S is given by:

$$I_S = \frac{QA}{E_H E_V T} \tag{1}$$

where A is the area of the raster. To calculate Q we must integrate the incremental build-up of charge over the frame period T. If G is the instantaneous gain:

$$dQ = JG \cdot dT \tag{2}$$

where J is the primary current density. Experiment shows that the gain of an SEC target has a maximum value, G_o, when the target surface potential, V, is zero and falls to zero when the target surface reaches its maximum potential V_S. This maximum potential is set either by the target voltage or the suppressor mesh voltage, whichever is higher. For a given primary

voltage we may write:

$$G = F(V, V_S) \tag{3}$$

and since $V = \frac{Q}{C}$ where C is the capacity per unit area of the target we may rewrite equation (3) as

$$G = F(\frac{Q}{C}, V_S)$$

Therefore, from equation (2) we have

$$dQ = J \cdot F(\frac{Q}{C}, V_S)\, dT$$

The total charge is found by integrating this equation for the appropriate integration period, in this case the frame period, T.

$$\int_0^Q \frac{dQ}{F(\frac{Q}{C}, V_S)} = \int_0^T J \cdot dT \tag{4}$$

Equation (4) is expressed in the most general terms. In order to clarify the discussion it is convenient to introduce a simple empirical expression for the gain equation, equation (3).

$$G = \frac{G_o}{V_S} (V_S - V) \tag{5}$$

or

$$G = \frac{G_o}{V_S} \left(V_S - \frac{Q}{C}\right) \tag{6}$$

Substituting in equation (4) and integrating, we find that:

$$Q = CV_S \left(1 - e^{-\frac{G_o JT}{V_S C}}\right) \tag{7}$$

Further substitution in equation (1) gives:

$$I_S = \frac{ACV_S}{E_H E_V T} \left(1 - e^{-\frac{G_o JT}{V_S C}}\right) \tag{8}$$

for the normal transfer function. When $\frac{G_o JT}{V_S C} \ll 1$ equation (8) reduces to the following expression:

$$I_S = \frac{JAG_o}{E_H E_V} \tag{9}$$

and when $\frac{G_o JT}{V_S C} \gg 1$

$$I_S = \frac{ACV_S}{E_H E_V T} \tag{10}$$

Equations (9) and (10) represent the two distinct regions of the transfer function described in the summary. They are shown schematically at the

left of Figure 4. The dotted line joining the two curves represents the transition region where neither equation (9) or (10) is applicable but where equation (8), or one similar, must be used.

The significance of equations (9) and (10) is that they represent two rather simple physical situations in the target. Equation (9) applies when the voltage excursion during the frame period, V, is small and the gain has a value close to G_o throughout integration. Equation (10) applies when the voltage excursion reaches its maximum value, V_S, before the end of the integration period and a further increase in the primary current density does not affect the amount of signal charge or signal current. Although we have derived these two asymptotic equations for a particular form of the gain variation, it can be seen that they apply whenever the gain variation satisfies the following conditions; $G = G_o$ when $V = 0$ and $G = 0$ when $V = V_S$.

2.2 CHARGING OF THE TARGET DURING THE LINE PERIOD - FIRST COMPONENT OF THE SUPERSATURATION SIGNAL CURRENT

It would appear from the discussion presented so far that the signal current should reach the so-called 'saturation' value given by equation (10) and then increase no further unless the primary current density attains a large enough value to actually change the physical structure of

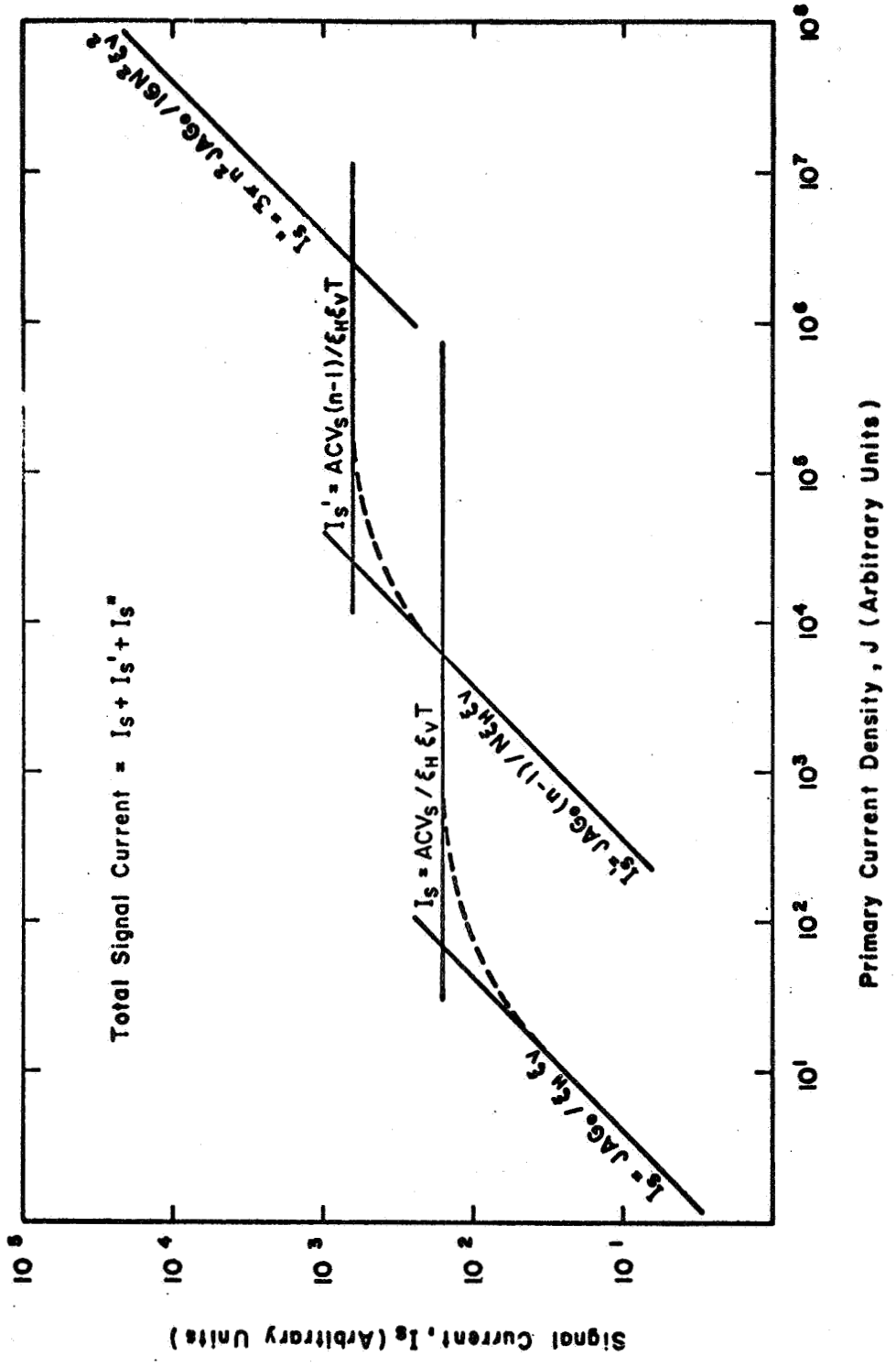

Figure 4

Theoretical Transfer Functions

the target. However, this argument turns out to be incorrect. We may identify two further contributions to the signal current which we will call the first and second components of the supersaturation signal current, I_S' and I_S''. The first component occurs in any SEC camera tube where the diameter of the scanning beam is greater than the spacing of the scanning lines. (This is a normal situation in many camera tubes.) The importance of the beam diameter may be best understood by reference to Figure 5.

If the beam diameter is greater than the line spacing only a small portion of the beam is normally responsible for depositing charge on the target. In Figure 5 this region is shown shaded and lies at the bottom of the beam cross-section when scanning takes place in the directions indicated. The reason for the inactivity of the rest of the beam cross-section is that it is covering a strip of target that has only recently been scanned and is, therefore, at cathode potential (provided no significant charging has taken place during the line period).

This last statement is the key to the origin of the first component of the supersaturation signal current. If the primary current density is high enough, significant charging will indeed take place during the line period. The normally inactive upper portion of the beam, covering an area of the target that has been returned to ground only one line period ago,

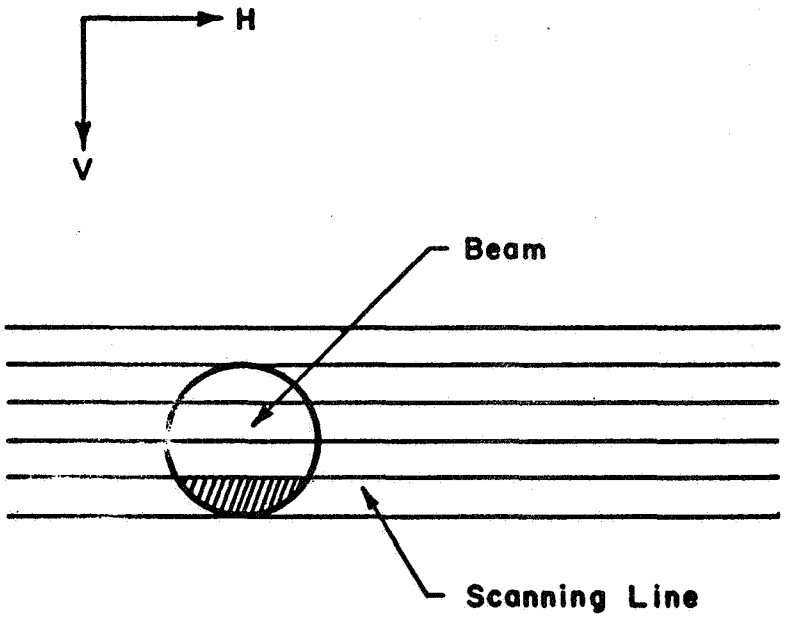

Figure 5

The Relation of Beam Diameter and Line Spacing

will deposit further charge and give rise to a further contribution to the signal current. This contribution is calculated in a similar fashion to the normal signal current. The reading time is $E_H T/N$, where N is the number of scanning lines. Since the actual number of lines in the raster is $E_V N$, the signal charge covers an area $(n - 1)\ A/E_V N$. Thus:

$$I_S' = \frac{QA\ (n - 1)}{E_H E_V T} \tag{11}$$

Q may be calculated, as before, by integrating equation (4), but in this case the integration time is the line period, T/N. For the specific gain function given in equation (5)

$$I_S' = \frac{(n - 1)ACV_S}{E_H E_V T} \left(1 - e^{-\frac{G_o JT}{NV_S C}}\right) \tag{12}$$

In general, for every point on the normal transfer curve, there is a corresponding point on this supersaturation current curve at N times the primary current density and (n - 1) times the signal current.

When

$$\frac{G_o JT}{NV_S C} \ll 1$$

$$I_S' = \frac{(n - 1)JAG_o}{NE_H E_V} \tag{13}$$

when

$$\frac{G_0 JT}{NV_S C} \gg 1$$

$$I_S' = \frac{(n - 1)ACV_S}{E_H E_T T} \tag{14}$$

These two curves are shown at the center of Figure 4. By adding the two terms, I_S and I_S', the full signal current can be obtained.

The following points are characteristic of the first component of the supersaturation current:

(a) The current is only observed in normal continuous scanning where there is simultaneous reading and writing. Where there is sequential reading and writing, charging of the target during the line period cannot take place.

(b) For a given beam diameter and a given raster size, increasing the number of scanning lines, N, will also increase the number of lines covered by the beam, N. The result is to shift the transfer function to higher signal current values along a line at 45° to the two axes on a log-log plot.

(c) Since an increasing fraction of the beam cross-section is involved in generating the supersaturation current, there should be a

simultaneous decrease in resolution.

(d) The normal signal current is not affected by an increase in the beam current beyond that required to discharge the target. This is not true of the supersaturation current. As the beam current is increased, the spot size tends to grow and hence both N and the signal current increase.

(e) Both the onset of normal saturation and of supersaturation will be easier to observe when the frame period, T, is long because they occur at lower current densities.

2.3 CHARGING OF THE TARGET DURING THE ELEMENTAL DWELL TIME - THE SECOND COMPONENT OF THE SUPERSATURATION CURRENT

The second contribution to the supersaturation current occurs at such high primary current densities that it has little practical significance. It is, however, included in this treatment for the sake of completeness. The normal signal current is produced by charging during the frame period. The first component of the supersaturation current is produced by charging during the line period. The second component discussed in this section is the result of charging during the dwell time of the reading beam on the individual picture element.

Over an area, a, of the target equal to the cross-section of the reading beam there will be a charging current, JaG_o, flowing in the target

even as the reading beam holds the target surface at cathode potential. As the beam delivers a current to replace this charge flow, there will be a corresponding signal current,

$$I_S'' = JaG_0 \tag{15}$$

For a standard 4 x 3 aspect ratio raster

$$a = \frac{3\pi n^2 A}{16\ N^2 E_V^2}$$

Therefore:

$$I_S'' = \frac{3\pi n^2 JAG_0}{16\ N^2 E_V^2} \tag{16}$$

This contribution to the signal current is shown at the right of Figure 4. It has similar characteristics to the first component of the supersaturation current.

(a) It is only observed in continuous scanning.

(b) The resolution will be limited by the full beam diameter.

3. COMPARISON WITH EXPERIMENT

3.1 SIMULTANEOUS AND SEQUENTIAL READ AND WRITE

Let us first make a direct test of the supersaturation current theory by comparing transfer curves obtained from the same SEC camera tube with simultaneous read and write (normal scanning) and with sequential read and write. In the latter case a 'normal' plateau should be observed. A comparison of the experimental results is given in Figure 2. The transfer curves shown in this Figure were measured with a 320 line non-interlaced scan and a frame time of 1/10 second. The tube was operated with a target voltage of 50 V, a suppressor mesh potential of 40 V, and a photocathode potential of 8 kV.

Up to a primary current density, J, of 10^{-8} A/cm^2, simultaneous and sequential operation give the same output current, (only one set of points is shown in the Figure). Above 10^{-8} A/cm^2 simultaneous operation results in a short plateau followed by a further increase in signal current as is normally observed with this type of tube. However, measurements made during sequential operation (marked by crosses) show the well defined plateau predicted by the normal signal current theory. Thus, the observed behavior provides qualitative confirmation for the supersaturation hypothesis advanced in Section 2.2.

To make a quantitative comparison with theory, we proceed as follows. First we insert in Figure 2 the two curves A and B corresponding to the best fit of the asymptotic equations (9) and (10) to the experimental data. These two curves represent the 'normal' signal current. Curve B is particularly easy to fit in this case as the measurements made during sequential operation clearly establish the saturation plateau. We now add curve C to the Figure. The form of this curve is given by the asymptotic equation (13) which represents the first component of the supersaturation current. The position of C is adjusted until the sum of B and C, shown by a dotted line, gives the best fit to the experimental points. It can be seen that, although there is only one degree of freedom in matching the theoretical curve to the experimental data, an excellent fit is obtained over a range of one order of magnitude in J. We shall see later that similar agreement is found with transfer curves from other SEC camera tubes. The excellent fit to the experimental data provides further support for the general validity of the theory.

3.2 ESTIMATES OF BEAM DIAMETER

A comparison of equation (9) and equation (13) shows that, for a given value of signal current, primary current densities on curves A and C are related by a factor, $N/(n - 1)$. Since, for the transfer curve shown in Figure 2, $N = 320$ and the value of $N/(n - 1)$ giving the best fit is 80,

we may deduce that $n - 1 = 4$ or that the beam covers 5 scanning lines.* A deterioration in resolution is observed at $J = 10^{-8}$ A/cm^2 which may be partly ascribed to the effect of the supersaturation current flowing in a beam of this diameter. However, other causes of poor resolution when the target is in saturation (such as beam-bending) should not be ignored.

This insight into the relation of the beam diameter and the line spacing now enables us to explain the striking dissimilarities between Figures 1 and 2 noted in the Introduction. The camera tube whose transfer curve is presented in Figure 1 does not show any of the characteristics of the supersaturation current even when operated with simultaneous read and write (normal scanning). It is a magnetically focused tube (unlike the tube whose characteristic is shown in Figure 2. This tube is electrostatically focused.) It was operated with a much larger raster area (6.2 cm^2 compared to 1.2 cm^2) and the scan is 525 line interlaced with a frame period of 1/30 second.

Since the tube of Figure 1 has a raster area five times that of the tube in Figure 2, a beam of the same diameter will cover only $3\frac{1}{2}$ lines (allowing for the difference in the number of lines). In fact, measurements indicate that the beam actually covers less than 2 lines, probably because of the superiority of magnetic focusing. Such a beam

* Measurements of the width of the unblanked vertical retrace lines have been made with the reading gun of this tube set to discharge the target at peak signal levels. Assuming that the beam diameter is equal to the width of the retrace lines, good agreement has been found with the deduction quoted above; that the beam covers five scanning lines.

size in a non-interlaced scan would give a long plateau with curves A and C spaced by a factor of approximately 500; that is 525/(2-1). However, because the transfer curve in Figure 1 was measured with an interlaced scan, where the beam moves 2 line widths after each line scan, there is no overlap with previously scanned areas, and no supersaturation current is observed. We see that the essential differences between the two camera tubes of Figures 1 and 2 contributing to the presence or absence of supersaturation current are as follows; differences in raster area, nature of beam focus and type of scan (interlace or non-interlace).

It should be noted in passing that if the beam diameter is greater than 1 but less than 2 lines wide in an interlaced scan, curve B should be calculated from equation (10) by using an integration period, T, intermediate between the frame period and the field period.

3.2 FRAME RATES

Figures 6 and 7 show measured transfer curves for camera tubes of the type illustrated in Figure 2. In Figures 6 and 7 the tubes were operated with a target voltage of 40 V, a suppressor mesh potential of 30 V, and a photocathode potential of 8 kV. The photocathode sensitivity of both tubes was 100 uA/lumen.

Results for two frame rates are shown, 10 frames/second (320 lines)

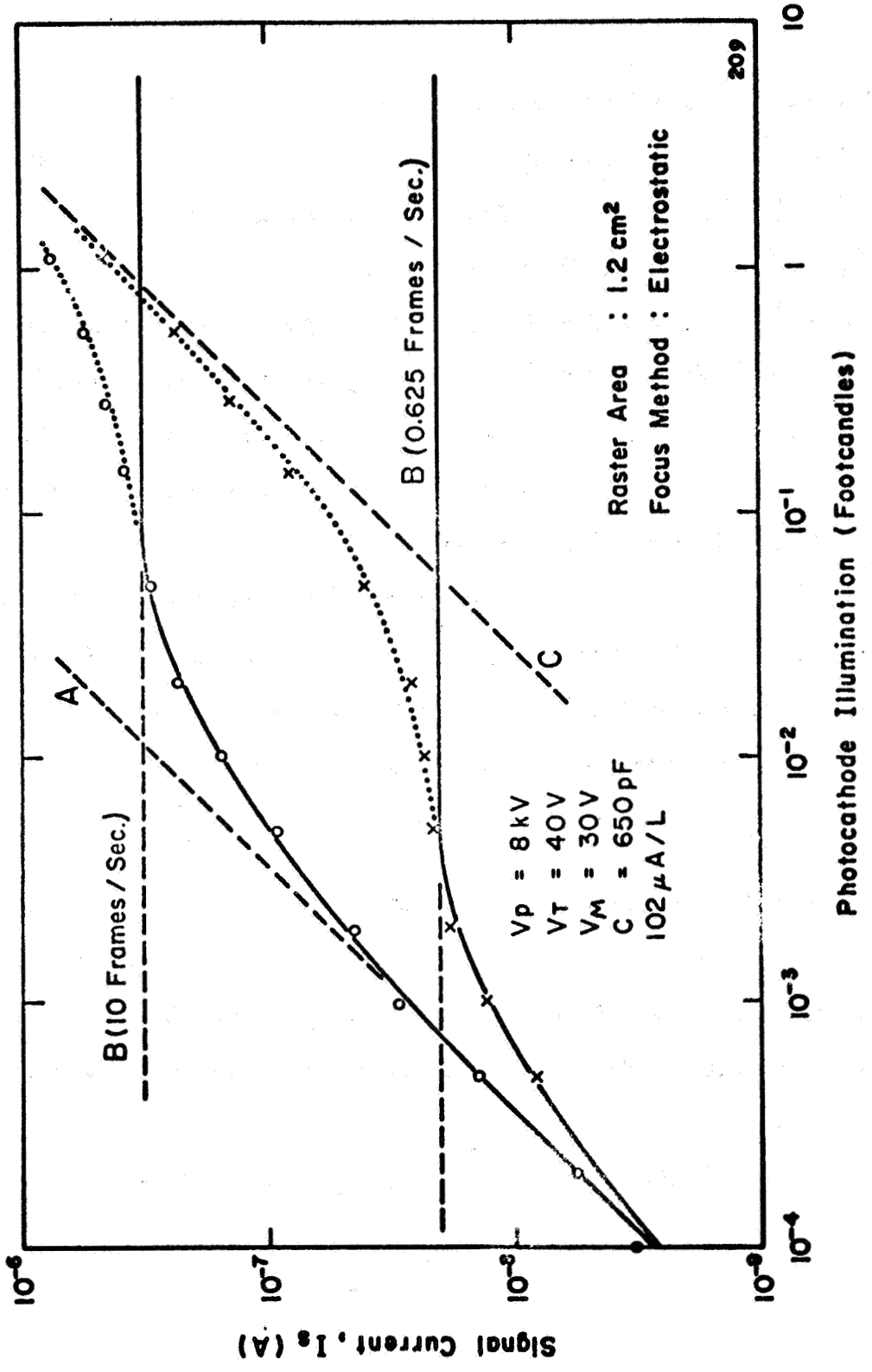

Figure 6

Transfer Function of an Electrostatically Focused SEC Camera Tube with a 16 mm Diameter Target - Tube 2

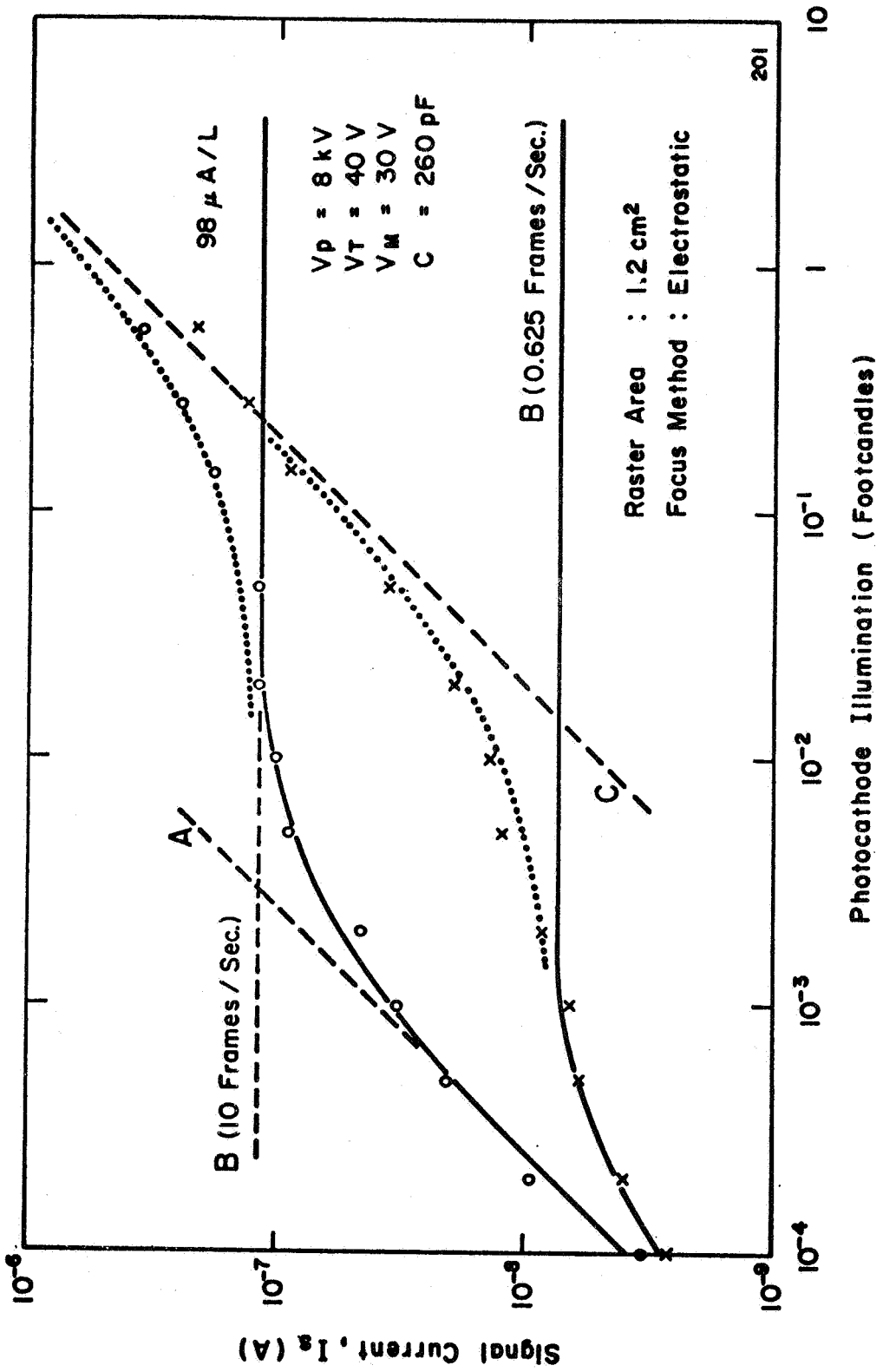

Figure 7

Transfer Function of an Electrostatically Focused SEC Camera Tube with a 16mm Diameter Target - Tube 3

and 0.625 frames/second (1280 lines). One rate is 16 times the other. Though the number of lines differs, it will be seen that for a constant raster size and beam diameter, $N/(n - 1)$ is the same for both curves. Consideration of equations (9), (10) and (13) shows that the theoretical curves A and C are the same for both frame rates and curve B is displaced by a factor of 16.

Examining the experimental data we observe that the B curves fit well with the theoretical spacing of 16. Furthermore, the combination of the B curves and a single C curve predicts most successfully the supersaturation current at both frame rates (the sum of B and C are shown by dotted lines). In both Figure 6 and Figure 7 the spacing of the A and C curves gives a beam diameter of equal to 5 line widths with the 320 line scan (as in Figure 2).

It is interesting to note that the 0.625 frame/second curve in Figure 7 is beginning to show "saturation" of the supersaturation current, as the photocathode illumination approaches one foot-candle. Also of interest is the general relation of the curves for the two frame rates. It can be shown that the signal current components I_S and I_S' can be written with greatest generality in the form

$$\text{constant} = \frac{1}{I_S T} \cdot f(JT) \qquad (17)$$

(see, for example, equation (8))

Thus, every point on a transfer curve measured with a frame period T_1 can be reproduced on another transfer curve measured with a frame period T_2 by scaling I_S and J by a factor T_1/T_2. In Figures 5 and 6, $T_1/T_2 = 16$. By scaling I_S and J by a factor of 16 it will be found that the experimental points on one curve accurately match the points on the other curve.

4. CONCLUSION

The absence of a well defined plateau in the transfer curves of certain SEC camera tubes can be explained as the consequence of charging of the target during the line period. Since this effect occurs at primary current densities greater than those required to saturate the target during the frame period, it has little practical significance. However, the search for an explanation has led to further understanding of the transfer characteristics of SEC camera tubes, and has provided new information about the diameter of the reading beam.

5. ACKNOWLEDGEMENTS

I would like to thank R. A. White, G. M. Bernhardt, and A. H. Boerio for providing the experimental data presented in this report.

6. REFERENCES

1. R. Theile, Journal of the Television Society 9, 45 (1959)

2. R. B. Janes and A. A. Rotow, RCA Review 11, 364 (1950).

APPENDIX I

HUMIDITY TEST

WESTINGHOUSE

ENGINEERING MEMORANDUM

ACTION

YES ☐ NO ☒

AEROSPACE DIVISION
BALTIMORE,MD.
ATTENTION: C. P. Hoffman
cc: A. J. Haley, D. E. Morenart
SUBJECT: Humidity Test

FROM: ELECTRONIC TUBE DIVISION
EM NO: 88
DATE: 9-16-66
G.O. NO:

In accordance with Paragraph 3.4.5.13 of P.D.S. 2134 (Revision C) Humidity Tests, we have prepared two tubes and initiated the specified test. Several problems have arisen which indicate that the test is difficult at best and probably not meaningful.

The test requires that the front end of the tube and the leads as they emerge from the gun be potted and that the tube be exposed to (10) 24-hour cycles of 95 ± 5% relative humidity. The tube must be operated and tested for corner and center resolution under these conditions.

Tube #432 was potted and placed in the chamber with leads extended to our test set. The resulting presentation was poor due to excessive lead length. Under test conditions there is a continuous film of water over the whole tube and associated circuitry making operation with specified voltages at the tube difficult.

Nevertheless, the tube was operated and pictures taken with the test setup before and after exposure to humidity conditions. This water film is also across the faceplate, creating water droplets that distort a projected image and which succeeded in disolving the emulsion from the test pattern placed on the faceplate. Subsequent to the 10 day exposure the tube was removed from the chamber, and it was discovered that the coil form material had absorbed so much moisture that the yoke has expanded, making it impossible to remove the tube to test it in the test set and to use the yoke for the second tube (#411), which also is to be tested in the humidity chamber.

In view of the above difficulties we have initiated the following steps:

1. Pictures were taken with #432 still in the test chamber to compare with initial setup.
2. #432 was removed from the chamber, potting was removed, and the tube checked visually for mechanical failure (none apparent). It was also unchanged electrically (photocathode, filaments, no opens or shorts). It cannot be operated in the test set until the yoke can be removed.

6693D-VA-24

3. Because of the press of time, Tube #411 was potted without the yoke (still on #432) and is now undergoing the humidity exposure without periodic checks of resolution, but will be tested in the test set at the conclusion of specified time.

Harold S Wilcox 9/21

H. S. Wilcox
Engineering Director
Lunar Camera Tube Project

dg

APPENDIX J

AN SEC TARGET WITH HIGH STORAGE CAPACITY

AN SEC TARGET WITH HIGH STORAGE CAPACITY

by

H. R. de Vries
K. F. Boll

The work reported here was performed in the Image Tube Department of the Westinghouse Electronic Tube Division, Elmira, New York under the direction of Dr. G. W. Goetze.

APPROVED BY:

R. A. Shaffer, Manager
Image Tube R & D Department

WESTINGHOUSE ELECTRONIC TUBE DIVISION
ELMIRA, NEW YORK

CONTENTS

Page

1. INTRODUCTION 1

2. THEORETICAL DISCUSSION 3

3. EXPERIMENTAL RESULTS 10

3.1 Physical Parameters 10

3.1.1 The Storage Capacity Per Area 11

3.1.2 The Electric Field at the Target Substrate 20

3.1.3 The Charge Density, the Electric Field, and the Potential in the Target 23

3.2 Practical Target Parameters 32

3.2.1 The Small Signal Gain 32

3.2.2 The Large Input Signal Storage Capacity 36

3.2.3 The Dynamic Range 39

3.2.4 The Storage Time 44

3.2.5 The Crossover Voltage 47

4. CONCLUSION 50

ACKNOWLEDGEMENT 51

REFERENCES 52

ILLUSTRATIONS

Figure No.		Page
2.1	Small Signal SEC Gain as a Function of Target Voltage	4
2.2	Sketch of Writing Section	4
2.3	Average Gain During Integration Time as a Function of Primary Current Density	4
3.1	Storage Capacity Per Area as a Function of Target Voltage	
	3.1A High Capacity Target	12
	3.1B Low Capacity Target	12
3.2	Storage Capacity Per Area as a Function of Target Voltage Measured with Two Different Methods	14
3.3	Charge Density as a Function of Distance From the Substrate	16
3.4	Field at the Target Substrate as a Function of Target Voltage	22
3.5	Charge Density as a Function of Target Voltage and Distance From Target Substrate	26
3.6	Charge Density as a Function of Target Voltage	27
3.7	Charge Density at the Target Substrate as a Function of Target Voltage	28
3.8	Electric Field as a Function of Distance from Substrate for Two Different Target Voltages (Target No. 3)	30
3.9	Potential as a Function of Distance From Substrate at the Target Voltage V_T = 50 Volts	31
3.10	Small Signal Gain versus Target Voltage Measured in Four Sealed-Off Tubes	34

Figure No.		Page
3.11	Normalized Small Signal Gain as a Function of Primary Voltage at Constant Target Voltage.....	35
3.12	Storage Capacity Per Area as a Function of Voltage Excursion and Target Voltage.....	38
3.13	Transfer Curves of a Low and a High Capacity Target, Measured at 10 Frames/Second.....	40
3.14	Transfer Curves of Two High Capacity Targets Measured in a Sealed-Off Tube and the Demountable System Respectively.....	42
3.15	Transfer Curve Measured at 0.625 Frames/Second.....	43
3.16	Voltage Excursion Caused by Discharge as a Function of Discharge Time Measured with Target No. 3 in Demountable Camera Tube System.....	45
3.17	The Square Wave Aperture Response of an Electro-Static Reading Gun with Different Voltages At the Suppressor Mesh.....	48

I. INTRODUCTION

A large signal-to-noise ratio is required at the output of any camera tube to permit the presentation of high resolution images of pleasing quality. In SEC camera tubes[1,2], where direct beam readout is used, high signal-to-noise ratios are obtained when the signal current is large compared to the equivalent RMS noise current of the preamplifier. The maximum signal current available from an SEC camera tube with a one inch diameter target results in a signal-to-noise ratio that is adequate for many applications. However, the signal current that can be generated with an SEC target of a given storage capacity/area is proportional to the frame rate and the raster area. Thus in tubes with a small target operated at low frame rates it is difficult to obtain a satisfactory maximum signal-to-noise ratio and hence an adequate dynamic range (the ratio of the weakest and the strongest illumination that can be presented in the same image without changing the operating parameters of the tube).

During the initial development of the SEC camera tube, 1 inch diameter targets were used to provide standard resolution performance (600 TV lines/picture height) at 30 frames/second, but recently there has been a growing interest in a wider range of operating conditions. Attention has been focused on (a) increased resolution with the 1 inch targets at 30 frames/second and (b) the development of camera tubes with

0.625 inch diameter targets operating at rates as low as 0.625 frames/ second. Both these trends required increased signal current in order to maintain or increase the maximum signal-to-noise ratio.

This report describes how far the desired increase in signal current has been achieved by using an SEC target with a large storage capacity/area. Before presenting the experimental results, we will discuss certain aspects of SEC target operation to establish in detail the relation between increased storage capacity and improved signal current.

2. THEORETICAL DISCUSSION

Let us consider a typical plot of small signal SEC gain, G, as a function of target voltage, V_T, such as that shown in Figure 2.1. At the target voltage $V_T = V_{To}$ the target has the SEC gain $G = G_0$. If now a certain target area is bombarded with electrons as sketched out in Figure 2.2, the voltage excursion V_E at the target surface will increase (starting from zero), and the voltage across the target (V_T - V_E) will decrease in the bombarded area. Hence the effective target voltage in the bombarded area is $V_T - V_E$. This means that during integration time the operating point on the gain curve in Figure 2.1 is moving from the point ($V_T = V_{To}$: $G = G_0$) to the point ($V_T = V_{To} - V_{Ef}$; $G = G_f$) where V_{Ef} is the final value of voltage excursion at the end of integration time (usually equal to the frame time) and G_f is the final value of the gain at the end of integration time. It can be seen that the average gain $\bar{G}$ during integration time will be smaller than G_0. If the average gain is plotted for different values of primary current density j_p (which is proportional to the photocathode illumination), the curve shown in Figure 2.3 is obtained. The average gain during the integration period is a function of j_p, V_{To} and integration time T. Let the point $\bar{G}$ (j_{p1}) in Figure 2.1 and 2.3 be the average gain $\bar{G}$ for the operating range indicated in Figure 2.1. By increasing the primary

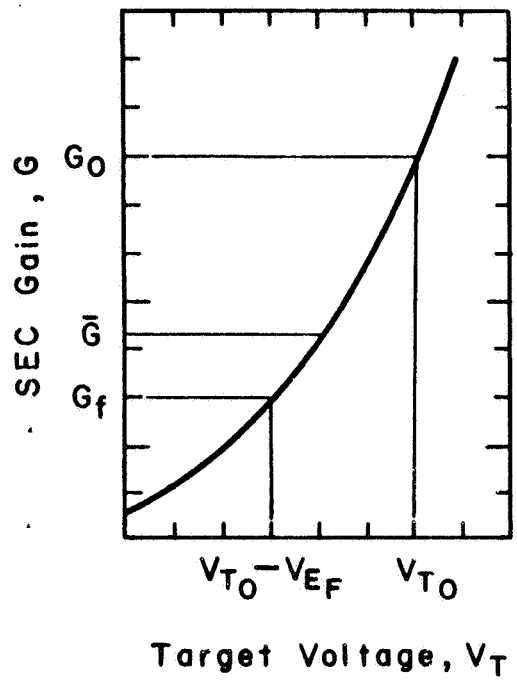

FIGURE 2.1: SMALL SIGNAL SEC GAIN AS A FUNCTION OF TARGET VOLTAGE

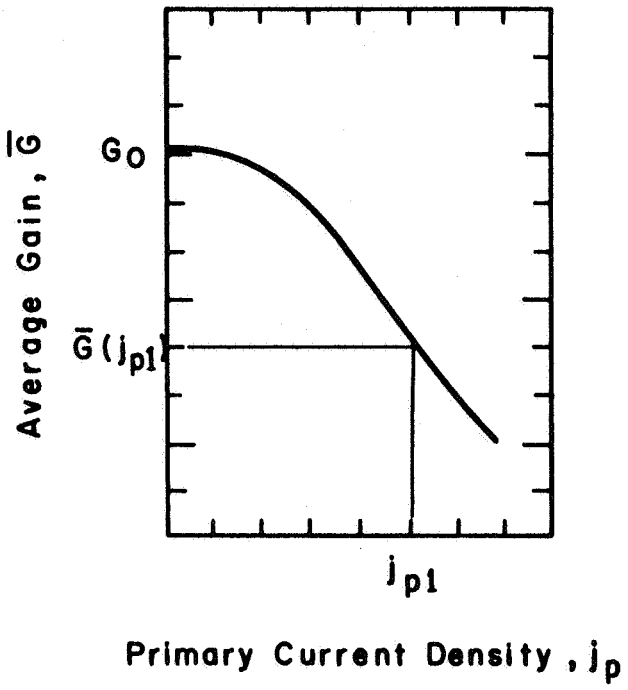

FIGURE 2.3: AVERAGE GAIN DURING INTEGRATION TIME AS A FUNCTION OF PRIMARY CURRENT DENSITY

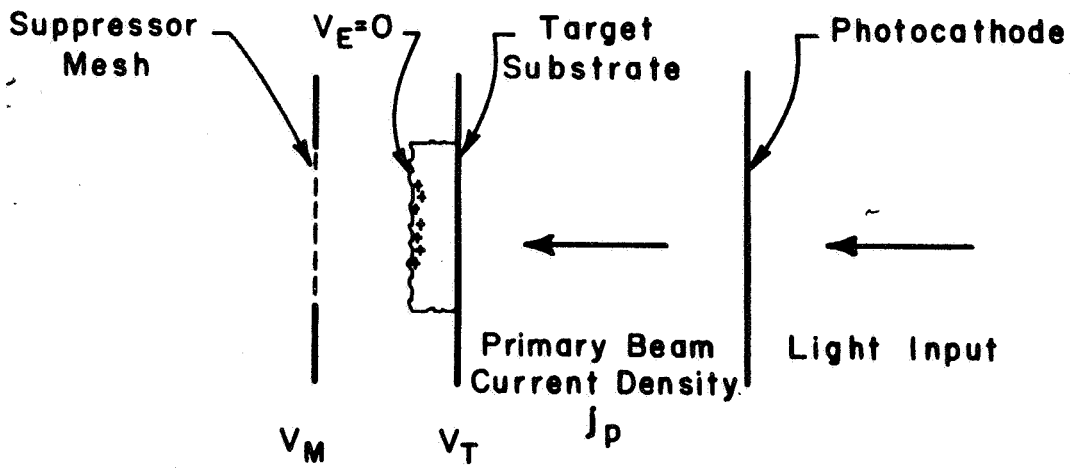

FIGURE 2.2: SKETCH OF WRITING SECTION

current density and therefore increasing V_{Ef} the point $\bar{G}$ (j_{P1}) slides down the curve in Figure 2.3.

The operating range is determined by the shape of the gain curve in Figure 1, the target voltage V_{To} and the voltage difference

$$V_{To} - (V_{To} - V_{Ef}) = V_{Ef} \tag{2.1}$$

The final voltage excursion V_{Ef} is given by

$$V_{Ef} = \int_0^T \frac{j_P}{C} G\,(V_{To} - V_E(t))\,dt = \bar{G}\,\frac{j_P\,T}{C} \tag{2.2}$$

where C is the target storage capacity/area (assumed constant). It can be seen from Figure 2.1 and Equation (2.2) that, for a given primary current density, by increasing C the surface excursion V_{Ef} can be decreased and $\bar{G}$ increased in such a way that the ratio $V_{Ef}/\bar{G}$ is increased in proportion to 1/C. For a given primary current density the increase in $\bar{G}$ yields a higher signal current. The reduction in V_{Ef} for a given primary current density enables the dynamic range to be increased. This follows because V_{Ef} may now be returned to the maximum value set by resolution considerations with a corresponding increase in the maximum light level that can be handled in a given scene. In order to see how the possibility outlined above may be realized in practice, it is necessary to analyze Equation (2.2) in more detail and provide further information about the target gain. In Equation (2.2) the function $V_E(t)$ is given by the integral equation

$$V_E(t) = \int_0^T \frac{j_P}{C} G\,(V_{To} - V_{E(t')})\,dt' \tag{2.3}$$

and may be obtained, for example, from the gain curve by solving the differential equation

$$\frac{dV_E(t)}{dt} = \frac{j_P}{C} G\ (V_{To} - V_E(t)) \tag{2.4}$$

which is the differential quotient of Equation (2.3).

Since the number of initially created secondary electrons is proportional to the energy dissipation in the target, the gain function has the form

$$G\ (V_{To} - V_E) = B\rho_M \Delta X\ f(E)\ h \tag{2.5}$$

where ρ_M = target mass density, ΔX = target thickness, h = collection efficiency, B is the constant describing the nature of the target material and f(E) is a function of the average energy E of the primary electrons in the target. B and f(E) may be calculated from the Bethe formula. The collection efficiency h is a function of the electric field across the target and the target density, so that h would be

$$h = h\ (\frac{V_{To} - V_E}{\Delta X};\ \rho_M). \tag{2.6}$$

Hence we have

$$G\ (V_{To} - V_E) = B\rho_M \Delta X\ f(E)\ h(\frac{V_{To} - V_E}{\Delta X}\ ;\ \rho_M). \tag{2.7}$$

Let us define the energy dissipation k by

$$k = B\rho_M \Delta X\ f(E) \tag{2.8}$$

and keep in mind that

$$C \propto \frac{1}{\Delta X} \tag{2.9}$$

To increase the target storage capacity we now consider two approaches:

<u>Approach 1</u>: We try to keep ρ_M = constant and decrease the target thickness by decreasing the amount of material evaporated. Under these conditions we have to expect that

k decreases in proportion to $\Delta X \propto \frac{1}{C}$

h should be constant if the electric field $\frac{V_{To} - V_E}{\Delta X}$ is kept constant. V_{To} has to be decreased because the maximum target voltage that can be applied to the target is determined by the maximum useful electric field and the maximum useful electric field is determined by the inner structure of the target that is not changed when ρ is kept constant. Hence according to Equation (2.7) a first order decrease in gain with ΔX will be expected.

If this is true the voltage excursion V_E at a given primary current density given by Equation (2.2) will decrease faster than proportional to ΔX. This effect will increase the dynamic range of the target, if the maximum useful final voltage excursion V_{Ef}^{max} is determined by resolutuon considerations and therefore possibly be independent from V_{To}, because the maximum useful signal current

$$I_S^{max} = V_{Ef}^{max}\, C\, \frac{A_T}{T_a} \tag{2.10}$$

of a target with the raster area A_T, operated with an active frame time T_a, increases with C. If, however, resolution is not important then the maximum useful signal current is equal to the saturation current.

$$I_{sat} = V_{To}\, C\, \frac{A_T}{T_a} \,. \tag{2.11}$$

The saturation current might not be increased since V_{To} has to be decreased with decreasing target thickness and constant mass density.

Approach 2: We try to increase ρ_M while decreasing ΔX in such a way that $\rho_M \Delta X$ = constant. Under these conditions we have to expect that

k = constant

h decreases with increasing ρ_M

h can be increased again by increasing the electric field across the target since targets with higher density can be operated at higher target voltages as will be seen in Section 3, where the experimental results are discussed.

Hence the gain represented in Equation (2.7) may be expected to show less than proportionate decrease with $\Delta X \propto \frac{1}{\rho_M} \propto \frac{1}{C}$. The maximum useful signal current represented in Equation (2.10) will increase to the same extent as the first approach if V_{Ef}^{max} is assumed to be unchanged. The saturation current, however, is increased substantially since C and V_{To} are increased by the second approach.

We have neglected that

(i) f(E) is not entirely independent of ΔX, and

(ii) the value of the integral in Equation (2.2) does not necessarily change in proportion to G since V_E has to obey the integral Equation (2.3).

However, both of the factors we have neglected effect the two approaches in the same way. Hence in order to compare the different approaches a discussion of f(E) and the integral Equation (2.4) is not necessary. As a result of these considerations it is obvious that the second approach is expected to yield the better result.

Another disadvantage of the first approach compared to the second one is seen when we consider the number of fibers of target material in an area representing a resolution element. This number will considerably decrease if the target is made thinner according to the first approach and, therefore, the relative local variation of the number of fibers per resolution element on the target will increase. This effect will result in an increase of image grain.

3. EXPERIMENTAL RESULTS

Although both approaches in Section 2 have been tried in the past, chiefly the results obtained with targets modified according to the second approach will be reported because of the better success.

In order to demonstrate the improvements in target performance which have been achieved, first physical parameters such as the storage capacity, electric field and charge density in the target will be discussed in Section 2.1; then the parameters of practical interest discussed in Section 3.2 will be seen to follow from the improvements in physical parameters.

3.1 Physical Parameters

Except for the storage capacity most of the interesting physical parameters such as the electric field at the target substrate and the charge density present in a completely scanned target, cannot be measured directly. In order to show how these parameters may be derived from measurements of the storage capacity, we start in Section 3.1.1 with a discussion of the storage capacity and its relation to the electric field at the target substrate and the charge density in the target. It will be seen in Section 3.1.2 that the electric field at the target substrate may be calculated directly from measurements without any additional assumptions, while in Section 3.1.3 the calculation of the charge density must be restricted to a first order approximation.

As far as data are available the results obtained with the improved high capacity target will be compared with those from low capacity targets.

3.1.1 The Storage Capacity Per Area

To determine the storage capacity per area

$$C = \frac{1}{A} \frac{dQ}{dV_E} \tag{3.1}$$

a known area A of the target was exposed to primary electrons for an integration time of a few seconds in such a way that only a voltage excursion V_E slightly exceeding two volts was obtained. The target voltage V_T then was decreased by two volts and the signal caused by the excess voltage V_E - 2 Volts was readout with a single scan. A second scan was applied to insure completion of the readout process. After this the target voltage V_T was increased by two volts (reset to its initial value) so as to produce a surface voltage difference dV_E = 2 Volts. The residual charge dQ was then readout with single frame readout. The output signal of the one line displayed on the scope compared with a calibrated comparator pulse, the output signal duration and the known number of lines in the area A were used to calculate the output charge dQ associated with a surface voltage difference dV_E of two volts.

In Figure 3.1A the storage capacity/area of some high capacity SEC targets is plotted versus target voltage. The increase of capacity/area that has been achieved by the modification of the SEC target can be seen by comparing Figure 3.1.A with Figure 3.1.B where a set of similar curves obtained with low capacity targets is presented. At first sight the curve No. 1 in Figure 3.1.A seems to indicate that this target would have the highest dynamic range. As has been pointed

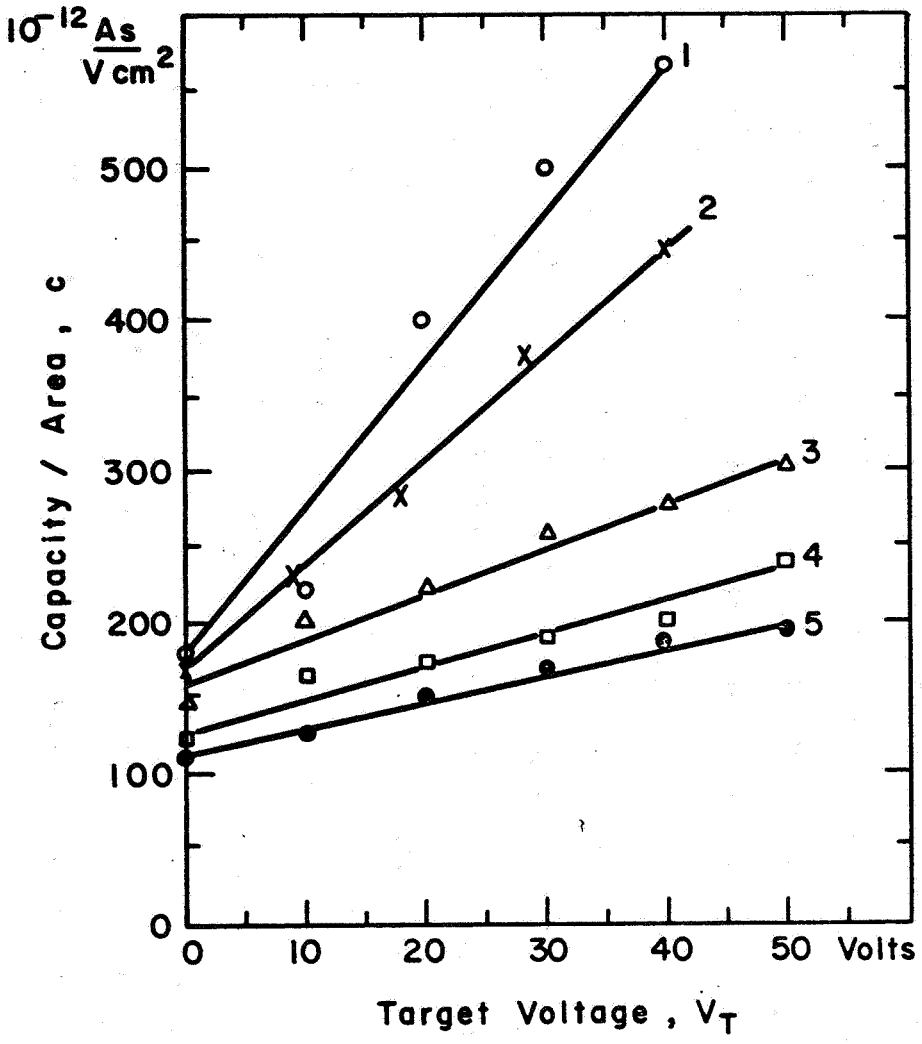

Figure 3.1A: High Capacity Target

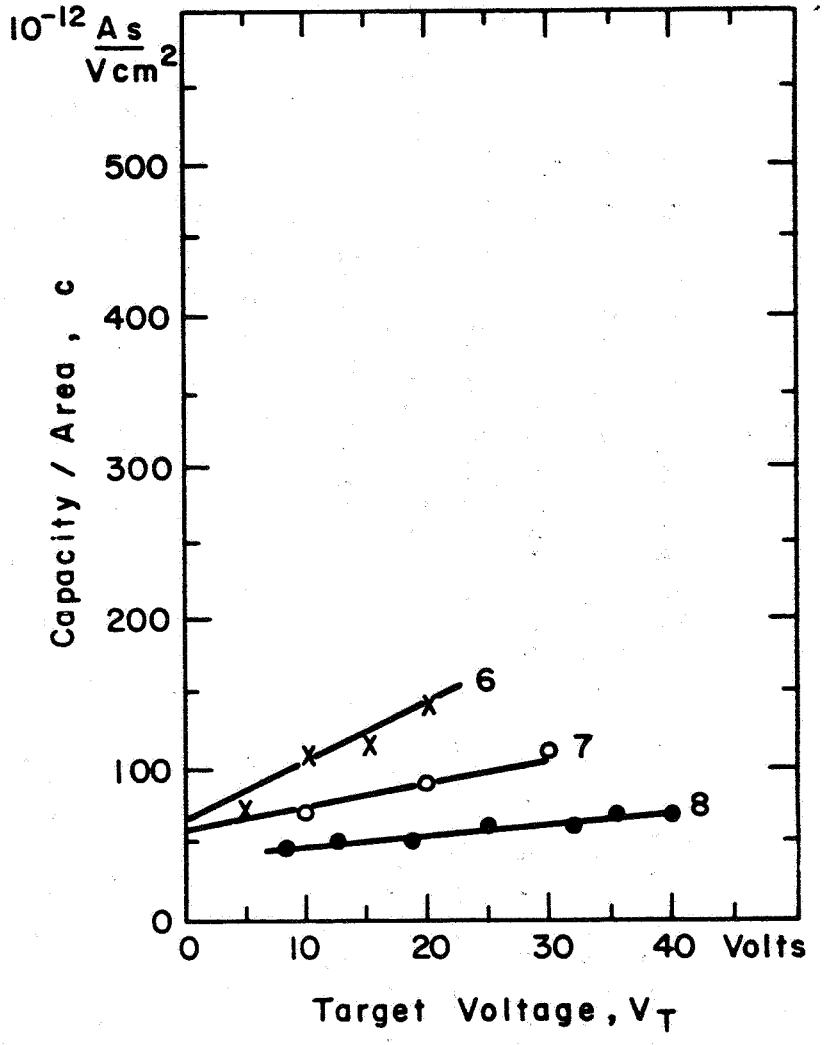

Figure 3.1B: Low Capacity Target

FIGURE 3.1: STORAGE CAPACITY PER AREA AS A FUNCTION OF TARGET VOLTAGE

out in Section 2.1, however, not only the storage capacity determines the dynamic range of the target but also the maximum useable target voltage does. In order to understand that the target voltage might be limited to lower values for a target with high capacity than it is for a target with low capacity we first have to consider the increase in storage capacity/area caused by increasing target voltage.

As has been pointed out by A. H. Boerio, et.al[3], the increase in capacity with increasing target voltage can be explained by the fact that in charging the target, the scanning beam electrons come under the influence of the internal electric field and can therefore penetrate a significant fraction of the target. If this is true it should be possible to measure the curves shown in Figure 3.1.A and B without applying a primary beam to the target merely by increasing the target voltage in steps of 2 volts and determining the charge added into the target by the scanning beam for each two volt step. This has been done and the results are shown in Figure 3.2. Obviously there is good agreement within the limitations of the measurement accuracy. Therefore we may now discuss the storage capacity without taking into account the primary beam.

When the target has been completely scanned with the reading beam at a given target voltage there exists throughout the target a negative charge distribution being described by the charge density ρ which in general is a function of the three space coordinates x, y, z and the target voltage V_T. For our further discussion, however,

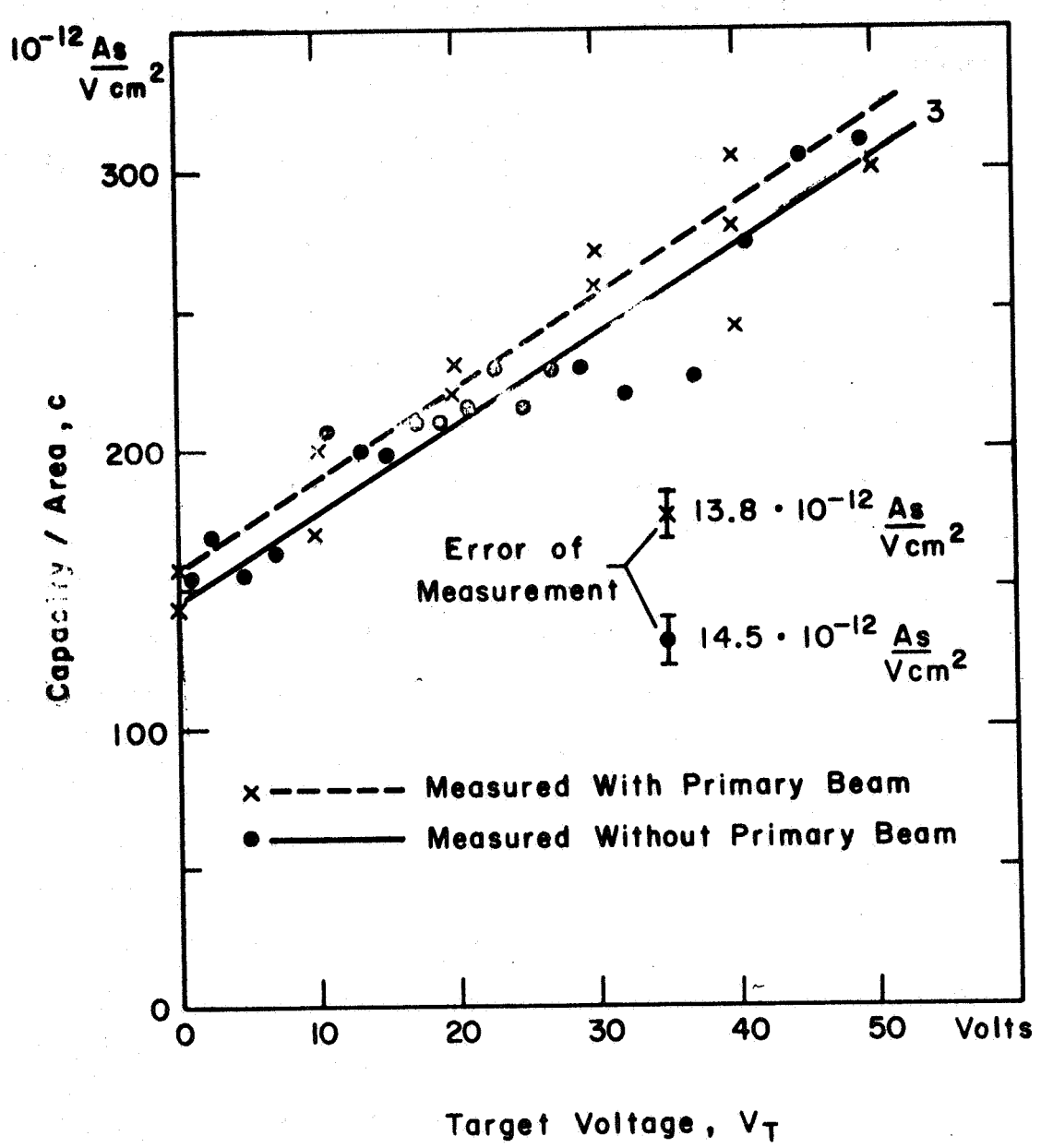

FIGURE 3.2: STORAGE CAPACITY PER AREA AS A FUNCTION OF TARGET VOLTAGE MEASURED WITH TWO DIFFERENT METHODS

we may assume the target to be uniform over its entire area and neglect any edge effects. In this case

$$\frac{\partial \rho\ (x;\ y;\ z;\ V_T)}{\partial y} = \frac{\partial \rho (x;\ y;\ z;\ V_T)}{\partial z} = 0 \qquad (3.2)$$

and therefore the charge density is $\rho = \rho\ (x;\ V_T)$. This distribution function is qualitatively illustrated in Figure 3.3 for low and high target voltages. The curves shown there cannot be measured directly. Some conclusions, however, may be drawn since $\rho\ (x;\ V_T)$ is determined to a certain extent by the measurement shown in Figure 3.1 and other observations, which will be discussed now.

The electric potential $\phi\ (x,\ V_T)$ in the target is connected with the charge density $\phi\ (x,\ V_T)$ by Poisson's equation which according to equation (3.2) has the form

$$\frac{d^2 \phi}{d\ x^2} = - \frac{\rho}{\epsilon\ \epsilon_o} \qquad (3.3)$$

If we neglect the thermionic distribution of the scanning beam electrons, consider the thermionic cathode to be on 7 potential and presume that the target is scanned completely so th more electrons are accepted by the target, the law of conservati energy then determines the potential at the target surface (sur tage excursion) to be

$$\phi\ (d,\ V_T) = 0 \qquad (3.4)$$

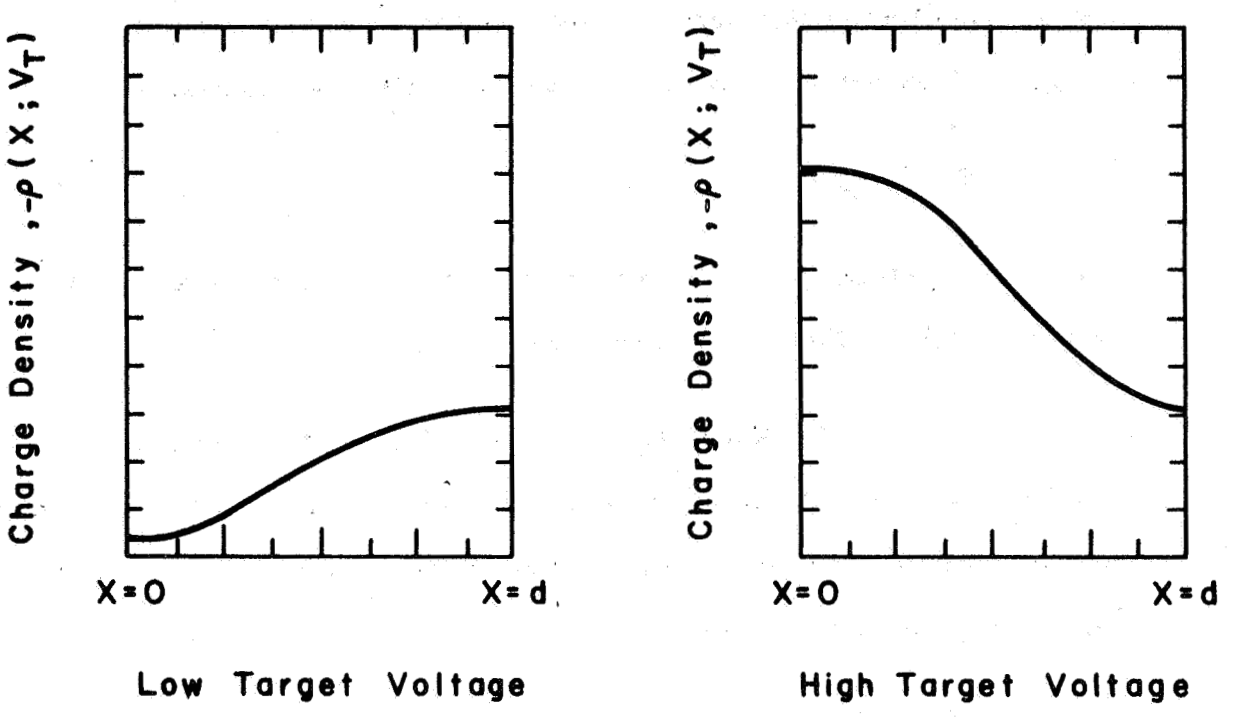

FIGURE 3.3: CHARGE DENSITY AS A FUNCTION OF DISTANCE FROM THE SUBSTRATE

where d is the target thickness.

Moreover the sume of the forces applied to an electron arriving at the target surface must be zero in order to prevent it from entering the target and hence the electric field is

$$\mathcal{E}\ (d,\ V_T) = 0 \tag{3.5}$$

if we neglect the electric field caused by the suppressor mesh. This assumption will be justified in Section 3.1.3.

The Equations (3.4) and (3.5) are the necessary and sufficient boundary conditions to determine the solution of Poisson's equation. However, there is another condition given by the conductive target substrate and which requires

$$\phi\ (o,\ V_T) = V_T. \tag{3.6}$$

This third condition therefore determines already to some extent the charge density $\rho\ (x,\ V_T)$. As result of this we may derive an interesting equation for the "integrated" storage capacity/area

$$C_i = \frac{-1}{V_T} \int_o^d \rho(x,\ V_T)\ dx \tag{3.7}$$

which is closely related to but must be distinguished from the differential storage capacity/area

$$C = \frac{\int_o^d \rho(x, V_T)\, dx - \int_o^d \rho(x, V_T)\, dx}{\Delta V_T} \longrightarrow$$

$$\frac{d}{dV_T} \left\{ \int_o^d \rho(s, V_T)\, dx \right\} \tag{3.8}$$

measured and represented in Figure 3.2. By inserting equation (3.3) in equation (3.7) and using equation (3.5) after integration we obtain

$$C_i = \frac{1}{V_T} \epsilon\epsilon_o \mathcal{E}(0, V_T). \tag{3.9}$$

If we now consider the primary beam to be turned on and the target being operated in such a way that during integration time the target is just neutralized (the target surface reaches the substrate potential) we then obtain during readout the saturation signal current*. In this case the effective storage capacity would just be the integrated storage capacity given in Equation (3.9). Hence the integrated storage capacity C_i determines the saturation current of the target and therefore the dynamic range. In Section 2 it has been explained that the dynamic range also increases with the target voltage. If we consider that the maximum usable electric field at the target substrate cannot exceed a certain value E_{max} given by the structure of the target the equation 3.9 sets the limitation.

$$C_i V_T \leq \epsilon\epsilon_o \mathcal{E}_{max} \tag{3.10}$$

*As will be discussed in Section 3.2 in more detail the saturation of the target by the primary beam pratically observed is not equal to the neutralization mentioned here. For the conclusions to be drawn in this section, however, a distinction is not necessary.

This means that under any circumstances the dynamic range of the target is limited by the maximum electric field that the target can withstand without breaking down or becoming seriously conductive. If, therefore, the maximum usable target voltage is limited by conduction in the target no increase in dynamic range can be expected by decreasing the target thickness alone.

Besides the limitation given by Equation (3.10) another limiting factor may be seen by interpreting Equation (3.7). The integral appearing in Equation (3.7) represents the total charge available for producing a signal current with normal target operation. This charge is trapped in trapping centers (stable energy levels). The electric charge density - $\rho(x, V_T)$ therefore is equal to the density ρ_t of trapping centers multiplied by the occupation probatility $p(x, V_T)$ and Equation (3.7) can be written as

$$C_i V_T = \int_o^d \rho_t \, p(x, V_T) \, dx. \qquad (3.11)$$

If we consider the density ρ_t of trapping centers to be constant throughout the target the Equation (3.11) becomes

$$C_i V_T = \rho_t \int_o^d p(x, V_T) \, dx. \qquad (3.12)$$

The maximum charge that can be stored in the target under most optimistic conditions is given when all trapping centers are occupied by electrons and therefore $p(x, V_T) = 1$. If at this point the target voltage V_T would be further increased more electrons would be accepted by the target but

could not be trapped. They would then be collected at the substrate and hence make the target appearing conductive. In practice this "saturation conduction" will be observed already before the maximum charge given by $\rho(x, V_T) = 1$ is stored in the target. Therefore we obtain from Equation (3.12)

$$C_i V_T \leq \rho_t d \qquad (3.13)$$

This limitation describes the fact that no substantial increase of dynamic range can be expected by making the target thinner without increasing the density of trapping centers in order to increase the storage capacity/area. The limitation (3.13) therefore seems to be the essential reason for the limited success of approach No. 1 discussed in Section 2.

Since the electric field $\mathcal{E}(0, V_T)$ at the target substrate and the maximum value of the charge density $\rho(x, V_T)$ in the target are the fundamental physical parameters which determine the dynamic range of the target, it is necessary to evaluate $\mathcal{E}(0, V_T)$ and $\rho(x, V_T)$ as far as possible from measurements done on the high capacity SEC target and on the low capacity target in order to explain the improvement that has been achieved. This will be done in the following two sections.

3.1.2 The Electric Field at the Target Substrate

To evaluate the electric field at the target substrate from Equation (3.9) we first have to determine the integrated storage

capacity/area C_I from the differential storage capacity/area C which has been measured. From Equation (3.7) and Equation (3.8) follows

$$C = \frac{d}{dV_T} (C_I \; V_T) \tag{3.14}$$

According to the experimental results represented in Figure (3.1) and (3.2) the differential storage capacity/area can be represented by

$$C = C_o + kV_T \tag{3.15}$$

where C_o and k are constants which can be determined from the capacity curves. Hence the electric field at the target substrate is

$$\mathcal{E}(0, V_T) = \frac{1}{\epsilon \epsilon_o} \left\{ C_o \; V_T + \frac{1}{2} \quad kV_T^{\,2} \right\} \tag{3.16}$$

Using the capacity curves of target No. 3 in Figure 3.2 (solid line), of target No. 7 and target No. 8 in Figure 3.1.B as examples for a high capacity target, a thin low capacity target and a thick low capacity target respectively, the electric field curves ($\epsilon\, \mathcal{E}(0, V_T)$ versus V_T) in Figure 3.4 were obtained. The high capacity target is indeed operated with considerable higher electric fields at the substrate than the low capacity target, when both targets are operated with the same target voltage. The total effect, however, is seen if we consider that by experience the low capacity target has a maximum target voltage ranging between 20 to 30 volts while the maximum target voltage of the high capacity target ranges between 35 to 45 volts. Assuming $\epsilon = 1$ the maximum electric field is in the order of 20 kV/cm for the low capacity target and 100 kV/cm for the high capacity target.

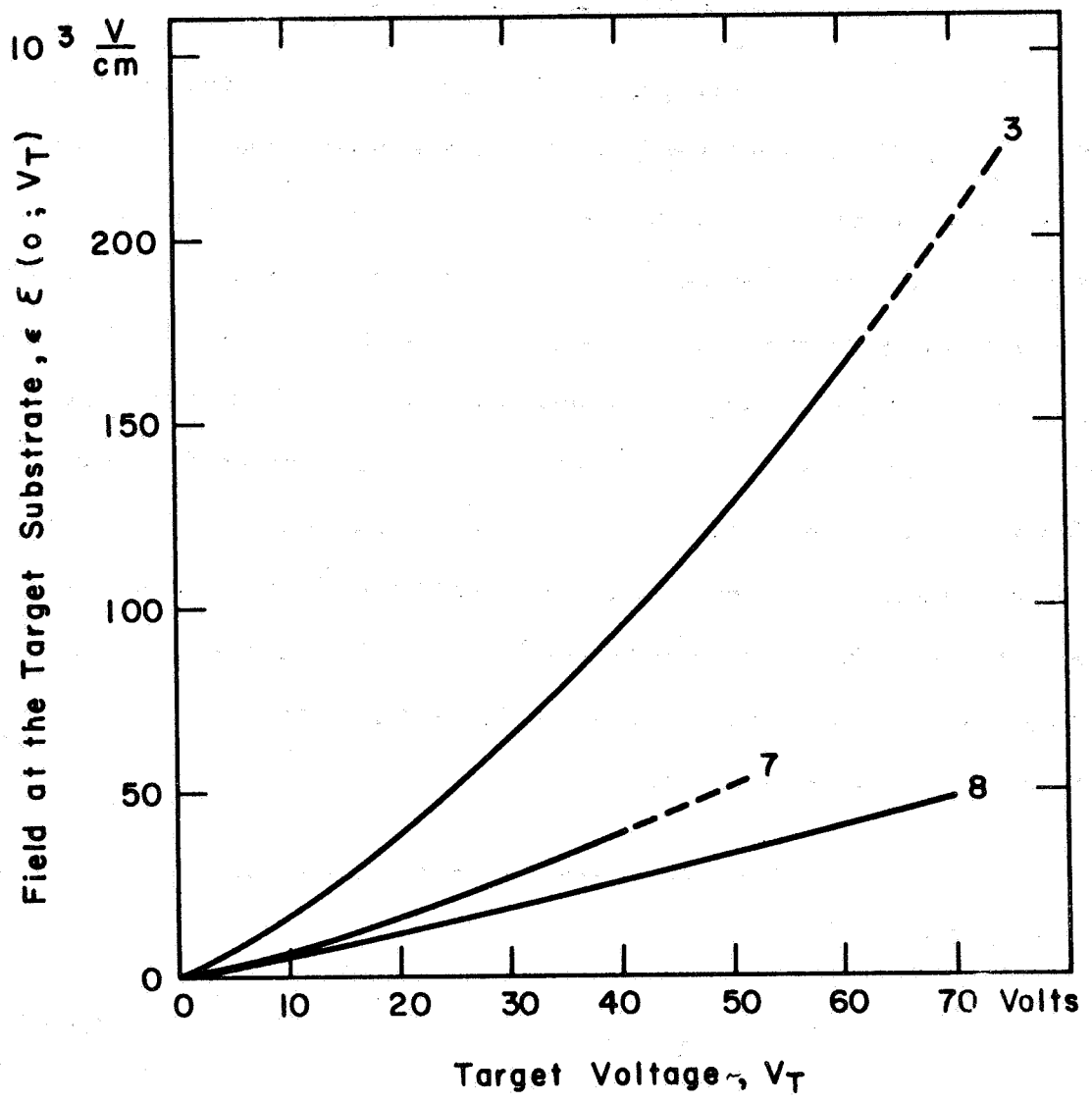

FIGURE 3.4: FIELD AT THE TARGET SUBSTRATE AS A FUNCTION OF TARGET VOLTAGE

3.1.3 The Charge Density, the Electric Field, and the Potential in the Target

The charge density $\rho(x, V_T)$, the electric field $\mathcal{E}(x, V_T)$ and the potential $\phi(x, V_T)$ in the target cannot be measured directly as functions of x; only parameters which are integrated values along the x-axis of the target can be observed experimentally. In order to determine parameters which are a function of x from integral values which have been measured, it is necessary either to make assumptions which already determine to some extent the parameters as function of x or to restrict the evaluation to a first or second order approximation which might be very crude. Since a general form of the charge density, the electric field and the potential can easily be derived without additional assumptions, a first order approximation for the three parameters as functions of x will be calculated.

The charge density in the target can be represented by the series

$$\rho(x, V_T) = \sum_{n=0}^{\infty} A_n(V_T)x^n \tag{3.17}$$

The coefficients A_n are functions of the target voltage V_T. By integrating Poisson's equation and using the boundary condition Equation (3.5) the electric field in the target is obtained.

$$\mathcal{E}(x) = \frac{-1}{\epsilon\epsilon_o} \sum_{n=0}^{\infty} A_n(V_T) \frac{d^{n+1} - x^{n+1}}{n+1} \tag{3.18}$$

The potential may be obtained by a second integration and using Equation (3.4).

$$\phi(x) = \frac{-1}{\epsilon\epsilon_o} \sum_{n=o}^{\infty} \frac{A_n(V_T)}{n+1} \left\{ \frac{n+1}{n+2} d^{n+2} - xd^{n+1} + \frac{1}{n+2} x^{n+2} \right\} \tag{3.19}$$

To determine the coefficients A_n we have from Equation (3.6)

$$V_T = \frac{-1}{\epsilon\epsilon_o} \sum_{n=o}^{\infty} \frac{A_n(V_T)}{n+2} d^{n+2} \tag{3.20}$$

and from Equation (3.18) and Equation (3.16)

$$C_o V_T + \frac{1}{2} k V_T^2 = -\sum_{n=o}^{\infty} \frac{A_n(V_T)}{n+1} d^{n+1} \tag{3.21}$$

From the last two equations the coefficients A_o and A_1 may be completely evaluated in the sense of a first order approximation ($A_n = 0$ for $n \geq 2$).

$$A_o = \frac{2}{d} V_T \left\{ \frac{3\epsilon\epsilon_o}{d} - 2C_o - kV_T \right\} \tag{3.22}$$

$$A_1 = \frac{6}{d^2} V_T \left\{ C_o - \frac{2\epsilon\epsilon_o}{d} + \frac{1}{2} k V_T \right\} \tag{3.23}$$

In order to calculate A_o and A_1, the measurement of ϵ and d seems to be necessary. Calculating the first order approximation consequently, however, the value of d/ϵ is determined by the fact that

$$\frac{\epsilon\epsilon_o}{C_o} = \bar{x}(o) = \lim_{V_T \to o} \frac{\int_o^d x \; \rho(x, V_T)\, dx}{\int_o^d \rho(x, V_T)\, dx} = \frac{2}{3} d \tag{3.24}$$

Since it is reasonable to assume that ϵ is close to one, we obtain from Figure 3.2 for target No. 3 the thickness $d = 10^{-3}$ cm. Based on this value and the experimental values of C_o and k the first order approximation of the charge density

$$\rho(x, V_T) = A_o (V_T) + A_1 (V_T) x \tag{3.25}$$

was evaluated and plotted in Figure 3.5 for several target voltages. In Figure 3.6 the charge density at the substrate and the charge density at the target surface are plotted versus the target voltage. The charge density at the substrate increases monotonously with V_T, while the charge density at the target surface has a maximum at $V_T = 40$ volts and decreases thereafter. The existance of this maximum cannot be real. If the target is continuously scanned and the target voltage is increased slowly from $V_T = 0$ to $V_T = 75$ volts, the charge density should assume the values indicated by the curves in Figure 3.5 and especially the charge density at the target surface should trace the lower curve in Figure 3.6. As long as no primary beam is applied to the target, however, there is no physical effect by which the scanning beam may "decrease" the negative charge density $\rho(x, V_T)$; hence no crossing points in Figure 3.5 are possible and in Figure 3.6 only curves monotonously increasing with target voltage can be true. The crossing points in Figure 3.5 and the maximum of the lower curve in Figure 3.6 therefore show that useful results may be expected from the first order approximation, Equation (3.25), only for the vicinity of the target substrate.

In Figure 3.7 the charge density $\rho(0, V_T)$ at the target substrate for a high capacity target and a low capacity target are

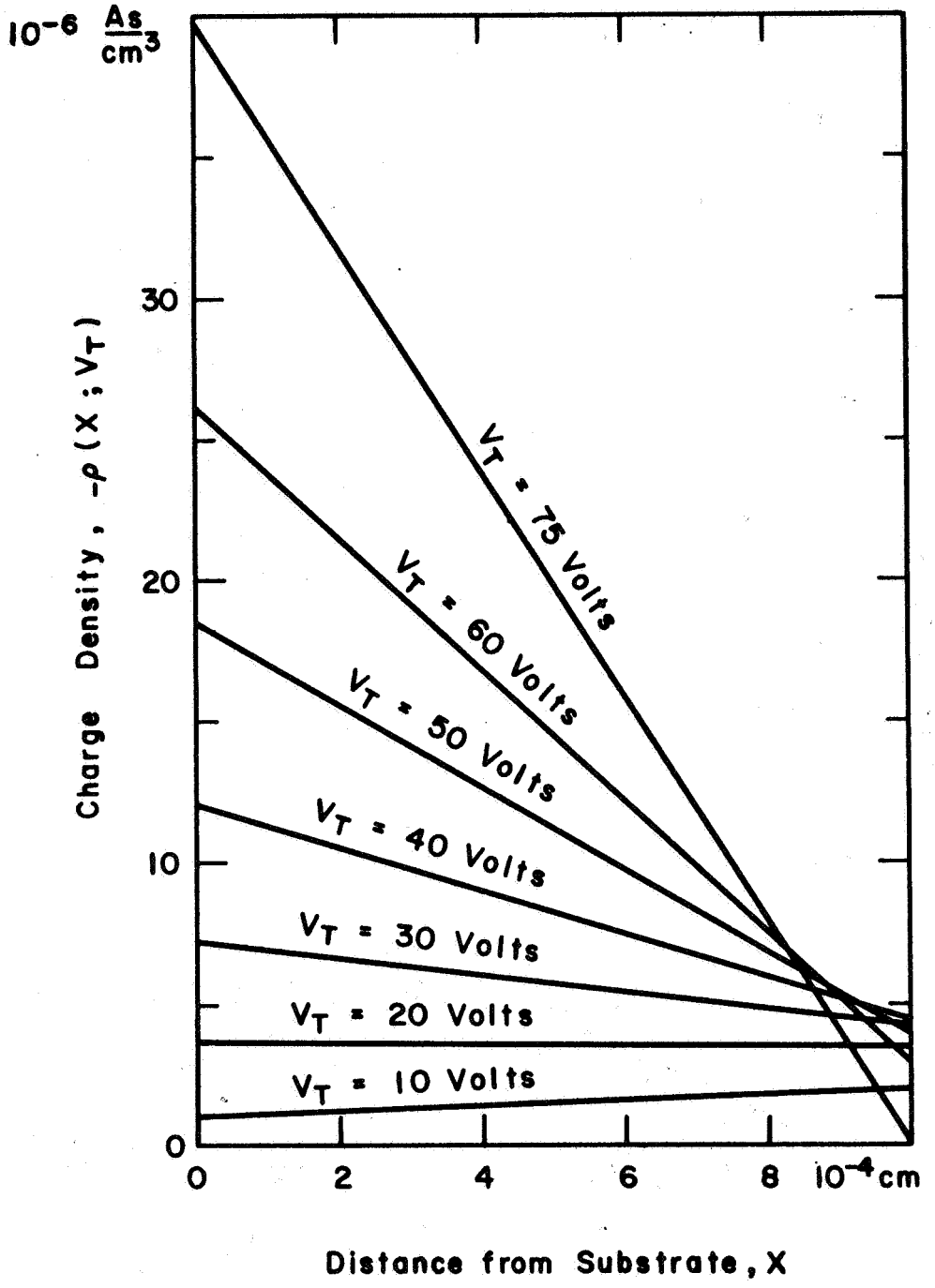

FIGURE 3.5: CHARGE DENSITY AS A FUNCTION OF TARGET VOLTAGE AND DISTANCE FROM TARGET SUBSTRATE

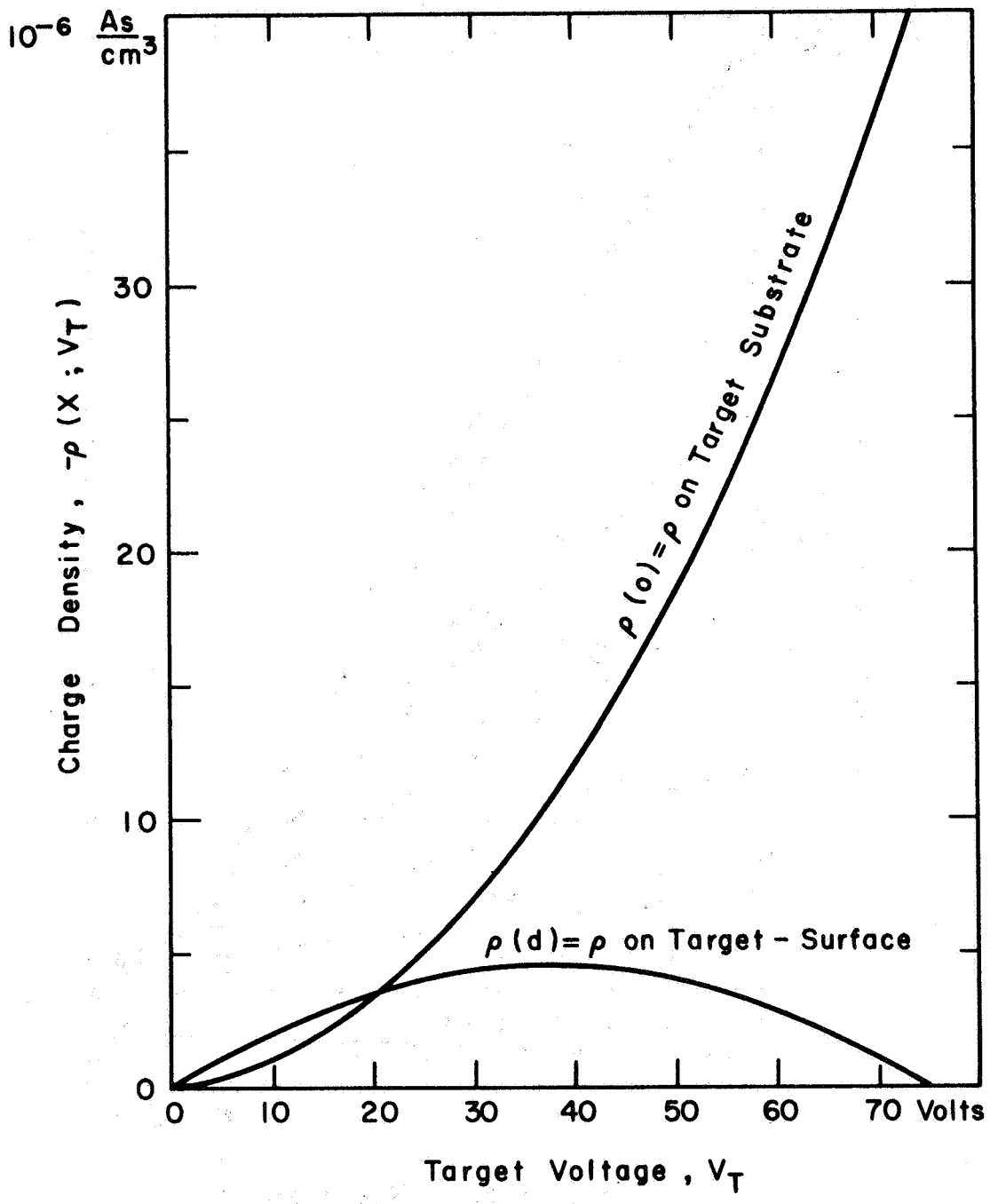

FIGURE 3.6: CHARGE DENSITY AS A FUNCTION OF TARGET VOLTAGE

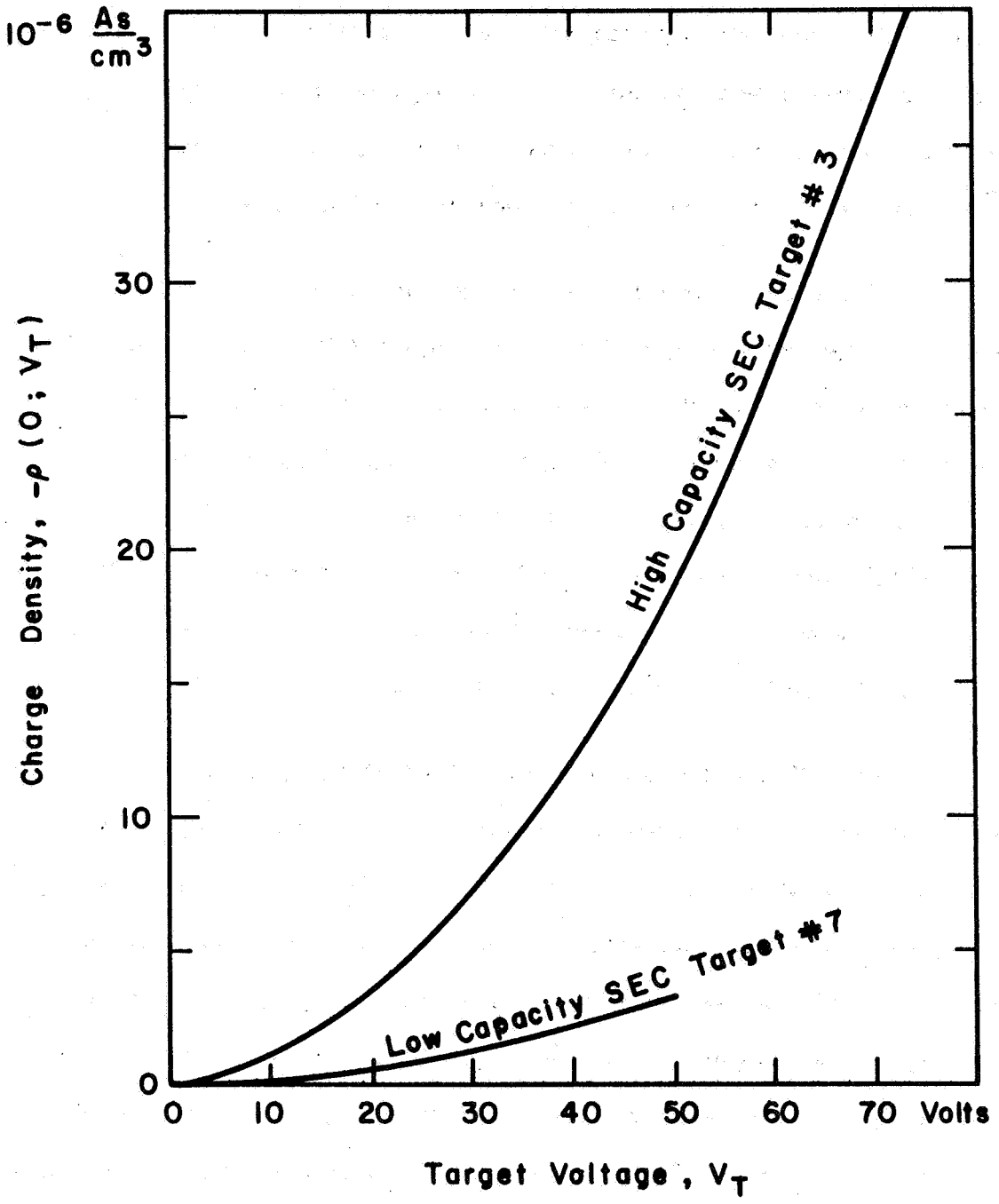

FIGURE 3.7: CHARGE DENSITY AT THE TARGET SUBSTRATE AS A FUNCTION OF TARGET VOLTAGE

plotted versus target voltage V_T. Considering the fact mentioned in Section 3.1.2 that the high capacity target usually can be operated at target voltages between 35 and 40 volts compared to 20 to 30 volts applicable to the low capacity target, the maximum useful charge density in the target has been increased by one order of magnitude.

The electric field in the target and the potential in the target are plotted in Figure 3.8 and in Figure 3.9 respectively. Although the curves were obtained by using the first order approximation for the charge density, Equation (3.25), their validity along the x-axis is better than Equation (3.25) because of the fact that the values for the electric field and the potential at x = o and x = d are not based on the first order approximation but are given either by the boundary conditions or experimental results as shown in Section 3.1.1.

With Figure 3.8 the validity of Equation (3.5) can be justified. This equation was introduced in Section 3.1.1 by neglecting the electric field caused by the suppressor mesh. Considering the mesh voltage, V_M, to be 30 volts and the distance between mesh and target 0.25 mm, the electric field between target and mesh then is 1.2×10^3 volt/cm and, therefore, small compared to the average electric field in the target at any target voltage of practical interest. Neglecting the induced charge on the target surface caused by the finite mesh voltage is equivalent to neglecting the electric field between target and mesh with respect to the electric field at the target substrate. As can be seen from Figure 3.8, this is a consequence of the first assumption.

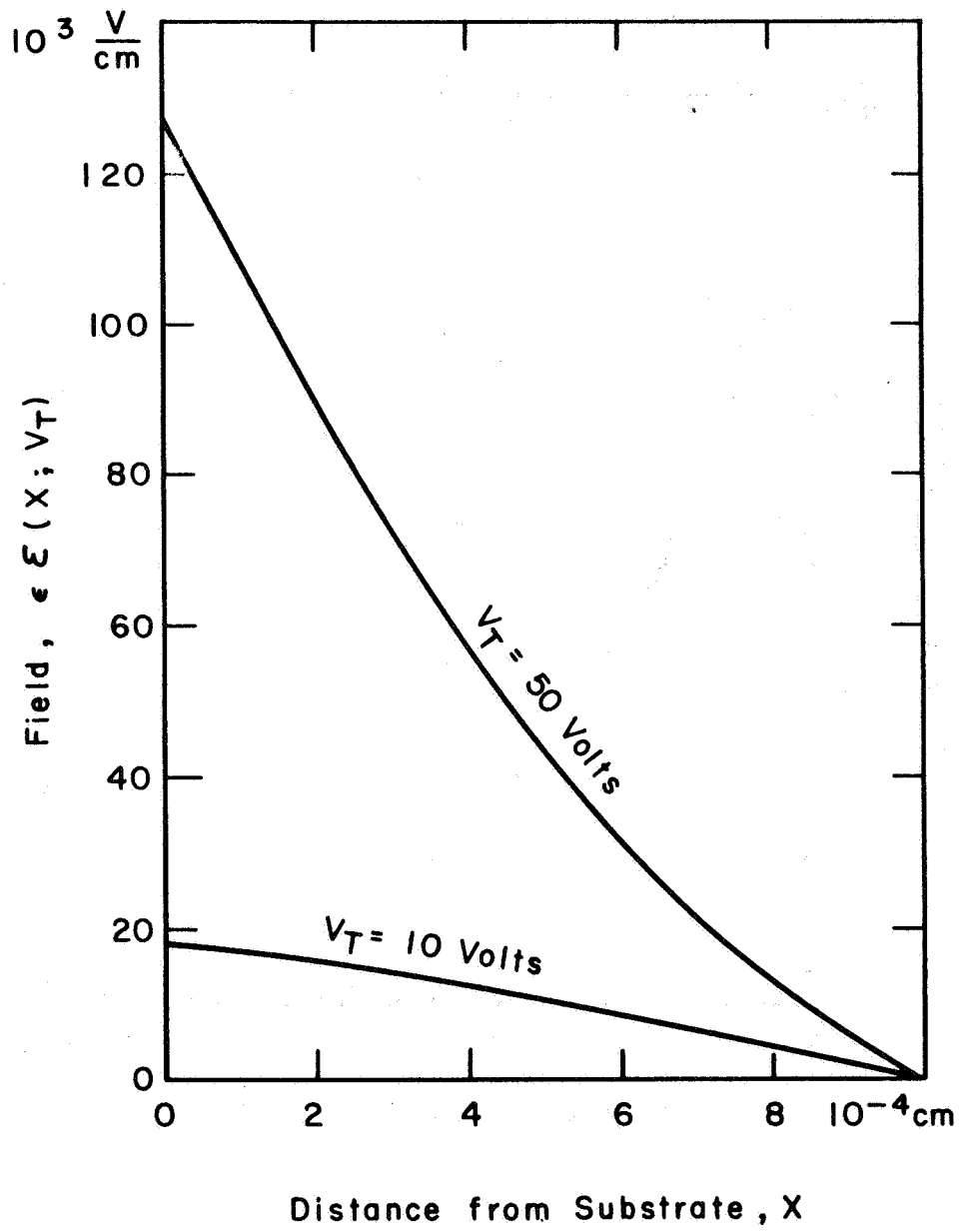

FIGURE 3.8: ELECTRIC FIELD AS A FUNCTION OF DISTANCE FROM SUBSTRATE FOR TWO DIFFERENT TARGET VOLTAGES (Target No. 3)

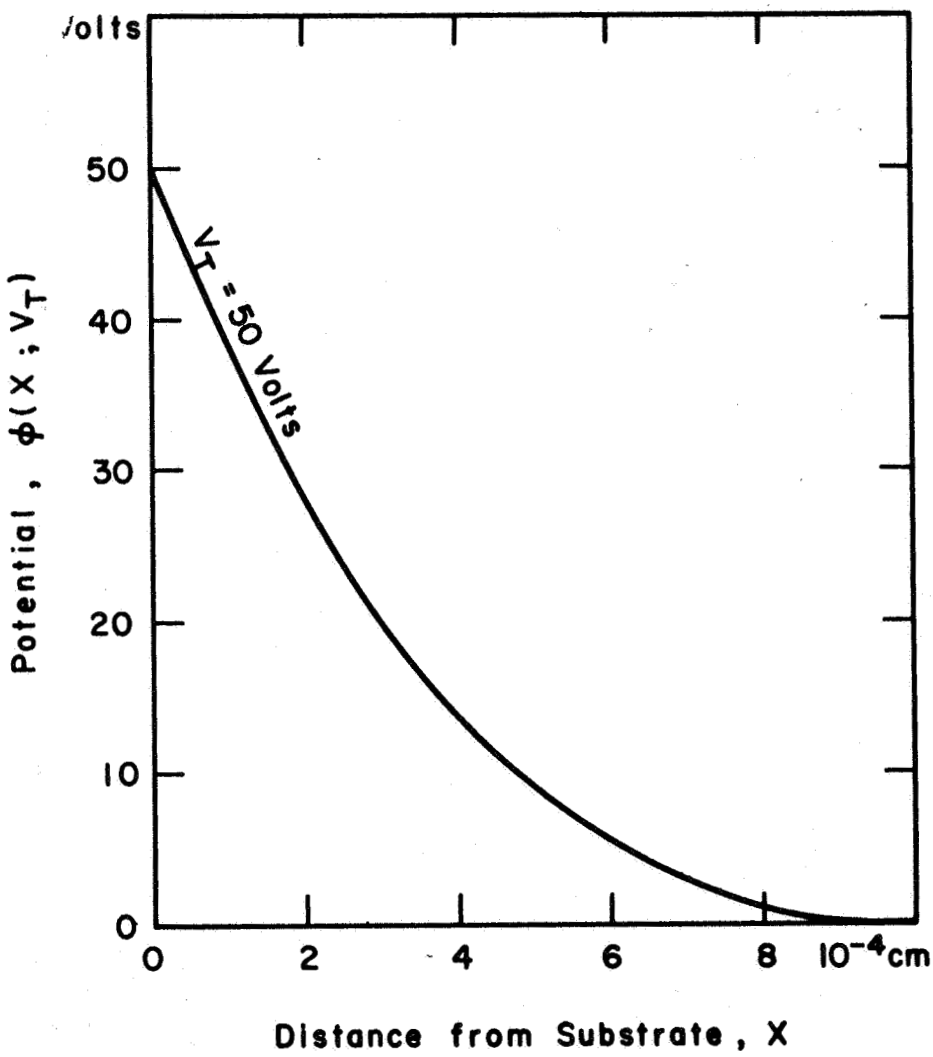

FIGURE 3.9: POTENTIAL AS A FUNCTION OF DISTANCE FROM SUBSTRATE AT THE TARGET VOLTAGE, V_T = 50 VOLTS

3.2 Practical Target Parameters

Target parameters of practical interest are the small signal gain, the large input signal storage capacity, the dynamic range and the storage time. According to Section 2, the dynamic range of the target depends on the storage capacity/area, the maximum useful target voltage and the small signal gain. Consequently, in Section 3.2.1, the small signal gain and the maximum useful target voltage of some typical high capacity targets will be compared with the results of some typical low capacity targets; the large input signal storage capacity and the dynamic range then will be presented in Section 3.2.2 and Section 3.2.3 respectively.

It will be seen in Section 3.2.4 that the storage time of the high capacity target is not as long as the storage time of the low capacity target. However, the storage time turned out to be more than adequate for continuous scanning operations. In Section 3.2.5 the effect of the high capacity target on the performance of the reading gun briefly will be discussed.

3.2.1 The Small Signal Gain

The small signal gain is one of the factors which determine the sensitivity of a camera tube. Since in Section 2 we saw some indication that the gain of a high capacity target might be lower than the gain of the low capacity target, it is of special interest to compare the practical results obtained with both targets. In Figure

3.10 the target gain curves of four camera tubes are plotted; the tubes were equipped with low and high capacity targets as indicated in the graph. The maximum usable target voltages shown in Figure 3.10 were found by increasing the target voltage, V_T, at constant illumination and determining the value of V_T at which the overall appearance of the target starts loosing its pleasing quality. This determination of the maximum usable target voltage infers a subjective judgment, but the values obtained seem to be in fair agreement with those determined by finding the target voltage at which the target shows conduction.

It can be seen from Figure 3.10 that a considerable increase of maximum usable target voltage has been achieved and a gain has been obtained at this voltage, which is comparable with the gain of a low capacity target.

It is well known that higher gain values than those represented in Figure 3.10 have been observed with low capacity targets, but this is also true for the high capacity target. Here, however, are typical and practical values under discussion, obtained from one tube type which was equipped over a long run with a low capacity target and over another long run with a high capacity target.

Of practical interest is the value of primary voltage necessary to get the maximum SEC gain. In Figure 3.11 the normalized gain is plotted versus primary voltage for a high capacity and a low capacity target. The curves are close together which indicates the energy

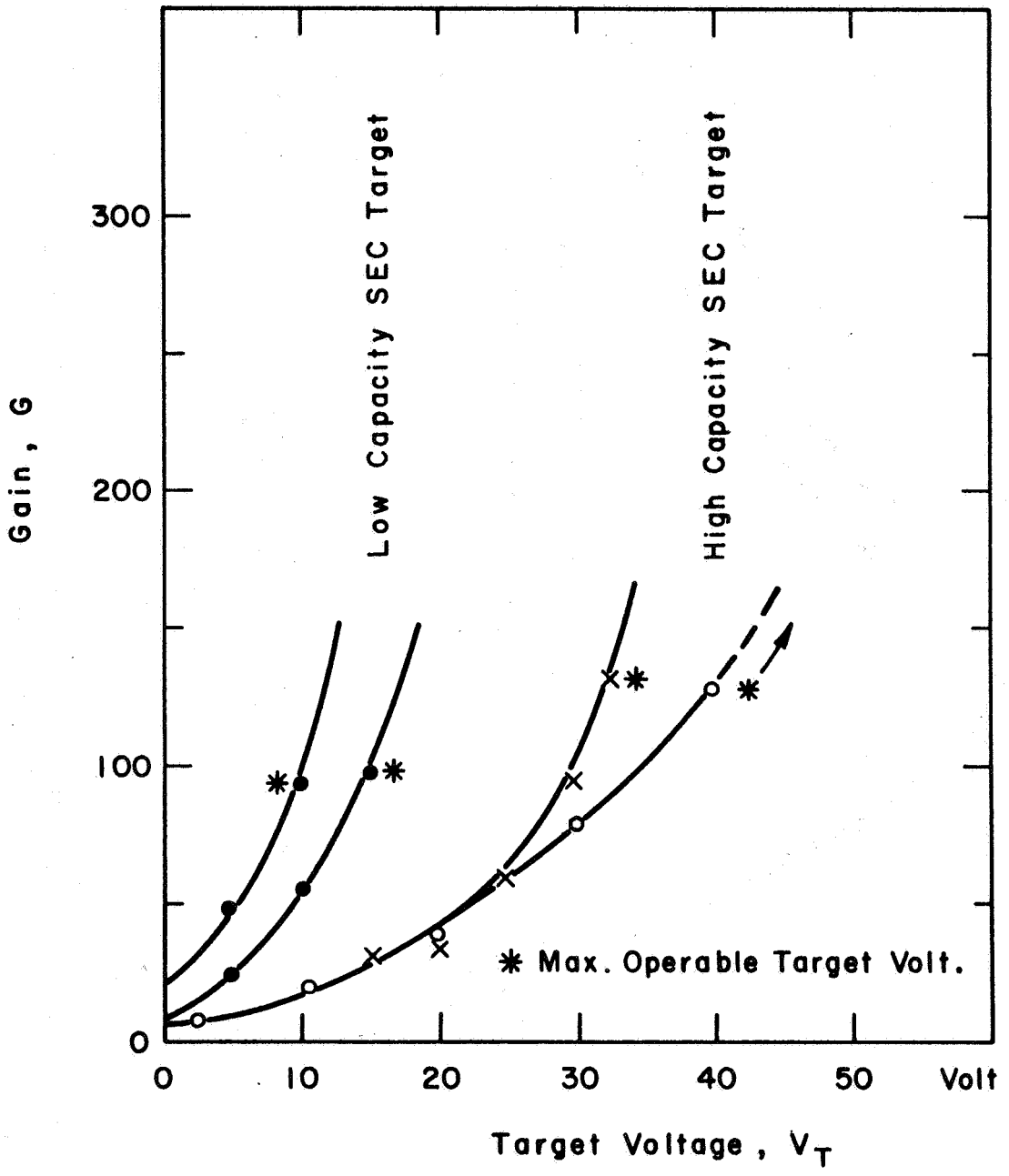

FIGURE 3.10: SMALL SIGNAL GAIN VERSUS TARGET VOLTAGE MEASURED IN FOUR SEALED-OFF TUBES

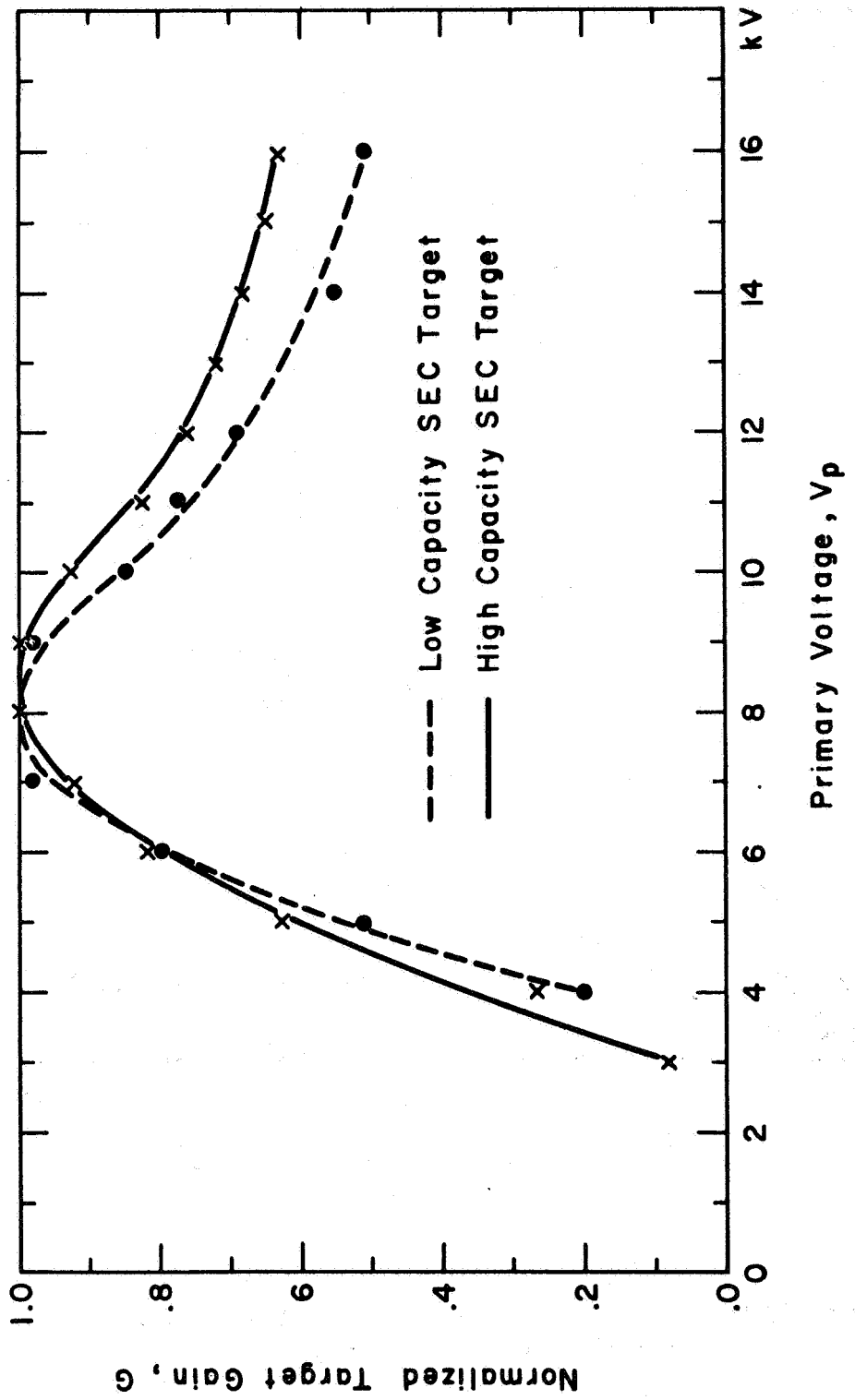

FIGURE 3.11: NORMALIZED SMALL SIGNAL GAIN AS A FUNCTION OF PRIMARY VOLTAGE AT CONSTANT TARGET VOLTAGE

dissipation to be approximately the same in both targets.

3.2.2 The Large Input Signal Storage Capacity

In Section 3.1.1 the "differential" storage capacity was defined by Equation (3.8) and the "integrated" storage capacity by Equation (3.7). Of practical interest, however, is especially the large input signal storage capacity. Only if the primary current would exactly neutralize the target when saturation is reached, the integrated storage capacity, as defined by Equation (3.7) would be equal to the large input signal storage capacity. In order to outline the trend of the storage capacity with increasing input current under this condition, we have to recall some results of Section 3.1.1.

As shown in Section 3.1.1, the differential storage capacity/area, C, is given by

$$C = C_o + kV_T \tag{3.26}$$

and the integrated storage capacity by

$$C_i = C_o + \frac{1}{2} kV_T. \tag{3.27}$$

Since, as also demonstrated in Section 3.1.1, the low input signal capacity is equal to the differential storage capacity, the storage capacity/area at a given target V_T is expected to start at low input signals with the value given by Equation (3.26) and approach the value given by Equation (3.27) as saturation is reached. Hence, under the condition of complete neutralization at the saturation point, the storage

capacity of the target should decrease with increasing input current. This is indeed not observed. In Figure 3.12 the storage capacity/area is plotted versus the voltage excursion V_E for the target voltage $V_T = 20$ volts (solid line) and $V_T = 40$ volts (solid line), in addition, the curve of the differential storage capacity/area versus target voltage (dotted line) is repeated from Figure 3.2. According to the results represented in Figure 3.2, the solid lines start at $V_E = 0$ with the value of the dotted line at $V_T = 20$ volts and $V_T = 40$ volts respectively, but increase with V_E (increasing primary current) rather than decrease. This effect has considerable practical importance since the higher values of the solid curves in Figure 3.12 that can be used practically determine the dynamic range.

In order to understand the increase of storage capacity with increasing input current, we have to remember the facts discussed in Section 3.1.3, especially those connected with Figure 3.6 and the discussion of the charge density $\rho(x)$ at the target surface ($x = d$) and its dependence on the target voltage. The curve $\rho(x = d, V_T)$ in Figure 3.6 cannot go below zero as long as only the reading beam operates. With primary current applied to the target, however, the target surface may well be loaded with positive charge and fulfill in the meantime the conditions given by Equations (3.4), (3.5), and (3.6) after having been scanned out. If this is the case, the amount of positive charge at the target surface should increase with increasing primary current and the center point of the negative charge-gravity comes closer to the target substrate with increasing primary current. Since

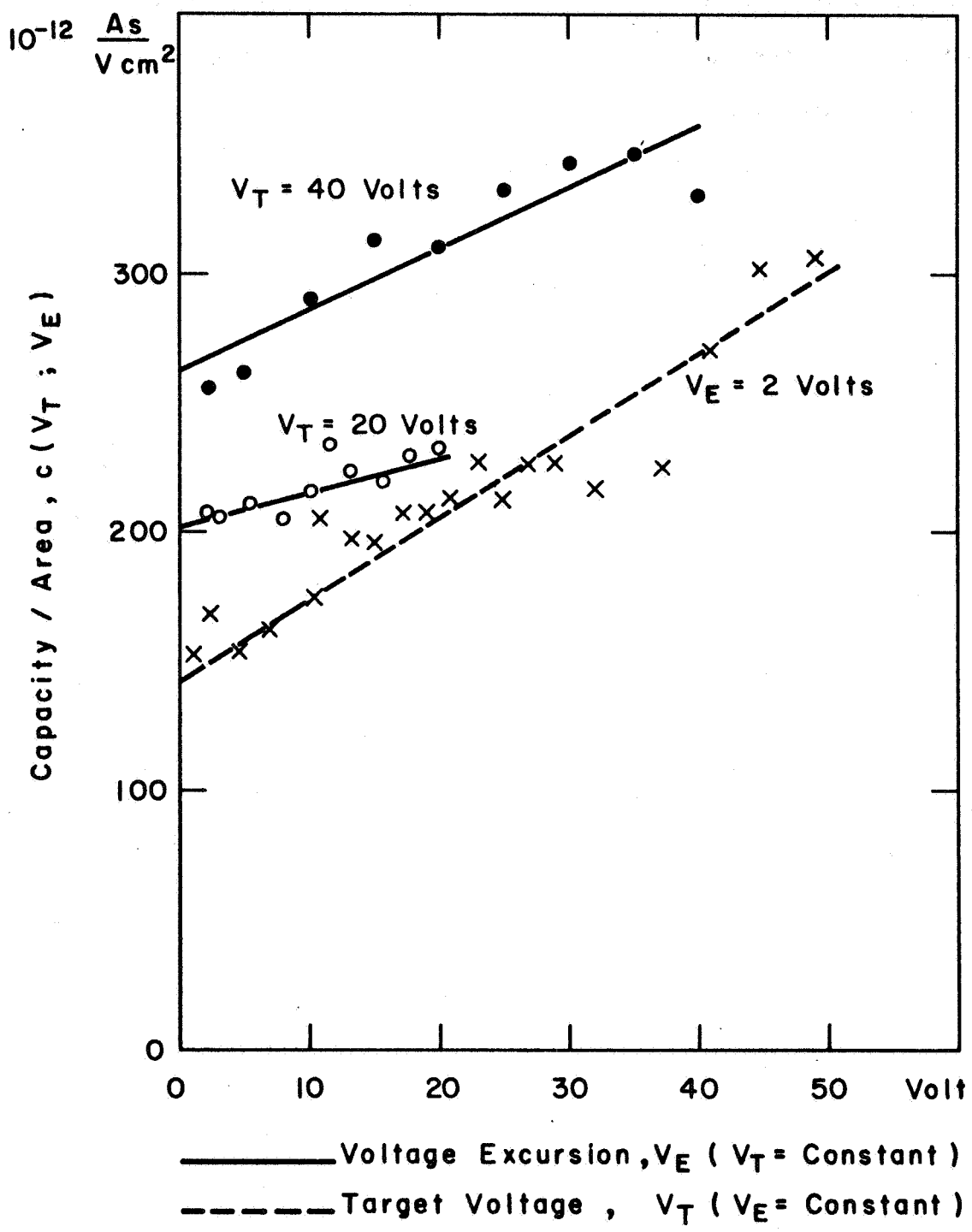

FIGURE 3.12: STORAGE CAPACITY PER AREA AS A FUNCTION OF VOLTAGE EXCURSION AND TARGET VOLTAGE

the target gain must be expected to increase with increasing negative charge density, the secondary electrons are created more closely to the target substrate as the input current is increased. The result is the positive slope of the storage capacity curves versus voltage excursion V_E in Figure 3.12.

The dependence of the storage capacity/area on the voltage excursion V_E can be handled in a similar fashion to the treatment of the differential storage capacity/area given in Section 3. From such a treatment one can deduce the electric field at the substrate, the charge density in the target, etc., when a primary beam is applied to the target. This discussion will be presented at a later date.

3.2.3 The Dynamic Range

The dynamic range of the target can be determined from the transfer curve (signal current versus primary current density). The improvement that has been achieved becomes especially evident if transfer characteristics are measured at low frame rates. In Figure 3.13 the transfer curve of a high capacity target is compared with the transfer curve of a low capacity target both measured at 10 frames/second. At the points on the curves indicated as "smear points", the resolution of the tubes started to decrease. The transfer curve of the low capacity target tends to saturate at the smear point, while this is not the case for the high capacity target. From Figure 3.13 again the good sensitivity of the high capacity target is seen.

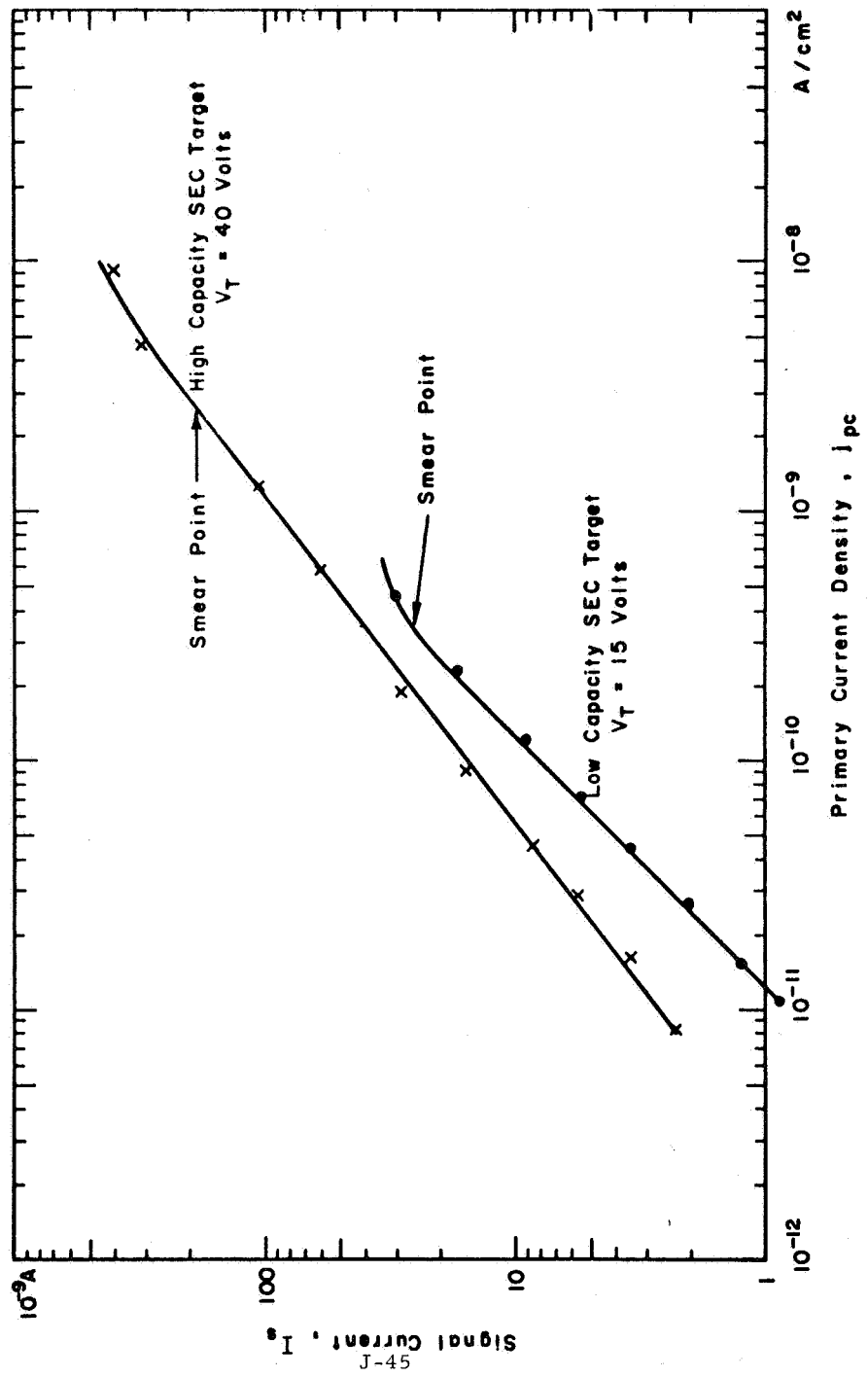

FIGURE 3.13: TRANSFER CURVES OF A LOW AND A HIGH CAPACITY TARGET, MEASURED AT 10 FRAMES/SECOND

In order to compare a high capacity target operated in a normal camera tube with target No. 3 which was operated and extensively measured (Section 3.1) in a demountable camera tube, the transfer curve of target No. 3, measured at 30 frames/second in the demountable camera tube, is added to the transfer curve of the high capacity target in Figure 3.14. The scanned target area was the same for both measurements. The reading beam current of the demountable system was limited as indicated in Figure 3.14. The maximum voltage excursion that could be readout in the demountable tube was $V_E = 2$ volt.

Since the curves in Figure 3.14 are measured at the same target voltage and agree very well, we may assume that both targets have approximately the same storage capacity. The surface voltage excursion at the smear point on the transfer curve of the high capacity target in Figure 3.13 can be estimated to be $V_E^{max} = 15$ Volts. A conclusive explanation of this limitation is not yet known; two possible explanations, however, can be given. The first one is the electric field disturbance between suppressor mesh and target surface caused by the variations of the surface voltage excursion which represents the brightness distribution of the scene. The second explanation might be found in a possible leakage current caused by the electric field parallel to the target surface which represents the brightness gradient in the scene. In Figure 3.15 the transfer curve of an SEC camera tube with high capacity target is shown which was measured at 0.625 frames/second. As far as known this was the first time that an SEC camera tube could be operated

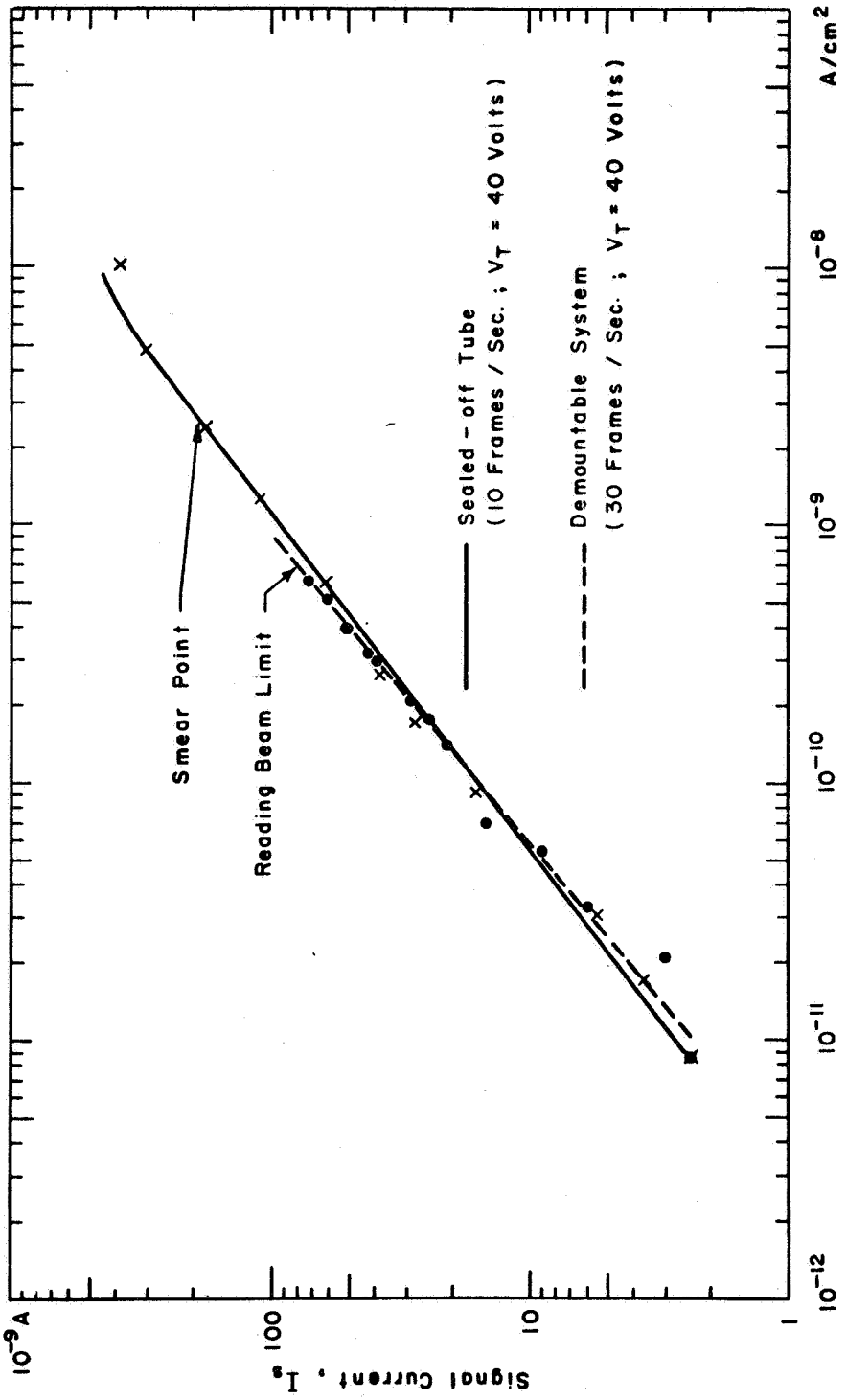

FIGURE 3.14: TRANSFER CURVES OF TWO HIGH CAPACITY TARGETS MEASURED IN A SEALED-OFF TUBE AND THE DEMOUNTABLE SYSTEM RESPECTIVELY

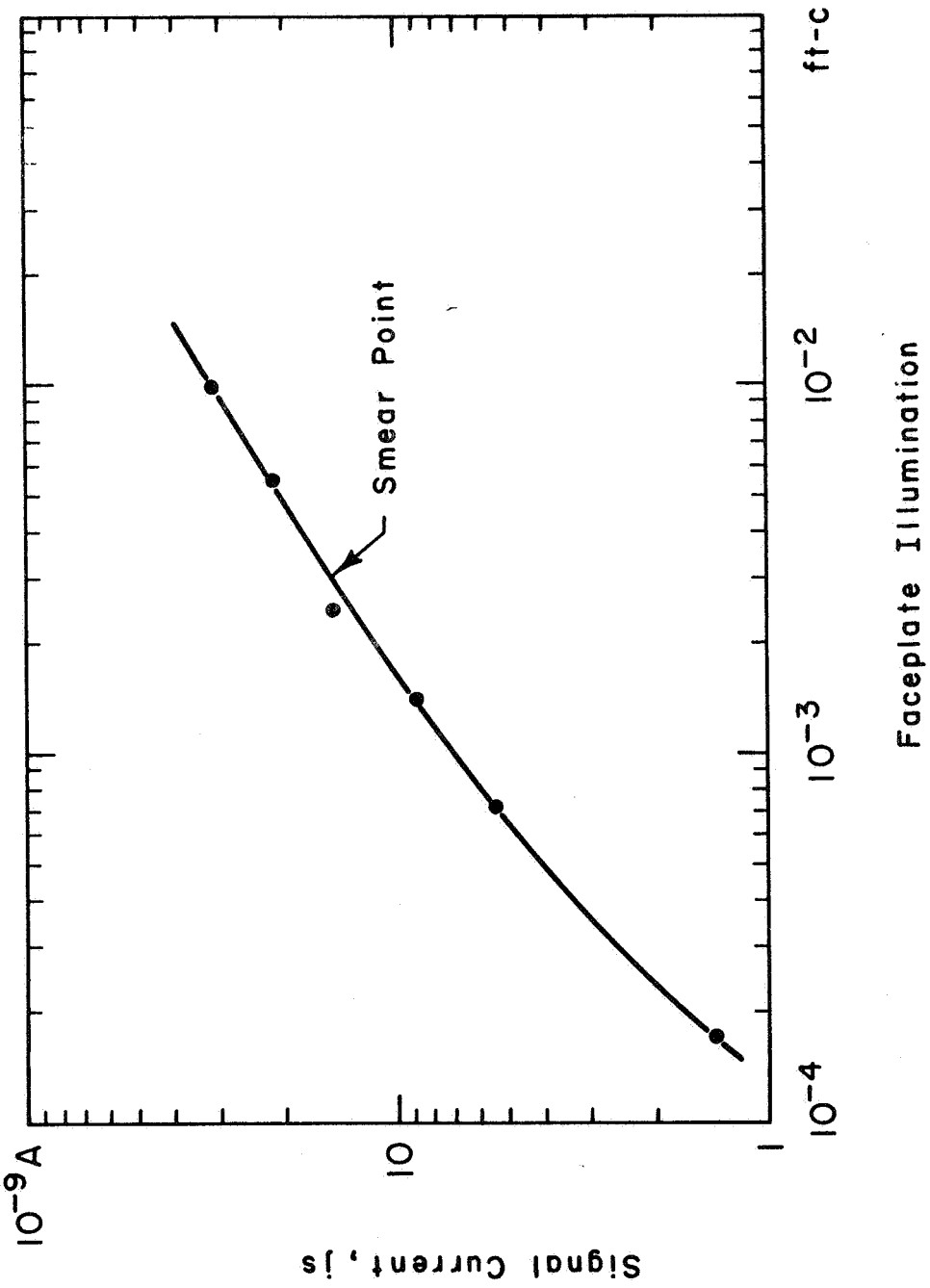

FIGURE 3.15: TRANSFER CURVE MEASURED AT 0.625 FRAMES/SECOND

successfully at such low frame rates.

3.2.4 The Storage Time

A given charge distribution in the target does not remain unchanged indefinitely, also if no primary beam or scanning reading beam is applied to the target. This fact indicates that at least some of the electrons trapped in the target have a finite lifetime in the trapping states. This lifetime limits the storage time of the target, that is, the time during which an image can be stored in the target without significant deterioration. If two or more different processes take place to release electrons out of the trapping states, more than one characteristic lifetime should be observed. However, only the shortest lifetime that becomes effective is of practical interest.

In order to measure the lifetime of the electrons trapped in the target, the primary beam was shut off and the target was scanned with the reading beam at a given target voltage, V_T, to such an extent that no further charge was accepted; and the voltage excursion, therefore, was zero. The reading beam was then turned off too. After the time t the decrease of charge in the target was determined by measuring the voltage excursion $V_E(t)$. The results are plotted in Figure 3.16 for $V_T = 40$ volts. Since the target was operated in a demountable camera tube, measurements could be made before and after the target had been baked. The crosses and circles in Figure 3.16 are the measured values of $V_E(t)$ while the solid lines are calculated according to

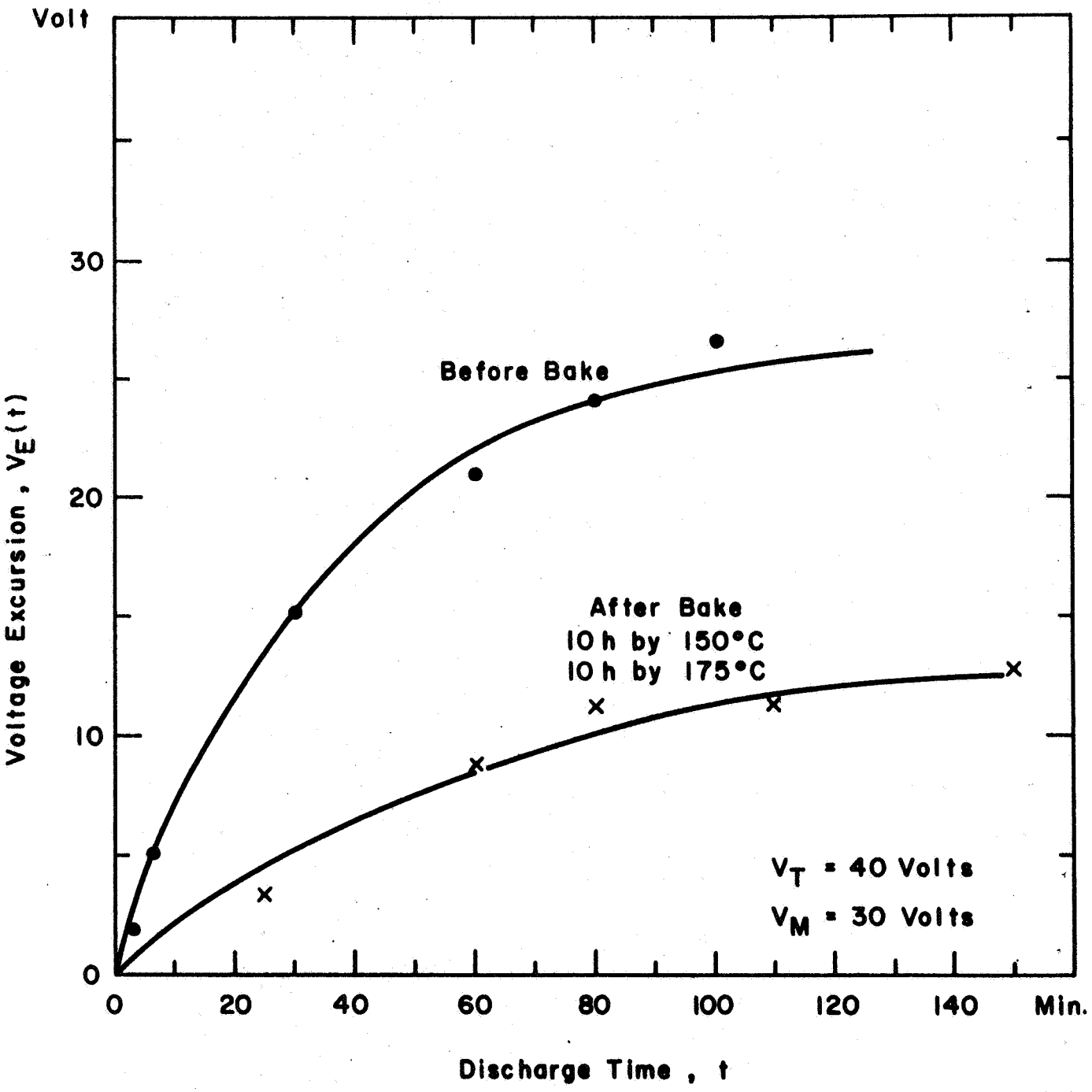

FIGURE 3.16: VOLTAGE EXCURSION CAUSED BY DISCHARGE AS A FUNCTION OF DISCHARGE TIME MEASURED WITH TARGET NO. 3 IN DEMOUNTABLE CAMERA SYSTEM

$$V_E(t) = V_{Ef}\,(1 - e^{-t/\tau}) \tag{3.28}$$

with the final voltage excursion $V_{Ef} = V_E\ (t = \infty)$ and the

$$\text{life time } \tau = V_{Ef}\left(\frac{dV_E}{dt}\right)^{-1}_{t=0} \tag{3.29}$$

adjusted to give the best fit. The curve obtained before baking levels off at 27 volts. After the target had been baked for ten hours at 150°C, and an additional ten hours bake at 175°C, the final value of the voltage excursion was only 14 volts. The relative charge loss

$$\frac{\Delta Q}{Q} = 1 - \frac{V_T - V_{Ef}}{V_T}\ \frac{C_i(V_T - V_{Ef})}{C_i(V_T)} \tag{3.30}$$

associated with the final voltage excursion V_{Ef} before and after baking was 0.74 and 0.42 respectively. The lifetime was according to Equation (3.29) 36 minutes before baking and 62 minutes after baking.

The signal current which is caused by the charge loss ΔQ when the target is operated with an active frame time T_a and a total frame time T is

$$I_S = \frac{\Delta Q}{T_a} \approx \frac{C_i\ A_T}{T_a}\ V_E(T) \tag{3.31}$$

where A_T is the scanned target area. Since from Equation (3.28) follows with t = T that

$$V_E(T) \leq \frac{V_{Ef}}{\tau}\ T \tag{3.32}$$

the signal current becomes

$$I_S \leq \frac{T}{T_a}\ A_T\ \frac{V_{Ef}}{\tau}\ C_i \tag{3.33}$$

Using the values V_{Ef} = 27 volts and τ = 36 minutes of the unbaked target No. 3 and replacing the integrated capacity by the large signal capacity given in Figure 3.12 at $V_T = V_E$ = 40 volts, we obtain from Equation (3.33)

$$I_S \leq \frac{T}{T_a} \frac{A_T}{cm^2} \quad 4.5 \times 10^{-12} \text{ Amp.} \qquad (3.34)$$

For practical target areas obviously this signal current is small compared to the noise in any camera system as long as the active frame time T_a is in the same order of magnitude as the total frame time T.

3.2.5 The Crossover Voltage

It has been observed that the first crossover voltage of the high capacity target appears to be higher than 15 volts and fluctuates when several high capacity targets are compared with each other. Voltages of first crossover in the range between 20 volts and 40 volts have been measured. This fact permits the voltage at the suppressor mesh to be higher than 15 volts. The advantage of an increased voltage at the suppressor mesh is the known improvement of the reading gun going along with it[4]. In order to show an example the square wave aperture response curve of an electrostatic reading gun is presented in Figure 3.17 for different values of the mesh voltage. The measurements were made in the demountable camera tube mentioned before with a suitable metal test pattern put in the target plane. The voltage at the test pattern was 8 volts in order to simulate high-light conditions in a camera tube. From Figure 3.17 it is seen that the most significant increase of resolution is obtained by increasing the suppressor mesh

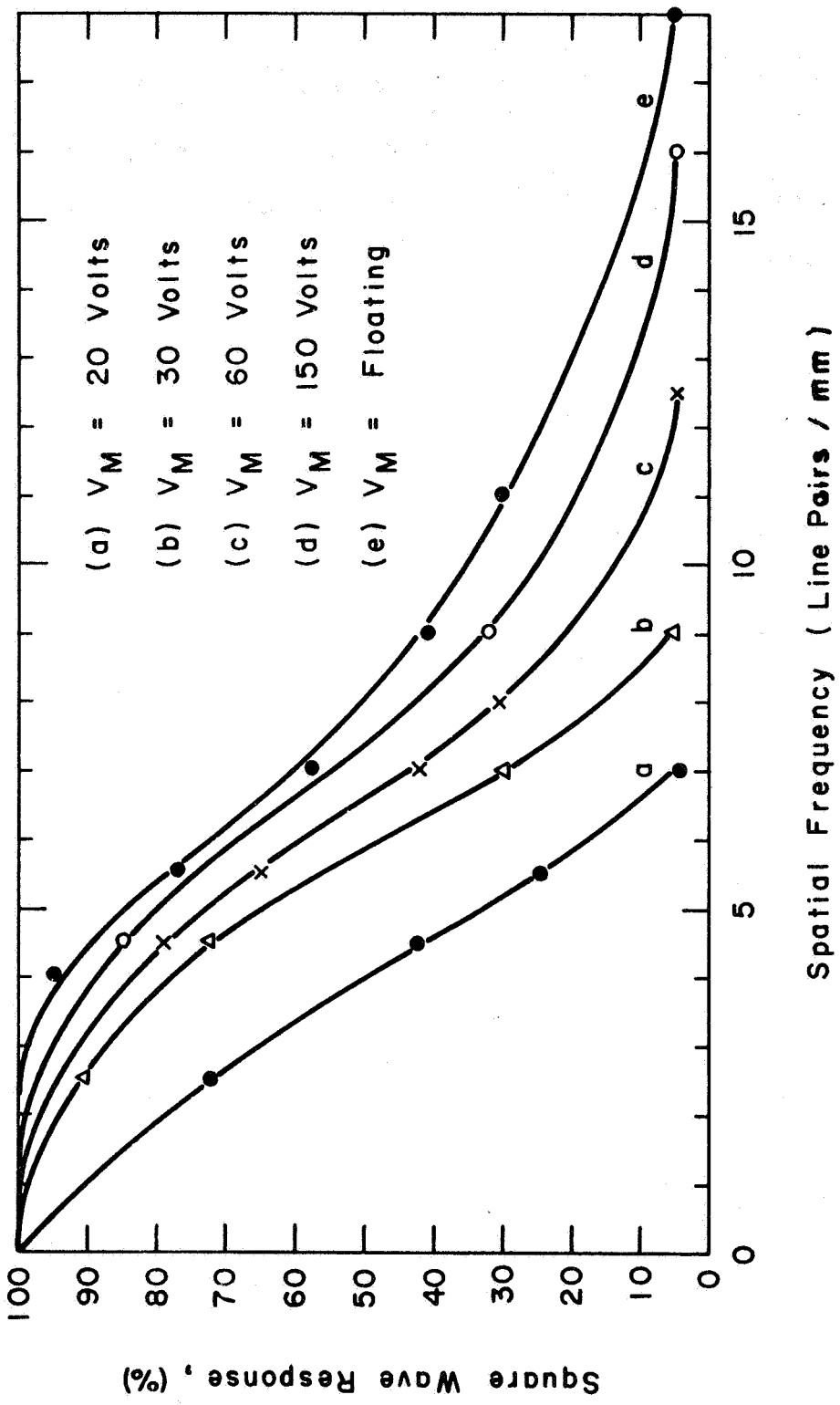

FIGURE 3.17: THE SQUARE WAVE APERTURE RESPONSE OF AN ELECTROSTATIC READING GUN WITH DIFFERENT VOLTAGES AT THE SUPPRESSOR MESH

voltage from 20 volts to 30 volts. Since most of the high capacity targets have a first crossover voltage exceeding 30 volts, the resolution of a camera tube equipped with a low capacity target usually increases if a high capacity target is inserted.

4. CONCLUSION

The storage capacity and therewith the dynamic range of the SEC target has been considerably improved. With the high capacity target an SEC camera tube could be operated at frame rates as low as 0.625 frames/second, as far as known, for the first time. The small signal gain seems to be approximately as good as the gain of the low capacity target. A disadvantage of the high capacity target, however, is its limited storage time which restricts the high capacity target to applications using the continuous scanning operation only.

ACKNOWLEDGEMENT

The authors would like to thank Dr. G. W. Goetze for initiating this work and for many helpful discussions. The authors are indebted to Mr. A. H. Boerio and Dr. M. Green who performed the first experiments on high capacity targets at the Westinghouse Research Laboratories in Pittsburgh and made their results available to the authors. Special thanks are due to Mr. R. R. Beyer who provided the demountable camera system which was used for most of the experiments presented in this report. The authors wish to thank Mr. J. C. Oswald and Mr. E. Boitin for their help in preparing and testing high capacity targets. Moreover thanks are due to Mr. G. M. Bernhardt who provided the transfer curves at low frame rates and Mr. A. Kuelling who provided the small signal gain curves.

REFERENCES

1. G. W. Goetze and A. H. Boerio, "Secondary Electron Conduction (SEC) for Signal Amplification and Storage in Camera Tubes." Proc. IEEE, Vol. 52, (1964) p. 1007.

2. G. W. Goetze, "Secondary Electron Conduction, (SEC), and its Application to Photoelectronic Image Devices" presented at the Third Symposium on Photoelectronic Image Devices as Aids to Scientific Observation, Imperial College, London, (September 1965).

3. A. H. Boerio, R. R. Beyer, and G. W. Goetze,"The SEC Target" presented at the Third Symposium of Photoelectronic Image Devices as Aids to Scientific Observation, Imperial College, London, (September 1965).

4. M. Green, R. R. Beyer and H. deVries, "Exploratory Development of the High Resolution Television Camera Tubes." Final Technical Report AFAL-TR-65-271(1965).

This page intentionally left blank.